



The University of
Nottingham

UNITED KINGDOM • CHINA • MALAYSIA

Biomass-derived Activated Carbon for Energy Storage Applications

Afnan Altwala

**Thesis Submitted to the University of Nottingham for
degree of Doctor of Philosophy**

Abstract

Activated carbon is a porous carbon material with a broad range of applications as adsorbents in liquid and gas treatment, as well as in catalytic applications. The need for activated carbons is continuing to expand, because environmental pollution is an increasingly serious issue. Activated carbons' (ACs) specific properties are determined by the properties of the starting materials and the activation methods utilised. Practically, the principal sources of commercial ACs are coal, wood and coconut shells. Given their low cost, sustainability and ready availability, various agricultural and forest by-products have recently gained considerable attention as alternative feedstock for the production of ACs. Accordingly, a major goal of this thesis is to explore and discover the synthesis conditions for generating highly porous materials from starting materials with little to no value, for example waste biomass. We employed (sawdust, SD), date seed (*Phoenix dactylifera*) and CNL carbon (from accidental and uncontrolled burning of wood under fierce fire conditions of the first Carbon Neutral Laboratory, CNL, building at Nottingham) as feedstock, in order to prepare the activated carbon. The principal objectives are to identify and investigate synthesis conditions for producing highly porous activated carbon for sustainable energy applications.

The first chapter presents an overview of the climate change issue, positing some strategies towards reducing the harmful effects of atmospheric pollution. Furthermore, it describes the several types of porous materials

used for gas adsorption, for instance MOFs, zeolites and porous carbon. Description of porous materials is a main focus of this chapter, which also covers pore classifications according to size, shape and type of the pores, as well as methods used to prepare activated carbons, and the use of the carbons in gas storage.

In the second chapter, the techniques adopted to analyse porous carbons are briefly discussed, with Brunauer, Emmett and Teller (BET) theory and CO₂ adsorption using gravimetric analysis methods using a XEMIS instrument being notable. The chapter also described the techniques that may be used to probe the nature of porous materials and includes description of Thermal Gravimetric Analysis (TGA), powder X-Ray Diffraction (XRD), Scanning Electron Microscopy Analysis (SEM), Transmission Electron Microscopy (TEM) and Elemental Analysis.

In the third chapter, date seed (*Phoenix dactylifera*) is used as an example of how biomass with a low O/C ratio can be used to prepare activated carbons in a targeted manner. The chapter describes how the choice of carbonisation mode may be adopted to produce activated carbons with optimised porosity for methane storage. The elemental composition of the biomass precursor, specifically, a low O/C atomic ratio, can be used as a universal predictor of the nature of porosity generated for activated carbon prepared via KOH activation. The carbons can be tailored to have a mix of microporosity/mesoporosity, with high surface area density, high volumetric surface area, in addition to a high packing density. The activated carbons produced are highly microporous with surface area of 995 – 2609

$\text{m}^2 \text{g}^{-1}$, pore volume of $0.43 - 1.10 \text{ cm}^3 \text{g}^{-1}$ and high packing density. The resulting carbons had pores of size $8 - 12 \text{ \AA}$, which are suitable for methane uptake. At 25°C and 35 bar , the carbons have an excess and total methane uptake of up to $196 \text{ cm}^3 \text{ (STP) cm}^{-3}$ and $222 \text{ cm}^3 \text{ (STP) cm}^{-3}$, respectively, which is superior to any previously reported carbon and comparable to the best MOFs.

In the fourth chapter, potassium oxalate (PO) and KOH were employed as activating agents to prepare activated carbons from date seed derived carbonaceous matter designated as ACDS (air-carbonised date seed). Previously, the action of the two activating agents has been compared but on different starting materials. In this study, identical procedures were used to synthesise the carbons with PO or KOH. The design of this study allowed a fuller understanding of the workings of the two activating reagents. The activated carbons resulting from PO activation had surface area of up to $1747 \text{ m}^2 \text{g}^{-1}$, with up to 94% of the surface area being attributed to micropores. Their porosity could be tailored towards $6-8 \text{ \AA}$ pore channels, which are excellent for CO_2 storage at low pressure. At 25°C , the PO activated carbons can store up to 1.9 and 4.8 mmol g^{-1} of CO_2 at 0.15 bar and 1 bar , respectively. Unlike what is observed for hydroxide (KOH) activation, changing the PO/ACDS ratio between 2 and 4 did not affect porosity. At any given activation temperature, carbons activated at PO/ACDS ratio of 2 or 4 have comparable porosity and therefore similar CO_2 uptake. On the other hand, KOH activated carbons reach higher surface area of up to $2738 \text{ m}^2 \text{g}^{-1}$. At 25°C , KOH activated carbons can store up to

4.5 mmol g⁻¹ of CO₂ compared to 4.8 mmol g⁻¹ for PO activated carbons. The PO activated carbons CO₂ uptake of 1.9 mmol g⁻¹ at 0.15 bar and 25 °C is amongst the highest for any porous material under those conditions.

In chapter five, highly microporous activated carbon materials are prepared via direct activation of biomass (sawdust, SD) with potassium oxalate (PO) as a non-corrosive and less toxic activating agent (compared to KOH). The direct activation negates the need for hydrothermal carbonisation or pyrolysis, and generates carbons that are similar to conventionally activated (via hydrothermal carbonisation) equivalents. Overall, the carbons display high microporosity with surface area ranging from 550 to 2100 m² g⁻¹, and pore volume between 0.3 and 1.0 cm³ g⁻¹. Unlike hydroxide activation, the PO/SD ratio does not have a significant effect on porosity, however the activation temperature plays a critical role in determining the textural properties at any PO/SD ratio. Porosity could thus be precisely controlled by varying the activation temperature only. This is a significant finding because it confirms that a more environmentally friendly and direct route to activation, using a milder activating agent, does not compromise achievable porosity. The direct activation, with potassium oxalate as an activating agent, generated activated carbons with pore sizes of 6–8 Å, which is conducive for post-combustion (low pressure) CO₂ storage; the carbons capture up to 1.6 and 4.3 mmol g⁻¹ of CO₂ at 0.15 and 1 bar, respectively, and 25 °C.

In chapter six, we synthesized activated carbons from pre-mixtures of polypyrrole (PPY) with CNL carbon or ACDS carbon. The pre-mixtures,

which combined precursors that would normally produce mesoporous carbons with high pore volume (PPY) or microporous carbons with moderate pore volume (CNL and ACDS carbons), produced activated carbons with ultra-high surface area (up to $3890 \text{ m}^2 \text{ g}^{-1}$) and pore volume (up to $2.40 \text{ cm}^3 \text{ g}^{-1}$). Use of pre-mixtures as precursors generates carbons with substantially greater surface area than single use of any one of the precursors. An improved understanding of the way in which the activation process is influenced by the carbonisation phase has been combined with knowledge of the effect of the oxygen to carbon (O/C) ratios of the utilised carbonaceous materials in order to provide activated carbons with a high packing density and porosity that are ideal for methane storage. The resulted activated carbons exhibit greater methane uptake capacity (gravimetric and volumetric) than those produced from single use of the precursors.

Declaration

I hereby declare that this thesis is my original work and it has been written by me in its entirety, under the supervision of Professor Robert Mokaya. It has also not been submitted for any degree in any university previously.

Name: Afnan Altwala

Signature:



Date: 14/01/2022

Publication:

- Predictable and targeted activation of biomass to carbons with high surface area density and enhanced methane storage capacity Afnan Altwala and Robert Mokaya, *Energy Environ. Sci.*, 2020, **13**, 2967-2978.
- Direct and mild non-hydroxide activation of biomass to carbons with enhanced CO₂ storage capacity Afnan Altwala and Robert Mokaya, *Energy Advances*, 2022, DOI: 10.1039/D1YA00085C.
- Modulating the porosity of activated carbons via pre-mixed precursors for simultaneously enhanced gravimetric and volumetric methane uptake, Afnan Altwala and Robert Mokaya, (Submitted to *Journal of Materials Chemistry A*)

Presentations:

- Afnan Altwala and Robert Mokaya, Department of Inorganic and Materials Chemistry 2nd year Talks, **11th March 2019**, Directly Activated and Compactivated Carbon From Biomass For Sustainable Energy Applications.
- Afnan Altwala and Robert Mokaya, Department of Inorganic and Materials Chemistry 3rd year Talk in PG Research symposium **18th September 2020**, Predictable and targeted activation of biomass to carbons with high surface area density and enhanced methane storage capacity.

Poster session:

- Afnan Altwala and Robert Mokaya, Inorganic and Materials Chemistry Postgraduate Research Symposium, university of Nottingham, **3^{ed} July 2019**, "Directly Activated and Compactivated Carbon From Biomass For Sustainable Energy Applications"
- Afnan Altwala and Robert Mokaya, RSC Biomaterials Special Interest Group meeting **12th January 2021**, Predictable and targeted activation of biomass to carbons with high surface area density and enhanced methane storage capacity. (awarded the 2nd Poster Prize).
- Afnan Altwala and Robert Mokaya, RSC Materials Chemistry Division Poster Symposium **20th January 2021**, Predictable and targeted activation of biomass to carbons with high surface area density and enhanced methane storage capacity
- Afnan Altwala and Robert Mokaya, 3rd Oldenburg Symposium on Chemical Bond Activation, **8th March 2021**, Directly Activated and Compactivated Carbon From Biomass For Sustainable Energy Applications".
- Afnan Altwala and Robert Mokaya, The 2021 Anglo-German Inorganic Chemistry Conference (AGICHEM 2021), **9-10 September 2021**, Date Seed-based Carbons for Methane Storage and Carbon Capture and Storage (CCS).

ACKNOWLEDGEMENT

Without the advice and support of many people, a PhD thesis such as this, which includes knowledge from various fields, would not be possible. I would therefore like to take this wonderful opportunity to thank everyone who has helped me along the journey.

First and foremost, I would like to thank the government of the Kingdom of Saudi Arabia for funding my PhD studentship together with Majmaah University.

I would also like to thank my supervisor, Robert Mokaya, for allowing me to join his team and to study with him. He has always given me the freedom to explore various research projects and welcomed me to discuss my findings with him. I am grateful for all the time he has spent reading and commenting on my work and reports.

I would like to give my special thanks to my mother, brothers and sisters, especially my close sister, Rehab. I wish I could say thank you to my father but unfortunately, he passed away; all my prayers are for him.

I would like to express my deepest gratitude to my dear husband for his unconditional love, encouragement, motivation and understanding.

I offer huge thanks to my friend, Tahani Alzkari, for her constant help and support.

I would also like to extend my particular thanks to Neil Barnes and Mark Guyler for their assistance with all the techniques. I am grateful to Dr. Tang

for helping with the elemental analysis. I am also grateful to Nanoscale and Microscale Research Centre (NMRC), and especially to Nigel Neate and Michael Fay for their help with the scanning electron microscopy and transmission electron microscopy images.

Finally, this thesis would not have been possible without the help and support of the members of our research group in the School of Chemistry.

Table of Contents

Chapter 1. Introduction	1
1.1 Climate change	1
1.2 Types of porous materials for gas adsorption.....	3
1.2.1 Liquid amines.....	3
1.2.2 Metal–organic frameworks (MOFs)	4
1.2.3 Zeolites	5
1.2.4 Porous Carbons	6
1.3 Carbonization step (pre-activation step).....	8
1.4 Activation carbon: activation methods	9
1.4.1 Activated carbon production through physical activation	9
1.4.2 Activated carbon production through chemical activation	10
1.5 Physisorption and chemisorption	11
1.6 Pore Classifications	12
1.7 Energy related gas storage applications	15
1.7.1 Carbon Capture and Storage (CCS).....	16
1.7.2 Hydrogen Storage.....	19
1.7.3 Methane Storage	20
1.8 Aim of this research	23
Chapter 2. Material Characterization.....	35
2.1 Analytical Techniques.....	35

2.1.1 Thermogravimetric Analysis (TGA)	35
2.1.2 Powder X-Ray Diffraction Analysis (XRD)	37
2.1.3 Scanning Electron Microscopy (SEM)	40
2.1.4 Transmission Electron Microscopy (TEM).....	42
2.1.5 Elemental Analysis	44
2.1.6 BET surface area and porosity measurement.....	45
2.1.7 Gas Uptake Analysis	55

Chapter 3. Predictable and targeted activation of biomass to carbons with high surface area density and enhanced methane storage capacity60

3.1 IntroductionError! Bookmark not defined.

3.2 Experimental Section.....Error! Bookmark not defined.

3.2.1 Material preparation..... **Error! Bookmark not defined.**

3.2.2 Material Characterisation **Error! Bookmark not defined.**

3.2.3 Methane uptake measurements **Error! Bookmark not defined.**

3.3 Results and DiscussionError! Bookmark not defined.

3.3.1 Nature of carbons **Error! Bookmark not defined.**

3.3.2 Porosity of carbons **Error! Bookmark not defined.**

3.3.3 Methane Storage **Error! Bookmark not defined.**

3.4 ConclusionError! Bookmark not defined.

Chapter 4. A Milder Non-Hydroxide Activation route for Activated Carbons 108

4.1	Introduction	110
4.2	Experimental Section.....	114
4.2.1	Material preparation.....	114
4.2.2	Material Characterisation	115
4.2.3	CO ₂ uptake measurements	116
4.3	Result and Discussion.....	116
4.3.1	Structural ordering, morphology and thermal stability	116
4.3.2	Textural properties and porosity	126
4.3.3	CO ₂ uptake	134
4.4	Conclusion	141
	<i>Chapter 5. Direct and mild non-hydroxide activation of biomass to carbons with enhanced CO₂ storage capacity</i>	<i>149</i>
5.1	Introduction	150
5.2	Experimental section.....	153
5.2.1	Material synthesis.....	153
5.2.2	Characterization methods	154
5.2.3	CO ₂ uptake measurements	155
5.3	Results and Discussion	155
5.3.1	Yield, nature and elemental composition of activated and compactivated carbons	155
5.3.2	Porosity of activated carbons and compactivated carbons	163
5.3.3	CO ₂ uptake of activated and compactivated carbons	171

5.4 Conclusion	177
<i>Chapter 6. Porosity modulation of activated carbons via pre-mixed precursors for enhanced methane storage</i>	185
6.1 Introduction	186
6.2 Experimental Section.....	192
6.2.1 Material preparation.....	192
6.2.2 Material Characterisation	193
6.2.3 Methane uptake measurements.....	194
6.3 Results and Discussion	194
6.3.1 Yield, nature and elemental composition of activated carbons ...	194
6.3.2 Textural properties and porosity.....	205
6.3.3 Methane Storage	218
6.4 Conclusions	240
<i>Chapter 7. Conclusion</i>	248

Chapter 1. Introduction

1.1 Climate change

The relationship between atmospheric warming and increases in 'greenhouse gases' present in the lower atmosphere has led to increased awareness of anthropogenic impact on global ecosystems and climate.^{1,2}

The changing global climate is predicted to have increasingly severe human, environmental and economic impacts. Emissions of greenhouse gases, especially CO₂, must be significantly reduced to prevent catastrophic global warming, a view accepted by the majority of researchers for more than four decades.³

A greenhouse gas (GHG) is defined as a gas that absorbs and emits infrared radiation. Water vapour, carbon dioxide, methane, nitrous oxide, and ozone are the primary greenhouse gases. The enhanced greenhouse effect, sometimes referred to as a global warming or climate change, is the impact on the climate due to the process of (positive) radiative forcing, whereby a greater amount of thermal energy is re-radiated back to the Earth's surface than is lost into space. A gradual rise in global surface temperature is the overall effect of the enhanced greenhouse effect.^{4,5} The use of fossil fuels that generate CO₂ is considered to be the primary contributing factor to global warming. Despite this, there is continuing worldwide growth in the use of gasoline and diesel. Control of gaseous CO₂ levels in the atmosphere is considered to be the main anthropogenic control

Introduction

knob on the climate and is therefore the focus of many studies. A number of potential solutions to mitigate CO₂ emissions prior to their release into the atmosphere, especially from flue gases emanating from fossil fuel power stations, are under active research.^{6,7}

Climate change has provided an incentive for increases in the use of renewable energy sources for electricity generation, transportation and other sectors. Such efforts need to be increased to achieve the required drastic reduction in the amount of anthropogenic CO₂ being released into the atmosphere, particularly from the burning of fossil fuels.^{6,8}

There are two major international agreements addressing Climate Change: the 1992 United Nations Framework Convention on Climate Change, and the 1997 Kyoto Protocol. More recently, in 2015, the United Nations Climate Change Conference held in Paris saw 195 countries agree on a plan to reduce emissions of CO₂ and other greenhouse gases, aiming to limit global temperature increases to well below 2 °C (relative to pre-industrial climate).^{1,9-11} Moving to the exclusive use of renewable energy – primarily solar, wind, hydro and biomass-based processes – and the reduction in industrial CO₂ use, are long-term goals.^{11,12} Due to the numerous barriers to achieving a future completely reliant on renewable energy, faster short-term solutions must be implemented immediately.

A leading solution is to switch to using natural gas, which is produced from the breakdown of organic matter, and largely consists of methane.

Introduction

Natural gas has become one of the more interesting renewable fuels and is widely used in an increasing number of countries.⁸

The removal of CO₂ from the atmosphere is another strategy towards reducing atmospheric CO₂. One solution is the adsorption of CO₂ onto solid materials.^{13,14} As a potential solution to methane and CO₂ storage, new ways of preparing porous carbons with properties for good performance in energy related applications have been recently reported. However, much of the work still relies on trial and error approaches.¹⁵

1.2 Types of porous materials for gas adsorption

Several approaches are currently being developed for the purpose of gas adsorption, with research focussing particularly on liquid amines,^{16,17} metal–organic frameworks (MOFs),^{18–20} zeolites,^{21,22} and porous carbon.^{13,23–25} Each material has a number of merits and disadvantages, with many still actively being developed and improved on today.

1.2.1 Liquid amines

Another way to do post-combustion capture is to use chemical absorption, such as liquid amine solvents which is known as 'amine scrubbing' and uses alkanolamines to absorb CO₂ from a flue stream. The 'rich' amine solution is next heated in order to remove the absorbed CO₂, which is subsequently condensed. Chemical absorbents have been demonstrated to have greater absorption capability at low CO₂ partial pressure than solid absorbents, with amine scrubbers capturing up to 99 % of CO₂.

Introduction

It is possibly that the most popular and well-established capture method, with major industrial trials and commercial demonstrations at plants all over the world. The common choice of amine solvent is monoethanolamine (MEA), due to its high reactivity with CO₂ and easy regenerability.²⁶ Despite being the most widely adopted approach to capture CO₂ in industry, the process is expensive, as it suffers from high energy consumption; around 30% of a power plant's energy is used in regenerating the amine.¹⁷ In addition, the corrosive nature of the amines utilised reduces the equipment's lifetime, increasing expenditures.¹⁷

1.2.2 Metal–organic frameworks (MOFs)

Metal–organic frameworks (MOFs) have many outstanding features making them very promising for a variety of important applications, especially in the adsorption and separation of small gases and hydrocarbons. In addition, MOFs are used for a wide range of applications, such as catalysis, drug delivery, purification, and gas separation and storage.^{27,28}

MOFs are versatile structures with tuneable porosity that allows almost unlimited approaches to improve their properties and optimise their functionality. By changing the metal ions and organic ligands (linkers), it is easy to tailor different MOFs for optimum adsorption.²⁹

In 2018, Hönicke et al. reported a new MOF, DUT-60, with the highest recorded surface area and accessible pore volume of any material; 7839 m² g⁻¹ and 5.02 cm³ g⁻¹ respectively.^{30,31} These characteristics make MOFs a good option for CO₂ uptake. In addition, MOFs are a promising field of

Introduction

research for methane storage materials, and a great deal of work is reported in the literature.³²⁻³⁵

However, MOFs are not always selective for CO₂; most MOFs not only adsorb CO₂ strongly, but also take up a large amount of other small gases, such as N₂, CH₄, CO and O₂.^{29,36} In addition, MOFs are expensive; for example, when comparing MOFs to activated carbon, the activated carbons are much cheaper (\leq 1\$/kg) compared to at best 10–20\$/kg for MOFs.³⁷ Also MOFs are time-consuming to produce and have varying associated environmental hazards (depending on their composition).

1.2.3 Zeolites

Zeolites have been explored as CO₂ capture materials for some time.^{21,38} Zeolites are crystalline aluminosilicates, and so have a uniform micropore structure that makes them interesting for CO₂ capture as the Al:Si:O ratios allow the design of a wide range of frameworks with various pore structures. Commonly, some silicon within the zeolite structure is substituted with aluminium, providing a negative charge within the framework, and these structural features of zeolites allow them to adsorb gas molecules such as CO₂. Cavenati *et al*³⁹ have shown that the zeolite 13X is highly effective for CO₂ adsorption, with an uptake of 4.66 mmol g⁻¹ at 1 bar and 25 °C, meaning it can be used for carbon dioxide sequestration from flue gas.

Zeolites are considered to have a slight advantage over MOFs in terms of suitability for post-combustion CO₂ adsorption. In addition, zeolites are

Introduction

comparatively cheaper to produce compared with MOFs. However, zeolites have a number of limitations, as they often adsorb water vapour in preference to CO₂, limiting uptake ability. At higher pressures, uptake capacity and selectivity for CO₂ significantly drops.³⁸⁻⁴⁴

Generally, the synthesis of zeolites is not always straightforward and zeolites show poor hydrothermal stability.³⁸⁻⁴⁴

1.2.4 Porous Carbons

The importance of porous materials has been recognized since antiquity, when porous charcoal was used for its medicinal properties.⁴⁵ Worldwide interest in environmental protection and energy conservation has revived research on porous materials,⁴⁶ as they have many potential applications, such as in catalysis, separation, insulation, sensors, chromatography, etc.⁴⁷

Activated carbon is a porous carbon material made by subjecting a char to reaction with gases (physically or chemically) before, during or after carbonization in order to increase its adsorptive properties.^{15,48,49}

Depending on the preparation conditions of a porous carbon, the structure generally has an amorphous, graphitic-like laminar structure.⁵⁰ Activated carbons are mainly used for the purification of liquids and gases, but they also find use as catalysts or catalyst supports.⁵¹ Since the 1700s, porous carbons have been reported for utilisation in medicine, food production and air and water purification.³ Activated carbons can have a highly developed internal surface area and porosity, obtained by controlling the process of carbonization and activation. The resulting structures give activated

Introduction

carbons a large capacity for adsorbing chemicals (normally small molecules) from gases and liquids.^{52,53} Activated carbons have shown great potential as a carbon capture solution. They show high CO₂ uptake, and have a high thermal and mechanical stability, and variable packing density.^{54,55} Importantly, they can be easily generated from cheap biomass using easily accessible and environmentally friendly starting materials.

Generally, the amount of gas (hydrogen or CO₂) adsorbed and stored on a solid depends on the porosity of the absorbent, and so the textural properties of activated carbons are vital for their performance. Careful activation of carbonaceous matter can dramatically improve properties for specific applications. For this reason, there have been increasing efforts to prepare tailorable porous materials with optimised porosity and gas uptake in order to fully exploit their potential, especially in energy related gas storage applications.⁵⁶⁻⁵⁸

The porosity and elemental composition of such carbons depends on the nature of the carbonaceous matter (precursor) used and the activation conditions. In this regard, biomass is considered a preferred choice of precursor for activated carbons, as it is readily available (usually as waste matter), renewable, and essentially offers a 'carbon neutral' route to porous carbons. A variety of biomasses have been used and successfully converted to activated carbon, such as coal,^{59,60} carbon nanotubes, corn cob⁴⁹, coconut shell,⁶¹ wood, rice husk⁶², kenaf fibre⁶³, paper mill sludge⁶⁴ and olive stones.⁶⁵ Their applications include electrodes in supercapacitors,⁶⁶ and in gas (CO₂ and H₂)^{55,67} storage. Moreover, porous carbons can be

Introduction

made from organic molecules such as polypyrrole, furfural, and cellulose, which are commonly used as carbon precursors.

Generally, for new activated carbons to be interesting, they need to fit into one of the three categories: (i) exhibit new or improved desirable properties, (ii) be easier or cheaper to prepare, and (iii) be sustainable.^{57,68}

1.3 Carbonization step (pre-activation step)

Before the activation steps, there are different ways of converting biomass to carbon-rich (carbonaceous) matter²³ by removing the volatile and small molecules. Conventionally, the methods are either hydrothermal carbonisation (HTC)⁶⁹⁻⁷¹ or pyrolysis.⁷¹⁻⁷³ Hydrothermal carbonisation involves the thermochemical decomposition of biomass. Typically, an aqueous dispersion of biomass is placed in a stainless steel autoclave at a target concentration, and heated (typically at 180-300 °C) for several hours. The pyrolysis process, on the other hand, involves generation of carbonaceous matter via enrichment of carbon content during thermal treatment at temperatures of 600–900 °C under oxygen-free conditions.^{25,56,73-76} The Mokaya group²³ has investigated an alternative process, termed flash carbonisation, which uses much shorter periods of time (5–10 minutes) and a lower temperature (400 °C) in the presence of air. The process makes use of the fact that volatiles (i.e., H₂O, CO_x, CH₄, and light hydrocarbons) are lost at temperatures as low as 200-350 °C, with little mass loss above 400 °C, negating the need to use the conventional energy-intensive pyrolysis processes. The resulting flash

Introduction

carbonisation process is significantly shorter than the typical 2 h procedure, and does not require specialised pressure equipment.^{23,77,78}

More recently, the Mokaya group has explored direct conversion of biomass to activated carbons in one step. This method has a significant influence on the properties of both the activatable carbonaceous matter and the final activated carbons.⁶⁸ In addition, the methodology has activated carbon yields that are comparable to or higher than those of conventional activation routes. The properties of the resulting materials are similar or superior to analogous carbons prepared via conventional methods.

1.4 Activation carbon: activation methods

In order to create a pore network (the “porous” in porous carbon) an activation step is needed. This activation step can be “chemical” or “physical”. Alternatively, the combination of both physical and chemical activation processes is also possible.

1.4.1 Activated carbon production through physical activation

The physical activation process is a two-step process. Firstly, pyrolysis of the precursor in an inert atmosphere is normally performed at 400-900 °C in order to remove any volatile matter. Secondly, partial gasification using an oxidising gas at 350–1000 °C is performed in order to develop the surface area and porosity. All factors, such as the degree of activation, the oxidising agent employed, and the temperature of activation and precursor, have a large effect on the physically-activated carbon and depending on

Introduction

those factors, the activated carbon can achieve high porosity, as well as varying surface chemistry (i.e. amount and type of oxygen groups). Generally, in order to have more porosity, higher activation temperatures and duration are needed.

1.4.2 Activated carbon production through chemical activation

The chemical activation of carbonaceous matter occurs in one step using a mixture of a carbon precursor and an activating agent, commonly a strong acid or base such as KOH, NaOH, ZnCl₂ or H₃PO₄, and is typically performed at 300-800 °C under inert atmosphere.⁷⁹ The development of porosity increases with the ratio of the activating agent used in the activation, with the activation temperature, and with duration. Moreover, the precursor used, the activating agent, and the ratio of the two, are considered to be important factors affecting the development of pore structure.

Potassium hydroxide (KOH) is the most commonly reported chemical activating agent. It is widely used to generate carbons with porosity characteristics such as high surface area, high pore volume and narrow pore size distributions (PSDs) with a higher proportion of microporosity.

Chemical activation is widely used and is often favoured over physical activation because it can generate activated carbons with higher surface areas and/or narrow pore size distributions.⁷⁹ Furthermore, the chemical activation process usually involves lower temperatures and shorter operation times, and can offer high carbon yields and better control of porosity.

Introduction

In order to make and develop more effective and efficient materials for solid sorbent applications, the process of physisorption of gas onto a solid material surface must be understood, as well as pore classifications.

1.5 Physisorption and chemisorption

In a porous materials system, gas adsorption is an important tool for characterisation. The adsorption of gases onto solid materials has been used in many applications such as air purification,⁸⁰ gas separation,⁸¹ and hydrogen storage.⁸² The term “adsorption” was first proposed in the late 1800s, by J. W. Gibbs. However, the process was employed previously in 1773 by Scheele, who measured the gas adsorption capacity of charcoal to determine adsorption forces. Later on, in 1881, Chappuis and Kayser introduced the term ‘adsorption’ and concluded that it was a surface phenomenon. They were also amongst the first researchers to measure adsorption isotherms.⁸³⁻⁸⁵

Generally, the definition of adsorption is the enrichment of molecules, atoms, or ions in the vicinity of the interface between a solid surface and the environment, in the case of gas/solid systems⁸⁶. The adsorption of gases onto a solid surface has been utilised in the field of carbon capture, air purification gas separation, and hydrogen storage.⁸⁶

There are some important terms to distinguish in the study of gas adsorption in porous materials: *adsorbate*, *adsorbent* and *adsorptive*.

Introduction

A material being adsorbed is known as the *adsorbate*. The solid material being used as the adsorbing phase is known as the *adsorbent*, while the *adsorptive* is the same component in the fluid phase.^{86,87}

There is a difference between adsorption and absorption; the term adsorption is used to describe the interaction when a molecule comes into contact with a surface, whereas the term absorption is used when the molecules of the adsorptive penetrate the surface layer and enter the structure of the bulk solid. On a surface, there are two principle modes of adsorption: Chemical adsorption (chemisorption) or physical adsorption (physisorption). Physisorption is a general phenomenon: it occurs whenever an adsorbable gas (the adsorptive) is brought into contact with the surface of a solid (the adsorbent). Chemisorption involves a chemical reaction between the surface and the adsorbate – that is, it involves the formation of new chemical bonds. In physisorption, the adsorptive and the adsorbent remain unchanged and the process is readily reversible, whereas in chemisorption, the adsorptive and the adsorbent are chemically changed during the process.⁸⁶

1.6 Pore Classifications

The term “porous” is used for any material that contains cavities, channels or interstices.⁸⁸ The pores of solids are classified according to size, shape and type. They can then be categorised into the following three divisions: their availability to an external fluid, their shape, and their pore diameter. In the early 1950s, work by Dubinin led to the theory now encompassed in

Introduction

the International Union of Pure and Applied Chemistry (IUPAC) classification.^{50,86,89} Starting with the classification based on the availability of the pore to an external fluid, the pores can be divided into two categories. The first category of pores are *closed pores*, which are totally isolated from their neighbours, as in region **a** (**Figure 1**).

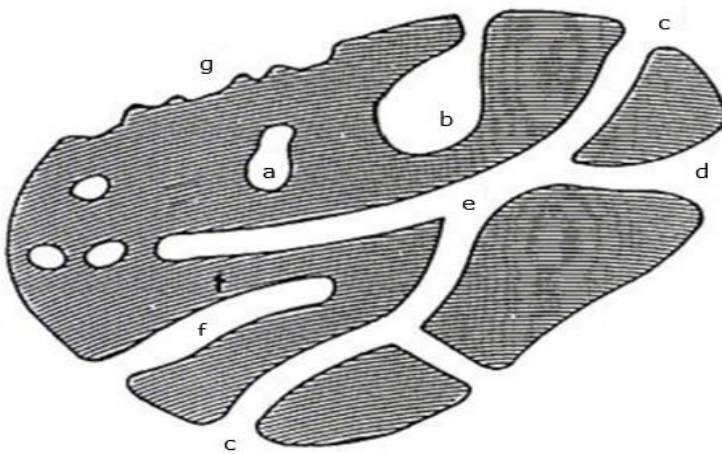


Figure 1. Pore classifications depend on their possibility to be accessed by an external fluid, shape, and pore diameter.

Pores such as **a** are not associated with adsorption or permeability of molecules, but these closed pores influence the mechanical properties of materials and are useful in lightweight structural applications and insulation.

The second category described are *open pores*, which have a continuous channel of communication with the external surface of the body, like pores **b-f**. Some of the *open pores* (like **b** and **f**) are open only at one

Introduction

end, and they are called '*blind*' or '*dead-end*' pores. Pores that are open at two ends (like **e**) are called *through* pores.

Pores are also classified according to their shape. These classifications are usually described in terms of geometric bodies, such as cylindrical, funnel, slit-shaped, and ink-bottle (**Figure 2**).

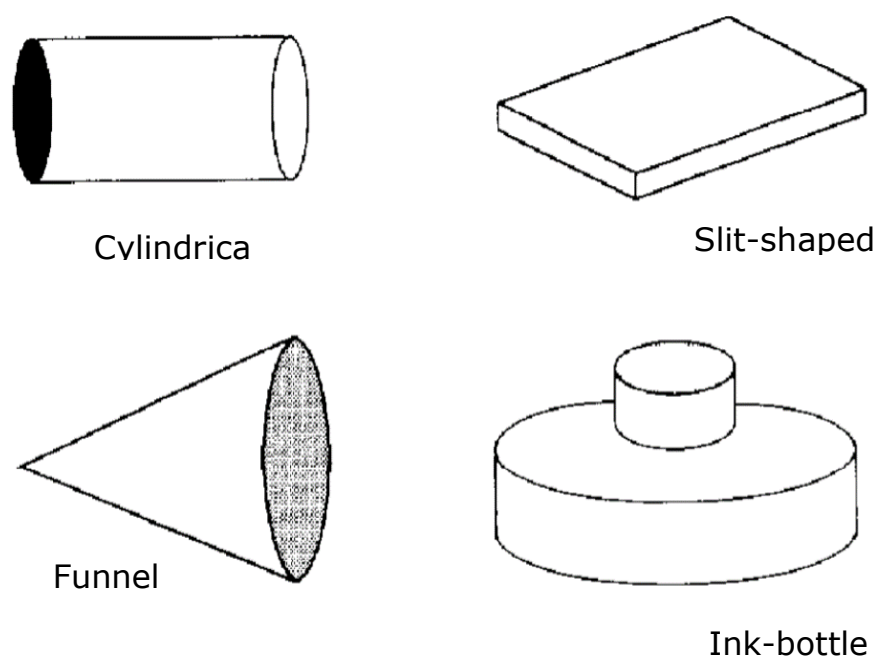


Figure 2. Pore classifications by shape.^{47,90}

Some materials characteristically show certain pore shapes: alumina often shows cylindrical pores, whereas activated carbons typically have two-dimensional slit-shaped pores with complicated network structures.^{91,92}

Pores can also be classified based on pore diameter. The IUPAC defines pore size classifications⁸⁶ according to pore width. Widths in the range of 20 Å and below are classified as micropores, and can be subdivided into supermicropores (> 7 Å) and ultramicropores (< 7 Å). In addition, those in

Introduction

the range of 20 – 500 Å are denoted mesopores, and those above 500 Å are macropores. In porous materials the size distribution, shapes and volumes of the void spaces directly relates to their ability to perform the desired function in a particular application. Over recent years the need to create uniformity within the pore size, shape, and volume has steadily increased because it can lead to superior applications properties.^{93–95}

Some materials, such as MOFs and zeolites, can show uniform porosity as the size and shape of the pore is mostly controlled by the structure of the material.^{46,70,96} Other porous materials, such as activated carbons, show hierarchical porosity as they contain a pore structure comprising pores of differing dimensions, which can be controlled by the materials used and the conditions of the synthesis.^{5,24,45,76} Porous materials are widely available with different porous properties and structures that play an important role in adsorption and also in other applications such as purification, medicine and superconductors.^{22,80} One of the most important applications, however, is in gas storage.

1.7 Energy related gas storage applications

The use of hydrocarbon fuels results in considerable environmental pollution and its consequences, such as ozone depletion, global warming, climate alteration, and human and animal health-related problems. The utilization of eco-friendly and reproducible fuels such as biomass, solar

Introduction

cells, wind power, and hydrogen has therefore attracted considerable attention.

In this regard, in order to reach the goal of a carbon neutral European Union for 2050, the use of cleaner electrical vehicles is desirable⁹⁷ to reduce CO₂ emissions, which are considered to be the main anthropogenic control knob on the climate. A promising solution to replace oil-based fuels is the use of hydrogen or natural gas fuels. The only by product of hydrogen combustion is water, and methane (natural gas) poses a lower environmental risk compared to oil, although it still produces CO₂ waste. Fuel cell technologies are a promising renewable energy source (often using hydrogen as fuel), and much research is being conducted to find efficient solutions for the storage of natural gas and hydrogen towards these applications.

This section will address the use of porous carbon in energy related applications. Firstly, carbon capture and storage (CCS) will be discussed and, secondly, a brief summary considering promising substitutes for oil-based fossil fuels will be covered, such as hydrogen and methane.

1.7.1 Carbon Capture and Storage (CCS)

Fossil fuel power stations are typically the largest source of CO₂, and thus emissions can be reduced by phasing out fossil fuel usage.²⁵ In the meantime, a necessary part of the solution to climate change is to mitigate

Introduction

CO₂ emissions, especially from flue gases emanating from fossil fuel power stations prior to their release into the atmosphere.

One of the ideas being explored for the removal of CO₂ is capture and utilization, which is achieved by adsorption of CO₂ onto solid adsorbents. Carbon capture and storage (CCS) is the process of capturing and storing carbon dioxide (CO₂) emissions from, for example, power generating industrial processes by using various technologies before it can be released into the atmosphere. Carbon capture and storage (CCS) is a more realistic climate change solution since it allows fossil fuels to be burned and industrial operations to continue without releasing CO₂ into the environment. Carbon capture does not have a "one-size-fits-all" solution; instead, a variety of technologies suited to particular industries are necessary. The technology of CO₂ capture can be broadly categorised into three different groups: oxy-fuel combustion, pre-combustion, and post-combustion processes. In the systems of oxy-fuel combustion the fuel is burned in pure oxygen to produce a flue stream rich in CO₂ (80-98 %) and free of nitrous compounds. This eliminates the need for any form of separation technique, but the expense of purifying oxygen is prohibitively expensive, both financially and environmentally.

A pre-combustion process involves gasification the fuel with steam and oxygen to produce 'syngas,' a mixture of H₂ and CO. A further steam reaction changes CO into CO₂, which is subsequently isolated from the gas mixture. Post-combustion capture involves isolating CO₂ from a flue gas stream after the fuel has been burned.⁹⁸

Introduction

A very common commercially available post-combustion technology for CO₂ capture is using the liquid amine monoethanolamine (MEA), which shows the advantage of high reactivity with CO₂. Despite this, MEA suffers from corrosion issues and has high regeneration costs, as CO₂ binds strongly to amines.

Recently, there has been a great deal of interest in the storage and transportation of hydrogen and CO₂ in energy related gas storage applications via various solid materials.

A variety of different materials are promising for the use of solid sorbents for CCS such as metal organic frameworks (MOFs),⁹⁶ porous silicas and carbon materials. Activated carbon has the advantage of being selective for CO₂, thermally and chemically stable, and cheap and simple to produce.^{41,50} Generally, the porosity of the absorbent is very important for the amount of gas (hydrogen or CO₂) adsorbed and stored on a solid material. As a consequence there have been increasing efforts to prepare tailorable porous materials with optimised porosity and gas uptake.¹⁵

Many studies report efficient CO₂ uptake. For instance, a CO₂ uptake of up to 3.1 mmol g⁻¹ at 25 °C and 1 bar was reported by Li et al. for carbons produced from a rice husk precursor using CO₂ activation at 900 °C for 1 hr.⁹⁹ Sevilla *et al.* reported very high CO₂ uptake of up to 4.8 mmol g⁻¹ at room temperature (25 °C) and 1 bar for a carbon activated at 600 °C using KOH as an activating agent.⁵²

1.7.2 Hydrogen Storage

Efforts towards energy consumption reduction and the utilization of renewable and sustainable energy sources have targeted the use of hydrogen as a fuel. Hydrogen is an attractive energy source, especially for motor vehicles, as it can be produced from renewable sources through non-toxic, non-corrosive, environmentally friendly, and high-efficiency techniques. However, the storage of hydrogen requires a very specific container due to the high pressure necessary to contain hydrogen at ambient temperature. The boiling point of hydrogen at 1 atm pressure is $-252.8\text{ }^{\circ}\text{C}$ so storage of hydrogen as a gas requires high-pressure tanks (350–700 bar) and storing hydrogen as a liquid requires cryogenic temperatures. So the challenge of storing hydrogen safely is a serious drawback for practical uses, as it needs to be stored in a more compact form.¹⁰⁰ Hydrogen is a clean energy carrier, as it does not produce any CO_2 emissions; the only by-product of hydrogen combustion is water.

Targets set by the United States Department of Energy (DOE) for hydrogen-powered cars include a gravimetric energy for the year 2020 of 1.8 kW h kg^{-1} (5.5 wt% H_2), an energy density of 1.3 kW h L^{-1} (0.040 kg L^{-1}). According to recent reports, porous carbons could be a viable material for achieving the required level of hydrogen storage.⁹⁷ Storage materials such as carbons and metal organic frameworks (MOFs) are typically highly porous materials with a high surface, and can store hydrogen via

Introduction

physisorption. It is now well established that the presence of micropores in materials of high surface area favour good hydrogen uptake.

An example of hydrogen storage using activated carbon is a study performed by the Mokaya group.⁵⁵ The study explored the valorisation of discarded smoked cigarette filters/butts. The authors successfully converted smoked cigarette waste into an activated carbon that exhibited an unprecedented hydrogen storage capacity of 8.1 wt% excess uptake, and 9.4 wt% total uptake at $-196\text{ }^{\circ}\text{C}$ and 20 bar, rising to a total uptake of 10.4 wt% and 11.2 wt% at 30 and 40 bar, respectively, due to the combined effects of high surface area, high microporosity and an oxygen-rich nature.

Whilst hydrogen production technologies and distribution are problematic, it is still an ideal replacement fuel, being renewable, sustainable, efficient, and cost-effective with a lower emission rate compared to oil-based fuels and in future, hydrogen storage, is expected to play an important role in a future energy economy.^{101,102}

1.7.3 Methane Storage

Although hydrogen is considered a promising candidate to substitute oil-based fossil fuels, it is still far from commercialization due to the remaining technological challenges. Natural gas (NG), which mainly (70%) consists of methane, CH_4 , is readily available, and when used as a fuel poses a lower environmental risk compared to conventional liquid hydrocarbon fuels. Although it still produces CO_2 , natural gas burns more cleanly than oil-

Introduction

based fuels as it has the highest H to C ratio of any fossil fuel, resulting in less CO and CO₂ released, and it may serve as a bridge to future clean renewable energy. The U.S. Department of Energy (DOE) has set a methane storage target, of 263 cm³ (STP) cm⁻³ at pressures of 35 to 100 bar, aimed at enabling widespread use.¹⁰³

Natural gas and CH₄ are most often transported and stored as compressed natural gas (CNG) or liquefied natural gas (LNG). However, the high cost of the processes involved (cryogenics and compression), the requirement for storage tanks (resistant metal alloys) and the high safety risk complicates the use of these technologies in the vehicle sector.³³

A promising solution is to store the natural gas in adsorbed form (ANG - Adsorbed Natural Gas technology) at relatively low pressure, onto a suitable adsorbent material such as porous carbon, which could reduce costs and improve safety.

For efficient methane storage, porous materials should be predominantly microporous, with a high surface area and low mesoporosity in order to achieve a high uptake at high pressure (35–100 bar).¹⁰⁴ A study of metal-organic frameworks (MOFs) suggested that materials with greater porosity (surface area and pore volume) and a high packing density would promote high methane storage.¹⁰⁵ Thus for porous carbon, in particular activated carbon, it is important to obtain materials that have a good balance between porosity and packing density.

Introduction

Among some of the best performing porous carbons for methane storage at 25 °C and 35 bar are mesophase pitch-derived activated carbons, LMA738 and D000-3:1_700, which store 142 and 160 cm³ cm⁻³ methane, respectively.^{106,107} Activated carbons have received more attention as methane storage materials, as they offer the advantages of being potentially much cheaper and more robust, and typically have good thermal and hydrolytic stability. The typical cost of activated carbons is ca. \$1 per kg, which is significantly lower than other porous materials.

1.8 Aim of this research

A major goal of this thesis is to explore and ascertain the synthesis conditions for generating highly porous carbon materials derived from starting materials with little to no value, for example waste biomass. In this thesis we employed (sawdust, SD), date seed (DS, *Phoenix dactylifera*) and CNL carbon (from accidental and uncontrolled burning of wood under fierce fire conditions of the first Carbon Neutral Laboratory, CNL, building at Nottingham) as feedstock, in order to prepare activated carbons. The principal objectives are to identify and investigate synthesis conditions for producing highly porous activated carbon for sustainable energy applications.

This thesis explored date seeds from which it is possible to generate highly microporous carbons with a high surface area density, a high volumetric surface area and a high packing density optimised for enhancing methane storage.

In addition, this thesis explored the direct activation of biomass using a mild non-hydroxide activating agent (potassium oxalate, PO) with the aim of simplifying the activation process and making it more sustainable by moving away from some of the challenges associated with the corrosive nature of KOH activation. This thesis is the first time that direct activation of biomass, i.e., without the need for HTC or pyrolysis has been attempted with a mild activating agent. Furthermore, compactivated carbons were also prepared to explore any benefits of compaction of the PO/SD mixture

Introduction

prior to thermal activation. This approach potentially offers several advantages that have, so far, not been probed in any one study as compactivation has only been explored for KOH activation, and has not been performed for direct activation of raw biomass regardless of the activating agent.

Furthermore, this thesis employed PO and KOH as activating agents to prepare activated carbons from biomass material (date seed) to allow for a comparative analysis. This is the first study that compares the use of these two activating agents for generating activated carbons from the same starting materials and under identical activation conditions.

This thesis, therefore, consists of four results and discussion chapters that explore the preparation of activated carbons from various sources and the application of the carbons for CO₂ uptake and methane storage. The first chapter explores the use of date seed as biomass source for predictable and targeted activation for methane storage. The second chapter reports the use of a milder non-hydroxide activation route for activated carbons. The third chapter addresses the direct activation and compactivation of carbon from sawdust for CO₂ uptake applications, and the final chapter explores the use of pre-mixed biomass precursors as a means to porosity modulation of activated carbons for enhanced methane storage.

References:

- 1 B. A. Kimball and S. B. Idso, *Agric. Water Manag.*, 1983, **7**, 55–72.
- 2 T. R. Anderson, E. Hawkins and P. D. Jones, *Endeavour*, 2016, **40**, 178–187.
- 3 S. A. Montzka, E. J. Dlugokencky and J. H. Butler, *Nature*, 2011, **476**, 43–50.
- 4 M. Perceptual, *Lett. to Nat.*, 1998, **392**, 881–884.
- 5 M. G. Plaza, A. S. González, C. Pevida, J. J. Pis and F. Rubiera, *Appl. Energy*, 2012, **99**, 272–279.
- 6 R. Kajaste and M. Hurme, *J. Clean. Prod.*, 2016, **112**, 4041–4052.
- 7 D. L. Hartmann, A. M. G. K. Tank, M. Rusticucci, L. Alexander, S. Brönnimann, Y. Charabi, F. Dentener, E. Dlugokencky, D. Easterling, A. Kaplan, B. Soden, P. Thorne, M. Wild and P. M. Zhai, *Clim. Chang. 2013 Phys. Sci. Basis Work. Gr. I Contrib. to Fifth Assess. Rep. Intergov. Panel Clim. Chang.*, 2013, 2SM-1-2SM – 30.
- 8 N. Adger and A. Coauthors including Fischlin, *Clim. Chang. 2007 Impacts, Adapt. vulnerability. Contrib. Work. Gr. II to Fourth Assess. Rep. Intergov. Panel Clim. Chang.*, 2007, 7–22.
- 9 G. Hansen and D. Stone, *Nat. Clim. Chang.*, 2016, **6**, 532–537.
- 10 H. Mikulčić, M. Vujanović and N. Duić, *Appl. Energy*, 2013, **101**, 41–48.
- 11 H. Mikulčić, J. J. Klemeš, M. Vujanović, K. Urbaniec and N. Duić, *J.*

Introduction

- Clean. Prod.*, 2016, **136**, 119–132.
- 12 M. Z. Jacobson and M. A. Delucchi, *Energy Policy*, 2011, **39**, 1154–1169.
- 13 B. Adeniran and R. Mokaya, *Nano Energy*, 2015, **16**, 173–185.
- 14 M. Sevilla and R. Mokaya, *Energy Environ. Sci.*, 2014, **7**, 1250–1280.
- 15 A. M. Aljumialy and R. Mokaya, *Mater. Adv.*, 2020, **1**, 3267–3280.
- 16 X. Wu, Y. Yu, Z. Qin and Z. Zhang, *Energy Procedia*, 2014, **63**, 1339–1346.
- 17 J. F. Brennecke and B. E. Gurkan, *J. Phys. Chem. Lett.*, 2010, **1**, 3459–3464.
- 18 H. Kajiro, A. Kondo, K. Kaneko and H. Kanoh, *Int. J. Mol. Sci.*, 2010, **11**, 3803–3845.
- 19 J. Yu, L. H. Xie, J. R. Li, Y. Ma, J. M. Seminario and P. B. Balbuena, *Chem. Rev.*, 2017, **117**, 9674–9754.
- 20 G. Xu, B. Ding, L. Shen, P. Nie, J. Han and X. Zhang, *J. Mater. Chem. A*, 2013, **1**, 4490–4496.
- 21 N. Balahmar, A. M. Lowbridge and R. Mokaya, *J. Mater. Chem. A*, 2016, **4**, 14254–14266.
- 22 R. E. Morris and P. S. Wheatley, *Angew. Chemie - Int. Ed.*, 2008, **47**, 4966–4981.
- 23 E. A. Hirst, A. Taylor and R. Mokaya, *J. Mater. Chem. A*, 2018, **6**,

Introduction

- 12393–12403.
- 24 C. Robertson and R. Mokaya, *Microporous Mesoporous Mater.*, 2013, **179**, 151–156.
- 25 E. Haffner-Staton, N. Balahmar and R. Mokaya, *J. Mater. Chem. A*, 2016, **4**, 13324–13335.
- 26 H. Yang, Z. Xu, M. Fan, R. Gupta, R. B. Slimane, A. E. Bland and I. Wright, *J. Environ. Sci.*, 2008, **20**, 14–27.
- 27 J. D. Evans, B. Garai, H. Reinsch, W. Li, S. Dissegna, V. Bon, I. Senkovska, R. A. Fischer, S. Kaskel, C. Janiak, N. Stock and D. Volkmer, *Coord. Chem. Rev.*, 2019, **380**, 378–418.
- 28 V. Benoit, N. Chanut, R. S. Pillai, M. Benzaqui, I. Beurroies, S. Devautour-Vinot, C. Serre, N. Steunou, G. Maurin and P. L. Llewellyn, *J. Mater. Chem. A*, 2018, **6**, 2081–2090.
- 29 Z. Zhang, Y. Zhao, Q. Gong, Z. Li and J. Li, *Chem. Commun.*, 2013, **49**, 653–661.
- 30 I. M. Hönicke, I. Senkovska, V. Bon, I. A. Baburin, N. Bönisch, S. Raschke, J. D. Evans and S. Kaskel, *Angew. Chemie - Int. Ed.*, 2018, **57**, 13780–13783.
- 31 O. K. Farha, I. Eryazici, N. C. Jeong, B. G. Hauser, C. E. Wilmer, A. A. Sarjeant, R. Q. Snurr, S. T. Nguyen, A. Ö. Yazaydin and J. T. Hupp, *J. Am. Chem. Soc.*, 2012, **134**, 15016–15021.
- 32 B. Li, H. M. Wen, W. Zhou, J. Q. Xu and B. Chen, *Chem*, 2016, **1**,

Introduction

- 557–580.
- 33 J. A. Mason, M. Veenstra and J. R. Long, *Chem. Sci.*, 2014, **5**, 32–51.
- 34 Y. He, W. Zhou, G. Qian and B. Chen, *Chem. Soc. Rev.*, 2014, **43**, 5657–5678.
- 35 T. A. Makal, J. R. Li, W. Lu and H. C. Zhou, *Chem. Soc. Rev.*, 2012, **41**, 7761–7779.
- 36 Q. Liu, L. Ning, S. Zheng, M. Tao, Y. Shi and Y. He, *Sci. Rep.*, 2013, **3**, 1–6.
- 37 A. Altwala and R. Mokaya, *Energy Environ. Sci.*, 2020, **13**, 2967–2978.
- 38 L. Nie, Y. Mu, J. Jin, J. Chen and J. Mi, *Chinese J. Chem. Eng.*, 2018, **26**, 2303–2317.
- 39 S. Cavenati, C. A. Grande and A. E. Rodrigues, *J. Chem. Eng. Data*, 2004, **49**, 1095–1101.
- 40 M. Moshoeshe, M. Silas Nadiye-Tabbiruka and V. Obuseng, *Am. J. Mater. Sci.*, 2017, **2017**, 196–221.
- 41 M. Abu Ghalia and Y. Dahman, *Energy Technol.*, 2017, **5**, 356–372.
- 42 G. Aguilar-Armenta, G. Hernandez-Ramirez, E. Flores-Loyola, A. Ugarte-Castaneda, R. Silva-Gonzalez, C. Tabares-Munoz, A. Jimenez-Lopez and E. Rodriguez-Castellon, *J. Phys. Chem. B*, 2001, **105**, 1313–1319.
- 43 N. Hedin, L. Chen and A. Laaksonen, *Nanoscale*, 2010, **2**, 1819–1841.

Introduction

- 44 Y. Li, L. Li and J. Yu, *Chem*, 2017, **3**, 928–949.
- 45 D. Nicholson, *J. Chem. Soc. - Faraday Trans.*, 1996, **92**, 1–9.
- 46 B. D. Zdravkov, J. J. Čermák, M. Šefara and J. Janků, *Cent. Eur. J. Chem.*, 2007, **5**, 385–395.
- 47 P. Russo, A. Hu and G. Compagnini, *Nano-Micro Lett.*, 2013, **5**, 260–273.
- 48 E. Fitzer, K. H. Köchling, H. P. Boehm and H. Marsh, *Pure Appl. Chem.*, 1995, **67**, 473–506.
- 49 C. F. Chang, C. Y. Chang and W. T. Tsai, *J. Colloid Interface Sci.*, 2000, **232**, 45–49.
- 50 M. D. Donohue and G. L. Aranovich, *Adv. Colloid Interface Sci.*, 1998, **76–77**, 137–152.
- 51 A. C. Forse, C. Merlet, P. K. Allan, E. K. Humphreys, J. M. Griffin, M. Aslan, M. Zeiger, V. Presser, Y. Gogotsi and C. P. Grey, *Chem. Mater.*, 2015, **27**, 6848–6857.
- 52 M. Sevilla and A. B. Fuertes, *Energy Environ. Sci.*, 2011, **4**, 1765–1771.
- 53 T. Kyotani, *Carbon Alloy. Nov. Concepts to Dev. Carbon Sci. Technol.*, 2003, **28**, 109–127.
- 54 M. Sevilla, A. B. Fuertes and R. Mokaya, *Energy Environ. Sci.*, 2011, **4**, 1400–1410.
- 55 T. S. Blankenship and R. Mokaya, *Energy Environ. Sci.*, 2017, **10**,

Introduction

- 2552–2562.
- 56 N. Balahmar, A. C. Mitchell and R. Mokaya, *Adv. Energy Mater.*, 2015, **5**, 1–9.
- 57 N. Balahmar and R. Mokaya, *J. Mater. Chem. A*, 2019, **7**, 17466–17479.
- 58 B. Adeniran and R. Mokaya, *J. Mater. Chem. A*, 2015, **3**, 5148–5161.
- 59 T. Pei, F. Sun, J. Gao, L. Wang, X. Pi, Z. Qie and G. Zhao, *RSC Adv.*, 2018, **8**, 37880–37889.
- 60 L. Wang, R. Wang, H. Zhao, L. Liu and D. Jia, *Mater. Lett.*, 2015, **149**, 85–88.
- 61 M. K. B. Gratiuto, T. Panyathanmaporn, R. A. Chumnanklang, N. Sirinuntawittaya and A. Dutta, *Bioresour. Technol.*, 2008, **99**, 4887–4895.
- 62 D. Kalderis, S. Bethanis, P. Paraskeva and E. Diamadopoulos, *Bioresour. Technol.*, 2008, **99**, 6809–6816.
- 63 A. A. H. Saeed, N. Y. Harun and N. Zulfani, *J. Ecol. Eng.*, 2020, **21**, 102–115.
- 64 K. Y. Foo and B. H. Hameed, *Adv. Colloid Interface Sci.*, 2009, **152**, 39–47.
- 65 S. Román, J. F. González, C. M. González-García and F. Zamora, *Fuel Process. Technol.*, 2008, **89**, 715–720.
- 66 J. Deng, M. Li and Y. Wang, *Green Chem.*, 2016, **18**, 4824–4854.

Introduction

- 67 A. Ghorbani, H. R. Rahimpour, Y. Ghasemi, S. Zoughi and M. R. Rahimpour, *Renew. Sustain. Energy Rev.*, 2014, **35**, 73–100.
- 68 N. Balahmar, A. S. Al-Jumialy and R. Mokaya, *J. Mater. Chem. A*, 2017, **5**, 12330–12339.
- 69 M. Sevilla and A. B. Fuertes, *Carbon N. Y.*, 2009, **47**, 2281–2289.
- 70 M. M. Titirici and M. Antonietti, *Chem. Soc. Rev.*, 2010, **39**, 103–116.
- 71 M. Paneque, J. M. De la Rosa, J. Kern, M. T. Reza and H. Knicker, *J. Anal. Appl. Pyrolysis*, 2017, **128**, 314–323.
- 72 S. Hameed, A. Sharma, V. Pareek, H. Wu and Y. Yu, *Biomass and Bioenergy*, 2019, **123**, 104–122.
- 73 C. Quan, A. Li and N. Gao, *Procedia Environ. Sci.*, 2013, **18**, 776–782.
- 74 N. Soltani, A. Bahrami, M. I. Pech-Canul and L. A. González, *Chem. Eng. J.*, 2015, **264**, 899–935.
- 75 C. R. Lohri, H. M. Rajabu, D. J. Sweeney and C. Zurbrügg, *Renew. Sustain. Energy Rev.*, 2016, **59**, 1514–1530.
- 76 J. F. González, J. M. Encinar, C. M. González-García, E. Sabio, A. Ramiro, J. L. Canito and J. Gañán, *Appl. Surf. Sci.*, 2006, **252**, 5999–6004.
- 77 Z. Hu, M. P. Srinivasan and Y. Ni, *Carbon N. Y.*, 2001, **39**, 877–886.
- 78 B. Adeniran, E. Masika and R. Mokaya, *J. Mater. Chem. A*, 2014, **2**, 14696–14710.

Introduction

- 79 M. Sevilla and R. Mokaya, *Energy Environ. Sci.*, 2014, **7**, 1250–1280.
- 80 M. Woellner, S. Hausdorf, N. Klein, P. Mueller, M. W. Smith and S. Kaskel, *Adv. Mater.*, 2018, **30**, 10.
- 81 A. D. Wiersum, J. S. Chang, C. Serre and P. L. Llewellyn, *Langmuir*, 2013, **29**, 3301–3309.
- 82 A. Martin-Calvo, J. J. Gutiérrez-Sevillano, I. Matito-Martos, T. J. H. Vlugt and S. Calero, *J. Phys. Chem. C*, 2018, **122**, 12485–12493.
- 83 Z. Ma and F. Zaera, *Surf. Sci. Rep.*, 2006, **61**, 229–281.
- 84 E. Robens and S. Jayaweera, *Adsorpt. Sci. Technol.*, 2014, **32**, 425–442.
- 85 A. Dabrowski, *Adv. Colloid Interface Sci.*, 2001, **93**, 135–224.
- 86 M. Thommes, K. Kaneko, A. V. Neimark, J. P. Olivier, F. Rodriguez-Reinoso, J. Rouquerol and K. S. W. Sing, *Pure Appl. Chem.*, 2015, **87**, 1051–1069.
- 87 C. Lu, Y. H. Huang, Y. J. Wu, J. Li and J. P. Cheng, *J. Power Sources*, 2018, **394**, 9–16.
- 88 M. M. Dubinin, *Chem. Rev.*, 1960, **60**, 235–241.
- 89 M. Thommes, K. Kaneko, A. V. Neimark, J. P. Olivier, F. Rodriguez-Reinoso, J. Rouquerol and K. S. W. Sing, *Pure Appl. Chem.*, 2015, **87**, 1051–1069.
- 90 K. Kaneko, *J. Memb. Sci.*, 1994, **96**, 59–89.

Introduction

- 91 P. González-García, *Renew. Sustain. Energy Rev.*, 2018, **82**, 1393–1414.
- 92 C. R. Correa and A. Kruse, *Materials (Basel)*., 2018, **11**, 1586.
- 93 M. E. Davis, *Nature*, 2002, **417**, 813–821.
- 94 T. Ramesh, N. Rajalakshmi and K. S. Dhathathreyan, *J. Energy Storage*, 2015, **4**, 89–95.
- 95 L. Estevez, D. Barpaga, J. Zheng, S. Sabale, R. L. Patel, J. G. Zhang, B. P. McGrail and R. K. Motkuri, *Ind. Eng. Chem. Res.*, 2018, **57**, 1262–1268.
- 96 J. R. Li, R. J. Kuppler and H. C. Zhou, *Chem. Soc. Rev.*, 2009, **38**, 1477–1504.
- 97 S. Foorginezhad, M. Mohseni-Dargah, Z. Falahati, R. Abbassi, A. Razmjou and M. Asadnia, *J. Power Sources*, 2021, **489**, 229450.
- 98 Q. Zhou, A. Manuilova, J. Koiwanit, L. Piewkhaow, M. Wilson, C. W. Chan and P. Tontiwachwuthikul, *Energy Procedia*, 2014, **63**, 7452–7458.
- 99 M. Li and R. Xiao, *Fuel Process. Technol.*, 2019, **186**, 35–39.
- 100 R. M. Baldwin, K. A. Magrini-Bair, M. R. Nimlos, P. Pepiot, B. S. Donohoe, J. E. Hensley and S. D. Phillips, *Appl. Catal. B Environ.*, 2012, **115–116**, 320–329.
- 101 M. Marinelli and M. Santarelli, *J. Energy Storage*, 2020, **32**, 101864.
- 102 Z. Yang, Y. Xia and R. Mokaya, *J. Am. Chem. Soc.*, 2007, **129**, 1673–

Introduction

- 1679.
- 103 J. H. Lee, Y. J. Heo and S. J. Park, *Int. J. Hydrogen Energy*, 2018, **3**, 22377–22384.
- 104 M. Feroldi, A. C. Neves, C. E. Borba and H. J. Alves, *J. Clean. Prod.*, 2018, **172**, 921–926.
- 105 Y. Peng, V. Krungleviciute, I. Eryazici, J. T. Hupp, O. K. Farha and T. Yildirim, *J. Am. Chem. Soc.*, 2013, **135**, 11887–11894.
- 106 M. E. Casco, M. Martínez-Escandell, E. Gadea-Ramos, K. Kaneko, J. Silvestre-Albero and F. Rodríguez-Reinoso, *Chem. Mater.*, 2015, **27**, 959–964.
- 107 N. Bimbo, A. J. Physick, A. Noguera-Díaz, A. Pugsley, L. T. Holyfield, V. P. Ting and T. J. Mays, *Chem. Eng. J.*, 2015, **272**, 38–47.

Chapter 2. Material Characterization.

2.1 Analytical Techniques

In order to design a porous material for any application, it is important to investigate the material properties. In this regard, pore structure, the nature of the materials, and the level of porosity are key features to study. There are several techniques that are used to analyse porous carbons, including porosity analysis using the Brunauer, Emmett and Teller (BET) theory, thermogravimetric analysis (TGA), powder X-ray diffraction (XRD), scanning electron microscopy (SEM), transmission electron microscopy (TEM) and elemental analysis. The main characterisation techniques used in this Thesis will be briefly discussed in this chapter.

2.1.1 Thermogravimetric Analysis (TGA)

TGA shows how the mass of a substance changes during heating as a function of temperature and time. The sample is heated under either static air conditions or in inert conditions such as flowing nitrogen or argon. For carbons, TGA is used to assess purity and thermal stability. Other characteristics of materials can be probed using TGA, for instance the percentage of inorganic and organic material in the sample, the temperature of degradation and any absorbed moisture content. The weight of the sample is calculated from the change in the mass as it is heated or cooled in a furnace.

Material Characterization.

Figure 1 shows a typical TGA curve in which the mass change is plotted against increasing temperature. T_i is the lowest temperature at which mass change is detected, and T_f is the lowest temperature when the mass change is completed.

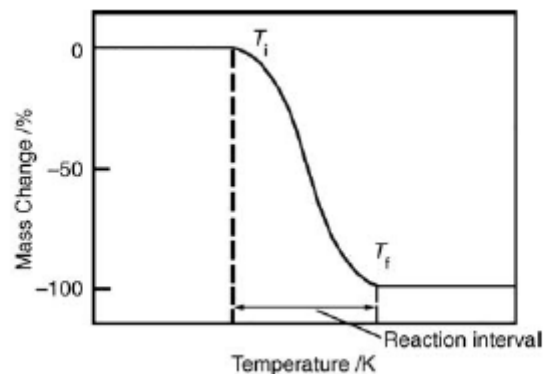


Figure 1. Thermogravimetric curves that exhibit decomposition between initial temperature T_i and final temperature T_f .1

For carbons, the expectation is that, under oxidising conditions, at a temperature of 1000 °C, the remaining carbon weight should be 0% indicating total burn off. However, if the residual weight is above 0%, it is inferred that there are other materials that burn off at temperatures higher than 1000 °C, such as inorganic oxides.

The TGA instrument typically consists of four major parts; firstly, the sample holder; secondly, the sensors to measure the temperature or detect a particular property of the sample; thirdly, an enclosure in which the parameters of the experiment are controlled (e.g. pressure and gas atmosphere); and, finally, the computer program to control the parameters

Material Characterization.

of the experiment (temperature programme) and to collect the data from the sensors.^{2,3}

In this Thesis, TGA was performed by placing a known mass (typically a few mg) of sample in an alumina pan contained within a furnace.

All thermogravimetric analysis was performed using a TA Instruments SDT Q600 analyser. TGA was performed in the temperature range of room temperature to 1000 °C in a static-air environment with a heating ramp rate of 10 °C min⁻¹.

2.1.2 Powder X-Ray Diffraction Analysis (XRD)

Powder X-ray diffraction is a technique used to determine the structure of porous materials. It is useful for obtaining the conformation of known structures and the identification and characterisation of unknown crystalline materials. XRD has been a most important technique in recent years for qualitative and quantitative analyses because the components within the materials can be identified as specific compounds.⁴ When a sample is exposed to X-rays there are two possible processes; the beam will be absorbed or scattered.^{4,5} Some of the X-rays will diffract and so contribute to diffraction beams, whereas others will be absorbed. The diffracted beams are used to produce a three-dimensional picture that allows the crystalline structure to be inferred.

Material Characterization.

The typical method for producing X-rays is to accelerate electrons with a high voltage and then allow them to collide with a metal target, often copper. A tungsten filament cathode is heated in a vacuum to generate electrons. The electrons are accelerated onto the anode (copper), which is at ground potential, since the cathode has a high negative potential. The electrons strike the anode at a high velocity, ejecting core shell electrons. X-rays are generated when energy is lost as a result of high energy outer shell electrons dropping into the vacated low energy inner electron shell. In copper anodes, the result of electron transition from 2p to 1s is the emission of CuK_{α} radiation with a characteristic wavelength of 1.5418 Å and an energy of 8.04 keV.^{6,7}

The X-ray beams incident on a crystalline solid will be diffracted by the crystallographic planes. The two in-phase incident waves are diffracted by two crystal planes so they follow Bragg's law as shown in Equation 1. Bragg's law³ is used to relate the X-ray wavelength, the diffraction angle and the lattice spacing:

$$n\lambda = 2d\sin\theta \quad \text{Equation 1}$$

where $n=1,2,3\dots$, θ is the diffraction angle, d is the interlayer spacing distance and λ is the x-ray wavelength (**Figure 2**).

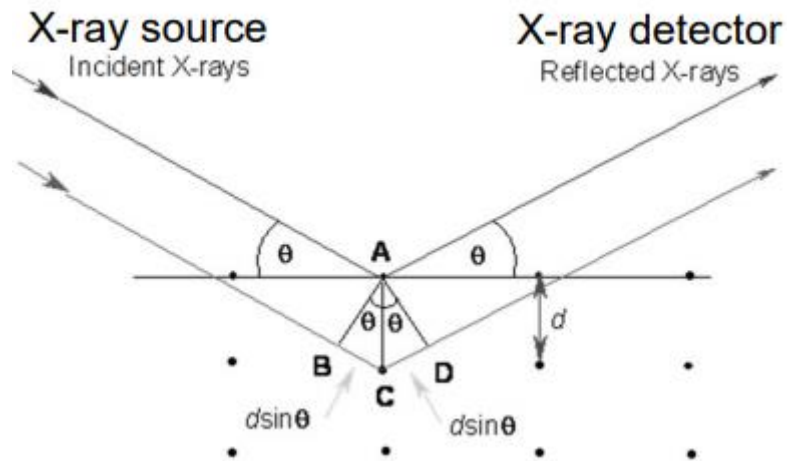


Figure 2. Bragg diffraction by crystal planes.⁷

Two X-ray beams with the same wavelength and traveling in the same direction can either reinforce or cancel each other, depending on their phase difference.¹ Constructive interference happens when they are in phase whereas destructive interference occurs when they are out of phase, as shown in **Figure 3**.

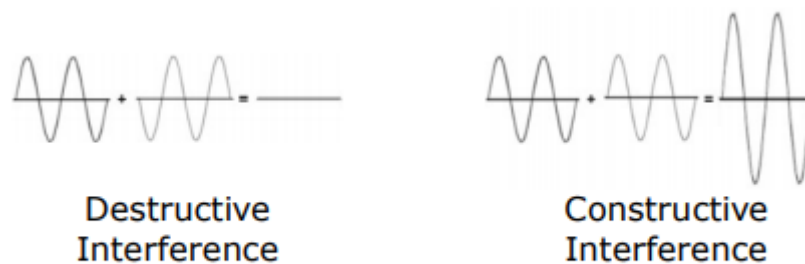


Figure 3. Constructive interference and destructive interference.⁷

In this Thesis, powder XRD was employed to assess the structural properties of the activated carbons, specifically the crystallinity. Analysis was performed using a PANalytical X'Pert PRO diffractometer with

Material Characterization.

CuK_α radiation ($\lambda = 1.5418 \text{ \AA}$) (40 kV, 40 mA), 0.02 step size and 2 s step time for values of 2θ between 2° and 80° .

2.1.3 Scanning Electron Microscopy (SEM)

Scanning electron microscopy uses an electron source to image the surfaces of a sample, by interacting it with a high energy stream of electrons to generate higher resolution images. The image produced can help determine information about the crystalline structure of the specimen, surface topography and composition.

A beam of electrons is produced by an electron gun at the top of the microscope, which is accelerated to energies in the range of 5-20 kv. The electron beam is focused through electromagnetic lenses towards the sample. This electron beam interacts with the sample producing secondary electrons, back-scattered electrons, X-rays, and heat. These signals are collected by the detectors to produce SEM images (**Figure 4**).¹

Material Characterization.

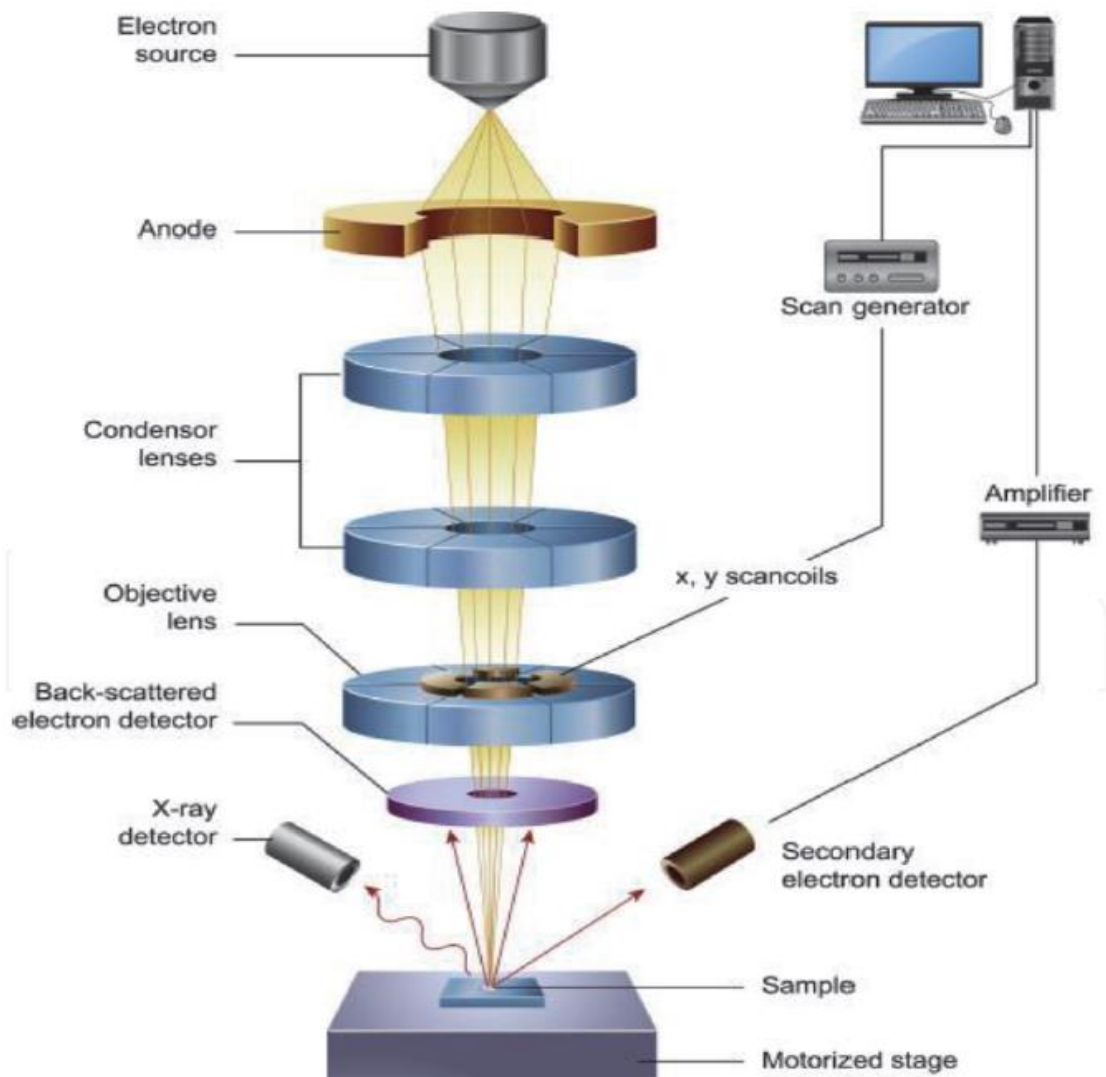


Figure 4. Schematic of a Scanning Electron Microscope setup.⁸

Some electrons will be reflected by the sample, and these backscattered electrons are detected and can give compositional information. In addition, some electrons will eject core electrons from surface atoms, which can cause outer shell electrons to drop down to fill the vacancy, emitting a photon characteristic of the element.

The resulting image depends on the nature of the samples. The heavier atoms will give relatively brighter images as they will deflect more electrons

Material Characterization.

due to their higher density nuclei. Emitted secondary electrons are detected, resulting in an image that provides surface topography and 3D structural information. It is important to treat some type of sample before analysis to remove any contaminants, and coat a conductive metal on the surface of sample, such as gold, is applied (using a sputter coater) to dissipate heat and avoid local heating effects that would blur the image.⁹In this Thesis scanning electron microscopy (SEM) images were recorded using an FEI Quanta200 microscope, operating at a 5 kV accelerating voltage. The carbon samples were loaded on a carbon conductive sticky tape prior to analysis. There was no need for a coating because the carbon is quite stable.

2.1.4 Transmission Electron Microscopy (TEM)

Transmission electron microscopy (TEM) is a technique in which a beam of electrons is transmitted through an ultra-thin specimen that is typically loaded on a lacy carbon. The interaction between the specimen (atoms) and the electron beams help to form the TEM image that displays the microstructure with atomic scale resolution. A transmission electron microscope has the following components along its optical path: a light source, a condenser lens, a specimen stage, an objective lens and a projector lens as shown in **Figure 5**.

When the incident electron beams are transmitted through the sample, depending on the density of the materials, some of the electrons will be

Material Characterization.

scattered, and the unscattered electrons will hit the fluorescent screen at the bottom of the microscope. These electrons carry information about the structure of the specimen. The samples need to be very thin, usually below 100 nm in thickness, in order to achieve high resolution images. The images produced by TEM are two-dimensional.^{1,8}In this Thesis Transmission electron microscopy (TEM) images were obtained using a JEOL 2100F instrument operating at 200 kV equipped with a Gatan Orius CCD for imaging. Prior to analysis, the carbon samples were suspended in distilled water and dispersed onto lacy carbon support films.

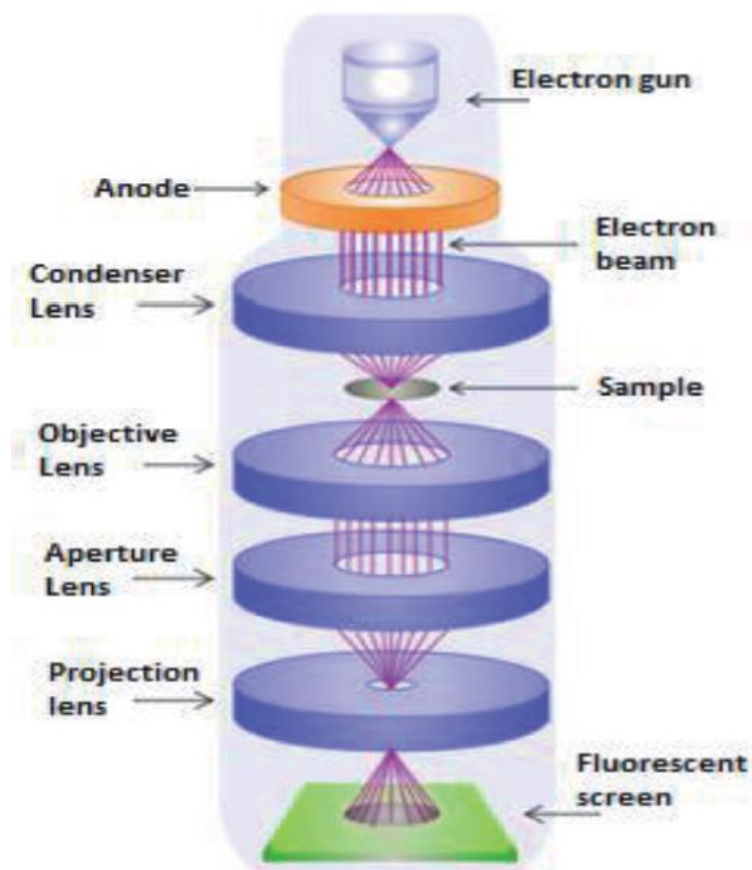


Figure 5. Schematic form of transmission electron microscopy.⁸

Material Characterization.

SEM is different to Transmission Electron Microscopy (TEM) both in terms of the intensity of the electron beams, and the characterisation provided. In SEM, the electron beam is incident on the surface of the sample, whereas in TEM the electron beam penetrates the sample, providing information about the internal structure. In addition, SEM images are three-dimensional because they provide large depth of field at resolutions up to approximately 20 Å.

2.1.5 Elemental Analysis

For carbons, a combustion analysis is used to determine the C, H and N content of the sample. A few grams of the sample is weighed and burned off in a high temperature furnace at 975 °C under a pure oxygen gas atmosphere. The C content is converted to CO₂, and all the H content converted to H₂O as a product of the combustion. The vaporized product travels through three pairs of thermal conductivity detectors, which are used to measure the carbon, hydrogen and nitrogen content. One of the pairs will absorb CO₂ allowing the amount of C to be measured. The other two pairs absorb H₂O and N₂. By weighing these materials before and after the experiment, the difference can be used to measure the carbon, hydrogen and nitrogen content in the sample. The carbon samples in this Thesis were analysed using a CE-440 Elemental Analyzer by Exeter Analytical, using sample masses of between 2–5 mg. Samples were typically submitted to Analytical Services within the School of Chemistry for analysis.

2.1.6 BET surface area and porosity measurement

When studying and designing porous materials, it is important to understand how porous structures fill with an adsorbing gas. Micropore filling, monolayer adsorption, multilayer adsorption, and capillary condensation are the four main phenomena that characterise the pore filling process.

In hierarchical pore structures, gas adsorption is efficient; micropores promote fast uptake at low pressures, while mesopores provide good channel connectivity and allow for quick gas diffusion through the pore structure. Macropores allow adsorptive molecules from the outside of the particle to quickly diffuse into the internal pore structure.

In a vacuum system, micropore filling occurs first as an adsorptive is introduced. In micropores, the interaction between the adsorbent and the adsorbate is greatest. In narrower pores, the adsorption potentials of opposite walls can overlap. As a result, the isosteric heat of adsorption in micropores is typically the largest, and micropore filling occurs at very low pressure. Mesopores begin to fill as the pressure in the system increases.

As the adsorbent surface is in contact with all adsorbed molecules, monolayer adsorption occurs first. As the pressure of the system increases, multilayer adsorption in the mesopores continues to occur. Capillary (or pore) condensation is the process through which a gas condenses into a liquid-like form in a pore at a pressure P less than the bulk liquid's

Material Characterization.

saturation pressure P_0 ; it represents a vapour-liquid phase change in a finite-volume system.¹⁰

Once multilayer adsorption has completed, as a result of increased van der Waals forces in the confined pore, capillary condensation occurs at higher relative pressure ($P/P_0 > \sim 0.2$).

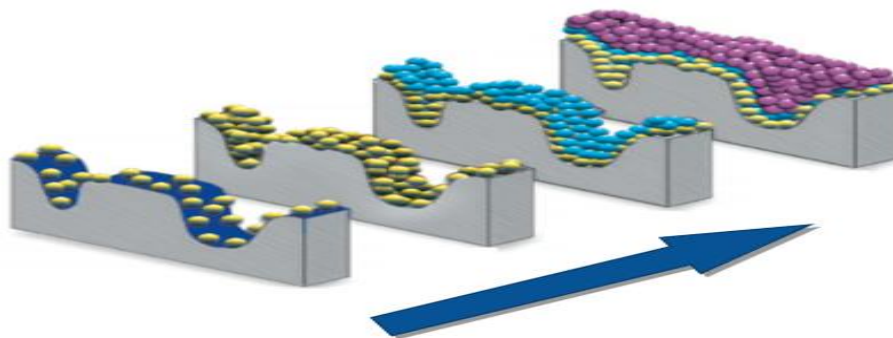


Figure 6. Representation of the pore filling process.¹¹

The relationship between the amount of gas adsorbed onto a material and the equilibrium pressure of the gas is described by a sorption isotherm, which plots adsorption and desorption measurements over varying pressures at a constant temperature. The measurement of a sorption isotherm is presented as the quantity of gas adsorbed (reported in $\text{cm}^3 \text{g}^{-1}$ or mol g^{-1}) vs pressure, and is used to analyse gas adsorption onto a material. Both the adsorption and desorption curves give details about the porous structure of a material. The data points are used to calculate information such as the surface area, pore volume and pore size distribution of the material.¹²

Material Characterization.

The BET theory is used to characterise the porosity of porous materials using the gas adsorption principle for solid surfaces to determine the specific surface area, the volume of the pores, pore size and pore size distribution. The BET method was developed by Stephen Brunauer, Paul Emmett and Edward Teller in 1938¹³ and is an extension to the Langmuir theory of adsorption, which was developed by Irvin Langmuir.¹²⁻¹⁴

There are a few assumptions required to extend Langmuir theory to BET theory (from monolayer adsorption to multilayer adsorption): the adsorption only takes place on a finite number of fixed sites, the adsorptive acts as an ideal gas with no lateral interactions or steric hindrance between adsorbed molecules, and only a monolayer exists since the adsorption layer is only one molecule thick.

According to the Langmuir assumptions, every adsorption site is full and the monolayer is assumed to be complete at the equilibrium saturation point – no further adsorption can take place beyond this point. By applying the Langmuir equation to each adsorption layer after the monolayer, the BET equation allows for multilayer adsorption. As a result, the BET equation will account for the sections of the adsorption process for the monolayer, multilayer and capillary condensation.^{12,15,16}

2.1.6.1 Classification of physisorption isotherms

The 1985 IUPAC classification of physisorption isotherms has six types, however, further research into pore structures over the past 30 years led to new characteristic types of isotherms (8 isotherm types, Figure 7).¹²

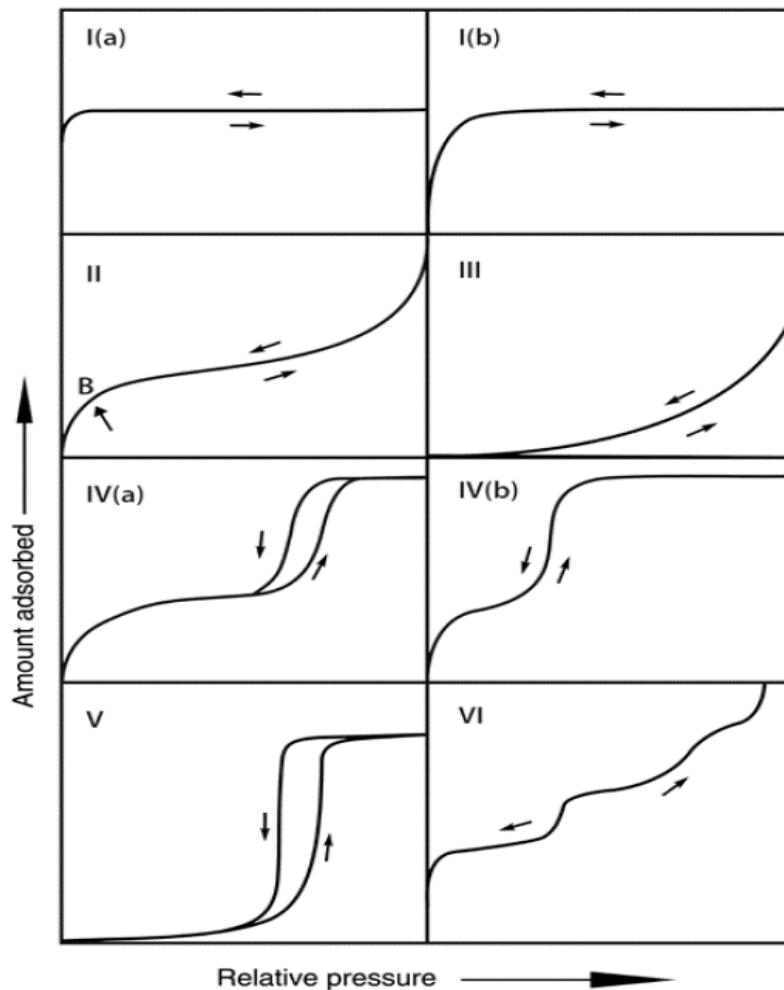


Figure 7. Classification of physisorption isotherms.¹²

Type I isotherms denote a microporous solid adsorbent with a small percentage of external surface. The isotherm's curve is concave to the relative pressure (P/P_0) axis and the amount adsorbed is limited by the accessibility of the microporous volume rather than by the internal surface area. A steep uptake at very low P/P_0 is due to enhanced favourable adsorbate-adsorbent interactions in small micropores.

Type I(a) isotherms indicate the presence of micropores (of width $<10 \text{ \AA}$); whereas Type I(b) isotherms are found with materials having a broader

Material Characterization.

pore size distribution, and the presence of larger micropores and small mesopores $< \sim 25 \text{ \AA}$.

Type II isotherms denote a macroporous or non-porous material. The first knee, 'point-B', denotes the stage where monolayer adsorption ends and multilayer adsorption begins.

Type III isotherms describe non-porous or macroporous materials. The absence of a 'point-B' knee and convex curve suggest poor adsorbate-adsorbent interactions with no discernible monolayer. Type III is not a very common isotherm.

Type IV isotherms suggest a mesoporous material. As monolayer-multilayer adsorption occurs on the mesopore walls, the initial absorption resembles that of a type II isotherm, which relates to capillary condensation. Capillary condensation in mesopores above a certain width causes hysteresis in Type IV(a) isotherms. Type IV(b) isotherms can also be found in conical and cylindrical mesopores with tapered ends.

Type V isotherms (also rare) show weak interactions between the adsorbate-adsorbent and low uptake at low relative pressure. The pore filling only occurs at higher relative pressures.

Type VI isotherms denote stepwise adsorption of layer-by-layer adsorption onto a uniform, non-porous solid. The layer capability is indicated by the step height.

2.1.6.2 Classifications of hysteresis loops

A hysteresis loop occurs when parts of the adsorption and desorption curves are not at the same relative pressure. By analysing the size, shape and position of a hysteresis loop, details about the structure of a pore network can be deduced. Hysteresis is often associated with capillary condensation.

Hysteresis loop classifications were defined by the IUPAC in 1985. The four main types were added to with the more recent finding of two new characteristic types correlated with the porous structure and adsorption.¹⁷

The type H1 loop is often associated with mesoporous structures with a narrow pore size distribution (PSD) of relatively uniform pores. The narrow loop present at high relative pressure correlates with delayed condensation on the adsorption branch.

The type H2 loop contains a more complex pore structure, in which network effects are significant. The very steep desorption branch, due to blocking in pore necks of narrow size distribution, is a characteristic feature of H2(a) loops. The H2(b) loop type is also associated with pore blocking, but is much wider than H1.

The type H3 loop resembles a Type II isotherm that does not exhibit any limiting adsorption at high P/P_0 .

The type H4 loop is a composite of Types I and II, containing both micropores and mesopores.

Material Characterization.

The type H5 loop is uncommon and related to mesoporous materials containing both open and partially blocked pores.

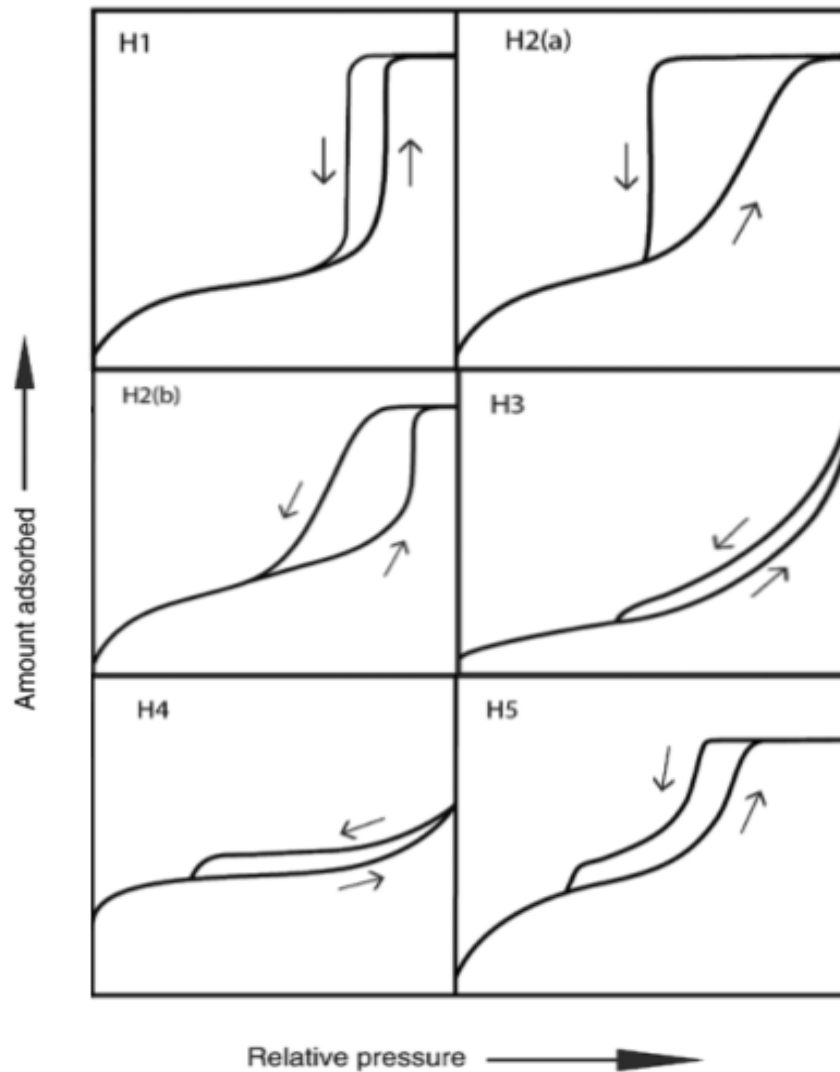


Figure 8. Classification of hysteresis loops.12

2.1.6.3 Porosity value calculations

Surface area, pore volume, pore size distribution, and microporosity are all porosity values that can be calculated using sorption isotherm data. BET

Material Characterization.

theory is widely accepted as the standard method to calculate the specific surface area of a material by using sorption isotherm.

The BET equation assumes a straight line in the specified partial pressure range, $P/P_0 \approx 0.02-0.25$, by estimating the volume of the adsorbed monolayer (V_m) from the linear section of the isotherm curve – within this range the BET specific surface area is calculated.

To estimate V_m , the BET equation in its linear form is applied to the linear section of the isotherm plot:

$$\frac{(P/P_0)}{V(1-(P/P_0))} = \frac{1}{V_m C} + \frac{(C-1)(P/P_0)}{V_m C} \quad \text{Equation 2}$$

Where V is the molar volume of the adsorbate gas at standard temperature and pressure (STP), V_m is the monolayer volume, P is the gas pressure, P_0 is the saturated pressure of adsorbed gas, and C is the intercept.

The BET surface area, S_{BET} , can be calculated using equation 3,

$$S_{\text{BET}} = \frac{V_m N_A A_x}{V} \quad \text{Equation 3}$$

where N_A is Avogadro's number, A_x is the adsorption cross-sectional area of the adsorbate, V_m is the amount of gas adsorbed in the monolayer, and V is the gram molecular volume (22414 ml).^{12,17,18}

From the isotherm data, pore volume and pore size information can be calculated. When the relative pressure is close to the saturation vapour pressure ($P/P_0 = 0.99$), the total pore volume (TPV) is determined from the

Material Characterization.

amount of gas adsorbed by converting the amount adsorbed to the corresponding volume of liquid at the adsorption temperature. This pressure point is used to ensure that the monolayer, multilayer, and capillary condensation stages have all completed.^{12,17-19}

Developed by Lippens and De Boer,²⁰ the t -plot method is commonly used to determine the microporous volume and microporous surface area in porous materials by using the adsorption isotherm. The method is based on plotting the volume of gas adsorbed against the adsorbate molecular film thickness.

$$V_{\text{micro}} = V_{\text{tot}} - V_{\text{ext}} \quad \text{Equation 4}$$

$$S_{\text{micro}} = S_{\text{tot}} - S_{\text{ext}} \quad \text{Equation 5}$$

Micropore volume can then be calculated using equation 4, where V_{micro} is the micropore contribution to the total pore volume, V_{tot} is the total pore volume, and V_{ext} is the external pore volume.

The micropore surface area can be calculated using equation 5, where S_{micro} is the micropore contribution to the total surface area, S_{tot} is the total surface area, and S_{ext} is the external surface area.

The external pore volume is the pore volume of the mesopores, macropores and external particle surface, whereas the external surface area is the surface area of the mesopores, macropores and external particle surface.^{21,22}

Material Characterization.

The pore size distribution can be determined using non-local density functional theory (NL-DFT) applied to nitrogen adsorption data.

Non-local density functional theory (NL-DFT) is a method based on statistical mechanics, and is used to determine, the pore size, and pore size distribution from gas adsorption isotherms measured across a pressure range that can extend from low relative pressure up to the saturation pressure of the fluid.²³

NL-DFT can be used to describe materials with porosity spanning three orders of magnitude, from micro- to meso- to macroporous, such as activated carbons. It can provide a single model that can extract a continuous pore size distribution to accurately quantify the complete porosity profile of the material. For example, in porous carbons, the one-dimensional infinite slit model, which assumes that pores are slits formed between infinite walls, generates a series of theoretical isotherms (kernels) that indicate the amount of gas adsorbed as a function of pore size and pressure at a specific temperature. By comparing the theoretical isotherms with experimentally measured isotherms, the pore size of the sample can be determined.

In this Thesis, nitrogen sorption (at -196 °C) was performed on a Micromeritics 3FLEX sorptometer. Prior to analysis, the carbon samples were degassed under vacuum at 200 °C for 12 h. The surface area was calculated using the Brunauer-Emmett-Teller (BET) method applied to adsorption data in the relative pressure (P/P_0) range of 0.05–0.3, and the

Material Characterization.

pore volume was estimated from the total nitrogen uptake at close to saturation pressure ($P/P_0 \approx 0.99$). The micropore surface area and micropore volume were determined via t -plot analysis. The pore size distribution was determined using non-local density functional theory (NL-DFT) applied to nitrogen adsorption data.

2.1.7 Gas Uptake Analysis

The physical adsorption of a gas on a solid material can be defined as the enrichment of gaseous molecules at the interface between the solid surface (adsorbent) and the gas phase (adsorbate) via van der Waals interactions between the adsorbent and adsorbate.

XEMIS is an advanced gas sorption analyzer, used for the characterisation of gas/vapour sorption properties of porous carbons. The gravimetric technique can be used to determine the methane, carbon dioxide and hydrogen capacity of solid materials by high accuracy gravimetric sorption analyzers.

Before adding the sample for analysis, the sample must be degassed at high temperature (up to 240 °C at a ramp rate of 5 °C/min) for several hours in order to remove any impurities. The pressure is varied during adsorption and then held constant at the set point pressure before equilibrium is achieved. The weight will change precisely as the gas is adsorbed and desorbed over varying pressure. Sorption uptake is determined from the measured weight changes and the resulting gas

Material Characterization.

sorption isotherm (as shown in **Figure 9**) can be used to calculate the molar adsorption of the gas.^{24,25}

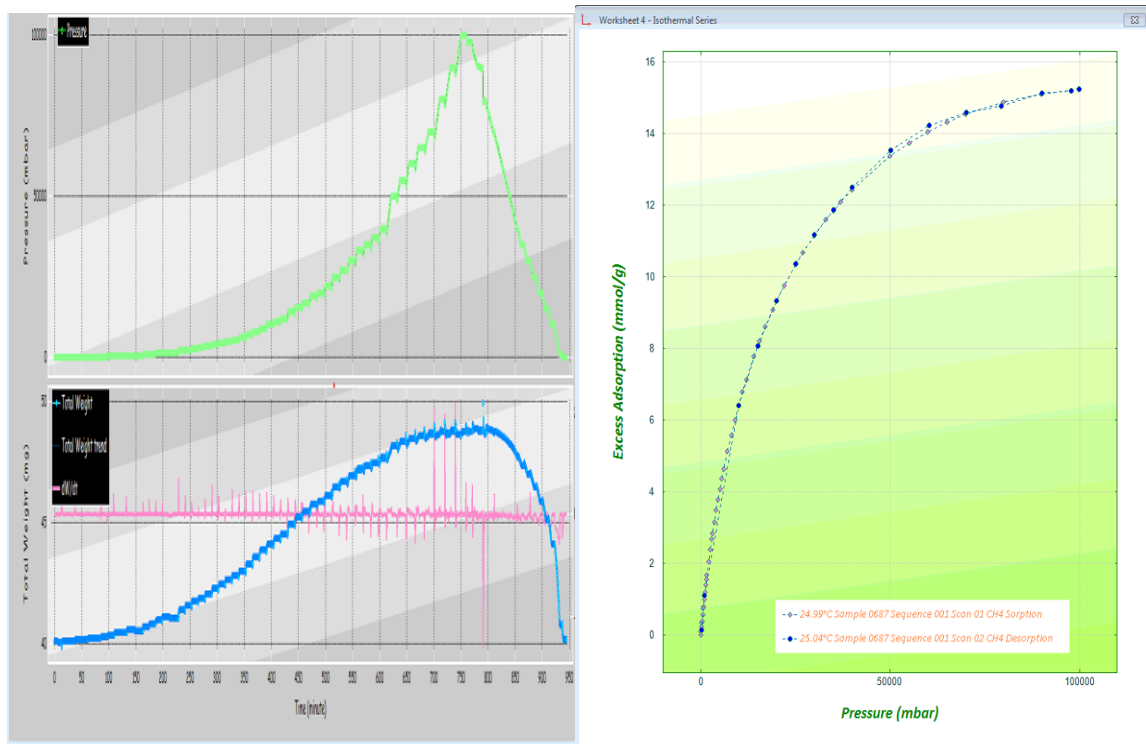


Figure 9. Gas measurement isotherm

In this Thesis methane uptake and CO₂ uptake were determined using a Hiden Isochema XEMIS Analyser. Before the uptake measurements, the carbon samples were degassed at 240 °C under vacuum for several hours. Adsorption-desorption isotherms were obtained at 25 °C over a pressure range of 0–40 bar for CO₂ uptake.

References:

- 1 Y. Leng, *Materials characterization: Introduction to microscopic and spectroscopic methods: Second edition*, 2013.
- 2 M. Wagner, *Therm. Anal. Pract.*, 2017, **1**, 162–186.
- 3 B. Adeniran, *PhD Thesis, University of Nottingham*, 2014.
- 4 M. Tulinski, *Handb. Nanomater. Hydrog. Storage*, 2017, 79–101.
- 5 G. Xu, B. Ding, P. Nie, L. Shen, H. Dou and X. Zhang, *ACS Appl. Mater. Interfaces*, 2014, **6**, 194–199.
- 6 O. Anderoglu, *PhD Thesis, Texas A&M University*, 2004.
- 7 J. G. Brown, *X-Rays Their Appl.*, 1966, 95–121.
- 8 A. S. Ali, *Application of Nanomaterials in Environmental Improvement*, 1989, vol. 32.
- 9 M. Walock, *Nanocomposite coatings based on quaternary metalnitrogen*, French., 2012.
- 10 S. Brunauer, P. H. Emmett and E. Teller, *J. Am. Chem. Soc.*, 1938, **60**, 309–319.
- 11 MicromeriticsInstrumentCorporation,
https://www.micromeritics.com/Repository/Files/Gas_Adsorption_Theory_poster.pdf, (accessed 20 April 2021).
- 12 M. Thommes, K. Kaneko, A. V. Neimark, J. P. Olivier, F. Rodriguez-Reinoso, J. Rouquerol and K. S. W. Sing, *Pure Appl. Chem.*, 2015, **87**, 1051–1069.

Material Characterization.

- 13 K. Sing, *Colloids Surfaces A Physicochem. Eng. Asp.*, 2001, **187–188**, 3–9.
- 14 B. D. Zdravkov, J. J. Čermák, M. Šefara and J. Janků, *Cent. Eur. J. Chem.*, 2007, **5**, 385–395.
- 15 G. Srinivas, V. Krungleviciute, Z. X. Guo and T. Yildirim, *Energy Environ. Sci.*, 2014, **7**, 335–342.
- 16 A. Dabrowski, *Adv. Colloid Interface Sci.*, 2001, **93**, 135–224.
- 17 M. Thommes, *Chemie-Ingenieur-Technik*, 2010, **82**, 1059–1073.
- 18 A. K. Ladavos, A. P. Katsoulidis, A. Iosifidis, K. S. Triantafyllidis, T. J. Pinnavaia and P. J. Pomonis, *Microporous Mesoporous Mater.*, 2012, **151**, 126–133.
- 19 M. Thommes, K. Kaneko, A. V. Neimark, J. P. Olivier, F. Rodriguez-Reinoso, J. Rouquerol and K. S. W. Sing, *Pure Appl. Chem.*, 2015, **87**, 1051–1069.
- 20 J. H. de Boer, B. G. Linsen, T. van der Plas and G. J. Zondervan, *J. Catal.*, 1965, **4**, 649–653.
- 21 F. Villemot, A. Galarneau and B. Coasne, *J. Phys. Chem. C*, 2014, **118**, 7423–7433.
- 22 A. Galarneau, F. Villemot, J. Rodriguez, F. Fajula and B. Coasne, *Langmuir*, 2014, **30**, 13266–13274.
- 23 micromeritics, *An Introduction To NLDFT Models for Porosity Characterization*, The Stables Hexton Manor Hexton.

Material Characterization.

- 24 C. Chilev, F. Darkrim Lamari, E. Kirilova and I. Pentchev, *Chem. Eng. Res. Des.*, 2012, **90**, 2002–2012.
- 25 I. Pentchev, B. Weinberger and F. D. Lamari, *J. Univ. Chem. Technol. Metall.*, 2007, **42**, 77–84.

Chapter 3. Predictable and targeted activation of biomass to carbons with high surface area density and enhanced methane storage capacity

Abstract

A challenge in the synthesis of activated carbons is that currently there is no way to prepare materials with predictable and targeted properties. In particular, there are no material parameters or characteristics of the starting carbonaceous matter that can be used to predict the porosity and packing density of the activated carbon. Here we report on the synthesis of biomass-derived activated carbons with targeted porosity and packing density that is suitable for methane storage. We show that the ratio of elemental oxygen to elemental carbon (i.e., O/C atomic ratio) of the precursor can be used as a universal predictor of the nature of porosity generated in an activated carbon. We use date seed (*Phoenix dactylifera*) as an example of how biomass starting material with a very low O/C ratio, and choice of mode of carbonisation, can be used to synthesise activated carbons with optimised porosity, as defined by the surface area density, and high packing density suitable for methane storage. The carbons store up to 222 cm³ (STP) cm⁻³ methane at 25 °C and 35 bar, which is much higher than any value reported to date for porous carbons, and is comparable to the best metal-organic-framework (MOF). However, the activated carbons are much cheaper (\leq 1\$/kg) compared to at best 10 – 20\$/kg for MOFs. Our findings present important insights on directed synthesis of optimised activated carbons and represent a

Predictable and targeted activation of biomass to carbons with high surface area density and enhanced methane storage capacity

significant step in the development of cheap porous carbons for high volumetric methane (or natural gas) storage. The findings are also applicable in informing preparation of activated carbons with targeted properties for other applications in energy storage and environmental remediation.

Predictable and targeted activation of biomass to carbons with high surface area density and enhanced methane storage capacity

Introduction

The continuing worldwide growth in the use of gasoline and diesel has led to increasing concerns over the sustainability of oil reserves. In addition, the mounting level of the greenhouse gas carbon dioxide (CO₂) in the atmosphere, much of it produced from burning of fossil fuels, has raised awareness of environmental impacts on global ecosystems and climate. A number of potential solutions are currently the focus of on-going research efforts that are aimed at mitigating the global effects arising from high levels of atmospheric CO₂.¹⁻³ Biogas, produced from the breakdown of organic matter, and which largely consists of methane, has become one of the more interesting renewable fuels and is widely used in an increasing number of countries.⁴ Technologies relating to biogas are also relevant to the use of natural gas. Natural gas (NG), which mainly (>70%) consists of methane, CH₄, is readily available, and when used as a fuel poses a lower environmental risk compared to oil as although it still produces CO₂, NG burns more cleanly than oil-based fuels. For these reasons, natural gas has attracted attention as an alternative fuel,⁵ and recently the U.S. Department of Energy (DOE) set a methane storage target, aimed at enabling widespread use, of 263 cm³ (STP) cm⁻³ at pressure of 35 to 100 bar. Natural gas may be stored as compressed natural gas (CNG) or liquefied natural gas (LNG). The former (CNG) requires high pressure vessels, which are heavy and pose safety concerns due to the high storage pressure (250 bar) required, while the latter (LNG) is limited by the high cost of cryogenic and compression processes. To

Predictable and targeted activation of biomass to carbons with high surface area density and enhanced methane storage capacity

circumvent the challenges of CNG and LNG, methane may be stored as adsorbed natural gas (ANG) via adsorption, at relatively low pressure, onto a suitable adsorbent material such as porous carbon.⁶⁻¹⁵

Recent research has developed new ways of preparing porous carbons with properties that are useful for good performance in energy-related applications but much of the work still relies on trial and error approaches.¹⁶⁻²⁵

Careful activation of carbonaceous matter can dramatically improve properties for specific applications but there is need for a more predictable synthesis approach. Chemical activation of carbonaceous matter, which uses activating agents such as potassium hydroxide (KOH), is widely used to generate carbons with a range of porosity characteristics^{17-19,22-28} The elemental composition and porosity of such carbons depends on the nature of the carbonaceous matter (hereinafter referred to as precursor) used and activation conditions. In this regard, biomass is a preferred choice of precursor for activated carbons due to being readily available (usually as waste matter), renewable, and essentially offering a 'carbon neutral' route to porous carbons.^{18-20,22,26,29}

The conventional methods of carbonising biomass prior to activation are hydrothermal carbonisation (HTC)³⁰⁻³² or pyrolysis.^{33,34} More recently, we have shown that for biomass-derived carbons, the mode of carbonisation prior to activation, or having no prior carbonisation, has a significant influence on the properties of both the activateable carbonaceous matter and the final activated carbons.³⁵⁻³⁸ More specifically, the mode of carbonisation can exert

Predictable and targeted activation of biomass to carbons with high surface area density and enhanced methane storage capacity

an influence on the elemental composition of biomass-derived carbonaceous matter.³⁵⁻³⁸ In this way, the atomic ratio between elemental oxygen and elemental carbon (i.e., O/C atomic ratio) can vary significantly depending on the nature of the biomass source and the mode of carbonisation.³⁶⁻³⁸ We have recently postulated that knowledge of the O/C ratio of carbonaceous matter may allow prediction of activation behaviour (i.e., susceptibility or resistance to activation) and the nature of porosity (micropore/mesopore mix) that can be achieved from any biomass.³⁸ These recent findings hint at the possibility of intentionally selecting or generating biomass-derived carbonaceous precursors that on activation will offer activated carbons with targeted properties for specific applications. Such an approach, which would offer directed or predictable carbon activation, is a complete departure from the current state-of-the-art that depends on trial and error activation with no way of determining in any directed way the properties of the final activated carbon.

As shown recently in a study on metal organic frameworks (MOFs), the key to achieving high methane storage in porous materials is not necessarily related to greater porosity (surface area and pore volume) but also to high packing density.³⁹ Thus for carbons, and in particular activated carbons, to achieve high methane storage, there is a need for synthesis routes that can predictably generate porous carbons that not only exhibit suitable porosity but also a good balance between the porosity and packing density. In this study, we have used our growing knowledge of how the carbonisation step and the O/C ratio of the activateable carbonaceous matter affect the activation process in an attempt to predictably generate activated carbons with high packing density

Predictable and targeted activation of biomass to carbons with high surface area density and enhanced methane storage capacity

and porosity that is suitable for methane storage. Through a selection process we settled on date seeds (*Phoenix dactylifera*) as a suitable starting biomass, and also used an alternative carbonisation process, termed flash air-carbonisation, which uses much shorter periods of time (5–10 minutes) and lower temperature (400 °C) in the presence of air to convert biomass into carbonaceous matter.^{35–37} Date seeds (*Phoenix dactylifera*) are inexpensive, and widely available as waste, the majority of which is disposed of *via* combustion at landfill sites. The valorisation of date seeds would therefore also reduce disposal costs, and the greenhouse gas emissions associated with their uncontrolled combustion. We show that it is possible to use a rational approach to prepare activated carbons with suitable porosity, high packing density and record levels of methane storage capacity.

Experimental Section

Material preparation

Air carbonisation

Date seeds (*Phoenix dactylifera*) was selected for use as the starting material. After thorough washing with water and drying, the date seeds (5 g) were placed in an alumina boat and heated in a horizontal tube furnace to 400 °C under an atmosphere of nitrogen with a heating ramp rate of 10 °C min⁻¹. At 400 °C, the date seed was exposed to a flow of air for 5–10 min, after which the furnace was left to cool under a flow of nitrogen gas. The resulting

Predictable and targeted activation of biomass to carbons with high surface area density and enhanced methane storage capacity

carbonaceous matter was designated as ACDS (i.e., air carbonised date seed) carbon.

Chemical activation

For activation, the ACDS carbon was mixed with the required amount of KOH at predetermined KOH/ACDS carbon ratios in an agate mortar. The KOH+ACDS carbon mixture was placed in an alumina boat and heated in a furnace to 600, 700 or 800 °C at a heating ramp rate of 3 °C min⁻¹ under an atmosphere of nitrogen gas and held at the final temperature for 1 h, after which the sample was allowed to cool under a flow of nitrogen. The resulting activated samples were then washed by stirring in 20% aqueous HCl at room temperature, and then repeatedly washed with deionised water until the filtrate was neutral (pH ~ 7). The samples were then dried in an oven at 120 °C, and designated as ACDSxT, where x is the KOH/ACDS carbon ratio, and T is the activation temperature (in °C). Thus, a carbon activated at a KOH/ACDS carbon ratio of 2 and at 800 °C is designated as ACDS2800. The packing density of the present samples was determined from pellets compacted in a 1.3 cm die for ca. 5 min at 7 MPa. Similar values were obtained from the general equation; $d_{\text{carbon}} = (1/\rho_s + V_T)^{-1}$, where ρ_s is skeletal density and V_T is total pore volume from nitrogen sorption analysis. The skeletal density was determined from helium pycnometry.

Predictable and targeted activation of biomass to carbons with high surface area density and enhanced methane storage capacity

Material Characterisation

Thermogravimetric analysis (TGA) was performed using a TA Instruments Discovery analyser or TA Instruments SDT Q600 analyser under flowing air conditions (100 mL/min). A PANalytical X'Pert PRO diffractometer was used to perform powder XRD analysis using Cu-K α light source (40 kV, 40 mA) with step size of 0.02° and 50 s time step. Elemental, CHN, analysis was performed on an Exeter Analytical CE-440 Elemental Analyser. Nitrogen sorption (at -196 °C) with a Micromeritics 3FLEX sorptometer was used for porosity analysis and to determination textural properties. Prior to analysis the carbon samples were degassed under vacuum at 200 °C for 12 h. Surface area was calculated using the Brunauer-Emmett-Teller (BET) method applied to adsorption data in the relative pressure (P/P_0) range of 0.02 – 0.22, and pore volume was estimated from the total nitrogen uptake at close to saturation pressure ($P/P_0 \approx 0.99$). The micropore surface area and micropore volume were determined via t -plot analysis. The pore size distribution was determined using Non-local density functional theory (NL-DFT) applied to nitrogen adsorption data. Scanning electron microscopy (SEM) images were recorded using an FEI Quanta200 microscope, operating at a 5 kV accelerating voltage. Transmission electron microscopy (TEM) images were obtained using a JEOL 2100F instrument operating at 200 kV equipped with a Gatan Orius CCD for imaging. Prior to analysis, the carbon samples were suspended in distilled water and dispersed onto lacey carbon support films.

Predictable and targeted activation of biomass to carbons with high surface area density and enhanced methane storage capacity

Methane uptake measurements

Methane uptake was determined using a Hiden Isochema XEMIS Analyser. Before the uptake measurements, the carbon samples were degassed at 240 °C under vacuum for several hours. Adsorption-desorption isotherms were obtained at 25 °C over methane (CH₄) pressure range of 0 – 35 bar.

Results and Discussion

Nature of carbons

The selection of date seeds (*Phoenix dactylifera*) as starting material, which involved extensive assessment of a wide range of biomass sources, was based on date seeds having relatively low elemental oxygen content compared to the elemental carbon content (**Table 1**). The elemental composition of date seed means that they have a relatively low O/C atomic ratio of 0.649 (**Table 1**) compared to a range of other biomass sources that were considered. The O/C ratio of 0.649 is the lowest we observed from a very wide range of biomass sources, which typically have O/C ratio of between 0.75 and 1.0 (**Table 1**). The next consideration was the choice of hydrothermal carbonisation (HTC), pyrolysis or flash air-carbonisation for carbonising the raw date seeds into carbonaceous matter that would then be activated. The aim was to achieve carbonaceous matter with the lowest O/C ratio. Based on a previous study, we know that both HTC and air-carbonisation reduce the O/C ratio but that the former causes greater decrease³⁵⁻³⁸ For example, when eucalyptus sawdust is subjected to HTC, the O/C ratio decreases from 0.773

Predictable and targeted activation of biomass to carbons with high surface area density and enhanced methane storage capacity

to 0.484 ($\sim 40\%$ decrease), while for air carbonisation the decrease is to 0.251 (ca. 70% decrease).³⁷ We therefore performed flash air-carbonisation on the date seeds.

We then explored the effect of flash air-carbonisation on the date seed, and also how the resulting carbonaceous matter (i.e., ACDS carbon) responded to activation. As shown in **Table 2**, the carbon content increased following the flash air-carbonisation step, from 49 wt% for the raw date seeds to 78.5 wt% for the ACDS carbon, while the H content reduced from 7 wt% to 4 wt%. This was accompanied by a large reduction in the apparent O content from 42.4 wt% (raw date seed) to 16.3 wt% for the ACDS carbon. These changes in elemental composition had the effect of reducing the atomic O/C ratio from 0.649 for the raw date seed to 0.156 for the ACDS carbon, a decrease of 76%. This decrease of 76% in O/C ratio is comparable to that ($\sim 70\%$) observed when raw sawdust is air carbonised.³⁷ However, the final O/C ratio for the ACDS carbon is lower due to the already lower O/C ratio of the date seeds. The O/C ratio of 0.156 for the ACDS carbon is the lowest we have observed for carbonaceous matter derived from biomass (**Table 3**) and other sources, and vindicates our choice of starting material (date seeds) and carbonisation process (flash air-carbonisation). More generally, we note that the elemental composition of the ACDS carbon is comparable to that of flash air-carbonised sawdust,³⁷ and CNL1 carbon obtained by burning of wood in air under fierce fire conditions.³⁵ This confirms that flash air-carbonisation of biomass, as described herein, yields carbon-rich carbonaceous matter with relatively low amounts of O and little or no N.

Predictable and targeted activation of biomass to carbons with high surface area density and enhanced methane storage capacity

The yield of activated carbon with respect to the starting biomass matter is an important consideration. The yield of carbonaceous matter (i.e., ACDS carbon) from flash air-carbonisation of raw date seeds was typically between 50 and 60%. On the other hand, the activated carbon yields (i.e., ACDS carbon to activated carbon), as shown in **Table 2** are between 50 and 65%. This yield is much higher than the yields (i.e., 4 to 20%) obtained when carbonaceous matter that is generated via conventional pyrolysis and hydrothermal carbonisation (HTC) routes is used as the starting material.^{5-11,40,41} We ascribe the higher yield to the fact that flash carbonisation, such as demonstrated here for date seeds and ACDS carbon, generates carbonaceous matter that is relatively resistant to activation with KOH due to having a low O/C ratio.³⁵⁻³⁸ However, the critical mass balance parameter is the overall biomass (date seeds) to activated carbon yield, which is between 25 and 40%. Such a yield is unprecedented with respect to the proportion of the original raw biomass that is converted to activated carbon, and is consistent with the effects of flash carbonisation. The nature of the raw date seeds (i.e., a low O/C ratio) also has a role to play in the high yield given that, when put through the same process, raw sawdust achieves lower yields.³⁷ For activation of the ACDS carbon, as expected, increasing the KOH/ACDS ratio decreases the overall yield of activated carbon from 56 – 64% at KOH/ACDS ratio 2, to 50 – 54% at ratio 4. The combined effects of the amount of KOH used and activation temperature mean that the highest yield (64%) is for sample ACDS2600, while the lowest (50%) is for ACDS4800.

Predictable and targeted activation of biomass to carbons with high surface area density and enhanced methane storage capacity

Table 1. Elemental composition and O/C atomic ratio of a range of activateable biomass precursors.

Biomass source	C [%]	H [%]	O [%]	(O/C) ^a
Eucalyptus sawdust ¹⁸	46.4	5.8	47.8	0.773
Seaweed ^b (<i>Sargassum fusiforme</i>) ³⁶	39.6	5.9	51.6	0.977
Jujun grass ⁴²	41.7	5.5	52.8	0.950
<i>Camellia Japonica</i> ⁴²	46.2	5.4	48.4	0.786
Cellulose ¹⁸	44.4	6.2	49.4	0.830
Date seed (<i>Phoenix dactylifera</i>) ^c	49.0	7.0	42.4	0.649

^aAtomic ratio. ^bSeaweed contains 2.9 wt% N. ^cDate seeds contain 1.6 wt% N (This work)

Table 2. Elemental composition of raw date seeds, air-carbonised date seed-derived carbon (ACDS) and activated carbons derived from the ACDS carbon.

Sample	Yield [wt %]	C [%]	H [%]	N [%]	O [%]
Date seeds		49.0	7.0	1.6	42.4
ACDS carbo		78.5	4.0	1.2	16.3
ACDS2600	64	67.0	2.0	0.6	30.4
ACDS2700	60	82.0	0.9	0.5	16.6
ACDS2800	56	90.0	0.1	0.2	9.7
ACDS4600	54	73.0	0.5	0.3	26.2
ACDS4700	54	83.9	0.2	0.3	15.6
ACDS4800	50	84.3	0.1	0.1	15.5

We note that hydrothermal carbonisation (HTC) of date seeds (at 250 °C) resulted in hydrochar with elemental composition (wt%) of C (68.7), H (6.0), N (1.5) and O (23.8) giving a O/C ratio of 0.25. Thus the carbon content (78.5 wt%) of the air carbonised ACDS carbon (with O/C ratio of

Predictable and targeted activation of biomass to carbons with high surface area density and enhanced methane storage capacity

0.156) is significantly higher than that of the hydrochar. It is, however, also noteworthy that the C content of the date seed hydrochar (68.7 wt%) is higher than that of sawdust hydrochar (57.4 wt%).^{36,37} On activation of the ACDS carbon, the content of elemental C varies between 67 and 90 wt% for activation at KOH/ACDS carbon ratio of 2, and between 73 and 85 wt% at ratio of 4. At both ratios, the C content increases for higher activation temperature. The H and N content reduce significantly on activation, with both reducing more at higher KOH/ACDS ratio and activation temperature, to the extent that they are close to nil after activation at 800 °C.

Predictable and targeted activation of biomass to carbons with high surface area density and enhanced methane storage capacity

Table 3. Elemental composition of flash air-carbonised activated ACDS carbon derived from date seed compared to other carbonaceous precursors, namely, flash air-carbonised sawdust (ACSD), CNL1 carbon (CNL1), raw sawdust (SDD), sawdust hydrochar (SD), lignin hydrochar (LAC), jujun grass hydrochar (ACGR), *Camelia Japonica* hydrochar (ACCA), cellulose hydrochar (C), cellulose acetate hydrochar (CA) and starch hydrochar.

Sample	C [%]	H [%]	O [%]	(O/C)
Flash air carbonised date seed (ACDS) ^a	78.5	4.0	16.3	0.156
Flash air carbonised sawdust (ACSD) ³⁷	72.4	3.2	24.2	0.251
CNL1 carbon (CNL1) ³⁵	77.7	3.1	19.2	0.185
Raw sawdust (SDD) ³⁶	46.4	5.8	47.8	0.773
Sawdust hydrochar (SD) ^{18,36,38}	57.4	5.6	37.0	0.483
Lignin hydrochar (LAC) ⁴³	66.6	5.1	28.3	0.319
Jujun grass hydrochar (AGGR) ⁴²	55.8	5.7	38.5	0.517
Camellia Japonica hydrochar (ACCA) ⁴²	49.1	5.2	45.7	0.698
Cellulose hydrochar (C) ^{18,44}	69.5	6.2	24.4	0.263
Cellulose acetate hydrochar (CA) ⁴⁴	66.2	3.9	29.9	0.339
Starch hydrochar (S) ¹⁸	68.8	6.6	24.6	0.269

^aThis work.

Thermogravimetric analysis (TGA) was performed to assess the purity and thermal stability of the carbons. The TGA curves in **Figure 1** indicate that the ACDS carbon is stable up to 300 °C, whereas the activated carbons (ACDSxT) are stable up to 400 °C. All samples show a small initial mass loss below 100 °C due to evaporation of residual moisture from the drying process. This is followed by a further single step mass-loss event due to the combustion of carbon. For all activated samples, the carbon burn off temperature is between 400 and 660 °C, with samples activated at 800 °C have greater thermal

Predictable and targeted activation of biomass to carbons with high surface area density and enhanced methane storage capacity

stability than those activated at 600 °C or 700 °C. All the carbons display residual mass typically less than 2 wt%, suggesting that they are essentially fully carbonaceous with only trace amounts of mineral matter.

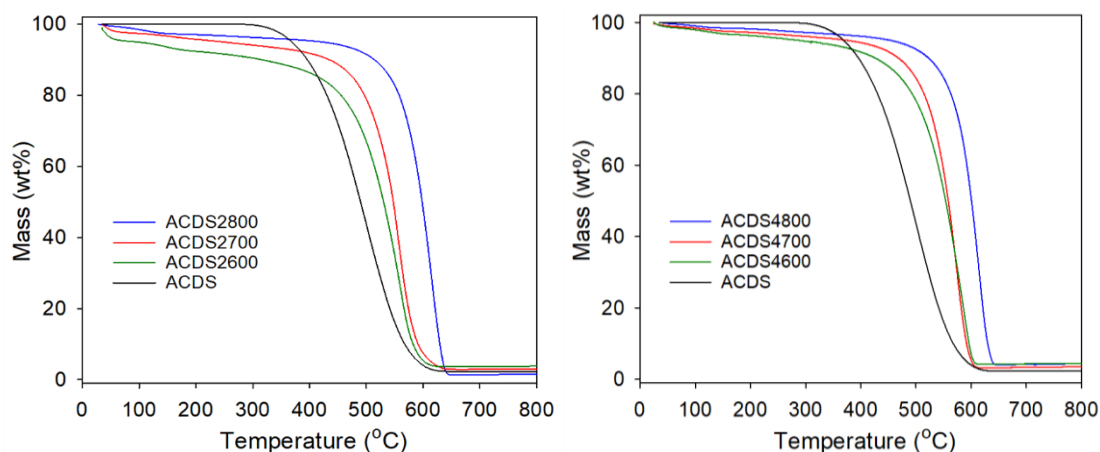


Figure 3. TGA curves of air-carbonised date seed-derived carbon (ACDS) and activated carbons derived from the ACDS carbon.

Powder X-ray diffraction was performed to confirm the nature and purity of the date seed-derived porous carbons. The XRD patterns of representative samples are shown in **Figure 2**. The broad peak at 2-theta of 22° and 44° in the XRD pattern of the ACDS carbon and some of the activated carbons correspond to the positions at which the (002) and (100) diffractions arising from graphene stacks are expected. This indicates that the ACDS carbon has some graphene-like stacking that is greatly reduced or lost for the activated carbons, which is consistent with the disruptive nature of the activation process. The activation temperature does not appear to have any significant or consistent effect of the level of graphene stacking. The overall picture that emerges from the XRD patterns is that the date seed derived carbons are

Predictable and targeted activation of biomass to carbons with high surface area density and enhanced methane storage capacity

essentially amorphous as is typical of KOH activated carbons. The morphology (**Figure 3**) of the carbons is dominated by honeycomb structure, and is similar to that previously observed in activated carbon. TEM images (**Figure 4**) reveal wormhole-type pore channels, and show no evidence of the presence of graphitic domains, which is in agreement with the XRD patterns (**Figure 2**), and previous studies on biomass derived activated carbons.^{33,35,45}

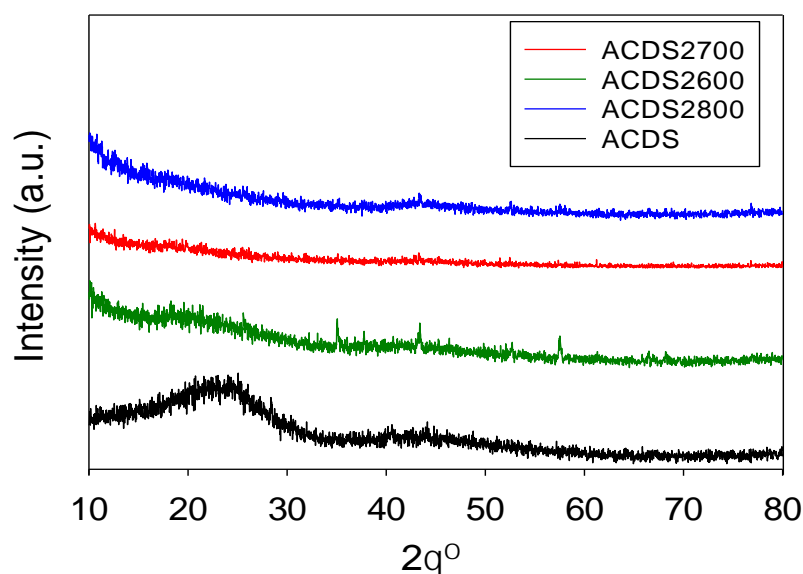


Figure 4. Powder XRD pattern of air-carbonised date seed-derived carbon (ACDS) and representative activated carbons derived from the ACDS carbon.

The date palm's fruit is well known as a staple food. It is made up of a fleshy pericarp and a seed. Date seeds also contain a high concentration of essential minerals. Potassium has the largest concentration, followed by phosphorus, magnesium, calcium, sodium, and iron in that order.⁴⁶⁻⁴⁸ Furthermore, as reported by Besbes and co-worker,⁴⁸ date seed oils have high relative percentages of oleic acid.

However, the TGA of the ACDS carbon indicates that it contains only trace amounts of inorganic matter meaning that it may be considered as being

Predictable and targeted activation of biomass to carbons with high surface area density and enhanced methane storage capacity

essentially fully carbonaceous. It is therefore unlikely that the minerals in date seed play any part in the activation process. In this regard, the date seed is no different from other types of biomass explored in the thesis.

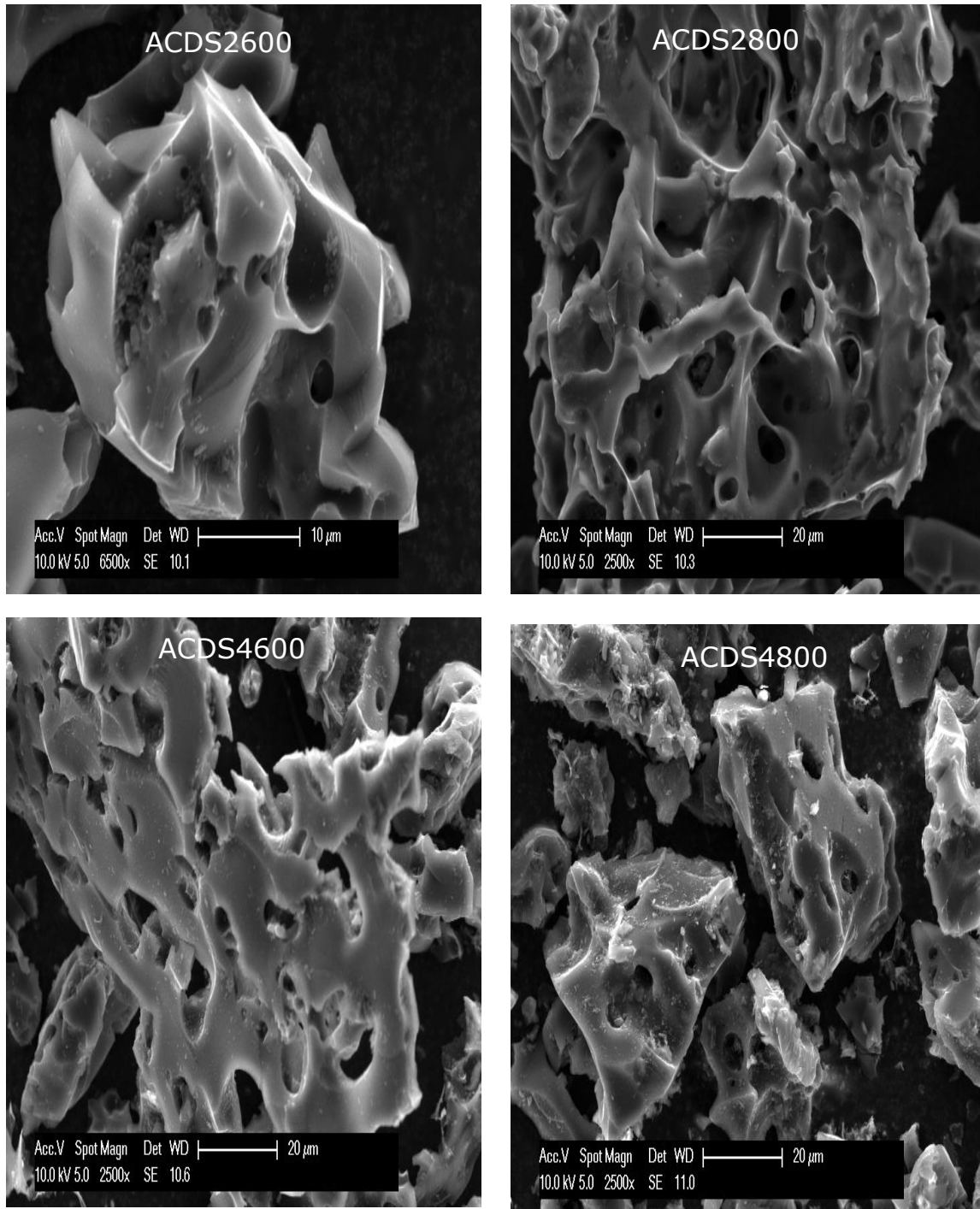


Figure 3. SEM images of air-carbonised activated date seed-derived carbons

Predictable and targeted activation of biomass to carbons with high surface area density and enhanced methane storage capacity

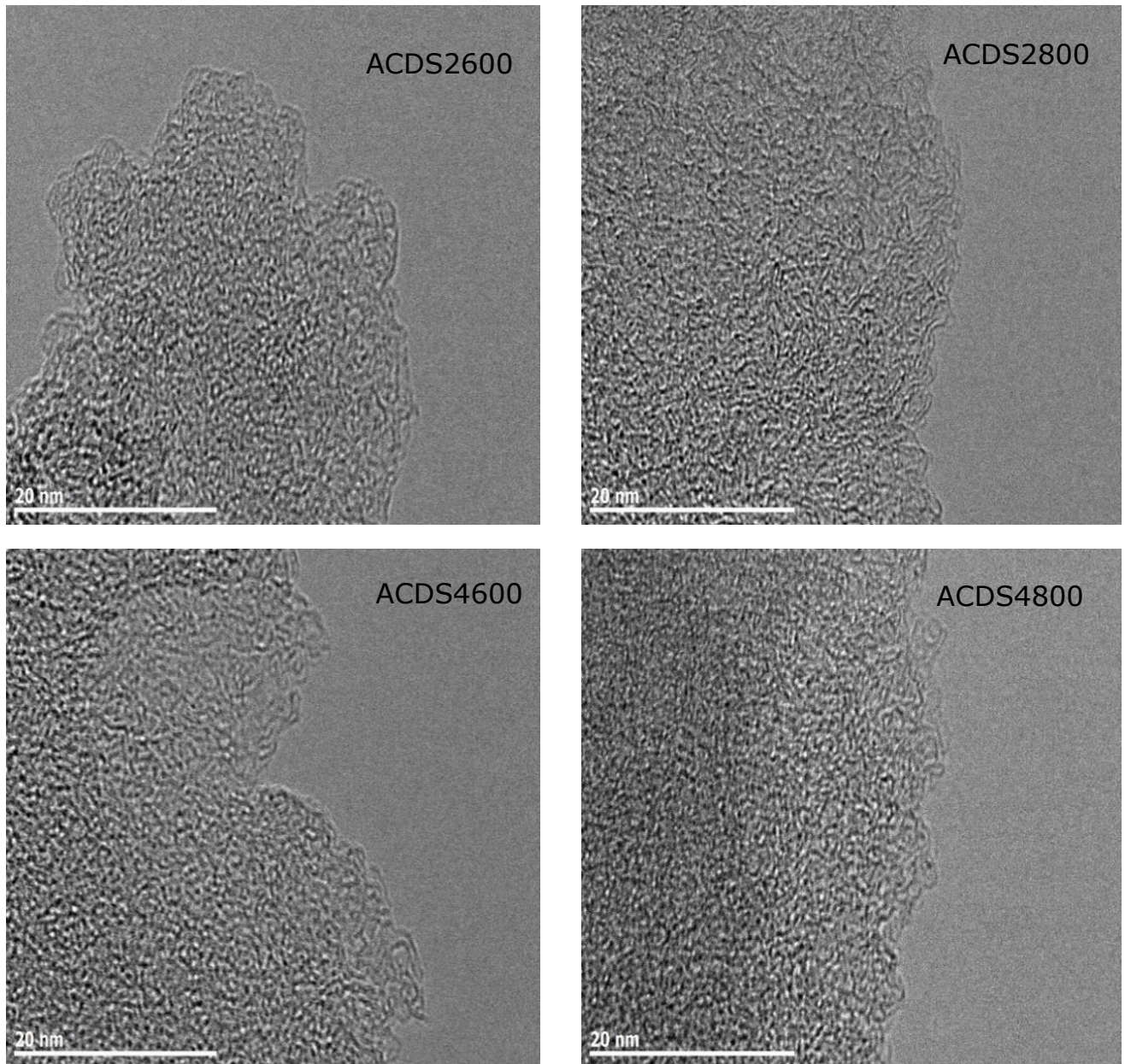


Figure 4. TEM images of air-carbonised activated date seed-derived carbons.

Porosity of carbons

The ACDS carbon was found to be virtually non-porous with a very low surface area of 2.5 m²/g and pore volume of 0.004 cm³/g. The nitrogen sorption isotherms and corresponding pore size distribution (PSD) curves of activated

Predictable and targeted activation of biomass to carbons with high surface area density and enhanced methane storage capacity

carbons prepared at KOH/ACDS ratio of 2 are displayed in **Figure 5**. All the isotherms, regardless of the activation temperature between 600 and 800 °C, are of type I, indicating that the ACDS2T carbons are microporous. The amount of nitrogen adsorbed, which is an indication of the level of porosity (i.e., surface area and pore volume) generated in the activated carbons, increases at higher activation temperature. It is interesting to note that despite the increase in amount of nitrogen adsorbed as activation temperature rises from 600 to 800 °C, there is little change in the shape of the isotherms as all three carbons exhibit isotherms with a sharp adsorption knee. Sharp adsorption knees are associated with the absence of pores of size larger than the micropore range (up to 2 nm). As shown in **Figure 5B**, the porosity of the ACDS2T carbons is dominated by 0.6 – 1.5 nm pore channels, with most pores being < 1 nm.

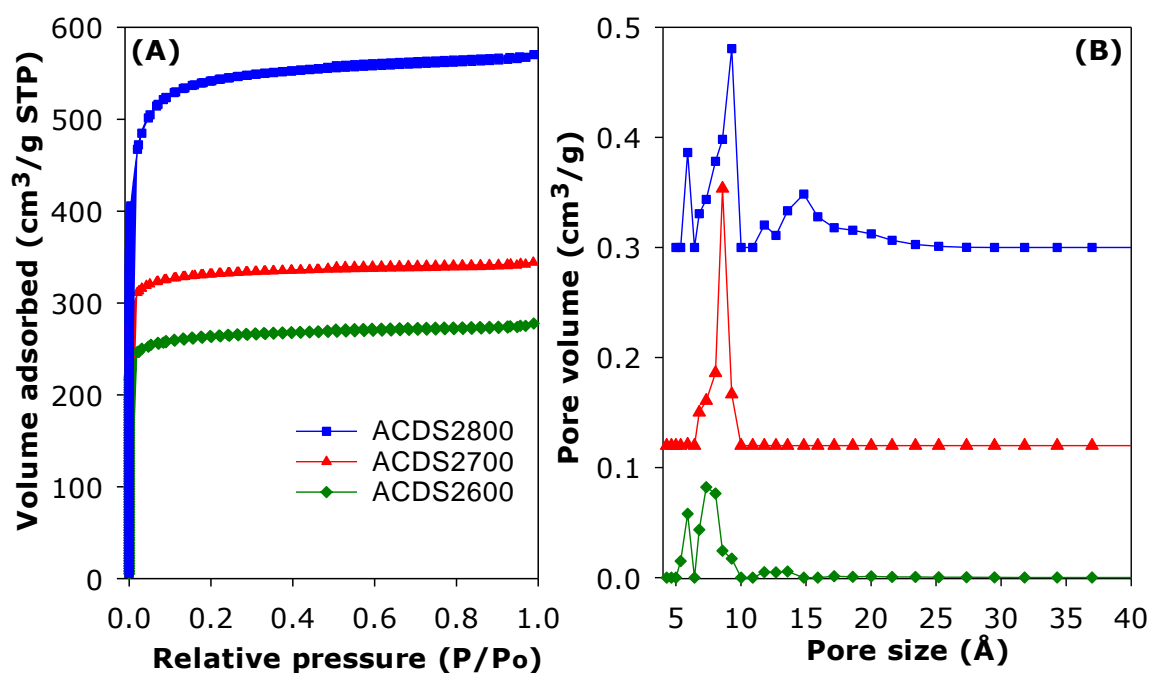


Figure 5. (A) Nitrogen sorption isotherms and (B) pore size distribution curves of activated carbons prepared from ACDS carbon at KOH/ACDS ratio of 2.

Predictable and targeted activation of biomass to carbons with high surface area density and enhanced methane storage capacity

Sample	Surface area (m ² g ⁻¹)	Micropore surface area ^a (m ² g ⁻¹)	Pore volume (cm ³ g ⁻¹)	Micropore volume ^b (cm ³ g ⁻¹)	Surface area density ^c (m ² cm ⁻³)	Packing density (g cm ⁻³)	Volumetric surface area ^d (m ² cm ⁻³)
ACDS2600	995	900 (90)	0.43	0.36 (83)	2314	1.12	1114
ACDS2700	1264	1170 (92)	0.53	0.47 (88)	2385	1.01	1277
ACDS2800	2068	1780 (86)	0.88	0.71 (80)	2350	0.82	1696
ACDS4600	1913	1736 (90)	0.80	0.62 (78)	2391	0.86	1645
ACDS4700	2192	1871 (85)	0.93	0.74 (79)	2357	0.81	1776
ACDS4800	2609	1825 (70)	1.10	0.70 (63)	2372	0.69	1774

Table 4. Textural properties of activated carbons derived from ACDS carbon.

The values in the parenthesis refer to: ^a% micropore surface area, and ^b% micropore volume. ^cSurface area density is obtained as ratio of total surface area to total pore volume. ^dVolumetric surface area determined as surface area x packing density.

Figure 6 shows the nitrogen sorption isotherms and corresponding PSD curves of activated carbons prepared at KOH/ACDS ratio of 4. The shape of isotherms for samples ACDS4600 and ACDS4700 suggest that they are predominantly microporous but with a significant proportion of supermicropores and some small mesopores. The isotherm of sample ACDS4800, while consistent with the sample being mainly microporous, exhibits a gentle adsorption knee, which is an indication of the presence of a significant proportion of supermicropores and small mesopores. Activation at KOH/ACDS ratio of 4 generates a greater proportion of larger pores compared

Predictable and targeted activation of biomass to carbons with high surface area density and enhanced methane storage capacity

to activation at ratio of 2. However, even at the most severe level of activation, (sample ACDS4800), the porosity is still dominated by micropores, which is unlike the behaviour of other biomass sources.¹⁶⁻²⁵

The PSD curves in **Figure 6B** confirm that ACDS4T samples possess a relatively wide size range of pores but still mainly within the micropore/supermicropore to small mesopore range, with most pores being of size below 1.5 nm and hardly any pores wider than 2.5 nm.

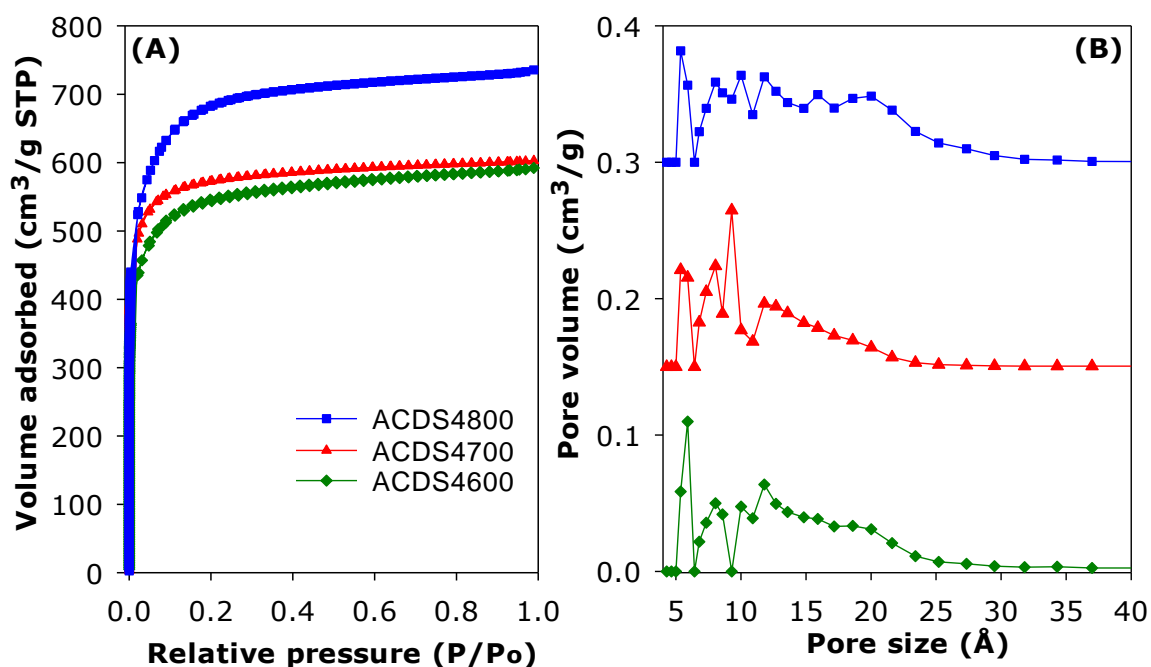


Figure 6. (A) Nitrogen sorption isotherms and (B) pore size distribution curves of activated carbons derived from ACDS carbon at KOH/ACDS carbon ratio of 4.

The textural properties of the activated carbons are given in **Table 4**. Depending on the severity of activation, the surface area (995 – 2610 m² g⁻¹) and pore volume (0.43 – 1.10 cm³ g⁻¹) are moderate to high compared to other forms of porous carbons. As expected, the lowest surface area is for the least activated sample (ACDS2600) and the highest surface is for the most severely activated carbon (ACDS4800). Nevertheless, the highest surface

Predictable and targeted activation of biomass to carbons with high surface area density and enhanced methane storage capacity

area and pore volume achieved is lower than for other types of biomass¹⁶⁻²⁵ or starting materials.^{35-38,49} We attribute this observation to the ACDS carbon being resistant to activation with KOH.^{35,37} The microporous nature of the carbons is more clearly illustrated by the extent and proportion of surface area and pore volume arising from micropores. As shown in **Table 4**, the proportion of microporosity for ACDS2T samples is typically ca. 90% of surface area and 80 – 90 % of pore volume, while for ACDS4T carbons the proportion is 70 – 90% (surface area) and 60 – 80% (pore volume).

In **Table 4**, we have also included calculated values of the surface area density defined as the ratio between total surface area and total pore volume. High surface area in porous materials is generally generated from a preponderance of small pores while, in contrast, large pore volume is associated with fewer but wider pores. Thus, any collapse of micropores (in a high surface area/low pore volume solid) into larger pores can generate a material with lower surface area/high pore volume. Given that low levels of activation tend to generate micropores (i.e., high surface area/pore volume ratio), while greater activation yields larger pores (supermicropores and mesopores, and therefore lower surface area/pore volume ratio), it follows that the surface area density is a parameter may be used as a measure of the susceptibility (or resistance) of carbonaceous matter to activation. It is interesting to note that, as shown in **Table 4**, the surface area density of the present carbons is within the narrow range of 2310 to 2390 m² cm⁻³ regardless of the severity of activation. This suggest that

Predictable and targeted activation of biomass to carbons with high surface area density and enhanced methane storage capacity

surface area density can in the present case be considered to be an inherent property of the starting carbonaceous material, and which may be used as an indicator of resistance to activation. In order to test this hypothesis in the context of a wide range of activateable carbonaceous matter, we compared the ACDS carbon with other starting materials that have been used for the preparation of activated carbons (**Table 3**), including flash air-carbonised sawdust,³⁷ air-carbonised CNL1 carbon,³⁵ raw sawdust,³⁶ hydrothermally carbonised hydrochar from biomass (sawdust,^{18,38} lignin,⁴³ jujun grass,⁴³ *Camellia Japonica*,⁴²), cellulose hydrochar,¹⁸ cellulose acetate hydrochar⁴⁴, and starch hydrochar¹⁸. The extensive comparative data (**Table 3**), firstly, indicates that ACDS carbon has the lowest O/C ratio amongst the wide range of carbonaceous matter. We then compared the surface area density of the ACDS-derived carbons with similarly activated carbons from the wide range of carbonaceous matter (**Table 5**). The data suggest that activations at 800 °C at the KOH/precursor ratio of 4, the date seed-derived ACDS4800 carbon have the highest surface area density consistent with their greater resistance to activation. The surface area density of the ACDS derived samples is comparable to that of carbons derived from air-carbonized sawdust or wood (i.e., CNL1 carbon),^{35,37} which is consistent with the three 'raw' (i.e., starting material) carbons being generated via flash air-carbonization of biomass.

It has been previously shown that a high surface area density (i.e., the tendency to generate micropores rather than larger pores) arises because air carbonization of biomass enriches the proportion of lignin products, which are

Predictable and targeted activation of biomass to carbons with high surface area density and enhanced methane storage capacity

less susceptible to activation.^{36-38,44,50-55} The comparative data (**Table 5**) clearly shows that activated carbons derived from the other sources have much lower surface area density indicating a greater susceptibility to activation with KOH. Furthermore, lower surface area density and susceptibility to activation is related to the ratio of elemental oxygen to that of elemental carbon (i.e., O/C atomic ratio) in the precursor materials (**Tables 5**). It has previously postulated that the elemental composition of activateable carbonaceous matter, and in particular the atomic ratio of oxygen to carbon (i.e., O/C atomic ratio) plays a role in the activation process with a high O/C ratio favouring ease of activation and generation of greater mesoporosity.³⁸ Indeed, the surface area density of activated carbons increases when carbonaceous matter with low O/C ratio is used as starting material (**Figure 7**). A close to linear relationship is observed between the surface area density and O/C ratio of the precursor for activation at KOH/precursor ratio of 4 and 800 °C (**Figure 7**). These findings demonstrate that selection of a starting carbonaceous precursor with a low O/C ratio can enable prediction of activation behaviour with the expectation, as confirmed herein, that the resulting activated carbons will be predominantly microporous and have high surface area density. A consequence of high surface area density is that the present activated carbons exhibit high packing density (**Table 4**), a key aim of this work. As described above, careful choice of precursor and understanding of the link between O/C ratio of a precursor and surface area density can enable synthesis of carbons with a targeted property (i.e., high packing density).

Predictable and targeted activation of biomass to carbons with high surface area density and enhanced methane storage capacity

Table 5. Textural properties and surface area density of flash air-carbonised activated ACDSxT carbons derived from date seed at activation temperature of 800 °C (T) and KOH/carbon ratio (x) of 4 compared to similarly activated carbons derived from flash air-carbonised sawdust (ACSD-xT), CNL1 carbon (CNL1-xT), raw sawdust (SDxTD), sawdust hydrochar (SDxT), lignin hydrochar (LACxT), jujun grass hydrochar (ACGRxT), *Camelia Japonica* hydrochar (ACCAxT), cellulose hydrochar (C-xT), cellulose acetate hydrochar (CA-xT), fresh cigarette filter hydrochar (FF-xT), smoked cigarette filter hydrochar (SF-xT), carbon nanotube composites (CNxT) and polypyrrole (PyxT).

Sample	Surface area ^a (m ² g ⁻¹)	Pore volume ^b (cm ³ g ⁻¹)	Surface area density (m ² cm ⁻³)	O/C ratio of precursor	Reference
ACDS4800	2609 (1825)	1.10 (0.70)	2372	0.156	This work
ACSD-4800 ³⁷	2610 (1892)	1.15 (0.74)	2270	0.251	34
CNL1-4800 ³⁵	2183 (1886)	1.05 (0.84)	2079	0.185	32
SD4800D ³⁶	2980 (478)	2.10 (0.30)	1419	0.773	33
SD4800 ^{36,38}	2783 (694)	1.80 (0.36)	1546	0.483	33,49
LAC4800 ⁴³	3235 (1978)	1.77 (0.93)	1828	0.319	39
ACGR4800 ⁴²	2957 (1578)	1.72 (0.75)	1719	0.517	40
ACCA4800 ⁴²	3537 (2557)	1.85 (1.21)	1912	0.698	40
C-4800 ^{18,44}	2125 (1707)	0.98 (0.74)	2168	0.263	21,38
CA-4800 ⁴⁴	2864 (2662)	1.32 (1.17)	2170	0.339	21
FF-4800 ²⁴	4113 (2075)	1.87 (0.79)	2199	0.380	50
SF-4800 ²⁴	2393 (1810)	1.09 (0.70)	2195	0.272	50
CN4800 ⁵⁶	3802 (33)	2.98 (0.22)	1276	0.672	51
Py4800 ⁵⁷	3450 (1910)	2.57 (1.22)	1342	0.875	17

The values in the parenthesis refer to: ^amicropore surface area and ^bmicropore volume.

Predictable and targeted activation of biomass to carbons with high surface area density and enhanced methane storage capacity

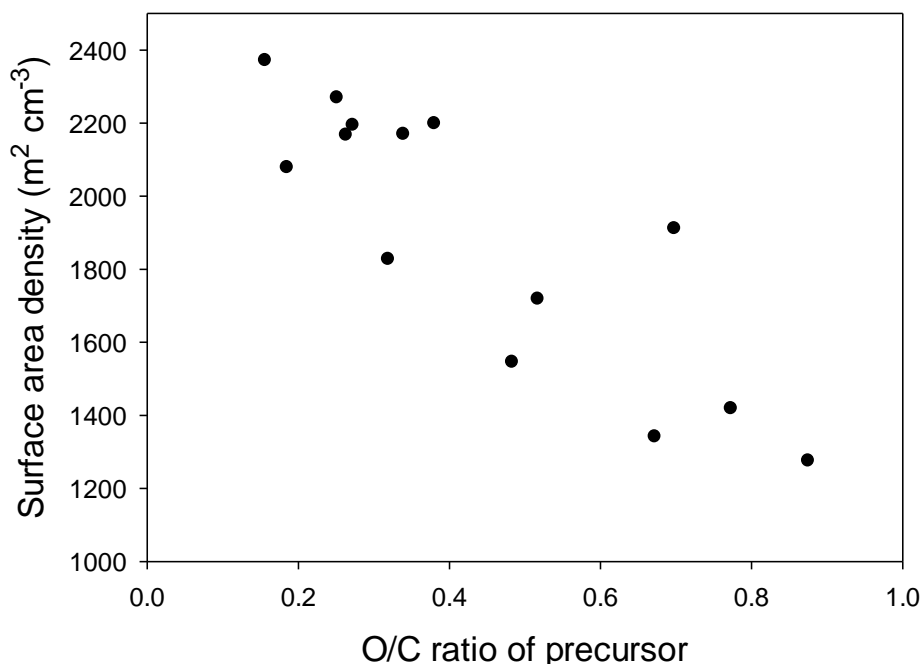


Figure 7. Surface area density of activated carbons as a function of the O/C ratio of precursor carbonaceous matter. All activations were at 800 °C at the KOH/precursor ratio of 4.

Methane Storage

For efficient methane storage at moderate to high pressure (35 – 100 bar), a porous material should be predominantly microporous with high surface area along with low mesoporosity.⁶⁻¹⁴ A high microporous volume is essential to ensure strong adsorption of methane molecules, while some mesoporosity is required for efficient sorption kinetics. Furthermore, pore channels of size 0.8 to 1.5 nm are best suited for the most favourable adsorption of 2 or 3 methane molecules in a manner that optimises the packing of the adsorbed phase within the pores.⁶⁻¹⁴ It has also been previously suggested that pore channels of size 1.1 nm are the most suited for methane storage.¹³ The present carbons, with their mix of microporosity/mesoporosity (**Table 4**), are therefore expected to be excellent candidates to achieve a high methane

Predictable and targeted activation of biomass to carbons with high surface area density and enhanced methane storage capacity

storage capacity at moderate pressures. The methane uptake capacity of the activated carbons was determined at room temperature (25 °C) and pressure of up to 35 bar. The focus was on uptake at 35 bar, a value that has been extensively used in previous studies and which therefore enables easy comparison with current state-of-the-art materials.⁶⁻¹⁴ The methane uptake measurements enabled direct determination of the excess uptake (**Figure 8**). The total gravimetric methane uptake isotherms of the ACDSxT carbons are shown in **Figure 9**. The total methane storage capacity can be calculated from the excess values by taking into account the density of the methane (under any given temperature and pressure conditions) and the total pore volume of the activated carbon (Figures 9, and 10). This was done by applying the equation; $\theta_T = \theta_{Exc} + d_{CH_4} \times V_T$, where; θ_T is total methane uptake, θ_{Exc} is excess methane uptake, d_{CH_4} is density (g cm^{-3}) of methane gas under the prevailing temperature and pressure, and V_T is total pore volume (cm^3g^{-1}) of the activated carbon. The methane density was obtained from the National Institute of Standards and Technology (NIST) website (<http://www.nist.gov/>). For all samples, the methane uptake at pressure of up to 35 bar was fully reversible with no hysteresis. The isotherms in **Figure 8** indicate that saturation was not attained in the 0 – 35 bar pressure range, meaning that the present carbons, and in particular the ACDS4T and ACDS2800 samples, can store greater amounts of methane at higher pressure. The present carbons have high to very high gravimetric methane storage capacity with the uptake being better for samples that have higher surface area and pore volume. It is also apparent that at low pressure (< 5 bar) the more

Predictable and targeted activation of biomass to carbons with high surface area density and enhanced methane storage capacity

microporous ACDS2T samples have higher methane uptake compared to their ACDS4T equivalents. However, above 6 bar, the methane uptake of ACDS4T samples gradually overtakes that of the ACDS2T group. The fact that the ACDS4T samples have high methane uptake at high pressure and relative lower uptake at low pressures is a preferred combination for achieving better performance with respect to working capacity.

Table 6. Methane uptake at 25 °C and pressure of 35 bar for of ACDS-derived activated carbons.

Sample	Excess uptake (35 bar)		Total uptake (35 bar)			Working capacity ^a cm ³ /cm ³	
	mmol/g	g/g	cm ³ /cm ³	mmol/g	g/g	cm ³ /cm ³	
ACDS2600	5.4	0.09	135	6.1	0.10	153	60
ACDS2700	6.8	0.11	154	7.5	0.12	170	71
ACDS2800	10.0	0.16	184	11.3	0.18	208	112
ACDS4600	8.0	0.13	154	9.3	0.15	180	106
ACDS4700	10.8	0.17	196	12.2	0.20	222	135
ACDS4800	11.4	0.18	176	13.0	0.21	201	126

^aWorking capacity is the difference in uptake between 35 bar and 5 bar.

Predictable and targeted activation of biomass to carbons with high surface area density and enhanced methane storage capacity

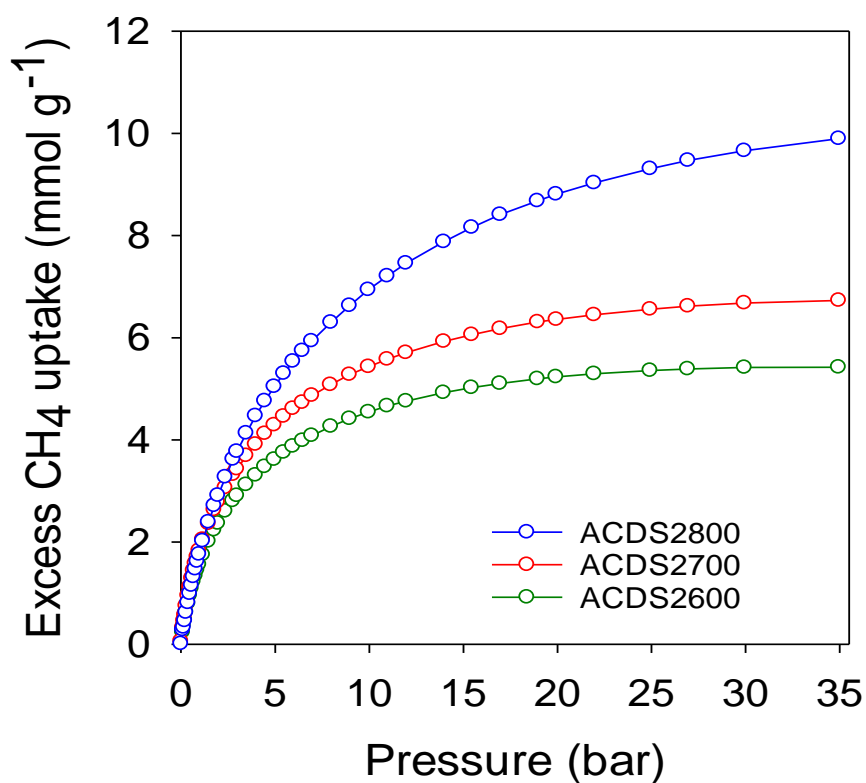
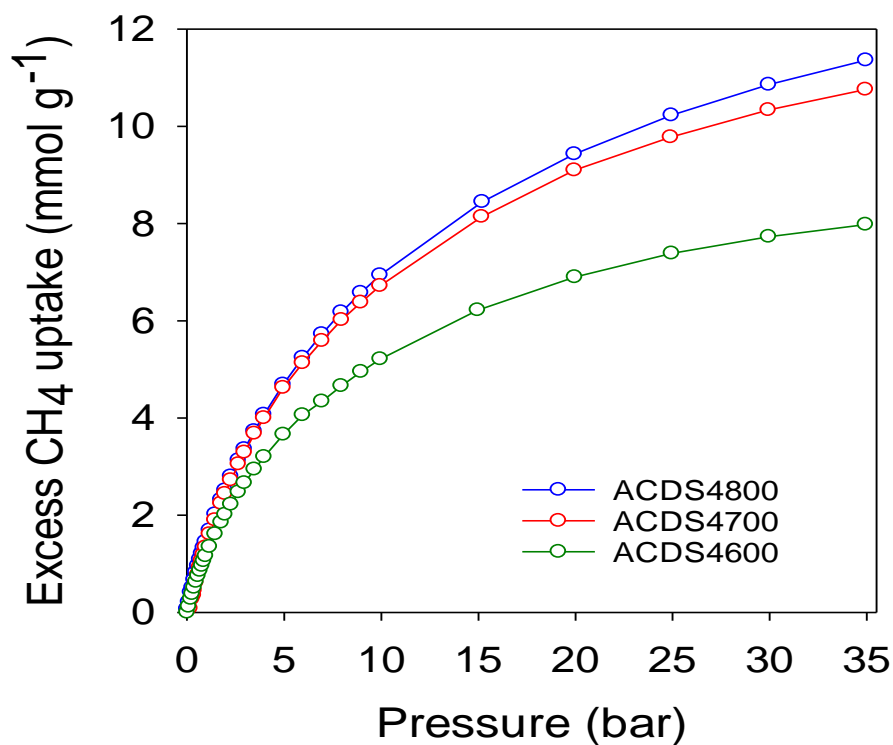


Figure 8. Excess gravimetric methane uptake at 25 °C of ACDS-derived activated carbons (ACDSxT), where x is KOH/ACDS ratio and T is activation temperature.

Predictable and targeted activation of biomass to carbons with high surface area density and enhanced methane storage capacity

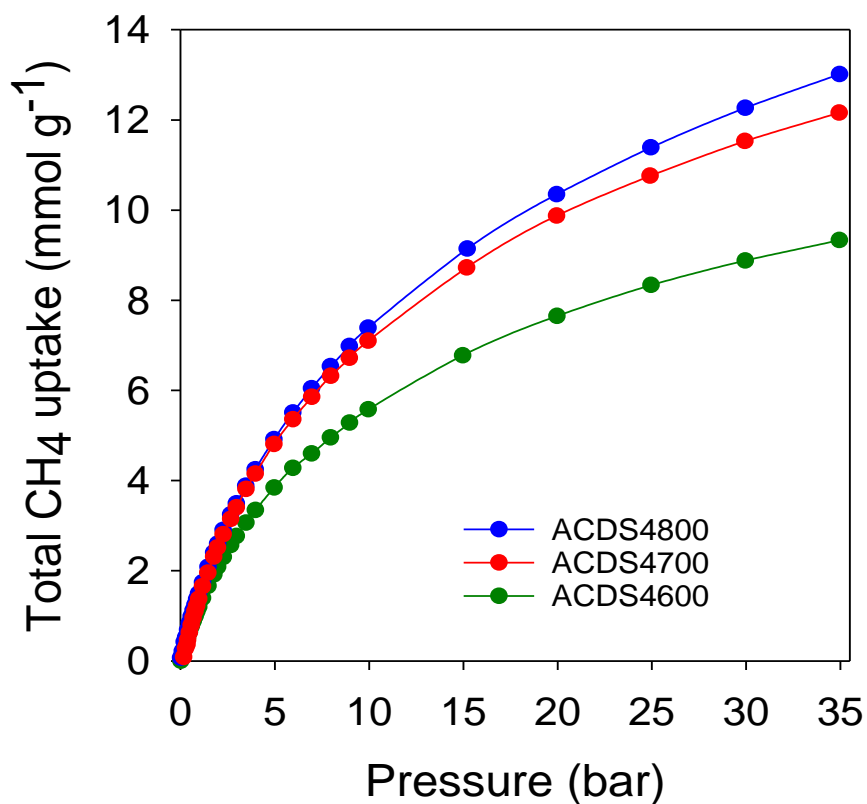
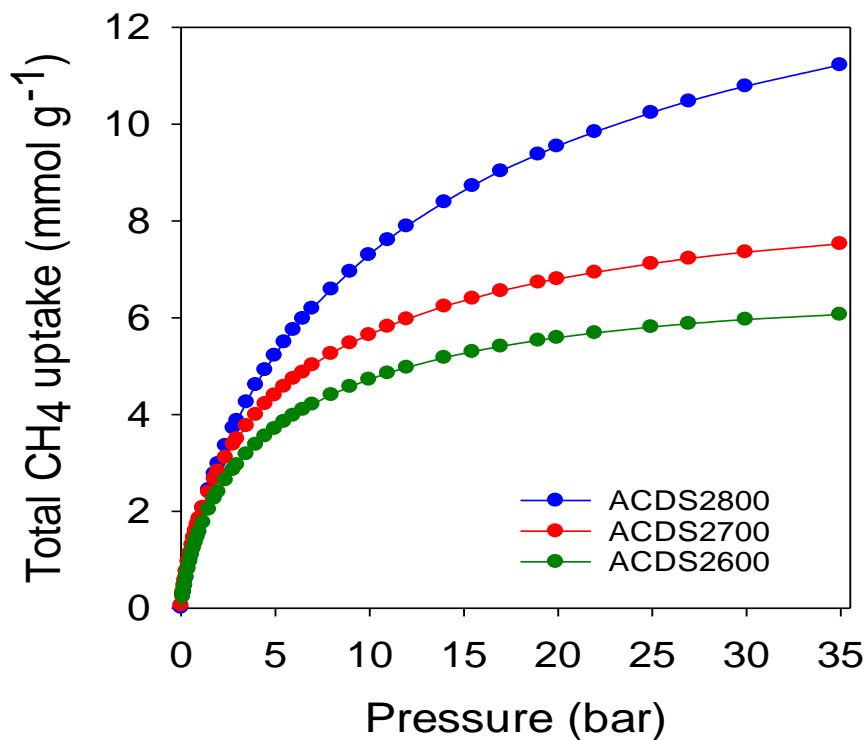


Figure 9. Total gravimetric methane uptake at 25 °C of ACDS-derived activated carbons (ACDSxT), where x is KOH/ACDS ratio and T is activation temperature.

Predictable and targeted activation of biomass to carbons with high surface area density and enhanced methane storage capacity

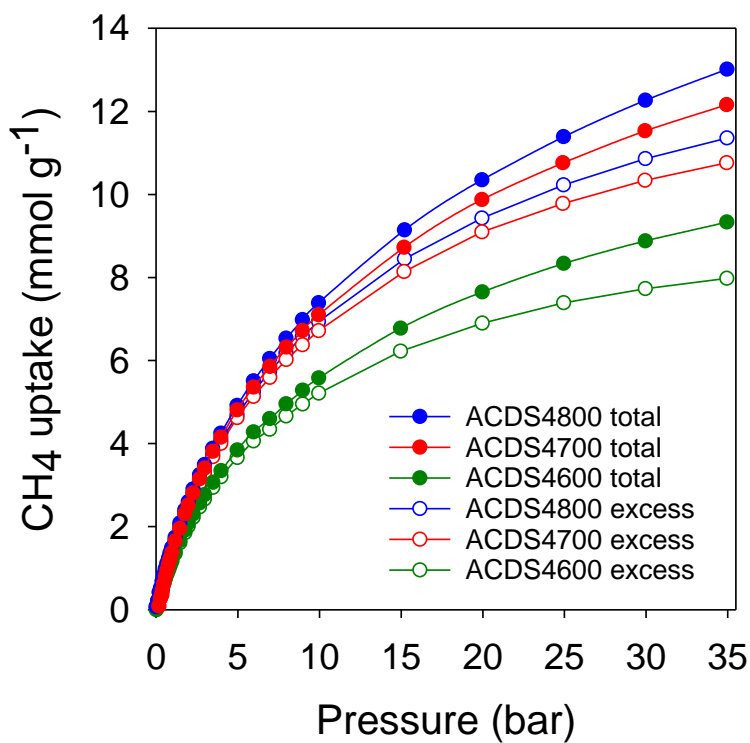
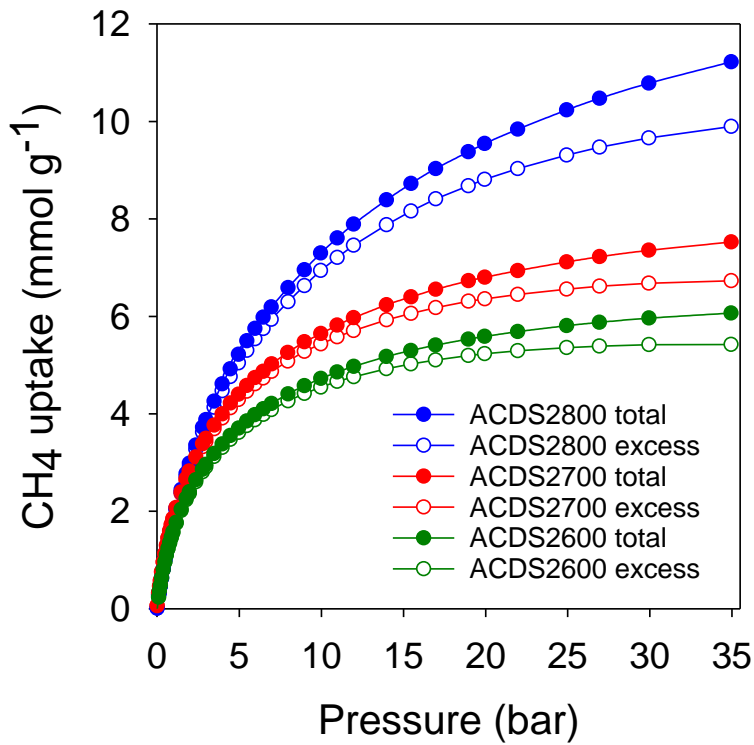


Figure 10. Total and excess gravimetric methane uptake at 25 °C of ACDS-derived activated carbons (ACDSxT), where x is KOH/ACDS ratio and T is activation temperature.

Predictable and targeted activation of biomass to carbons with high surface area density and enhanced methane storage capacity

Table 6 summarizes the amount of methane adsorbed at 35 bar, expressed as gravimetric (mmol g^{-1} and g g^{-1}) or volumetric (cm^3 (STP) cm^{-3}) uptake. The excess gravimetric methane uptake is in the range $5.4 - 11.4 \text{ mmol g}^{-1}$, (equivalent to $0.09 - 0.18 \text{ g g}^{-1}$). Sample ACDS2800, ACDS4700 and ACDS4800 have higher gravimetric methane uptake, which is consistent with their greater surface area and pore volume. On the other hand, sample ACDS2600 has both the lowest porosity and methane uptake. We note that excess methane uptake of 11.4 mmol g^{-1} (0.18 g g^{-1}), at $25 \text{ }^\circ\text{C}$ and 35 bar, is amongst the best ever reported for any porous material.⁶⁻¹² The total methane uptake is in the range $6.1 - 13.0 \text{ mmol g}^{-1}$, ($0.10 - 0.21 \text{ g g}^{-1}$). In this regard, the uptake of sample ACDS4700 and ACDS4800, which is above 12.0 mmol g^{-1} ($> 0.20 \text{ g g}^{-1}$) is very impressive and compares with the best benchmark materials reported to date.⁶⁻¹² It is clear that the targeted porosity development in the present carbons achieves impressive gravimetric methane storage capacity at $25 \text{ }^\circ\text{C}$ and 35 bar. However, the more important measure of a solids performance in methane storage is the volumetric uptake, which takes into account the packing density of the adsorbent. The key targets for methane storage in porous materials are set with respect to volumetric uptake capacity expressed as cm^3 (STP) cm^{-3} (i.e., cm^3 of methane per unit tank volume occupied by the adsorbent). An often-quoted target is that set by the US Department of Energy (DOE) of 263 cm^3 (STP) cm^{-3} at ambient temperature ($25 \text{ }^\circ\text{C}$) and moderate pressure (35 – 100 bar). **Figure 11** shows the excess and total volumetric uptake of the ACDSxT carbons. In general, the ACDS4T samples perform better than their equivalents in the ACDS2T

Predictable and targeted activation of biomass to carbons with high surface area density and enhanced methane storage capacity

group. All the carbons, except sample ACDS2600, do not reach saturation at 35 bar, with the ACDS4T samples appearing to be much further away from saturation and therefore capable of achieving much greater volumetric uptake at higher pressure (36 – 100 bar). The highest gravimetric uptake was observed for sample ACDS4800, which also has the highest surface area and pore volume, but the best volumetric uptake is for sample ACDS4700. The better volumetric uptake performance of sample ACDS4700 is ascribed to a more optimized combination of porosity and packing density (**Table 4**).

Table 7. Methane uptake at 25 °C and pressure of 35 bar for ACDS-derived activated carbons compared to the best performing porous carbons

Sample	Excess uptake (35 bar) cm ³ /cm ³	Total uptake (35 bar) ^a cm ³ /cm ³	Reference
ACDS2800	184	208 (205)	This work
ACDS4700	196	222 (217)	This work
ACDS4800	176	201 (199)	This work
DO00-3:1_700 ⁵⁸	160	184	55
LMA738 ⁵⁹	142	165	56
BEA-ZTC ⁶⁰	125	148	57
BEA-ZTC-873 ⁶⁰	142	165	57
AX-21 ⁸		154	7

^aValues in the parentheses are calculated using the equation; $V_{st} = V_{exc} + d_{CH_4} (1 - \rho_{pd}/\rho_{He})$, where V_{st} (g/cm³) is total storage inside a unit tank volume filled with an adsorbent, V_{exc} (g/cm³) is the excess volumetric uptake per unit volume of an adsorbent, d_{CH_4} is the methane gas density (g/cm³) at 25°C and 35 bar, ρ_{pd} is the packing density of the carbon, and ρ_{He} is the skeletal (or helium) density of the carbons, which was determined using helium pycnometry to be 2.1 g/cm³.

Predictable and targeted activation of biomass to carbons with high surface area density and enhanced methane storage capacity

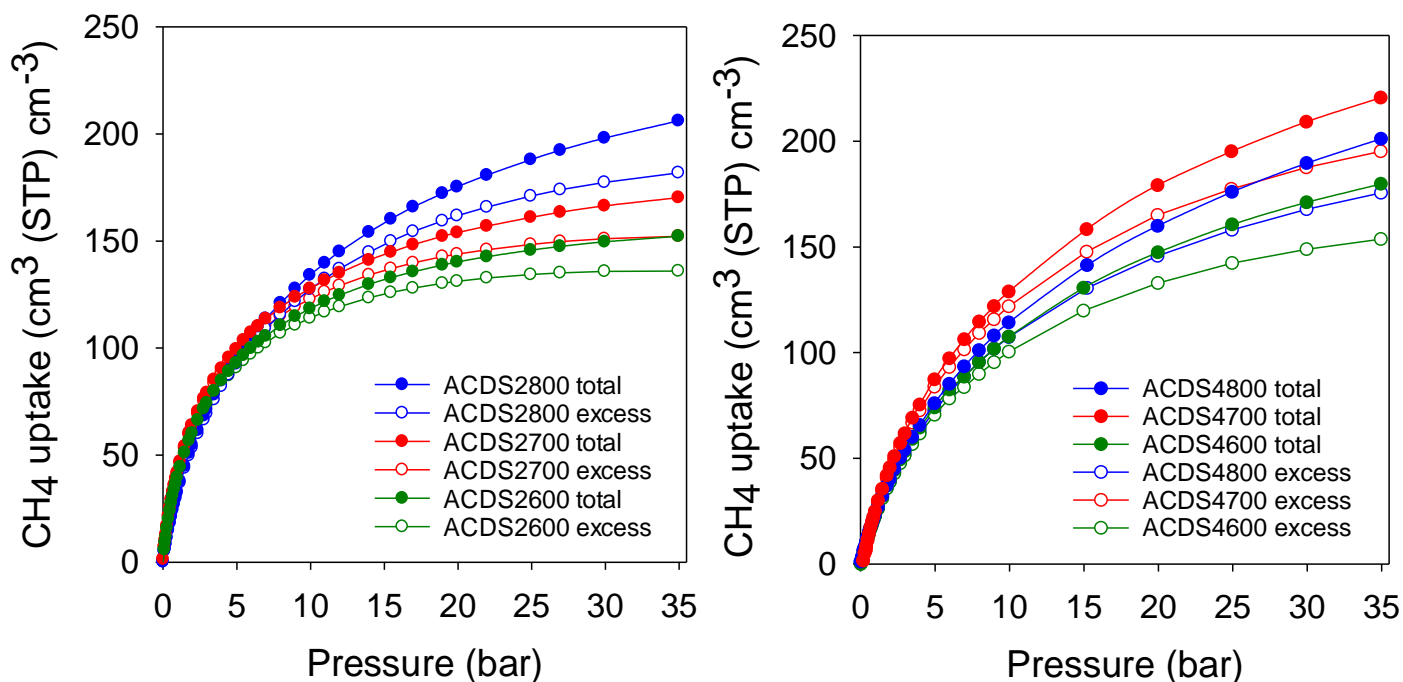


Figure 11. Excess and total volumetric methane uptake at 25 °C for ACDS-derived activated carbons (ACDSxT), where x is KOH/ACDS ratio and T is activation temperature.

The carbons have excess volumetric methane uptake (at 25 °C and 35 bar) of 135 to 184 $\text{cm}^3 \text{cm}^{-3}$ for ACDS2T samples, and 154 to 196 $\text{cm}^3 \text{cm}^{-3}$ for the ACDS4T group. This excess volumetric uptake is much higher than for the best of previously reported porous carbons (**Table 7**).^{7,58-61} To date, the best performing porous carbons for volumetric methane storage at 25 °C and 35 bar are mesophase pitch derived activated carbons, LMA738 and DO00-3:1_700 that store 142 and 160 $\text{cm}^3 \text{cm}^{-3}$ methane, respectively,^{58,59} and zeolite templated carbons, ZTC, (BEA-ZTC)⁶⁰ and thermally treated BEA-ZTC (BEA-ZTC-873)⁶⁰ that store 125 and 145 $\text{cm}^3 \text{cm}^{-3}$ methane, respectively (**Table 7**). In comparison, the best performing ACDS4700 sample achieves much higher excess methane uptake of 196 $\text{cm}^3 \text{cm}^{-3}$ (**Table 6 and 7**). The total methane uptake of the present carbons is between 153 and 208 $\text{cm}^3 \text{cm}^{-3}$ for ACDS2T samples, and 180 to 222 $\text{cm}^3 \text{cm}^{-3}$ for the ACDS4T group. Such

Predictable and targeted activation of biomass to carbons with high surface area density and enhanced methane storage capacity

total storage capacity, of up to $222 \text{ cm}^3 \text{ cm}^{-3}$, is significantly better than for all previously reported porous carbons (**Table 7**).⁵⁸⁻⁶⁰ We note that the current benchmark carbon materials are the aforementioned mesophase pitch derived activated carbons, LMA738 and DO00-3:1_700 with storage of 185 and $184 \text{ cm}^3 \text{ cm}^{-3}$, respectively,^{58,59} and the ZTCs with $148 \text{ cm}^3 \text{ cm}^{-3}$ for BEA-ZTC and $165 \text{ cm}^3 \text{ cm}^{-3}$ for BEA-ZTC-873.⁶⁰ A commercially available high surface area carbon, AX21, has uptake of $148 \text{ cm}^3 \text{ cm}^{-3}$. A comparison between the best performing ACDS-derived samples (ACDS2800, ACDS4700 and ACDS4800) and benchmark carbons^{58-60,62} (**Table 7**) indicates that it is important to optimise, as we have herein attempted, several factors, namely, total porosity (surface area and pore volume), level of microporosity, pore size distribution and packing density.

For a proper and broader context of the methane storage performance of the present ACDSxT carbons, we compared them to benchmark MOF materials. MOFs have been touted as the most promising methane storage materials, and a great deal of work is reported in the open literature.⁶⁻⁹ It is, however, important to note that most reported volumetric methane uptake values of MOFs is computed using crystallographic density (rather than packing density).⁶⁻⁹ The use of crystallographic density results in overestimated values and unrealistic scenarios requiring that MOFs be packed into constrained space such as a cylinders as single crystals. The Advanced Research Projects Agency-Energy (ARPA-E) of the US DOE has recently offered a new volumetric methane storage target of $350 \text{ cm}^3 \text{ (STP) cm}^{-3}$, that incorporates use of the crystallographic density of MOFs.^{8,9} Given that the actual packing density of

Predictable and targeted activation of biomass to carbons with high surface area density and enhanced methane storage capacity

MOFs is typically much lower (up to 50% less) than their crystallographic density, this new target allows for a 25% reduction in volumetric capacity (to ca. $263 \text{ cm}^3 \text{ cm}^{-3}$) as a result of packing MOFs into a storage tank. To date, the highest reported values for methane storage at $25 \text{ }^\circ\text{C}$ and 35 bar, for powder forms of MOFs are; $225 \text{ cm}^3 \text{ cm}^{-3}$ for HKUST-1 (crystal density of 0.881 g/cm^3),⁸ $230 \text{ cm}^3 \text{ cm}^{-3}$ for Ni-MOF-74 (crystal density of 1.195 g/cm^3),⁸ $221 \text{ cm}^3 \text{ cm}^{-3}$ for Co-MOF-74 (crystal density of 1.173 g/cm^3),⁸ $235 \text{ cm}^3 \text{ cm}^{-3}$ for PCN-14 (crystal density of 0.829 g/cm^3),⁶³ and $227 \text{ cm}^3 \text{ cm}^{-3}$ for HKUST-1 (with crystal density of 0.883 g/cm^3).⁶⁴ The storage capacity of the best performing ACDS4700 sample ($222 \text{ cm}^3 \text{ cm}^{-3}$) is comparable to that of these benchmark MOFs^{8,63-66} Crucially, the MOF values can be expected to reduce by between 25 and 50% when used in real applications,⁶⁻⁹ which means that the present ACDS4700 sample has far higher capacity compared to the MOFs. Indeed, a recent study has shown that the uptake of HKUST-1 at 65 bar reduces by $>50\%$ from $267 \text{ cm}^3 \text{ cm}^{-3}$ when crystal density (0.883 g cm^{-3}) is used to $130 \text{ cm}^3 \text{ cm}^{-3}$ for hand packing density (0.43 g cm^{-3}).³⁹

Recently Tian and co-workers reported on a sol-gel monolithic MOF that exhibits high packing density and enhanced volumetric methane uptake.³⁹ The so-called monoHKUST-1 , which has a packing density of 1.06 g cm^{-3} , is currently the record holder for volumetric methane storage in porous materials.^{9,39} We compared the performance of the best ACDSxT carbons with that of monoHKUST-1 (**Figure 12**, and **Table 8**). The ACDSxT carbons have higher gravimetric uptake than monoHKUST-1 at pressure of 35 bar due to their higher surface area and pore volume.³⁹ However, the situation is reversed for the

Predictable and targeted activation of biomass to carbons with high surface area density and enhanced methane storage capacity

volumetric uptake (**Figure 12** and **Table 8**) where the uptake of monoHKUST-1 is higher than that of ACDS2800 and ACDS4800 and comparable to that of ACDS4700. At 35 bar the excess uptake of ACDS4700 is $196 \text{ cm}^3 \text{ cm}^{-3}$ compared to $205 \text{ cm}^3 \text{ cm}^{-3}$ for monoHKUST-1 . The total uptake is closely matched at 222 and $224 \text{ cm}^3 \text{ cm}^{-3}$ for ACDS4700 and monoHKUST-1 , respectively. The shape of the uptake isotherm of the ACDS4700 sample (**Figure 12**) suggest that it is potentially likely to be at par or higher than that of monoHKUST-1 at pressures higher than 35 bar.

Predictable and targeted activation of biomass to carbons with high surface area density and enhanced methane storage capacity

Table 8. Methane uptake and working capacity at 25 °C and pressure of 35 or 30 bar for ACDS-derived activated carbons compared to the best performing MOF, monoHKUST-1

Sample	Excess uptake @35 (30)	Total uptake @35 (30)	Working capacity ^{c,d}
	<u>bar^a</u> cm ³ /cm ³	<u>bar^b</u> cm ³ /cm ³	
ACDS2800	184 (177)	208 (198)	107 (97)
ACDS4700	196 (188)	222 (211)	128 (117)
ACDS4800	176 (168)	201 (190)	118 (107)
monoHKUST-1 ³⁹	205 (199)	224 (213)	137 (126)

^aValues in the parentheses are excess uptake at 30 bar. ^bValues in the parentheses are total uptake at 30 bar. ^cWorking capacity is the difference in uptake between 35 bar and 5.8 bar. ^dThe values in the parenthesis refer to working capacity as the difference in uptake between 30 bar and 5.8 bar.

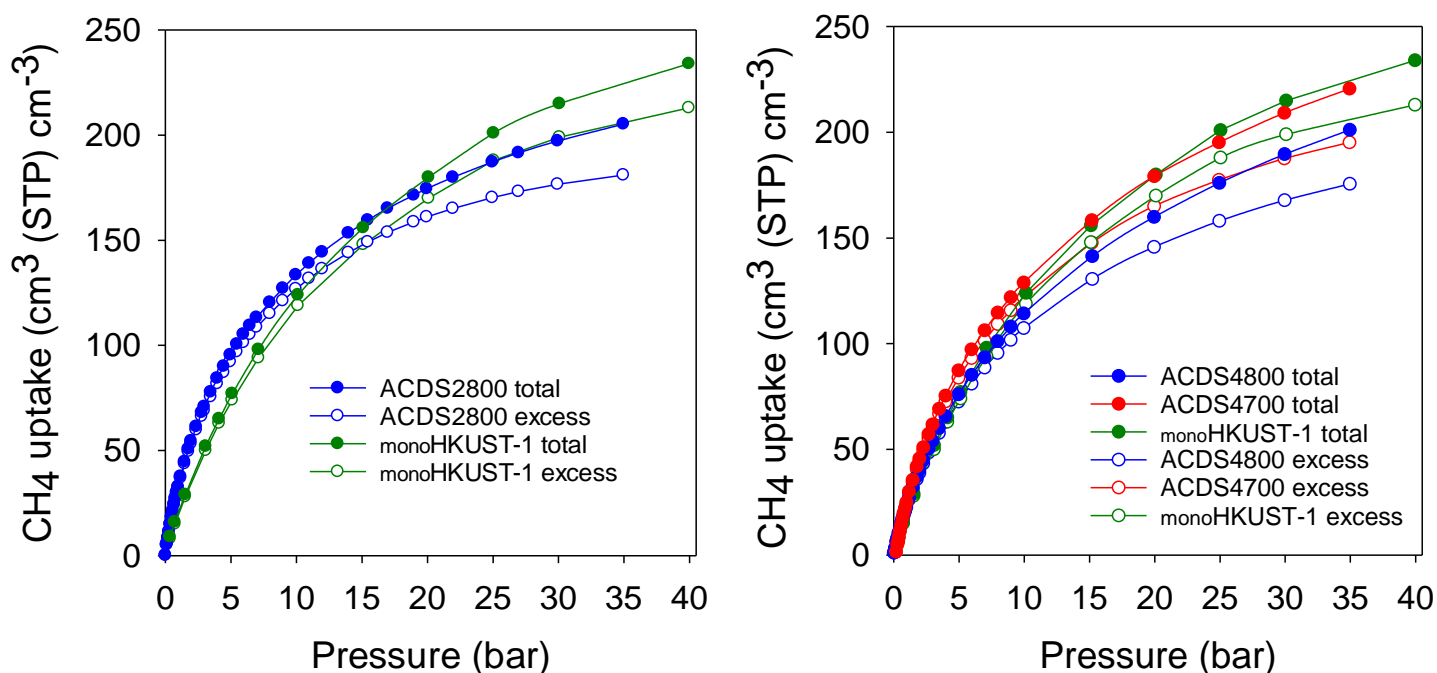


Figure 12. Total and excess volumetric methane uptake at 25 °C of ACDS-derived activated carbons (ACDSxT) compared to the benchmark MOF, monoHKUST-1 . Data for monoHKUST-1 obtained from reference 45.

A key measure of the performance of a porous material for methane storage is the working capacity, which is the difference in uptake between the adsorption and desorption (regeneration) pressure. For methane storage, a desorption pressure of 5.8 bar is suggested, and we applied an adsorption pressure of 35 bar (**Table 8**).^{6-9,39} The working capacity of the ACDS4700

Predictable and targeted activation of biomass to carbons with high surface area density and enhanced methane storage capacity

sample is comparable to that of monoHKUST-1 (**Table 8**). This is a noteworthy finding given that monoHKUST-1 is 50% better than any other MOF and is the current record holder for methane storage in porous materials. The monoHKUST-1 sample has a volumetric surface area (surface area x packing density) of $1288 \text{ m}^2 \text{ cm}^{-3}$, compared to ca. $800 \text{ m}^2 \text{ cm}^{-3}$ for powder form of HKUST-1.³⁹ Interestingly, the volumetric methane uptake shows a similar trend to the volumetric surface area. The present ACDSxT carbons have volumetric surface area of between 1114 and $1776 \text{ m}^2 \text{ cm}^{-3}$ (**Table 4**), and the methane volumetric uptake (**Table 6**) is best for samples with the highest volumetric surface area, which is consistent with the work of Tian and co-workers.³⁹ MOFs with higher volumetric surface area have been reported, such as $2060 \text{ m}^2 \text{ cm}^{-3}$ for NU-1501-Al, but are based on crystallographic density and therefore overestimated.⁶⁷ That such volumetric surface area computed from crystallographic density are overestimated is consistent with NU-1501-Al having a total methane uptake of only $148 \text{ cm}^3 \text{ cm}^{-3}$ at $25 \text{ }^\circ\text{C}$ and 35 bar,⁶⁷ compared to $> 220 \text{ cm}^3 \text{ cm}^{-3}$ for monoHKUST-1 and sample ACDS4700. The present carbons, therefore, match the best MOF in terms of volumetric methane storage,³⁹ but offer the advantage of being much cheaper and more robust. Affordability of an adsorbent is an important consideration, and the high cost of MOFs is a likely obstacle to their commercial take up.⁶⁻⁹ Indeed, a recent techno-economic analysis for MOFs as candidates for light-duty vehicle on-board natural gas storage found baseline MOF costs to range from \$35/kg to \$71/kg, with the possibility of reduction of costs to \$13/kg to \$36/kg, and perhaps to \$10/kg in best case scenarios.⁶⁸ On the other hand,

Predictable and targeted activation of biomass to carbons with high surface area density and enhanced methane storage capacity

the typical cost of activated carbons is *ca.* \$1 per kg, which is significantly lower than the best scenario (*i.e.*, lowest cost) for MOFs.

Conclusion

Activated carbons may be prepared from a wide range of carbonaceous precursors. To date, it is accepted that the properties (e.g., porosity, packing density) generated in the activated carbons are optimised via trial and error. In a departure from this current norm, we have shown that the properties of activated carbons can be predictably tailored by choice of the biomass precursor and mode of carbonisation to generate carbons that are highly microporous with high surface area density, high volumetric surface area and high packing density that is optimised for enhanced methane storage at medium pressure (35 bar). We show that the elemental composition of the biomass precursor, and more specifically a low ratio of elemental oxygen to elemental carbon (*i.e.*, low O/C atomic ratio), can be used as a universal predictor of the nature of porosity to be generated for activated carbon prepared via KOH activation. Using date seeds (*Phoenix dactylifera*) as starting biomass material, along with flash air-carbonisation, which requires much shorter time (5 – 10 min. and lower temperature (400 °C), we have synthesised activated carbons with an optimised mix of microporosity/mesoporosity, high surface area density, high volumetric surface area and high packing density than translates to record levels of volumetric methane storage. By examining a wide range of materials, we show that the surface area density is inversely related to the O/C ratio of the precursor carbonaceous matter. The carbonaceous matter obtained from flash air

Predictable and targeted activation of biomass to carbons with high surface area density and enhanced methane storage capacity

carbonisation of date seeds is resistant to activation and thus generates highly microporous activated carbons (with surface area of 995 – 2609 m² g⁻¹ and pore volume of 0.43 – 1.10 cm³ g⁻¹) with high packing density even after severe activation. The porosity of the resulting carbons is dominated by 0.8 – 1.2 nm pores, which are suitable for methane uptake. The carbons have excess methane uptake, at 25 °C and 35 bar, up to 196 cm³ cm⁻³ and total uptake of up to 222 cm³ cm⁻³, which is better than any previously reported carbon, and comparable to the best metal organic framework but at a much lower cost. Our findings provide new insights on the targeted, predictable and controlled activation of carbonaceous matter, and also offer a new pathway for addressing the challenge of developing porous materials with optimised balance between gravimetric and volumetric surface areas suitable for the on-board storage of methane gas.

Predictable and targeted activation of biomass to carbons with high surface area density and enhanced methane storage capacity

References:

- 1 M. S. Dresselhaus and I. L. Thomas, *Nature*, 2001, **414**, 332–337.
- 2 S. Choi, J. H. Drese and C. W. Jones, *ChemSusChem*, 2009, **2**, 796–854.
- 3 U. Eberle, B. Müller and R. Von Helmolt, *Energy Environ. Sci.*, 2012, **5**, 8780–8798.
- 4 I. Angelidaki, L. Treu, P. Tsapekos, G. Luo, S. Campanaro, H. Wenzel and P. G. Kougias, *Biotechnol. Adv.*, 2018, **36**, 452–466.
- 5 K. V. Kumar, K. Preuss, M. M. Titirici and F. Rodríguez-Reinoso, *Chem. Rev.*, 2017, **117**, 1796–1825.
- 6 Y. He, W. Zhou, G. Qian and B. Chen, *Chem. Soc. Rev.*, 2014, **43**, 5657–5678.
- 7 T. A. Makal, J. R. Li, W. Lu and H. C. Zhou, *Chem. Soc. Rev.*, 2012, **41**, 7761–7779.
- 8 J. A. Mason, M. Veenstra and J. R. Long, *Chem. Sci.*, 2014, **5**, 32–51.
- 9 B. Li, H. M. Wen, W. Zhou, J. Q. Xu and B. Chen, *Chem*, 2016, **1**, 557–580.
- 10 J. Romanos, S. Sweany, T. Rash, L. Firlej, B. Kuchta, J. Idrobo and P. Pfeifer, *Adsorpt. Sci. Technol.*, 2014, **32**, 681–691.
- 11 D. A. Gómez-Gualdrón, C. E. Wilmer, O. K. Farha, J. T. Hupp and R. Q. Snurr, *J. Phys. Chem. C*, 2014, **118**, 6941–6951.

Predictable and targeted activation of biomass to carbons with high surface area density and enhanced methane storage capacity

- 12 D. Lozano-Castelló, J. Alcañiz-Monge, M. A. De La Casa-Lillo, D. Cazorla-Amorós and A. Linares-Solano, *Fuel*, 2002, **81**, 1777–1803.
- 13 C. M. Simon, J. Kim, D. A. Gomez-Gualdron, J. S. Camp, Y. G. Chung, R. L. Martin, R. Mercado, M. W. Deem, D. Gunter, M. Haranczyk, D. S. Sholl, R. Q. Snurr and B. Smit, *Energy Environ. Sci.*, 2015, **8**, 1190–1199.
- 14 R. E. Morris and P. S. Wheatley, *Angew. Chemie - Int. Ed.*, 2008, **47**, 4966–4981.
- 15 M. Namvar-Asl, M. Soltanieh and A. Rashidi, *Energy Convers. Manag.*, 2008, **49**, 2478–2482.
- 16 J. Wang and S. Kaskel, *J. Mater. Chem.*, 2012, **22**, 23710–23725.
- 17 M. Sevilla and R. Mokaya, *Energy Environ. Sci.*, 2014, **7**, 1250–1280.
- 18 M. Sevilla, A. B. Fuertes and R. Mokaya, *Energy Environ. Sci.*, 2011, **4**, 1400–1410.
- 19 L. Wei and G. Yushin, *Nano Energy*, 2012, **1**, 552–565.
- 20 N. Balahmar, A. C. Mitchell and R. Mokaya, *Adv. Energy Mater.*, 2015, **5**, 1–9.
- 21 J. P. Marco-Lozar, M. Kunowsky, F. Suárez-García, J. D. Carruthers and A. Linares-Solano, *Energy Environ. Sci.*, 2012, **5**, 9833–9842.
- 22 M. Sevilla, W. Sangchoom, N. Balahmar, A. B. Fuertes and R. Mokaya, *ACS Sustain. Chem. Eng.*, 2016, **4**, 4710–4716.

Predictable and targeted activation of biomass to carbons with high surface area density and enhanced methane storage capacity

- 23 J. S. M. Lee, M. E. Briggs, T. Hasell and A. I. Cooper, *Adv. Mater.*, 2016, **28**, 9804–9810.
- 24 T. S. Blankenship and R. Mokaya, *Energy Environ. Sci.*, 2017, **10**, 2552–2562.
- 25 M. Cox and R. Mokaya, *Sustain. Energy Fuels*, 2017, **1**, 1414–1424.
- 26 B. Adeniran and R. Mokaya, *Nano Energy*, 2015, **16**, 173–185.
- 27 J. Wang and S. Kaskel, *J. Mater. Chem.*, 2012, **22**, 23710–23725.
- 28 Y. Zhu, S. Murali, M. D. Stoller, K. J. Ganesh, W. Cai, P. J. Ferreira, A. Pirkle, R. M. Wallace, K. A. Cychosz, M. Thommes, D. Su, E. A. Stach and R. S. Ruoff, *Science*, 2011, **332**, 1537–1542.
- 29 M. Sevilla and A. B. Fuertes, *Energy Environ. Sci.*, 2011, **4**, 1765–1771.
- 30 M. Paneque, J. M. De la Rosa, J. Kern, M. T. Reza and H. Knicker, *J. Anal. Appl. Pyrolysis*, 2017, **128**, 314–323.
- 31 M. M. Titirici and M. Antonietti, *Chem. Soc. Rev.*, 2010, **39**, 103–116.
- 32 M. M. Titirici, R. J. White, C. Falco and M. Sevilla, *Energy Environ. Sci.*, 2012, **5**, 6796–6822.
- 33 C. R. Lohri, H. M. Rajabu, D. J. Sweeney and C. Zurbrügg, *Renew. Sustain. Energy Rev.*, 2016, **59**, 1514–1530.
- 34 S. Hameed, A. Sharma, V. Pareek, H. Wu and Y. Yu, *Biomass and Bioenergy*, 2019, **123**, 104–122.

Predictable and targeted activation of biomass to carbons with high surface area density and enhanced methane storage capacity

- 35 E. Haffner-Staton, N. Balahmar and R. Mokaya, *J. Mater. Chem. A*, 2016, **4**, 13324–13335.
- 36 N. Balahmar, A. S. Al-Jumialy and R. Mokaya, *J. Mater. Chem. A*, 2017, **5**, 12330–12339.
- 37 E. A. Hirst, A. Taylor and R. Mokaya, *J. Mater. Chem. A*, 2018, **6**, 12393–12403.
- 38 N. Balahmar and R. Mokaya, *J. Mater. Chem. A*, 2019, **7**, 17466–17479.
- 39 T. Tian, Z. Zeng, D. Vulpe, M. E. Casco, G. Divitini, P. A. Midgley, J. Silvestre-Albero, J. C. Tan, P. Z. Moghadam and D. Fairen-Jimenez, *Nat. Mater.*, 2018, **17**, 174–179.
- 40 D. Lozano-Castelló, M. A. Lillo-Ródenas, D. Cazorla-Amorós and A. Linares-Solano, *Carbon N. Y.*, 2001, **39**, 741–749.
- 41 A. C. McKinlay, B. Xiao, D. S. Wragg, P. S. Wheatley, I. L. Megson and R. E. Morris, *J. Am. Chem. Soc.*, 2008, **130**, 10440–10444.
- 42 H. M. Coromina, D. A. Walsh and R. Mokaya, *J. Mater. Chem. A*, 2016, **4**, 280–289.
- 43 W. Sangchoom and R. Mokaya, *ACS Sustain. Chem. Eng.*, 2015, **3**, 1658–1667.
- 44 T. S. Blankenship, N. Balahmar and R. Mokaya, *Nat. Commun.*, , DOI:10.1038/s41467-017-01633-x.
- 45 A. Policicchio, E. MacCallini, R. G. Agostino, F. Ciuchi, A. Aloise and G.

Predictable and targeted activation of biomass to carbons with high surface area density and enhanced methane storage capacity

- Giordano, *Fuel*, 2013, **104**, 813–821.
- 46 I. Nehdi, S. Omri, M. I. Khalil and S. I. Al-Resayes, *Ind. Crops Prod.*, 2010, **32**, 360–365.
- 47 I. A. Nehdi, H. M. Sbihi, C. P. Tan, U. Rashid and S. I. Al-Resayes, *J. Food Sci.*, 2018, **83**, 624–630.
- 48 S. Besbes, C. Blecker, C. Deroanne, N. E. Drira and H. Attia, *Food Chem.*, 2004, **84**, 577–584.
- 49 J. Song, W. Shen, J. Wang and W. Fan, *Carbon N. Y.*, 2014, **69**, 255–263.
- 50 H. Yang, R. Yan, H. Chen, C. Zheng, D. H. Lee, V. Uni, N. D. V, R. V March, V. Re, M. Recei and V. September, 2006, 388–393.
- 51 M. J. Antal, S. G. Allen, X. Dai, B. Shimizu, M. S. Tam and M. Grønli, 2000, 4024–4031.
- 52 M. Brebu and C. Vasile, *Cellul. Chem. Technol.*, 2010, **44**, 353–363.
- 53 M. J. Antal, E. Croiset, X. Dai, C. Dealmeida, W. S. Mok, N. Norberg, J. Richard and M. Al Majthoub, 1996, 652–658.
- 54 W. M. A. W. Daud and W. S. W. Ali, *Bioresour. Technol.*, 2004, **93**, 63–69.
- 55 Z. Fang, T. Sato, R. L. Smith, H. Inomata, K. Arai and J. A. Kozinski, 2008, **99**, 3424–3430.
- 56 B. Adeniran and R. Mokaya, *J. Mater. Chem. A*, 2015, **3**, 5148–5161.

Predictable and targeted activation of biomass to carbons with high surface area density and enhanced methane storage capacity

- 57 M. Sevilla, R. Mokaya and A. B. Fuertes, *Energy Environ. Sci.*, 2011, **4**, 2930–2936.
- 58 M. E. Casco, M. Martínez-Escandell, E. Gadea-Ramos, K. Kaneko, J. Silvestre-Albero and F. Rodríguez-Reinoso, *Chem. Mater.*, 2015, **27**, 959–964.
- 59 M. E. Casco, M. Martínez-Escandell, K. Kaneko, J. Silvestre-Albero and F. Rodríguez-Reinoso, *Carbon N. Y.*, 2015, **93**, 11–21.
- 60 S. Choi, M. A. Alkhabbaz, Y. Wang, R. M. Othman and M. Choi, *Carbon N. Y.*, 2019, **141**, 143–153.
- 61 P. Navarro Quirant, C. Cuadrado-Collados, A. J. Romero-Anaya, J. Silvestre Albero and M. Martinez Escandell, *Ind. Eng. Chem. Res.*, 2020, **59**, 5775–5785.
- 62 D. Lozano-Castelló, D. Cazorla-Amorós and A. Linares-Solano, *Energy and Fuels*, 2002, **16**, 1321–1328.
- 63 S. Ma, D. Sun, J. M. Simmons, C. D. Collier, D. Yuan and H. C. Zhou, *J. Am. Chem. Soc.*, 2008, **130**, 1012–1016.
- 64 Y. Peng, V. Krungleviciute, I. Eryazici, J. T. Hupp, O. K. Farha and T. Yildirim, *J. Am. Chem. Soc.*, 2013, **135**, 11887–11894.
- 65 P. Chowdhury, S. Mekala, F. Dreisbach and S. Gumma, *Microporous Mesoporous Mater.*, 2012, **152**, 246–252.
- 66 A. D. Wiersum, J. S. Chang, C. Serre and P. L. Llewellyn, *Langmuir*, 2013, **29**, 3301–3309.

Predictable and targeted activation of biomass to carbons with high surface area density and enhanced methane storage capacity

- 67 Z. Chen, P. Li, R. Anderson, X. Wang, X. Zhang, L. Robison, L. R. Redfern, S. Moribe, T. Islamoglu, D. A. Gómez-Gualdrón, T. Yildirim, J. F. Stoddart and O. K. Farha, *Science*, 2020, **368**, 297–303.
- 68 D. DeSantis, J. A. Mason, B. D. James, C. Houchins, J. R. Long and M. Veenstra, *Energy and Fuels*, 2017, **31**, 2024–2032.

Chapter 4. A Milder Non-Hydroxide Activation route for Activated Carbons

Abstract

As pollution levels increase worldwide, energy production processes that are sustainable, and other mitigations are required to minimise adverse effects. Activated carbon is an example of a green and sustainable material within which gases may be stored due to internal extensive surface area. Recently, studies on so-called green activators for generating activated carbons have attracted research interest with the aim of making the preparation of activated carbons more sustainable. Potassium hydroxide (KOH), a corrosive and toxic activating reagent, is the most commonly used activating agent in the chemical activation of carbons. In this chapter, a less corrosive activating agent, potassium oxalate (PO), was explored as activator. To allow for a comparative analysis, PO and KOH were employed as activating agents to prepare activated carbons from biomass material (date seed) that is typically considered as date waste. The raw date seed was transformed to carbonaceous matter (designated as ACDS) via the so-called flash air-carbonisation route developed by the Mokaya group at Nottingham. The design of this study allowed a fuller understanding of the workings of the two activating reagents. The resulting PO activated carbons have surface area of up to $1747 \text{ m}^2 \text{ g}^{-1}$ and are highly microporous with up

A Milder Non-Hydroxide Activation route for Activated Carbons

to 94% of surface area arising from micropores. The porosity of the PO activated carbons can be readily tailored towards having pores of size 6 – 8 Å, which are highly suited for CO₂ storage at low pressure (*i.e.* post-combustion capture). Thus at 25°C, the PO activated carbons can store up to 1.9 and 4.8 mmol g⁻¹ of CO₂ at 0.15 bar and 1 bar, respectively. Unlike what is observed for hydroxide (KOH) activation, changing the amount of PO in the activation mixture, within the applied range, does not alter the porosity. At any given activation temperature, carbons activated at the PO/ACDS ratio of 2 or 4 have comparable porosity and therefore similar CO₂ uptake. On the other hand, KOH activated carbons reach higher surface area of up to 2738 m² g⁻¹. At 25°C, KOH activated carbons can store up to 4.5 mmol g⁻¹ of CO₂ compared to 4.8 mmol g⁻¹ for PO activated carbons. The PO activated carbons uptake at 0.15 bar and 25 °C of 1.9 mmol g⁻¹ is amongst the highest uptake for any porous material under those conditions.

4.1 Introduction

The concentration of CO₂ in the atmosphere is rapidly increasing. This increase is a significant global challenge as CO₂ is a significant greenhouse gas in terms of contributing to global warming. Some of the main contributors to release of CO₂ to the atmosphere are fossil-fuel-based power plants, cement industries, steel manufacturing deforestation and other modes of burning fossil fuels. Carbon capture and storage (CCS) is among the few remaining options for preserving the environment. CCS is a technique in which CO₂ emissions are captured and sequestered thus preventing entry to the atmosphere. Activated porous carbons have long been used to remove pollutants, in water and sewage treatment, air filters, industrial purification and energy storage applications. As a result of suitable chemical and thermal stability, high porosity and high specific surface area, activated carbons are a promising material for CO₂ capture and storage.¹⁻⁷ In recent years, new ways of preparing porous carbons with properties directly targeted at energy-related applications have been developed.

With careful choice of activation methods, the surface area and pore structure of carbonaceous materials can be dramatically altered for targeted applications. Activation can be either chemical or physical with the former offering several advantages including lower preparation temperature and higher yield. Nonetheless, chemical activation still has some severe limitations, including a large wastewater stream for chemical

A Milder Non-Hydroxide Activation route for Activated Carbons

disposal and high cost for maintaining and replacing equipment corroded by the activating agent. On the other hand, physical activation can be less expensive and more eco-friendly, although high temperatures and carbon gasification reactants, such as steam, CO₂, and air, are required.

The most frequently used chemical activating agents are inorganic acids (HCl, H₂SO₄, and H₃PO₄), alkali hydroxides (KOH, NaOH), ZnCl₂, and K₂CO₃.⁸⁻¹¹ Potassium hydroxide is the best-studied activating agent, as it can generate activated carbon with a defined pore size distribution and high surface area from a wide range of carbon precursors.^{12,13} Nevertheless, the use of KOH has disadvantages associated with its toxic and corrosive nature. Milder activating agents that yield carbons with comparable or superior textural properties compared to KOH activation are therefore a key research target.¹⁴ In the search for activating agents beyond hydroxides, the use of potassium oxalate (PO) as activator for a range of precursors, including sawdust hydrochar, polypyrrole or pre-mixed precursors has been explored.¹⁵ Previous studies on PO activated carbons have reported that, in general, carbons with a low to medium surface area (typically < 1500 m² g⁻¹) are obtained at activation temperatures below 800°C

The elemental composition and pore structure of activated carbons depend on the carbon sources used and the activation parameters. Parameters include activation duration, type of inert gas used, inert gas flow rate, heating ramp rate and, most importantly, the activation temperature and the amount of activating agent. Additionally, as demonstrated in chapter 3, the O/C ratio of any carbonaceous matter utilised as a starting material

A Milder Non-Hydroxide Activation route for Activated Carbons

(i.e. precursor) is an essential factor in determining the porosity of KOH-activated carbons, with a lower O/C ratio favouring greater surface area and pore volume. The properties of porous carbons can, therefore, be influenced by choice of precursors, allowing for tailoring of porosity towards specific energy applications as described in chapters 3 and 6.^{13,16-20}

Biomass is widely available as a renewable resource, is cheap and is, theoretically, 'carbon neutral'. Examples of biomass sources used as starting materials for activated carbon include eucalyptus sawdust,²¹ coconut shell²² and rice husk.²³ As described in chapter 3, this Thesis explored date seeds (*Phoenix dactylifera*) from which it is possible to generate highly microporous carbons with a high surface area density, a high volumetric surface area and a high packing density optimised for enhancing methane storage at medium pressure (35 bar). In this chapter, PO activation of air carbonised date seed was performed and compared to the KOH activation described in chapter 3.²⁴ However, in this chapter, the target application is CO₂ storage at 25 °C and low to moderate pressure (1 to 20 bar).

Before activation, there are various ways of converting biomass to carbon-rich (carbonaceous) matter.²¹ Conventionally, hydrothermal carbonisation (HTC)²⁵⁻²⁷ or pyrolysis²⁷⁻²⁹ are the most commonly used. Hydrothermal carbonisation involves the thermochemical decomposition of biomass wherein an aqueous biomass dispersion is placed in a stainless steel autoclave at a target concentration and heated (typically 180–300°C) for several hours. On the other hand, the pyrolysis process involves the

A Milder Non-Hydroxide Activation route for Activated Carbons

generation of carbonaceous matter via enrichment of carbon content during thermal treatment at temperatures of 600–900°C under oxygen-free conditions.^{10,29–33}

In an alternative process investigated by the Mokaya group, the so-called flash air carbonisation, much shorter periods (5–10 min) and a lower temperature (400°C) are used to transform biomass to carbon-rich matter in the presence of air. The process is based on the fact that volatiles (i.e., H₂O, CO_x, CH₄, and light hydrocarbons) in biomass are lost at temperatures as low as 200–350°C, with little mass loss above 400°C. The attraction of the flash carbonisation method is that it negates the need to use conventional energy-intensive processes and that the process is significantly shorter than the typical several hour procedures, and it does not require specialised high pressure (for HTC) equipment.^{21,34,35}

In this chapter, the synthesis of PO activated carbons from air-carbonised date seed (ACDS) is explored. Date seed is inexpensive and widely available in the Kingdom of Saudi Arabia, more than one million metric tonnes of date seed are produced annually. The majority of date seed waste is disposed of via combustion at landfill sites. Therefore, disposal costs would also be reduced by date seed valorisation, further reducing greenhouse gas emissions associated with its uncontrolled combustion. In chapter 3, with potassium hydroxide as activating agent, carbon materials with high surface area density, high volumetric surface area and high packing density optimised for enhanced methane storage at medium pressure (35 bar) have been described. The focus of this chapter shifts to CO₂ uptake at low to

A Milder Non-Hydroxide Activation route for Activated Carbons

medium pressures that mimic post-combustion capture from fossil fuel power station flue gases.

4.2 Experimental Section

4.2.1 Material preparation

Date seed (*Phoenix dactylifera*) was selected for use as the starting material. After thorough washing with water and drying, the date seeds (5 g) were placed in an alumina boat and heated in a horizontal tube furnace to 400 °C under an atmosphere of nitrogen with a heating ramp rate of 10 °C min⁻¹. At 400 °C, the date seed was exposed to a flow of air for 5–10 min, after which the furnace was left to cool under a flow of nitrogen gas. The resulting carbonaceous matter was designated as ACDS (*i.e.*, air carbonised date seed) carbon. For activation, the ACDS carbon was mixed with the required amount of potassium oxalate (PO) at predetermined PO/ACDS carbon ratios in an agate mortar. The PO + ACDS carbon mixture was placed in an alumina boat and heated in a furnace to 700 or 800 °C at a heating ramp rate of 3 °C min⁻¹ under an atmosphere of nitrogen gas and held at the final temperature for 1 h, after which the sample was allowed to cool under a flow of nitrogen. The resulting activated samples were then washed by stirring in 20% aqueous HCl at room temperature, and then repeatedly washed with deionised water until the filtrate was neutral (pH ~ 7). The samples were then dried in an oven at 120 °C, and designated as ACDS_xT(PO), where *x* is the PO /ACDS carbon ratio, *T* is the activation temperature (in °C) and PO means potassium oxalate is being

A Milder Non-Hydroxide Activation route for Activated Carbons

used as an activating agent. Thus, a carbon activated at a PO /ACDS carbon ratio of 2 and at 800 °C is designated as ACDS2800(PO) or ACDS2800P(PO), P means the sample was compacted before the activation step. The compacted samples were obtained from pellets compacted in a 1.3 cm die for *ca.* 5 min at 7 MPa.

Moreover, the carbons activated at a KOH/ACDS carbon ratio of 2 or 4 and at 700 or 800 °C in chapter 3 are explored in this chapter for CO₂ uptake in order to make a clear comparison with PO activation. As described in chapter 3, a carbon activated at a KOH/ACDS carbon ratio of 2 and at 800 °C is designated as ACDS2800.

4.2.2 Material Characterisation

Thermogravimetric analysis (TGA) was performed using a TA Instruments Discovery analyser or TA Instruments SDT Q600 analyser under flowing air conditions (100 mL/min). A PANalytical X'Pert PRO diffractometer was used to perform powder XRD analysis using Cu-K α light source (40 kV, 40 mA) with step size of 0.02° and 50 s time step. Elemental, CHN, analysis was performed on an Exeter Analytical CE-440 Elemental Analyser. Nitrogen sorption (at -196 °C) with a Micromeritics 3FLEX sorptometer was used for porosity analysis and to determination textural properties. Prior to analysis the carbon samples were degassed under vacuum at 200 °C for 12 h. Surface area was calculated using the Brunauer-Emmett-Teller (BET) method applied to adsorption data in the relative pressure (P/P_0) range of 0.02 – 0.22, and pore volume was estimated from the total nitrogen uptake at close to saturation pressure (P/P_0).

A Milder Non-Hydroxide Activation route for Activated Carbons

≈ 0.99). The micropore surface area and micropore volume were determined via t -plot analysis. The pore size distribution was determined using Non-local density functional theory (NL-DFT) applied to nitrogen adsorption data. Scanning electron microscopy (SEM) images were recorded using an FEI Quanta200 microscope, operating at a 5 kV accelerating voltage. Transmission electron microscopy (TEM) images were obtained using a JEOL 2100F instrument operating at 200 kV equipped with a Gatan Orius CCD for imaging. Prior to analysis, the carbon samples were suspended in distilled water and dispersed onto lacey carbon support films.

4.2.3 CO₂ uptake measurements

CO₂ uptake was determined using a Hiden Isochema XEMIS instrument at 25 °C and pressure of up to 20 bar. The carbons were outgassed for 3 h under vacuum at 240 °C prior to performing the CO₂ uptake measurements. The measurements directly determined the excess CO₂ uptake.

4.3 Result and Discussion

4.3.1 Structural ordering, morphology and thermal stability

We looked at how flash air-carbonisation affected the date seed, as well as how the carbonaceous matter that formed (ACDS carbon) behaved to activation. **Table 1** shows that after the flash air-carbonisation stage, the carbon content increased from 49 wt% for raw date seeds to 78.5 wt% for ACDS carbon, whereas the H content decreased from 7 wt% to 4 wt%. This

A Milder Non-Hydroxide Activation route for Activated Carbons

was accompanied by a significant decrease in apparent O content, which dropped from 42.4 wt% (raw date seed) to 16.3 wt% for ACDS carbon. Activation was conducted by heating the ACDS with PO, either as pellets or in powder form, to the target temperature (700 °C to 800 °C) and holding for 1 hr. The yield of the activated carbons in relation to the initial biomass matter is a critical factor to consider. **Table 1** summarises the carbon yields of samples activated at PO/ACDS ratio of 2 or 4 at 700 °C or 800 °C.

For the PO activated carbons, as shown in **Table 1**, the yield is in the range of 52% to 60%, for samples activated at a high temperature (800 °C), and is 58% to 64% for samples activated at lower temperature (700 °C). The highest yield obtained is for sample ACDS4700P(PO). The yields of KOH activated carbons are summarised in **Table 2**. The carbon yields vary from 46% to 60%, with sample ACDS2700 having the highest yield obtained of 60%. The yield achieved from PO activated carbon is clearly higher than that obtained from KOH activated carbon. In addition, we compared the yield of the PO activated carbons with the recently published study of PO as an activating agent with hydrochar (obtained from sawdust via hydrothermal carbonisation) as a precursor.¹⁵ Under similar activation conditions (i.e., PO/hydrochar ratio 2 or 4 and activation temperature of 700 and 800), the yield was in the range of 36 % to 41%, which is lower than the yield of ACDS activated carbon for both PO and KOH activating carbon as reported here.¹⁵ This result clearly demonstrates the benefits, in terms of greater yield, of utilizing the air carbonisation route and the date seed as a biomass resource for activating carbon preparation. The genesis

A Milder Non-Hydroxide Activation route for Activated Carbons

of this benefit lies with the nature of the ACDS carbon, its low O/C ratio (as described in chapter 3) and resistance to activation.

The elemental C content of the PO activated carbon increases from 78.5 wt% in the ACDS carbon to a high of 87.0 wt% (sample ACDS2800P(PO)). The H content dropped from 4% for the ACDS and was nil for some samples. A similar trend is observed for the N content, which decreased from 1.2 wt% for ACDS to virtually nil (0.1 wt%) after activation. The KOH activated carbons show a similar trend in CHN content to PO activated carbons with the highest C content reaching 90 wt% for sample of ACDS2800.

For both PO and KOH activating carbons, therefore, the activation of ACDS results in an increase in the C content, with the increase being generally greater at higher activation temperatures. On the other hand, the H content decreases significantly, and the nitrogen content shows a less drastic reduction. These results are similar to those obtained by Mokaya and co-workers in a study using carbon from cigarette butts as precursor.¹²

A Milder Non-Hydroxide Activation route for Activated Carbons

Table 1 Yield and elemental composition of carbons activated at PO/ACDS ratio of 2 or 4 as powder or pellet.

Sample	Yield [wt %]	C [%]	H [%]	N [%]	O [%]
Date seeds		49.0	7.0	1.6	42.4
ACDS carbon		78.5	4.0	1.2	16.3
ACDS2700(PO)	58	80.6	1.0	2.6	15.8
ACDS2800(PO)	52	83.0	0.1	0.2	16.7
ACDS4700(PO)	62	80.0	1.2	1.8	17.0
ACDS4800(PO)	60	84.0	0	0.2	15.8
ACDS2700P(PO)	60	79.3	1.0	1.0	18.7
ACDS2800P(PO)	56	87.0	0.1	0.3	12.6
ACDS4700P(PO)	64	79.5	0.2	0.1	20.2
ACDS4800P(PO)	58	82.5	0	0.3	17.2

Table 2 Yield and elemental composition of carbons activated at KOH/ACDS ratio of 2 or 4 as powder or pellet.

Sample	Yield [wt %]	C [%]	H [%]	N [%]	O [%]
Date seeds		49.0	7.0	1.6	42.4
ACDS carbon		78.5	4.0	1.2	16.3
ACDS2700	60	82.0	0.9	0.5	16.6
ACDS2800	56	90.0	0.1	0.2	9.7
ACDS4700	54	83.9	0.2	0.3	15.6
ACDS4800	50	84.3	0.1	0.1	15.5
ACDS2700P	58	81.4	1.1	0.3	17.2
ACDS2800P	54	83.3	0.1	0.2	16.4
ACDS4700P	48	82.0	0.7	0.2	17.1
ACDS4800P	46	84.5	0.1	0.3	15.1

A Milder Non-Hydroxide Activation route for Activated Carbons

Figures 1 and 2, show the TGA curves of the activated carbons. TGA was performed to assess the purity (with respect to presence of any non-combustible inorganic matter) and thermal stability. The TGA involved thermal treatment of the carbons to 1000 °C at a ramp rate of 10 °C min⁻¹ under flowing air conditions. The curves show that the PO or KOH activating carbon are stable up to 400 °C. All samples show a small initial mass loss below 100 °C, which is due to evaporation of residual moisture. This is followed by a further single mass loss step, which is due to the combustion of carbon. For both PO and KOH activated carbons, the carbon burn-off temperature is between 400 °C and 660 °C, with samples activated at 800 °C having greater thermal stability. The wide range of the burn-off temperature (400 to 660 °C) is consistent with the nature of the ACSD carbon, which is mostly non-graphitic (i.e., amorphous), as might be expected for carbonaceous materials produced via low-temperature carbonisation. All the PO or KOH activated carbons display a residual mass typically less than 2 wt%, suggesting that they are essentially carbonaceous with only trace amounts of inorganic matter.

Figures 3 and 4 show the XRD patterns of PO or KOH activated carbons. Powder XRD was performed to confirm the nature and purity of the date seed-derived porous carbons. The broad peak in the XRD pattern of the activated carbons at 2-theta of 22 °C and 44 °C corresponds to the positions where the (002) and (100) diffractions are expected to arise from graphene stacks.

A Milder Non-Hydroxide Activation route for Activated Carbons

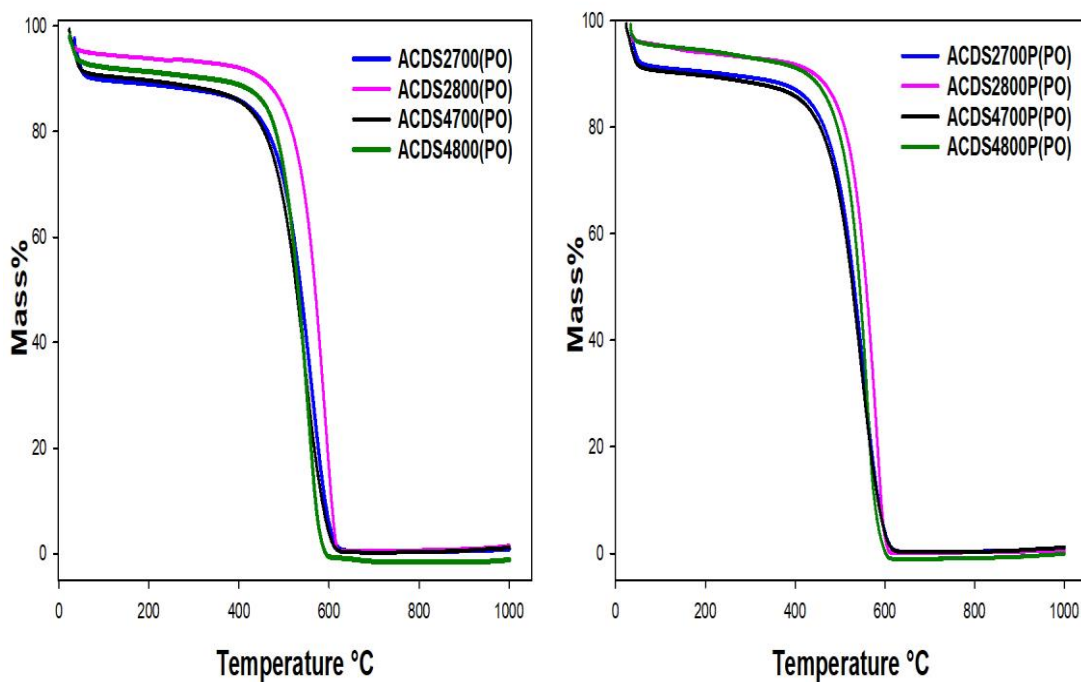


Figure 1. Thermogravimetric analysis curves of carbons activated at PO/ACDS ratio of 2 or 4 as powder or pellet

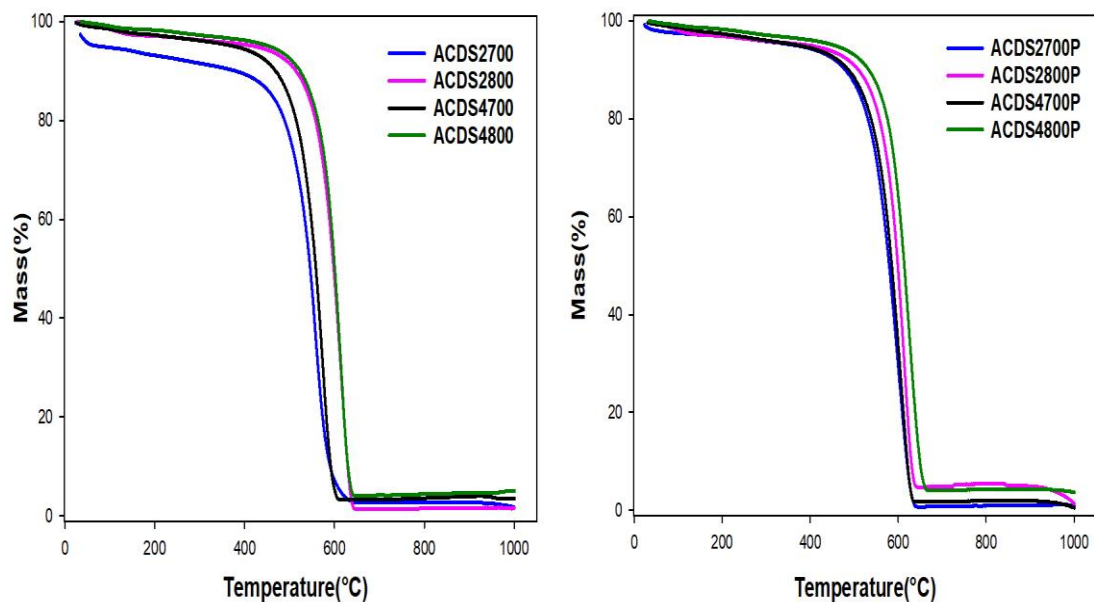


Figure 2. Thermogravimetric analysis curves of carbons activated at KOH/ACDS ratio of 2 or 4 as powder or pellet.

A Milder Non-Hydroxide Activation route for Activated Carbons

This suggests that the ACDS carbon has some graphene-like stacking, which is considerably reduced or absent in activated carbons; this is consistent with the disruptive nature of the activation process. The level of graphene stacking does not appear to be affected by the activation temperature in any significant or consistent way. The overall picture shown by the XRD patterns is that the carbons generated from the date seeds are largely amorphous, as is typical of PO activated carbons.^{15,36} The general absence of sharp peaks in the XRD patterns confirms the absence of inorganic matter, which is consistent with the TGA curves.

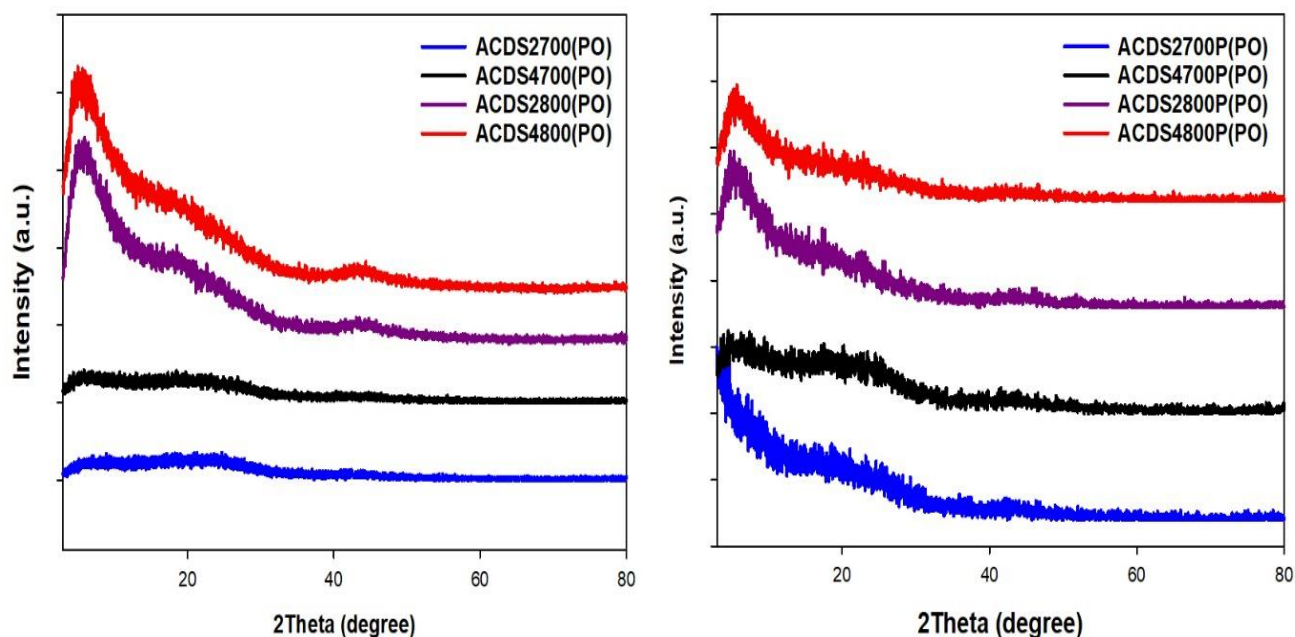


Figure 3. Powder XRD pattern of carbons activated at PO/ACDS ratio of 2 or 4 as powder or pellet.

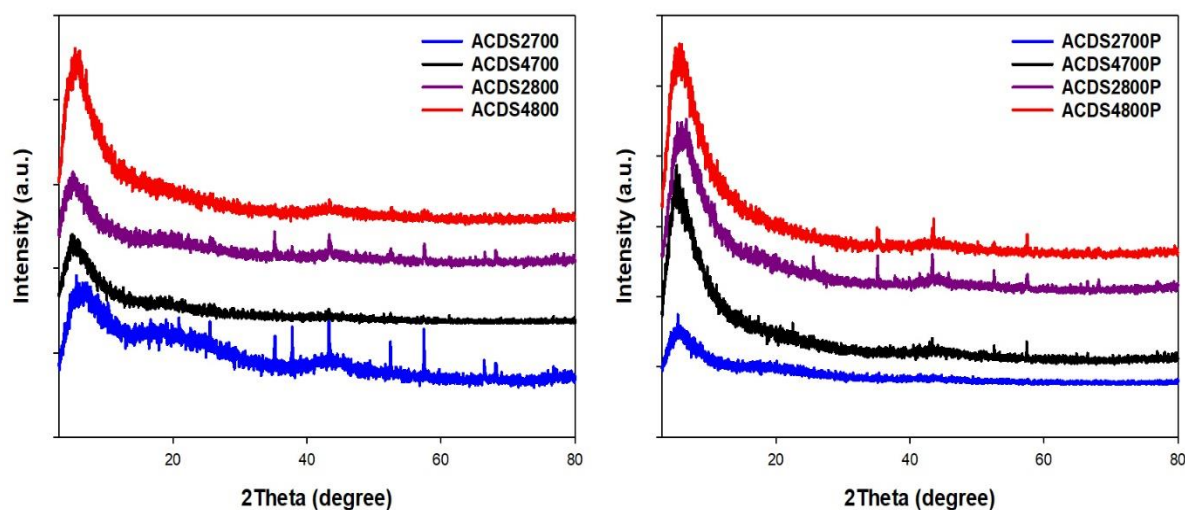


Figure 4 Powder XRD pattern of carbons activated at KOH/ACDS ratio of 2 OR 4 as powder or pellet.

To ascertain the morphology and microstructural ordering of the carbon materials, SEM and TEM images were obtained. The SEM and TEM images of selected carbon samples are shown in **Figure 4** and **5** respectively. As revealed by the SEM micrographs in **Figure 4**, the morphology is dominated by honeycomb structures, and is similar to that previously observed in activated carbon.²¹ A close inspection of the date-seed derived particles by TEM (**Figure 5**) reveals wormhole-type pore channels, which is typical for activated carbons. The TEM images for both sets show no significant evidence of the presence of graphitic domains, which is in agreement with previous studies.^{18,21,37}

A Milder Non-Hydroxide Activation route for Activated Carbons

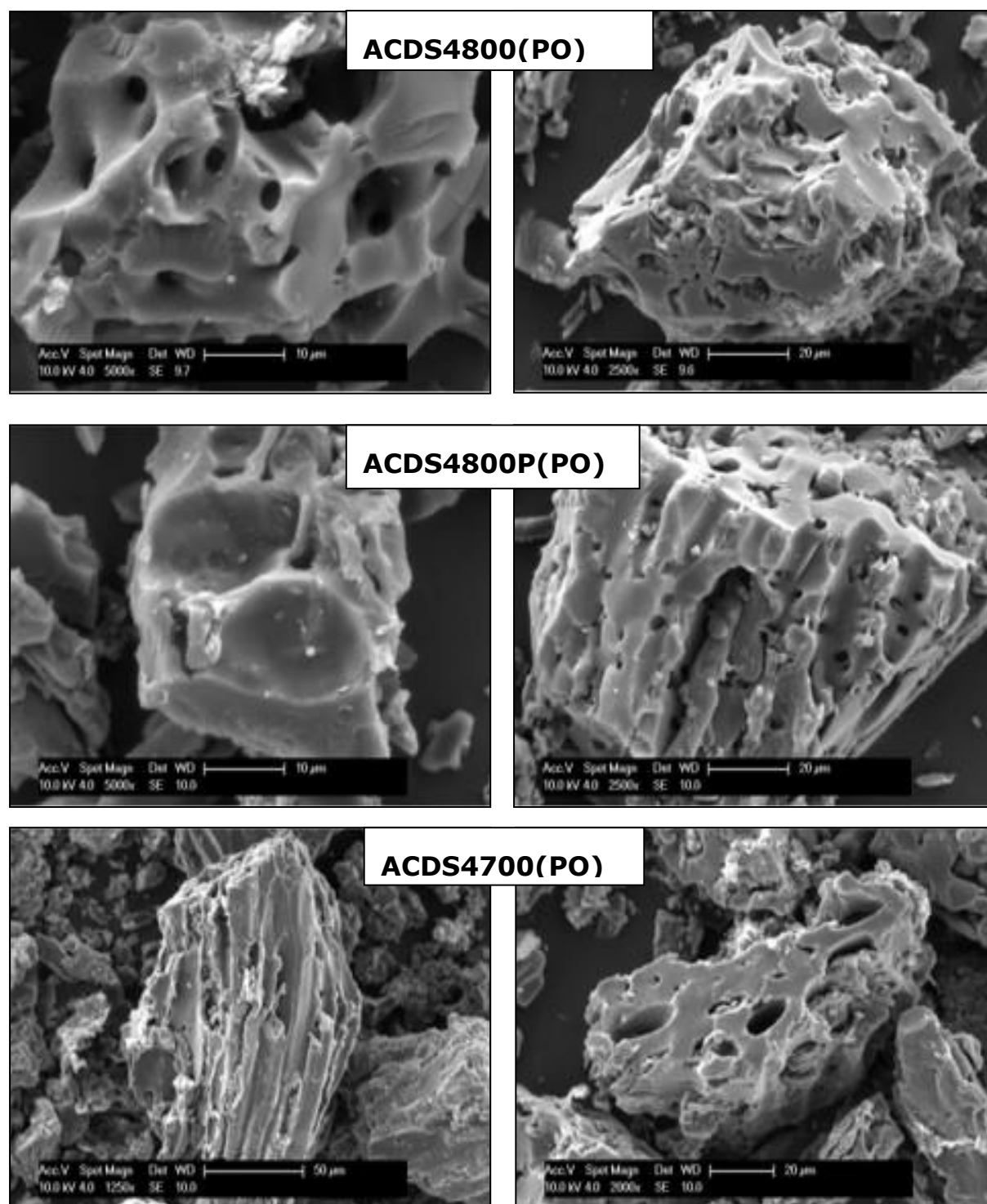


Figure 5. SEM images of air-carbonised activated date seed-derived carbon at PO/ACDS carbon ratio of 2 or 4.

A Milder Non-Hydroxide Activation route for Activated Carbons

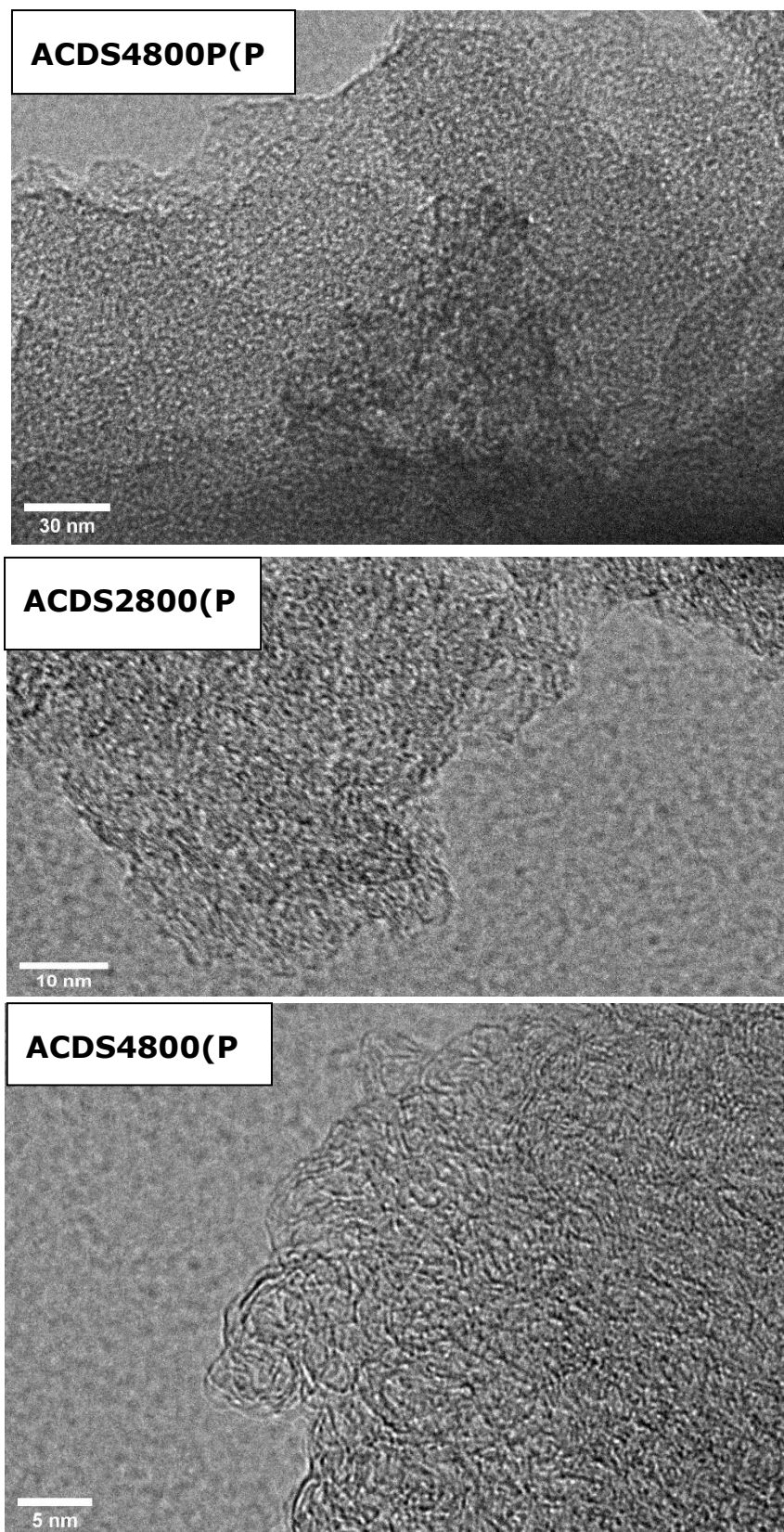


Figure 6. TEM images of air-carbonised activated date seed-derived carbon at PO/ACDS carbon ratio of 2 or 4.

4.3.2 Textural properties and porosity

The main goal of this chapter was to investigate how the activating agent affected carbon porosity and how the less toxic activating agent, PO, behaved in comparison to the KOH activated carbons prepared in Chapter 3. The ACDS carbon was found to be nearly non-porous, with a surface area of $2.5 \text{ m}^2 \text{ g}^{-1}$ and a pore volume of $0.004 \text{ cm}^3 \text{ g}^{-1}$, as previously mentioned in Chapter 3. **Figure 7** and **8** show the nitrogen sorption isotherms and corresponding pore size distribution (PSD) curves of activated carbons prepared at PO/ACDS ratio of 2 or 4. All the isotherms, regardless of the activation temperature between 700 and 800 °C, are of type I, indicating that the *carbons* are microporous. Due to micropore filling, high nitrogen sorption occurs at a low relative pressure ($P/P_0 < 0.1$),³⁸ and no significant adsorption occurs at P/P_0 greater than 0.1. At higher activation temperatures, the amount of nitrogen adsorbed increased, indicating a higher level of porosity (i.e., surface area and pore volume) generated in the activated carbons.

It is interesting to note that despite the increase in amount of nitrogen adsorbed as activation temperature rises from 700 to 800 °C, there is little change in the shape of the isotherms as all PO activating carbons exhibit isotherms with a sharp adsorption knee. Sharp adsorption knees are associated with the absence of pores of size larger than the micropore range (up to 2 nm). It is clear to see that the porosity of PO

A Milder Non-Hydroxide Activation route for Activated Carbons

activating carbons at any given ratio is dominated by 0.5–1.3 nm pore channels, with most pores being <1 nm.

The nitrogen sorption isotherms and corresponding PSD curves of activated carbons prepared at KOH/ACDS ratio of 2 or 4 carbons are shown in **Figures 9** and **10**. Unlike PO activation, the isotherms shape show that some samples have a significant proportion of supermicropores (*i.e.*, pore channels of size 0.7–2.0 nm) and some small mesopores.^{12,39–41}

Clearly, KOH activation generates a greater proportion of larger pores compared to PO activation, and the proportion of mesopores is higher at KOH/ACDS ratio of 4. As shown in **Figure 9** and **10**, the samples possess a relatively wide pore size range but still mainly within the micropore/supramicropore to small mesopore range, with most pores being of size lower than 1.5 nm and hardly any pores wider than 2.5 nm.

A Milder Non-Hydroxide Activation route for Activated Carbons

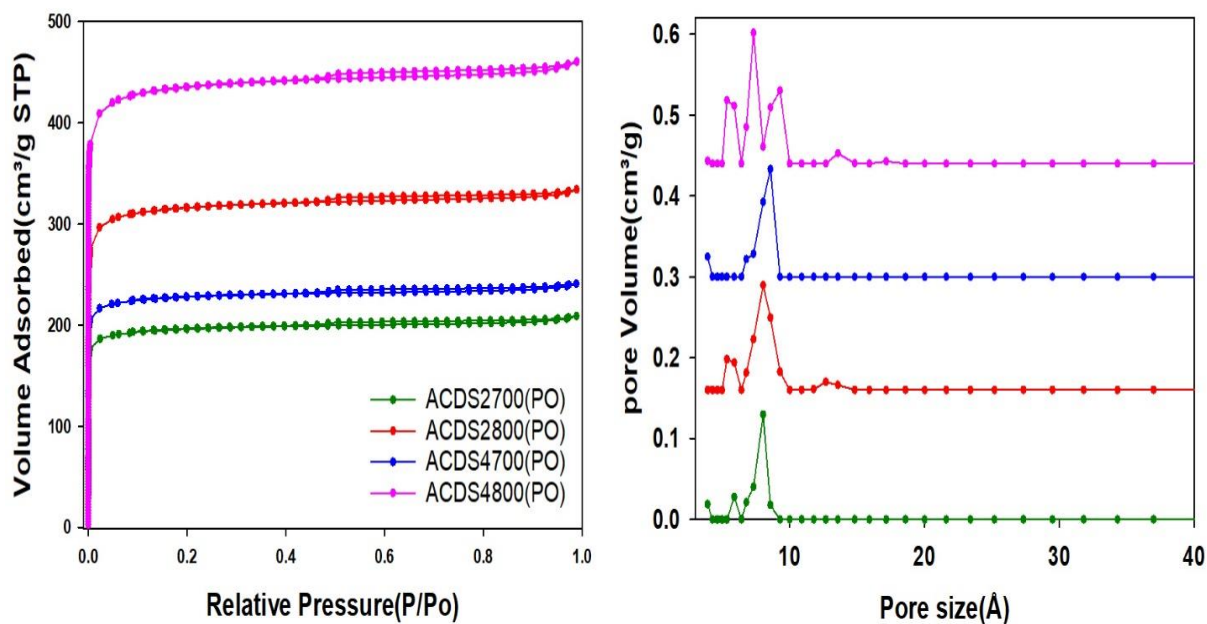


Figure 7 Nitrogen sorption isotherms and pore size distribution curves of activated carbons derived from ACDS carbon at PO/ACDS carbon ratio of 2 or 4 as powder samples.

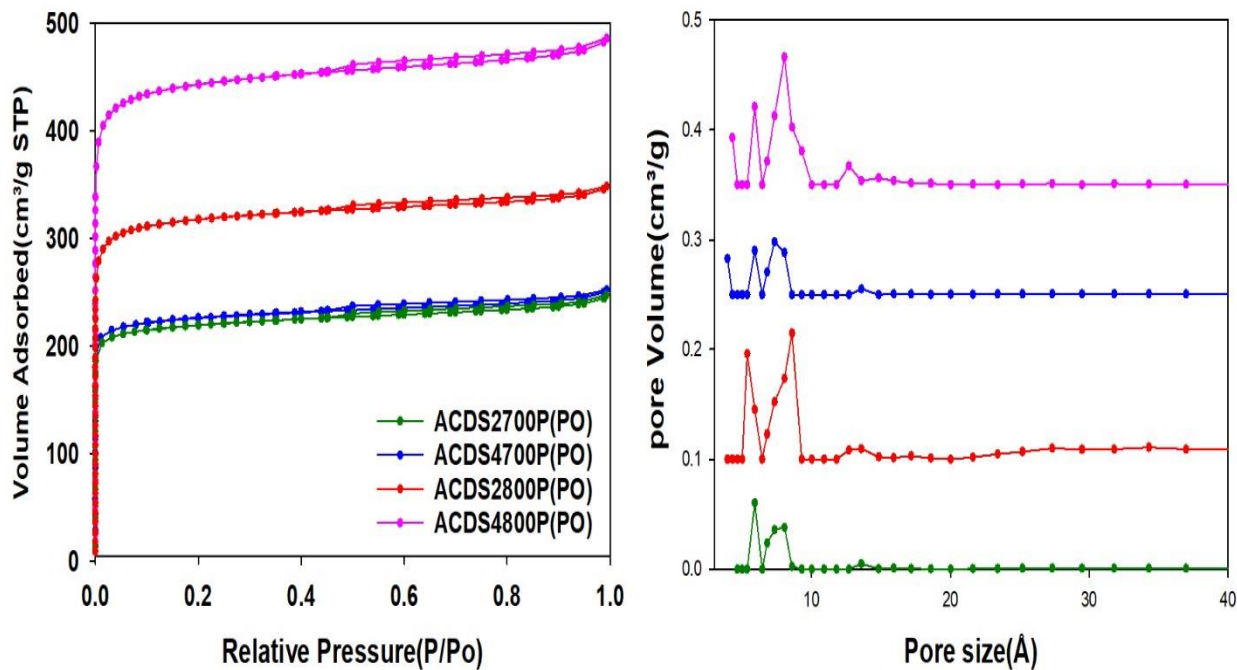


Figure 8 Nitrogen sorption isotherms and pore size distribution curves of activated carbons derived from ACDS carbon at PO/ACDS ratio of 2 or 4 as compacted samples.

A Milder Non-Hydroxide Activation route for Activated Carbons

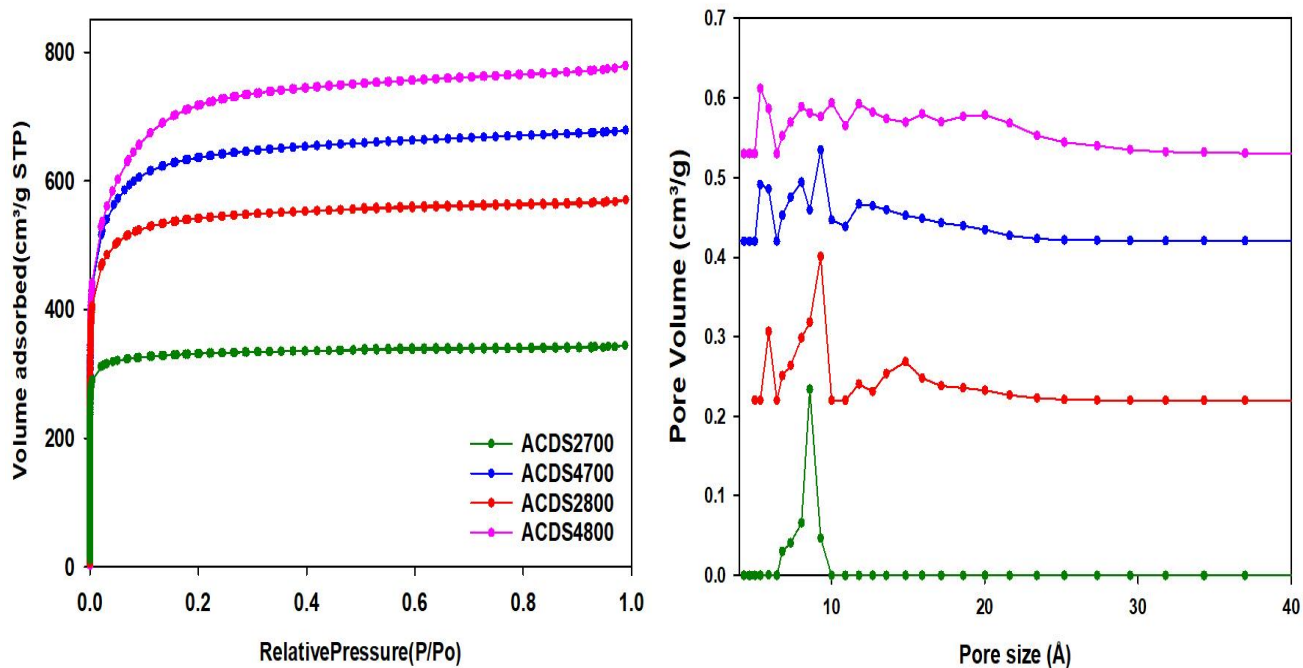


Figure 9 Nitrogen sorption isotherms and pore size distribution curves of activated carbons derived from ACDS carbon at KOH/ACDS ratio of 2 or 4 for powder samples.

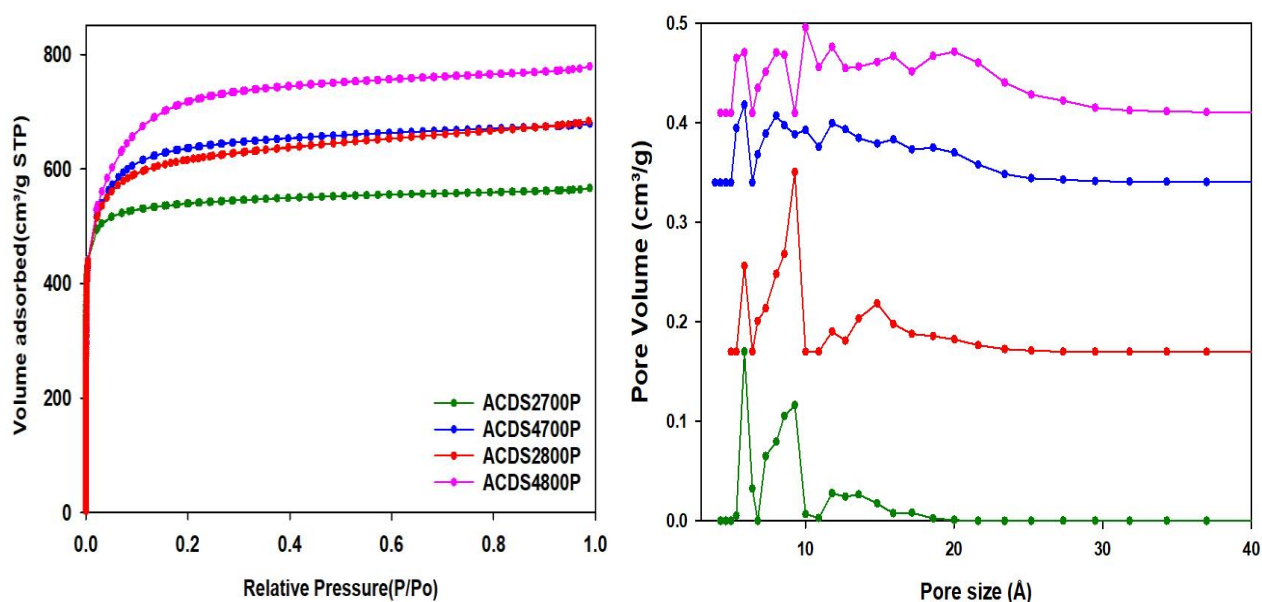


Figure 10 Nitrogen sorption isotherms and pore size distribution curves of activated carbons derived from ACDS carbon at KOH/ACDS ratio of 2 or 4 for compacted samples.

A Milder Non-Hydroxide Activation route for Activated Carbons

The textural properties of PO activated carbons are shown In **Table 3**. The total surface area is in the range of (790-1767 m² g⁻¹), which is low to moderate compared to other porous carbons. As expected, the surface area and pore volume of PO activated carbons increased with the activation temperature. At the lower activation temperature, sample ACDS2700(PO) has the lowest surface area, whereas sample ACDS4800P(PO) has the highest surface area.

Importantly, the PO activated carbons show a high proportion of microporosity of up to 94% surface area. The magnitude of micropore surface area increases as the activation temperature rises from 700°C to 800°C such that the micropore surface area is 767 m² g⁻¹ for sample ACDS2700(PO) compared to 1696 m² g⁻¹ for sample ACDS4800(PO).

There are no significant differences between compacted and powder samples. However, it appears that compaction has the effect of reducing the level of microporosity. It can be expected the change in the pores due to the compaction. Applying pressure to the pores after compaction process seems to change the nature of the pores which include increased mesoporosity. The highest proportion of microporosity decreased from 97% for the powder sample to 81% for compacted samples.

A Milder Non-Hydroxide Activation route for Activated Carbons

Table 3 Textural properties of carbons activated at PO/ACDS ratio of 2 or 4 as powder or pellet.

Sample	Surface area (m ² g ⁻¹)	Micropore surface area ^a (m ² g ⁻¹)	Pore volume (cm ³ g ⁻¹)	Micropore volume (cm ³ g ⁻¹) ^b	Pore size (Å)
ACDS2700(PO)	790	767	0.31	0.29	4/6/8
ACDS4700(PO)	918	893	0.37	0.34	4/6/8
ACDS2800(PO)	1261	1223	0.51	0.47	6/8/13
ACDS4800(PO)	1747	1696	0.70	0.65	6/8/9/13
ACDS2700P(PO)	881	825	0.38	0.31	6/8/13
ACDS4700P(PO)	908	855	0.38	0.32	6/8/13
ACDS2800P(PO)	1276	1029	0.75	0.47	6/8/13
ACDS4800P(PO)	1767	1676	0.75	0.65	4/6/8/13

Table 4 Textural properties of carbons activated at KOH/ACDS ratio of 2 or 4 as powder or pellet.

sample	Surface area (m ² g ⁻¹)	Micropore surface area ^a (m ² g ⁻¹)	Pore volume (cm ³ g ⁻¹)	Micropore volume (cm ³ g ⁻¹) ^b	pore size (Å)
ACDS2700	1264	1170	0.53	0.47	8.5
ACDS2800	2068	1780	0.88	0.71	6/9.2/11.7/14.5
ACDS4700	2192	1871	0.93	0.74	5.5/8/9/11.5
ACDS4800	2609	1825	1.10	0.70	5.5/8/10/16/20
ACDS2700P	2051	1845	0.87	0.74	6/9/11.8
ACDS2800P	2356	1888	1.05	0.74	6/8.5/12.5/16
ACDS4700P	2449	1962	1.05	0.76	5.8/8/10/11.8/16
ACDS4800P	2738	1793	1.20	0.68	5.8/8/10/11.8/16/20

A Milder Non-Hydroxide Activation route for Activated Carbons

For KOH activated sample ACDS2700 has surface area of $1264 \text{ m}^2 \text{ g}^{-1}$ and pore volume of $0.53 \text{ cm}^3 \text{ g}^{-1}$, which increase to $2609 \text{ m}^2 \text{ g}^{-1}$ and $1.10 \text{ cm}^3 \text{ g}^{-1}$ for sample ACDS4800. For compacted samples. ACDS2700P has surface area and pore volume of $2051 \text{ m}^2 \text{ g}^{-1}$ and $0.87 \text{ cm}^3 \text{ g}^{-1}$, respectively, while the highest surface area obtained is for ACDS4800P at $2738 \text{ cm}^3 \text{ g}^{-1}$. In contrast to PO activation, increasing the activation temperature resulted in a reduction in the proportion of microporosity. The proportion of microporosity decrease from 80% for sample ACDS4700P to 65% for sample ACDS4800P. It is noteworthy that carbons synthesised with PO as an activating agent can achieve a very high proportion of microporosity. The highest surface area obtained for PO activation is $1767 \text{ m}^2 \text{ g}^{-1}$ for sample ACDS4800P(PO) and the highest surface obtained of KOH activation is $2738 \text{ m}^2 \text{ g}^{-1}$, and their proportion of microporosity is 95% and 65%, respectively. **Table 3** and **4** show that the proportion of microporosity for PO activating carbons is typically *ca.* 94% of surface area while for KOH activating carbons the proportion is between 65–93%.

Larger pores were found in KOH activated carbons may be attributable to the mechanism of activation. For KOH, the hydroxide reacts directly with C, even at a low temperature, generating carbonate. On the other hand, PO activation occurs *via* oxalate decomposition to the carbonate, followed by gasification reactions at high temperatures. The PO activation mechanism is as follows; In a temperature range of $500\text{--}600^\circ\text{C}$, PO decomposition occur as $\text{K}_2\text{C}_2\text{O}_4 \rightarrow \text{K}_2\text{CO}_3 + \text{CO}$. This is followed by a reaction between C within the precursor at 700°C , generating potassium

A Milder Non-Hydroxide Activation route for Activated Carbons

carbonate, which will result in the etching of C atoms (*i.e.* pore formation) according to the reaction $K_2CO_3 + 2C \rightarrow 2K + 3CO$.

Moreover, the potassium carbonate can also decompose according to the reaction $K_2CO_3 \rightarrow K_2O + CO_2$. The gases produced by carbonate decomposition result in pore formation in the precursor, followed by the reaction $C + CO_2 \rightarrow 2CO$ at temperatures above 700°C. This mechanism explains why PO is a mild activating agent compared to KOH. The mechanism also confirms that the activation temperature plays an essential role in determining the properties of carbon activated with PO while there is no significant effect of changing the amount of PO in the range of PO/ACDS ratio between 2 and 4. With this result, it is shown that using potassium oxalate as an activating agent allows for porosity control by simply changing the activation temperature and benefiting from being a less corrosive and toxic activating agent than KOH. It has been demonstrated that the specific surface area has an essential role in the adsorption of gases by activated carbon. However, adsorption of gases is a complex process that is also affected by factors other than the specific surface area, such as the pore size and surface functionality. The overall porosity trends that emerge from the PO and KOH comparison are that, at temperatures of 700–800°C, the former generates carbons with a surface area of up to ca. 1800 m² g⁻¹, whereas KOH activation achieves carbons with a surface area of up to 2700 m² g⁻¹. However, carbons with a higher proportion of micropore surface area, which is preferred for CO₂ uptake at low pressure, are generated with PO.

4.3.3 CO₂ uptake

The CO₂ uptake was measured at pressure range of 0–20 bar and 25 °C.

Figure 11 shows the CO₂ uptake isotherms for PO activated carbons and

Table 5 summarises the uptake at pressure of 0.15 bar, 1 bar, and 20 bar.

In addition, **Figure 12** and **Table 6** present the data for KOH activated carbons.

4.3.3.1 PO activated carbons

At pressure of 0.15–0.5, the CO₂ uptake of PO activated carbons ranged between 1.6–1.9 mmol g⁻¹ and 3.0–3.4 mmol g⁻¹, respectively. Sample ACDS4700(PO) has the highest CO₂ uptake at 0.15 bar of 1.9 mmol g⁻¹, and sample ACDS4800P(PO) has the highest CO₂ uptake at 0.50 bar of 3.4 mmol g⁻¹. As far as we know, this is the highest CO₂ uptake at 0.15 and 0.50 bar for any activated carbon prepared with PO as activating agent. It is apparent that at low pressure (0.15 to 0.5 bar), there is an increase in CO₂ uptake as the pore size decreases such that there is a proportionality between microporosity and CO₂ uptake. In this sense, the highest CO₂ uptake of 1.9 mmol g⁻¹, at 0.15 bar, is for sample ACDS4700(PO) with 97% of surface area arising from micropores. This trend applies to the fact that sample ACDS4800P(PO), which has the lowest CO₂ uptake of 1.6 mmol g⁻¹ also has the lowest proportion (80%) of surface area arising from micropores.

A Milder Non-Hydroxide Activation route for Activated Carbons

At 1 bar, which is often used as a measure of performance for post-combustion capture from flue gas streams from fossil fuel power stations,^{15,19} the CO₂ uptake ranged between 3.8–4.8 mmol g⁻¹. For the present samples, the CO₂ uptake at 1 bar rises significantly from 3.8 mmol g⁻¹ for the sample activated at 700°C to 4.8 mmol g⁻¹ for the sample activated at 800°C. This rise in CO₂ uptake despite an overall increase in surface area is due to the fact that PO activation retains extremely high microporosity even for activation at 800°C. This is further indication of the mild nature of PO activation compared to KOH.

At a higher pressure of 20 bar, CO₂ uptake is in the range of 6.4–11 mmol g⁻¹, where the highest uptake of 11 mmol g⁻¹ is for samples ACDS4800P(PO) and ACDS2800P(PO). It is clear to see that, at high pressure of 20 bar, the highest uptake is for sample ACDS4800P(PO), which has the highest surface area. This indicates that microporosity is more critical for low-pressure uptake than the total surface area except for scenarios where high microporosity is retained as surface area increases. The CO₂ uptake is clearly dependent on the total surface area rather than on the pore size at high pressure. The data supports the idea that CO₂ uptake at high pressure is determined by total surface area rather than pore size and that the CO₂ uptake at low pressure is dependent on the micropore surface area ^{15,30,35,42–44}.

A Milder Non-Hydroxide Activation route for Activated Carbons

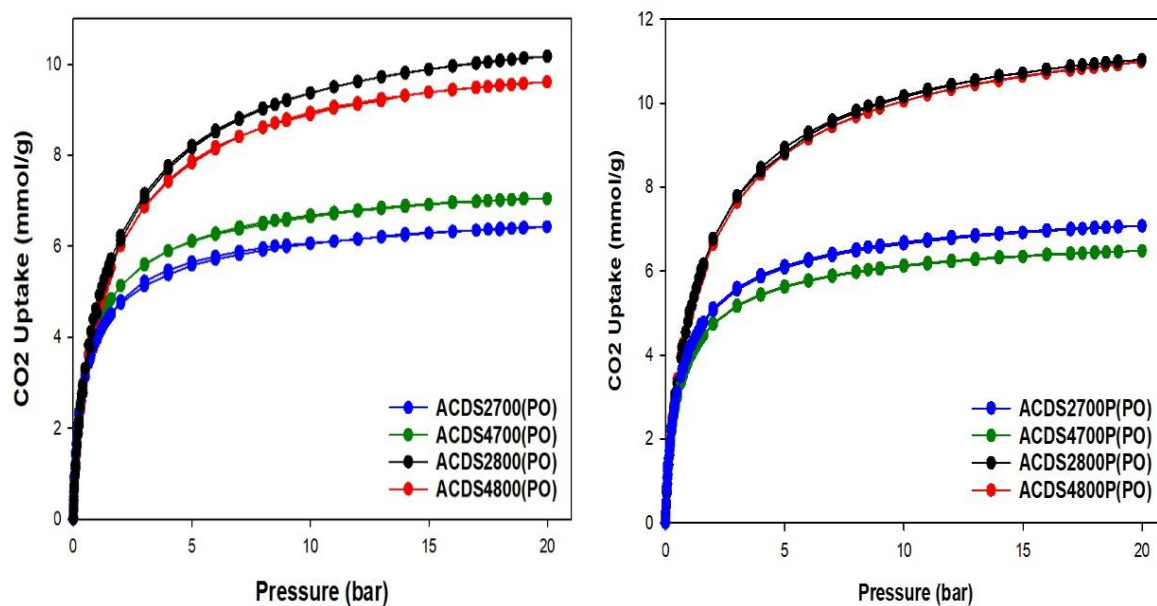


Figure 11 CO₂ uptake (mmol/g) isotherms of carbons activated at PO/ACDSratio of 2 or 4 as powder or pellet at 25 °C and 0-20 bar.

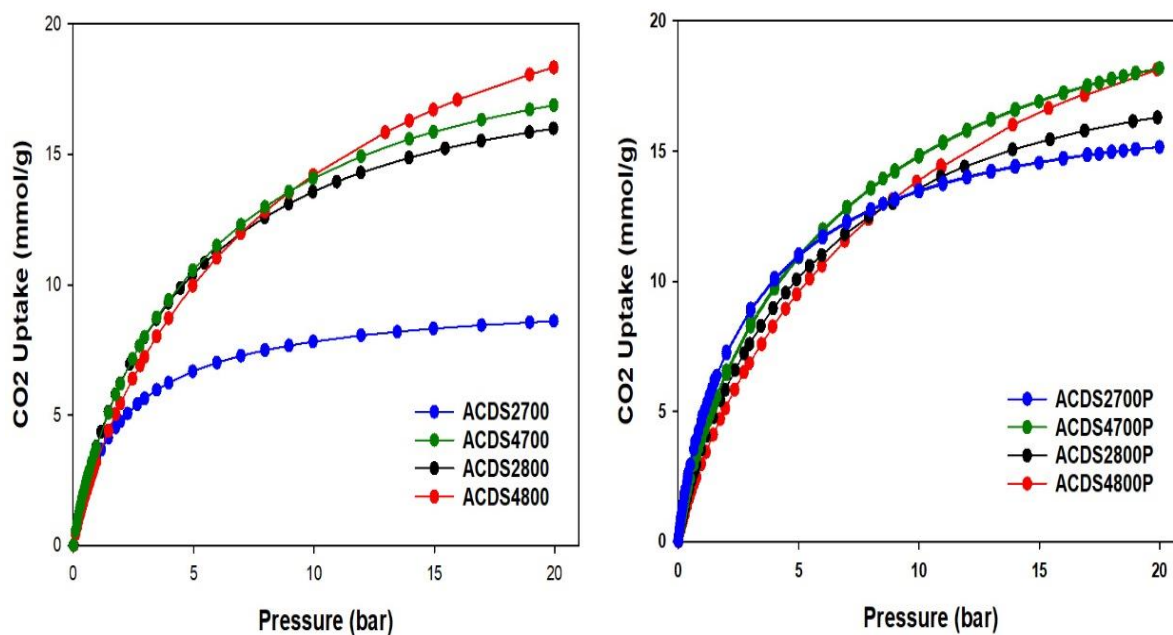


Figure 12 CO₂ uptake (mmol/g) isotherms of carbons activated at KOH/ACDS ratio of 2 or 4 as powder or pellet at 25 °C and 0-20 bar.

A Milder Non-Hydroxide Activation route for Activated Carbons

Table 5. CO₂ uptake at 25 °C and various pressures (i.e., 0.15 bar, 0.5 bar, 1 bar and 20 bar) for carbons activated at PO/ACDS ratio of 2 or 4 as powder or pellet.

Sample	0.15 bar	0.5 bar	1 bar	20 bar
ACDS2700(PO)	1.8	3.1	3.8	6.4
ACDS4700(PO)	1.9	3.2	4.1	7.0
ACDS2800(PO)	1.7	3.3	4.6	10
ACDS4800(PO)	1.6	3.1	4.6	9.5
ACDS2700P(PO)	1.7	3.1	4.0	7.0
ACDS4700P(PO)	1.7	3.0	3.8	6.5
ACDS2800P(PO)	1.6	3.3	4.8	11
ACDS4800P(PO)	1.7	3.4	4.8	11

Table 6. CO₂ uptake at 25 °C and various pressures (i.e., 0.15 bar, 0.5 bar, 1 bar and 20 bar) for carbons activated at KOH/ACDS ratio of 2 or 4 as powder or pellet.

Sample	0.15 bar	0.5 bar	1 bar	20 bar
ACDS2700	0.7	2.3	3.6	8.6
ACDS4700	0.8	2.3	3.7	16.8
ACDS2800	0.7	2.5	4.3	16.0
ACDS4800	0.7	1.9	3.2	18.3
ACDS2700P	1.2	2.8	4.5	15.0
ACDS4700P	0.1	2.4	3.8	18.0
ACDS2800P	0.7	2.3	4.5	16.2
ACDS4800P	0.6	1.9	3.5	18.0

A Milder Non-Hydroxide Activation route for Activated Carbons

Moreover, according to the uptake data in **Table 5**, there is no clear correlation between the amount of PO in activation and the CO₂ uptake of the samples. Therefore, changing the PO/ACDS ratio between 2 to 4 does not significantly affect the CO₂ uptake. For instance, the CO₂ uptake at 1 bar is 4.8 mmol g⁻¹ for both samples ACDS2800P(PO) and ACDS4800P(PO). Additionally, the CO₂ uptake at 20 bar is 11 mmol g⁻¹ for both samples ACDS2800P(PO) and ACDS4800P(PO) and is very similar (9.5 - 10 mmol g⁻¹) for sample ACDS2800(PO) and ACDS4800(PO). This means that there is no need to use the higher amount of PO as a means to optimising the CO₂ uptake. Use of lower amounts of PO is attractive as it reduces the costs of activation thus making the process more sustainable. This is in addition to the milder nature (in terms of corrosion) of PO activation, which will translate to lower costs with respect to equipment maintenance. In contrast, the activation temperature has an essential role in determining the CO₂ uptake. Higher activation temperature does in some cases translate to greater CO₂ uptake especially at pressures above 1 bar. In a sense, the activation temperature can be used to tailor the porosity of the PO activated carbons so as to target optimised CO₂ uptake at low or high pressure. The uptake data shows that the highest CO₂ uptake at 0.5, 1 and 20 bar was for samples activated at the higher temperature of 800°C, which is consistent with previous studies.^{21,36,40,45-49} In this regard, temperature variations combined with a meagre PO/ACDS ratio of 2 can be employed to synthesise a suite of carbons with a wide range of porosity. In this scenario, a more ecologically friendly and sustainable activation

A Milder Non-Hydroxide Activation route for Activated Carbons

procedure is allowed, along with easier porosity control, by adjusting the activation temperature.

4.3.3.2 KOH activated carbons

The CO₂ uptake isotherms of KOH activated carbons are shown in **Figure 12**, and the uptake at 0.15, 0.50, 1 bar and 20 bar are summarised in **Table 6**. The CO₂ uptake at 1 bar, which is commonly used as a metric for post-combustion capture from flue gas streams from fossil fuel power stations,^{15,19} is in the range of 3.5–4.5 mmol g⁻¹. Sample ACDS2700P has the highest uptake of 4.5 mmol g⁻¹. Similarly to PO activating carbons, this sample with the highest CO₂ uptake at 1 bar, has the highest proportion of surface area arising from micropores at 90%. Sample ACDS4800P has the least microporosity (65%), and the lowest CO₂ uptake of 3.5 mmol g⁻¹.

At lower pressures of 0.15 and 0.5 bar, the highest CO₂ uptake is for the ACDS2700P at 1.2 and 2.8 mmol g⁻¹, respectively. As mentioned above, this sample has the high level of microporosity.

In contrast, the lowest CO₂ uptake of 0.6 mmol g⁻¹ was for ACDS4800P, with 65% of surface area arising from micropores.

Unlike PO activation, for uptake at 20 bar, changing the KOH/ACDS ratio from 2 to 4 does improve the CO₂ uptake, as the uptake increased from 8.6 mmol g⁻¹ to 16.8 mmol g⁻¹ for samples ACDS2700 and ACDS4700, respectively. Therefore, the larger the specific surface area, the higher the adsorption capacity. For example, the highest CO₂ uptake of 18 mmol g⁻¹ is

A Milder Non-Hydroxide Activation route for Activated Carbons

for samples with a higher surface area $\leq 2400 \text{ m}^2 \text{ g}^{-1}$, which is consistent with previous studies using other forms of activation.^{18,41,42,50-52}

By comparing CO_2 uptake levels at low pressure between KOH and PO activation, we observed that PO activation has the advantage of generating activated carbons with high microporosity and high CO_2 uptake at low relative pressure. PO activation generates carbons with higher CO_2 uptake of 1.9, 3.4 and 4.8 mmol g^{-1} compared to 1.2, 2.8 and 4.5 mmol g^{-1} for KOH activation at 0.15, 0.50 and 1 bar, respectively. In contrast, at 20 bar, KOH activation generated carbons with higher CO_2 uptake of up to 18.3 mmol g^{-1} compared to 11 mmol g^{-1} for PO activation.

This result is in line with previous studies in which low pressure CO_2 uptake was increased by the presence of small pores.^{7,15,53} In contrast, the lowest CO_2 uptake of 0.6 mmol g^{-1} is for sample ACDS4800P with the lowest proportion (65%) of microporosity. On the other hand, it is clear that the surface area has a vital role in determining uptake for KOH activated carbons. Thus, the larger the specific surface area, the higher the adsorption capacity at 20 bar. The highest CO_2 uptake of 18 mmol g^{-1} was obtained for the sample with a high surface area $\leq 2400 \text{ m}^2 \text{ g}^{-1}$. It has also been reported that, for KOH activation, a large specific surface area usually indicates a high adsorption capacity for most activated carbon.^{30,50,54-56} However, surface area of only up to $1767 \text{ m}^2 \text{ g}^{-1}$ for activation at 800°C are achieved with PO activation, meaning that the CO_2 uptake of PO activated carbons at 20 bar is limited. However, at 1 bar, the PO activation has the advantages over KOH activation. The highest CO_2 uptake at 1 bar

A Milder Non-Hydroxide Activation route for Activated Carbons

is 4.8 mmol g^{-1} , as shown by sample ACDS2700P(PO), which is higher than that for KOH activation carbon.⁵⁷ In addition to this characteristic, the current PO activated carbons benefit from being simple to optimise pore size without considering the amount of activator used. According to the data discussed above, PO appears to be a promising and effective activating agent for creating activated carbons from ACDS with a high micropore surface area and high CO_2 uptake at low pressure.

4.4 Conclusion

We have demonstrated that a less corrosive and toxic activating agent, potassium oxalate (PO), may be used to produce activated carbons from a recently discovered precursor, date seed-derived ACDS, in a targeted manner. By carefully choosing activation conditions it is possible to obtain highly microporous activated carbons through PO activation with surface areas up to $1747 \text{ m}^2 \text{ g}^{-1}$ and pore volumes up to $0.75 \text{ cm}^3 \text{ g}^{-1}$ with up to 93% of surface area arising from micropores.

At temperatures of $700\text{--}800^\circ\text{C}$, the surface area of PO activated carbons is limited to below $1800 \text{ m}^2 \text{ g}^{-1}$, while carbons with surface area of up to $2700 \text{ m}^2 \text{ g}^{-1}$ may be obtained under similar activation conditions from KOH activation. However, due to the high micropore surface area, carbons with high CO_2 uptake at low pressure (*i.e.* post-combustion CO_2 capture conditions) are generated by PO activation. At 25°C , the PO activated carbons capture up to 1.9 and 4.8 mmol g^{-1} of CO_2 at 0.15 bar and 1 bar, respectively. On the other hand, KOH activated carbons have higher CO_2

A Milder Non-Hydroxide Activation route for Activated Carbons

uptake at 20 bar (18.3 mmol g^{-1}) due to their higher surface area of up to $2738 \text{ m}^2 \text{ g}^{-1}$. At $25 \text{ }^\circ\text{C}$, up to 1.2 mmol g^{-1} and 4.5 mmol g^{-1} of CO_2 can be stored by KOH activated carbons compared to 1.8 and 4.8 mmol g^{-1} for PO activation carbons at pressure of 0.15 bar and 1 bar , respectively.

Unlike what is observed for KOH activation, changes in the PO/ACDS ratio, from 2 to 4, has no significant influence on the porosity of the PO activated carbons. In contrast, the activation temperature is the most critical variable in controlling the porosity of the PO activated carbons. As a result, a meagre PO/ACDS ratio of 2 can be used, coupled with temperature changes, to synthesise a suite of carbons with the whole porosity range. In terms of the required amount of activating agent, a more environmentally friendly and sustainable activation process and easier porosity control are enabled by this scenario of modifying only the activation temperature.

References

- 1 M. Molina-Sabio, M. T. González, F. Rodríguez-Reinoso and A. Sepúlveda-Escribano, *Carbon N. Y.*, 1996, **34**, 505–509.
- 2 M. C. Bohm, H. J. Herzog, J. E. Parsons and R. C. Sekar, *Int. J. Greenh. Gas Control*, 2007, **1**, 113–120.
- 3 M. Sevilla and A. B. Fuertes, *Energy Environ. Sci.*, 2011, **4**, 1765–1771.
- 4 D. Y. C. Leung, G. Caramanna and M. M. Maroto-Valer, *Renew. Sustain. Energy Rev.*, 2014, **39**, 426–443.
- 5 H. Mikulčić, J. J. Klemeš, M. Vujanović, K. Urbaniec and N. Duić, *J. Clean. Prod.*, 2016, **136**, 119–132.
- 6 G. Aguilar-Armenta, G. Hernandez-Ramirez, E. Flores-Loyola, A. Ugarte-Castaneda, R. Silva-Gonzalez, C. Tabares-Munoz, A. Jimenez-Lopez and E. Rodriguez-Castellon, *J. Phys. Chem. B*, 2001, **105**, 1313–1319.
- 7 H. Yang, Z. Xu, M. Fan, R. Gupta, R. B. Slimane, A. E. Bland and I. Wright, *J. Environ. Sci.*, 2008, **20**, 14–27.
- 8 J. Alvarez, G. Lopez, M. Amutio, J. Bilbao and M. Olazar, *Ind. Eng. Chem. Res.*, 2015, **54**, 7241–7250.
- 9 I. Wróbel-Iwaniec, N. Díez and G. Gryglewicz, *Int. J. Hydrogen Energy*, 2015, **40**, 5788–5796.
- 10 N. Soltani, A. Bahrami, M. I. Pech-Canul and L. A. González, *Chem.*

A Milder Non-Hydroxide Activation route for Activated Carbons

- Eng. J.*, 2015, **264**, 899–935.
- 11 J. H. Lee, Y. J. Heo and S. J. Park, *Int. J. Hydrogen Energy*, 2018, **3**, 22377–22384.
 - 12 T. S. Blankenship and R. Mokaya, *Energy Environ. Sci.*, 2017, **10**, 2552–2562.
 - 13 M. Sevilla and R. Mokaya, *Energy Environ. Sci.*, 2014, **7**, 1250–1280.
 - 14 M. M. Johns, W. E. Marshall and C. A. Toles, *J. Chem. Technol. Biotechnol.*, 1999, **74**, 1037–1044.
 - 15 A. M. Aljumialy and R. Mokaya, *Mater. Adv.*, 2020, **1**, 3267–3280.
 - 16 M. Sevilla and A. B. Fuertes, *Energy Environ. Sci.*, 2011, **4**, 1765–1771.
 - 17 M. M. Titirici, R. J. White, C. Falco and M. Sevilla, *Energy Environ. Sci.*, 2012, **5**, 6796–6822.
 - 18 W. Sangchoom and R. Mokaya, *ACS Sustain. Chem. Eng.*, 2015, **3**, 1658–1667.
 - 19 H. M. Coromina, D. A. Walsh and R. Mokaya, *J. Mater. Chem. A*, 2016, **4**, 280–289.
 - 20 C. Robertson and R. Mokaya, *Microporous Mesoporous Mater.*, 2013, **179**, 151–156.
 - 21 E. A. Hirst, A. Taylor and R. Mokaya, *J. Mater. Chem. A*, 2018, **6**, 12393–12403.

A Milder Non-Hydroxide Activation route for Activated Carbons

- 22 M. K. B. Gratuito, T. Panyathanmaporn, R. A. Chumnanklang, N. Sirinuntawittaya and A. Dutta, *Bioresour. Technol.*, 2008, **99**, 4887–4895.
- 23 D. Kalderis, S. Bethanis, P. Paraskeva and E. Diamadopoulos, *Bioresour. Technol.*, 2008, **99**, 6809–6816.
- 24 A. Altwala and R. Mokaya, *Energy Environ. Sci.*, 2020, **13**, 2967–2978.
- 25 M. Sevilla and A. B. Fuertes, *Carbon N. Y.*, 2009, **47**, 2281–2289.
- 26 M. M. Titirici and M. Antonietti, *Chem. Soc. Rev.*, 2010, **39**, 103–116.
- 27 M. Paneque, J. M. De la Rosa, J. Kern, M. T. Reza and H. Knicker, *J. Anal. Appl. Pyrolysis*, 2017, **128**, 314–323.
- 28 S. Hameed, A. Sharma, V. Pareek, H. Wu and Y. Yu, *Biomass and Bioenergy*, 2019, **123**, 104–122.
- 29 C. Quan, A. Li and N. Gao, *Procedia Environ. Sci.*, 2013, **18**, 776–782.
- 30 N. Balahmar, A. C. Mitchell and R. Mokaya, *Adv. Energy Mater.*, 2015, **5**, 1–9.
- 31 C. R. Lohri, H. M. Rajabu, D. J. Sweeney and C. Zurbrügg, *Renew. Sustain. Energy Rev.*, 2016, **59**, 1514–1530.
- 32 J. F. González, J. M. Encinar, C. M. González-García, E. Sabio, A. Ramiro, J. L. Canito and J. Gañán, *Appl. Surf. Sci.*, 2006, **252**, 5999–6004.
- 33 E. Haffner-Staton, N. Balahmar and R. Mokaya, *J. Mater. Chem. A*,

A Milder Non-Hydroxide Activation route for Activated Carbons

- 2016, **4**, 13324–13335.
- 34 Z. Hu, M. P. Srinivasan and Y. Ni, *Carbon N. Y.*, 2001, **39**, 877–886.
- 35 B. Adeniran, E. Masika and R. Mokaya, *J. Mater. Chem. A*, 2014, **2**, 14696–14710.
- 36 Y. D. Chen, W. Q. Chen, B. Huang and M. J. Huang, *Chem. Eng. Res. Des.*, 2013, **91**, 1783–1789.
- 37 J. Wang, A. Heerwig, M. R. Lohe, M. Oschatz, L. Borchardt and S. Kaskel, *J. Mater. Chem.*, 2012, **22**, 13911–13913.
- 38 L. Zhang, J. Zhang, H. Fu, H. Zhang, H. Liu, Y. Wan, S. Zheng and Z. Xu, *Microporous Mesoporous Mater.*, 2018, **260**, 59–69.
- 39 Z. Zhang, J. Zhou, W. Xing, Q. Xue, Z. Yan, S. Zhuo and S. Z. Qiao, *Phys. Chem. Chem. Phys.*, 2013, **15**, 2523–2529.
- 40 J. Ludwinowicz and M. Jaroniec, *Carbon N. Y.*, 2015, **82**, 297–303.
- 41 J. Wang and S. Kaskel, *J. Mater. Chem.*, 2012, **22**, 23710–23725.
- 42 D. Lozano-Castelló, D. Cazorla-Amorós and A. Linares-Solano, *Energy and Fuels*, 2002, **16**, 1321–1328.
- 43 S. Liu, R. Ma, X. Hu, L. Wang, X. Wang, M. Radosz and M. Fan, *Ind. Eng. Chem. Res.*, 2020, **59**, 7046–7053.
- 44 L. Estevez, D. Barpaga, J. Zheng, S. Sabale, R. L. Patel, J. G. Zhang, B. P. McGrail and R. K. Motkuri, *Ind. Eng. Chem. Res.*, 2018, **57**, 1262–1268.

A Milder Non-Hydroxide Activation route for Activated Carbons

- 45 M. Sevilla, G. A. Ferrero and A. B. Fuertes, *Carbon N. Y.*, 2017, **114**, 50–58.
- 46 H. Lin, C. Xu, Q. Wang, J. Wu, Y. Wang, Y. Zhang and G. Fan, *Int. J. Hydrogen Energy*, 2019, **44**, 21527–21535.
- 47 M. Sevilla, G. A. Ferrero and A. B. Fuertes, *Chem. Mater.*, 2017, **29**, 6900–6907.
- 48 J. S. Wei, S. Wan, P. Zhang, H. Ding, X. B. Chen, H. M. Xiong, S. Gao and X. Wei, *New J. Chem.*, 2018, **42**, 6763–6769.
- 49 J. Li, Q. Jiang, L. Wei, L. Zhong and X. Wang, *J. Mater. Chem. A*, 2020, **8**, 1469–1479.
- 50 T. Ramesh, N. Rajalakshmi and K. S. Dhathathreyan, *J. Energy Storage*, 2015, **4**, 89–95.
- 51 J. Wang and S. Kaskel, *J. Mater. Chem.*, 2012, **22**, 23710–23725.
- 52 M. Sevilla, W. Sangchoom, N. Balahmar, A. B. Fuertes and R. Mokaya, *ACS Sustain. Chem. Eng.*, 2016, **4**, 4710–4716.
- 53 A. Ghorbani, H. R. Rahimpour, Y. Ghasemi, S. Zoughi and M. R. Rahimpour, *Renew. Sustain. Energy Rev.*, 2014, **35**, 73–100.
- 54 A. Ganesan and M. M. Shaijumon, *Microporous Mesoporous Mater.*, 2016, **220**, 21–27.
- 55 M. G. Plaza, A. S. González, C. Pevida, J. J. Pis and F. Rubiera, *Appl. Energy*, 2012, **99**, 272–279.
- 56 A. S. Ali, *Application of Nanomaterials in Environmental Improvement*,

A Milder Non-Hydroxide Activation route for Activated Carbons

1989, vol. 32.

- 57 N. Balahmar, A. S. Al-Jumialy and R. Mokaya, *J. Mater. Chem. A*, 2017, **5**, 12330–12339.

Chapter 5. Direct and mild non-hydroxide activation of biomass to carbons with enhanced CO₂ storage capacity

Abstract

Potassium oxalate (PO) was trialled as a non-corrosive and less toxic activating agent for the direct activation of biomass (sawdust, SD). The PO+SD mixtures were activated either in powder form or after compaction into pellets. The resulting activated carbons are highly microporous with surface area in the range of 550 to 2100 m² g⁻¹ and pore volume between 0.3 and 1.0 cm³ g⁻¹. The porosity of the directly activated and compactivated carbons is similar to that of conventionally activated (via hydrothermal carbonisation) equivalents. In general, pelletized (i.e., compactivated) carbons achieved higher levels of porosity for any identical set (with respect to amount of PO and temperature) of preparation conditions. Unlike hydroxide activation, the amount of PO used, for PO/SD mass ratio between 2 and 4, does not have a significant effect on porosity. On the other hand, the activation temperature plays a critical role in determining the textural properties at any given PO/SD ratio. The porosity of the carbons is dominated by pores of size 6 – 8 Å, which are suitable for post-combustion (low pressure) CO₂ storage. At 25 °C, the carbons capture up to 1.6 and 4.3 mmol g⁻¹ of CO₂ at 0.15 bar and 1 bar, respectively. Our findings show that the use of potassium oxalate as a mild activating agent

Direct and mild non-hydroxide activation of biomass to carbons with enhanced CO₂ storage capacity

via direct activation succeeds in addressing the need for non-corrosive and less toxic activators and also negates the need for hydrothermal treatment or pyrolysis of biomass prior to activation. The present carbons are attractive as sustainable energy materials especially for post-combustion CO₂ capture and storage.

5.1 Introduction

Meeting the demand of low cost and environmentally friendly energy storage methods and avoiding the emission of environmental pollutants in mobile and portal applications remains a challenge. To meet this challenge, new materials with properties targeted at specific applications are required. One such target is the storage of gases, such as H₂, CO₂ and CH₄, which are relevant to energy production or environmental remediation. In this regard, porous solids are amongst the most studied materials for use in gas storage applications.¹⁻⁴ One area of recent research on gas storage has focused on obtaining activated carbons from biomass, which is considered to be an environmentally sustainable source, is cheap and readily available.⁵⁻⁷ There are two main routes for generating activated carbon from biomass, namely physical or chemical activation.⁷ Physical activation is via high temperature thermal treatment of biomass in the presence of oxidising gases such as air, O₂, CO₂ and steam. Chemical activation, on the other hand, utilises activating agents such as KOH, H₃PO₄, ZnCl₂ and NaOH as porogens for generating porosity in carbonaceous matter at medium to

Direct and mild non-hydroxide activation of biomass to carbons with enhanced CO₂ storage capacity

high temperature. KOH, via so-called hydroxide activation, is one of the most extensively explored activating agents for activated carbons. However, it has disadvantages due to the toxicity and corrosive nature of the KOH. Milder activating agents that offer carbons with similar or better textural qualities are therefore highly sought after. Therefore, beyond hydroxide activation, there is growing interest in the use of less corrosive and toxic activating agents.⁸⁻¹⁷ A number of studies have reported the use of potassium oxalate (PO) as activating agent for carbons with low to medium surface area (typically <1500 m² g⁻¹) for activation at 800 °C or below.⁸⁻¹⁷

Another important consideration is that, for new activated carbons to be of interest, they should fall into one of the following categories: have new or improved properties, be easy/cheap to prepare, and be sustainable. Lower cost/easier to prepare materials typically result from a reduction in the number of fabrication steps required. Biomass is normally activated after the process of hydrothermal carbonisation (HTC) or pyrolysis, which converts the biomass into carbon-rich carbonaceous matter. Hydrothermal carbonisation involves (typically at 180-300 °C) in water under pressure to enable thermochemical decomposition of biomass to carbon-rich carbonaceous matter.¹⁸⁻²¹ The pyrolysis process, on the other hand, involves generation of carbonaceous matter via enrichment of carbon content during thermal treatment at temperatures of 600-900 °C under oxygen-free conditions.²²⁻²⁸ Our groups have recently explored a direct and cheaper route to KOH activated biomass-derived carbons, which excluded

Direct and mild non-hydroxide activation of biomass to carbons with enhanced CO₂ storage capacity

the need for HTC or pyrolysis prior to activation.²⁹ Recently, they have also reported on the process of compactation, also known as mechanochemical activation, wherein mixtures of the precursor and KOH are compacted into pellets prior to activation.³⁰ Given that the activation process is initially based on solid-solid interaction between the activating agent and the precursor, the compactation method was developed with the aim of increasing proximity (solid-solid contacts) between the precursor and KOH.^{28,30} The desired outcome of compactation is to improve the efficiency of the KOH with respect to the porosity generated. It is now known that compactation with KOH can generate carbons with higher (compared to conventional powder activation) surface area and pore volume.^{28,30} However, so far, compactation has only been explored for KOH activation, and has not been performed for direct activation of raw biomass.

In this chapter, we explore the use of PO for the direct activation and compactation of raw biomass (sawdust). This approach potentially offers several advantages that have, so far, not been probed in any one study, namely (i) use of a milder non-hydroxide activating agent, (ii) direct activation of biomass that negates the need for HTC or pyrolysis, and (iii) porosity modulation and optimisation (with respect to amount of activating agent) via the compactation route. Overall, therefore, this approach offers a direct process that is simpler, cheaper, and more sustainable. Importantly, it is necessary that these advantages not compromise the porosity of the resulting carbons, i.e., the carbons should have similar

Direct and mild non-hydroxide activation of biomass to carbons with enhanced CO₂ storage capacity

properties to analogous carbons prepared via conventional methods. Based on the porosity of the resulting activated and compacted carbons, we investigated their CO₂ uptake and show that they offer very attractive trends especially for low-pressure (post-combustion) uptake.

5.2 Experimental section

5.2.1 Material synthesis

Raw sawdust was sieved using 212 MC sieves to obtain homogenous powder. Potassium oxalate (PO) was ground into a fine powder and thoroughly mixed with the sawdust (SD) at PO/SD mass ratio of 2 or 4. Half of the PO/SD mixture was compacted for 10 min at a load of 10 tonnes in a 1.3 cm diameter die (equivalent to a compression pressure of 740 MPa) prior to activation. The light brown PO/SD mixtures (powders or pellets) were then loaded on alumina boats and then placed in a furnace and heated, at ramp rate of 5 °C min⁻¹, to 600, 700 or 800 °C under a flow of nitrogen. Samples were held at the target temperature for 1 h before being cooled to room temperature, whilst still under a flow of nitrogen. The resulting black matter was washed with 20 wt% HCl at ambient temperature to remove any inorganic species. The mixtures were then washed with deionised water until neutral pH was achieved for the filtrate, and dried in an oven. The activated carbons were denoted as DSDxT or DSDxTP where x is the PO/SD ratio (2 or 4) and T is the activation

Direct and mild non-hydroxide activation of biomass to carbons with enhanced CO₂ storage capacity

temperature (600, 700 or 800 °C), and P denotes compaction (i.e., palletisation) prior to activation. Thus, a powder sample activated at a PO/SD ratio of 4 and 700 °C is designated as DSD4700, while a compactivated sample prepared at a PO/SD ratio of 4 and 700 °C is designated as DSD4700P.

5.2.2 Characterization methods

Thermogravimetric analysis (TGA) was performed using a TA Instruments Discovery analyser or TA Instruments SDT Q600 analyser under flowing air conditions (100 mL/min). A PANalytical X'Pert PRO diffractometer was used to perform powder XRD analysis using Cu-K α radiation (40 kV, 40 mA) with step size of 0.02° and 50 s time step. Elemental, CHN, analysis was performed on an Exeter Analytical CE-440 Elemental Analyser. Nitrogen sorption (at -196 °C) with a Micromeritics 3FLEX sorptometer was used for porosity analysis and to determine textural properties. Prior to analysis, the carbon samples were degassed under vacuum at 200 °C for 12 h. Surface area was calculated using the Brunauer-Emmett-Teller (BET) method applied to adsorption data according to Roquerol rules, in the relative pressure (P/P_0) range of 0.02 – 0.22, and pore volume was estimated from the total nitrogen uptake at close to saturation pressure ($P/P_0 \approx 0.99$). The micropore surface area and micropore volume were determined via t -plot analysis. The pore size distribution was determined using Non-Local Density Functional Theory (NL-DFT) applied to nitrogen adsorption data. Scanning

Direct and mild non-hydroxide activation of biomass to carbons with enhanced CO₂ storage capacity

electron microscopy (SEM) images were recorded using an FEI Quanta200 microscope, operating at a 5 kV accelerating voltage.

5.2.3 CO₂ uptake measurements

CO₂ uptake was determined using a Hiden Isochema XEMIS instrument at 25 °C and pressure of up to 20 bar. The carbons were outgassed for 3 h under vacuum at 240 °C prior to performing the CO₂ uptake measurements.

5.3 Results and Discussion

5.3.1 Yield, nature and elemental composition of activated and compactivated carbons

This study explored the direct activation of biomass using a mild non-hydroxide activating agent with the aim of simplifying the activation process and making it more sustainable by moving away from some of the challenges associated with the corrosive nature of KOH activation. This work is the first time that direct activation of biomass, i.e., without the need for HTC or pyrolysis has been attempted with a mild activating agent. Furthermore, compactivated carbons were also prepared to explore any benefits of compaction of the PO/SD mixture prior to thermal activation. The elemental composition of the sawdust and the activated carbon yields, and the yields of the direct activation or direct compactivation are given in **Table 1**. The yield of activated (i.e., powder) samples ranges from 22% to

Direct and mild non-hydroxide activation of biomass to carbons with enhanced CO₂ storage capacity

28% while for compacted (i.e. pelletised) samples it is between 20% and 34%. It is important to note that the reported yields are with respect to the raw sawdust. This differs from most activated carbon yields in the literature that are typically reported with respect to carbonised matter derived from biomass via HTC or pyrolysis. This is an important distinction as conversion of raw biomass to carbonaceous matter (via HTC or pyrolysis) has a typical yield of between 30% and 45%. Previous studies have shown that the activated carbon yield from PO activation of sawdust hydrochar (i.e., after HTC) varied as follows; 35% (800 °C), 40% (700 °C) and 44% (600 °C).¹⁰ This means that the yield of activated carbon with respect to the raw sawdust was at most (assuming 45% yield for HTC) 16% (800 °C), 18% (700 °C) and 20% (600 °C).¹⁰ Thus, the data in **Table 1** indicates that at any given temperature, the activated carbon yields for the direct PO activation of sawdust is higher than what is achieved via HTC. This greater yield, which is higher by nearly 50% at 600 °C, appears to be a general advantage of direct activation and has also been previously observed for KOH activated carbons.²⁹

For the present direct activation process, it is noteworthy that compaction of the PO/SD mixtures before activation (i.e., activation of pelletized mixtures) generates generally similar yields to activation of powder mixtures. Compaction of the PO/SD mixture is expected to engender closer contact between the PO and SD particles and under any given activation conditions (i.e., amount of PO and temperature) should lead to greater levels of activation and therefore lower activated carbon

Direct and mild non-hydroxide activation of biomass to carbons with enhanced CO₂ storage capacity

yields. Such a trend is now well established for KOH activation; in effect, compactions acts to improve the efficient use of KOH.^{24,28,30} The fact that the trend is not observed here for PO activation suggests that, unlike for hydroxide activation where the amount of KOH is critical, the PO/SD ratio is not a critical factor in determining the level or extent of activation. It is clear from the data in **Table 1** that, in general, only the activation temperature determines the carbon yield; change of PO/SD ratio from 2 to 4 at any given temperature does not appear to have any significant effect on the carbon yield. On the other hand, higher activation temperatures lead to a lowering of carbon yield.

Table 1. Yield and elemental composition of carbons directly activated or compacted from sawdust at 600, 700 or 800 °C, and PO/sawdust ratio of 2 or 4.

Sample	Yield [wt%]	C [%]	H[%]	N[%]	O[%]
Sawdust		47.0	5.6	0.4	47.0
DSD2600	28	71.3	1.0	0.5	27.2
DSD2700	28	65.6	1.1	0.2	33.1
DSD2800	22	65.5	0	0	34.5
DSD4600	28	65.5	0.5	0.3	33.7
DSD4700	26	71.5	0.7	0.2	27.6
DSD4800	22	72.5	0.1	0	27.4
DSD2600P	34	75.0	1.2	0.6	23.2
DSD2700P	20	73.0	0.8	0.2	26.0
DSD2800P	20	80.0	0.5	0.0	19.5
DSD4600P	30	72.0	0.5	0.5	27.0
DSD4700P	26	76.5	1.3	0.7	21.5
DSD4800P	20	86.0	0.1	0.1	13.8

Direct and mild non-hydroxide activation of biomass to carbons with enhanced CO₂ storage capacity

As expected, following activation, the carbon content (given as wt%) increases from 47% for the sawdust to a high of 86% for the sample compacted at 800 °C (DSD4800P). The effect of activation temperature is such that *carbons activated* at the highest temperature (800 °C) have the most elemental C content (72.5% and 86% for powder and compacted samples, respectively). In general, compacted carbons have higher C content compared to powder samples under any given activation conditions. The content of N, H and O decreases at higher activation temperature, which is the expected trend at higher levels of activation.

Figure 1 shows thermogravimetric analysis of the activated carbons, under flowing air conditions, was performed in order to assess the carbon purity (i.e., lack of inorganic matter) and thermal stability. The TGA curves (**Figure 1**) show a large mass loss between 450 and 650 °C due to carbon combustion, with an initial mass loss below 120 °C due to water removal. The TGA curves show that the residual mass, after heating in air at 800 °C, is typically lower than 5 wt%, which indicates that the activated carbons are generally free of inorganic residues. Samples activated at 600 °C have maximum burn-off at 500 °C compared to up to 650 °C for carbons activated at 800 °C, which exemplifies the effect of activation temperature on thermal stability. Higher activation temperatures results in greater thermal stability in the activated carbons, which is consistent with previous observations.³¹⁻³⁷

Direct and mild non-hydroxide activation of biomass to carbons with enhanced CO₂ storage capacity

The powder XRD patterns of the activated carbons (**Figure 2**) show that the amount of PO does not have any significant effect on the nature of the carbons – the XRD patterns of representative samples suggest a comparable level of graphitic ordering at any given activation temperature. The XRD patterns have very broad peaks at $2\theta = 26^\circ$ and 43° , which correspond to a very weakly graphitic/turbostratic nature in the carbons. The XRD patterns of carbons activated at higher temperature show a very weak peak, which indicates greater disruption of any graphitic ordering. Given that higher activation temperature leads to more thermally stable activated carbons, the 'disruption' of graphitisation as evidenced by the XRD patterns may be more to do with decrease in size of 'graphitic' domains rather than actual overall lowering of the level of graphitisation. The XRD patterns of some of the activated carbons exhibit sharp peaks, which could indicate the presence of inorganic residues left over by the activating agent. However, the TGA curves suggest that the presence of any inorganic impurities occurs only at a minor level.^{16,18-20}

Direct and mild non-hydroxide activation of biomass to carbons with enhanced CO₂ storage capacity

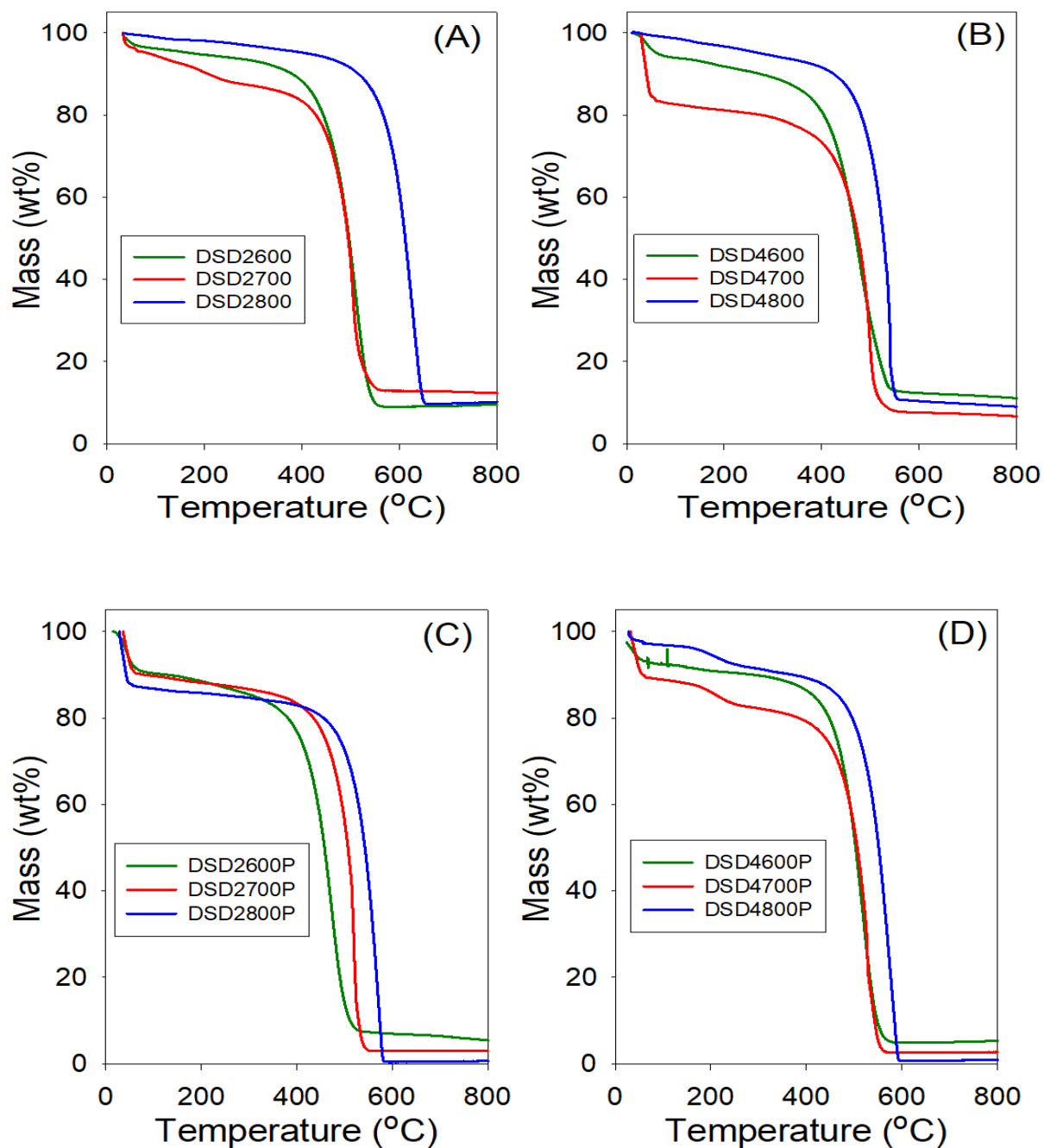


Figure 1. Thermogravimetric analysis (TGA) curves of carbons directly activated (A and B) or compactivated (C and D) from sawdust (SD) at 600, 700 or 800 °C, and PO/SD ratio of 2 (A and C) or 4 (B and D).

Direct and mild non-hydroxide activation of biomass to carbons with enhanced CO₂ storage capacity

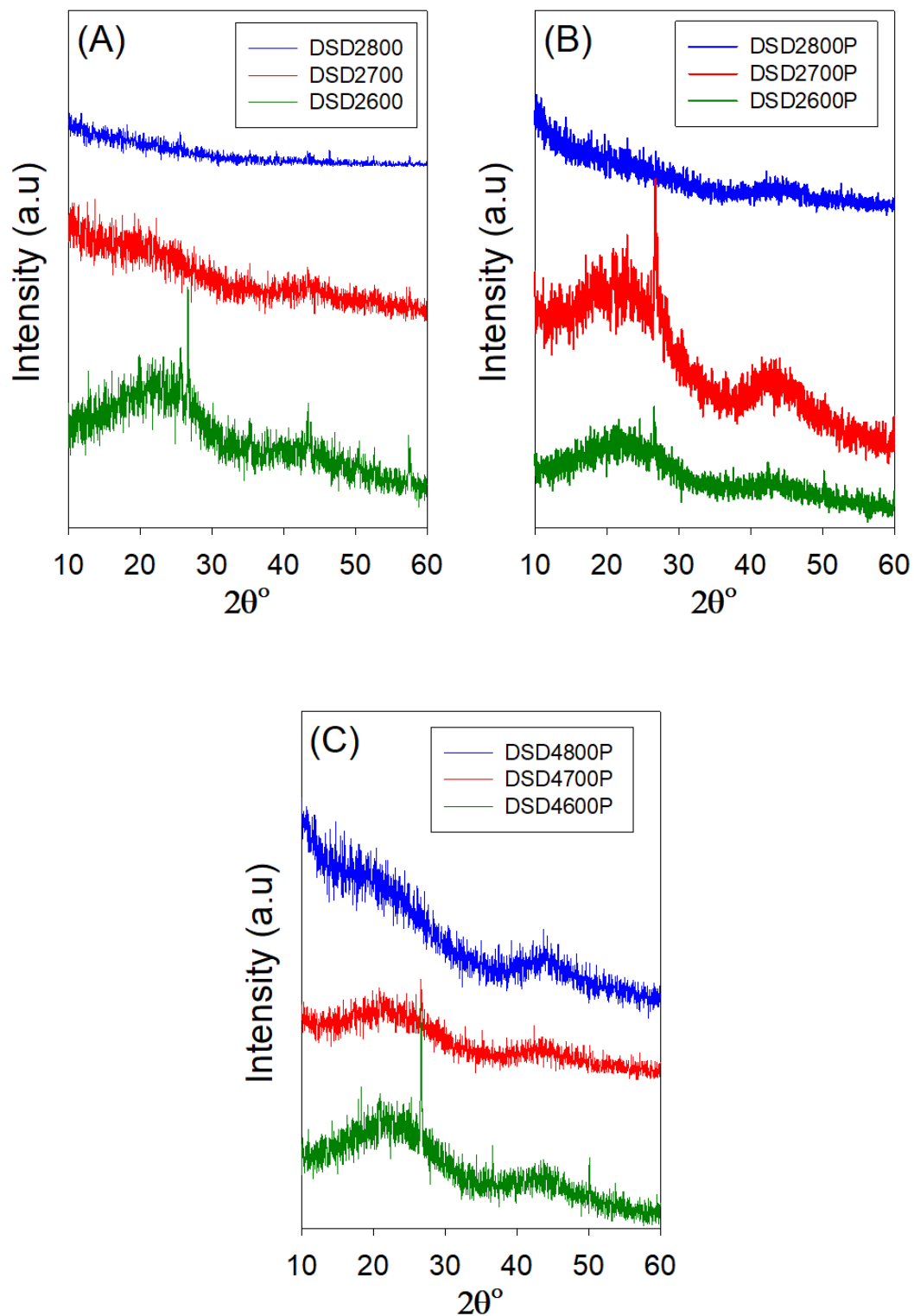


Figure 2. Powder XRD patterns of carbons directly activated (A) or compactivated (B and C) from sawdust (SD) at 600, 700 or 800 °C, and PO/SD ratio of 2 (A and B) or 4 (C).

Direct and mild non-hydroxide activation of biomass to carbons with enhanced CO₂ storage capacity

Scanning electron microscopy was used to probe the morphology of the carbons. The SEM images of the raw sawdust and activated carbons DSD4800 and DSD4800P are shown in **Figure 3**. The morphology of the raw sawdust is comprised of extended fibrous structures typical for woody matter. After activation, the morphology shows some retention of fibrous and honeycomb-like structures. The morphology of the activated carbons includes smooth surfaces characterised by large conchoidal cavities, which is similar to what has previously been reported for carbons generated via direct or flash carbonisation activation routes.^{21,29,32} The aforementioned retention of some woody morphology is consistent with the milder nature of PO activation compared to KOH where the morphology is completely altered (compared to that the biomass) especially at high levels of activation.^{33-35,38}

Direct and mild non-hydroxide activation of biomass to carbons with enhanced CO₂ storage capacity

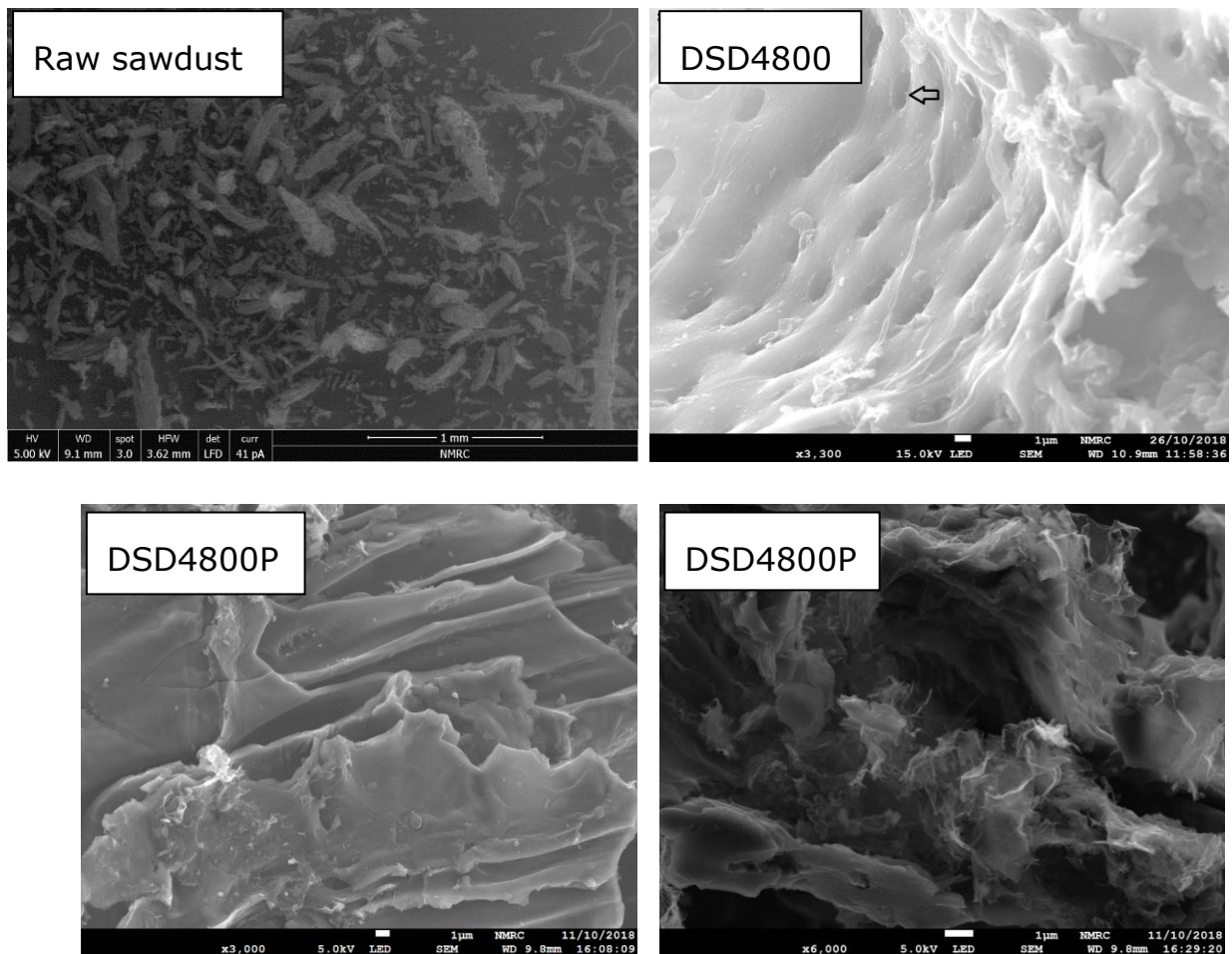


Figure 3. SEM images of raw sawdust and selected activated and compactivated carbons.

5.3.2 Porosity of activated carbons and compactivated carbons

The nitrogen sorption isotherms and the corresponding pore size distribution (PSD) curves for carbons directly activated or compactivated at PO/SD ratio of 2 are shown in **Figure 4**. All samples exhibit type I isotherms typical of microporous materials. Due to micropore filling, a significant proportion of nitrogen sorption takes place at a relative pressure (P/P_0)

Direct and mild non-hydroxide activation of biomass to carbons with enhanced CO₂ storage capacity

below 0.1, followed by a sharp knee and plateau with no significant adsorption occurring at P/P_0 greater than 0.1. For samples activated at 800 °C, the isotherms show a slight broadening of the adsorption 'knee', which suggests limited widening in the pore size distribution. The amount of nitrogen adsorbed appears to be correlated with the temperature of activation, and increases at higher activation temperature. The isotherms of the compactivated carbons (**Figure 4C**) are similar to those of powder samples (**Figure 4A**), except for higher amounts of nitrogen adsorbed. This is the first indication that direct compactivation with PO generates higher levels of porosity compared to direct activation. The pore size distribution curves of powder samples (**Figure 4B**) show no pores of width greater than 20 Å with most pores being of size less than 10 Å. A similar trend is observed for the compactivated samples except that they have a slightly higher proportion of pores in the 10 – 20 Å range. Regarding pore maxima, increasing the activation temperature from 600 to 800 °C leads to an increase such that while samples prepared at 600 °C or 700 °C show an average pore width of 6 – 8 Å, this rises to 6–12 Å at 800 °C. Compactivation does not significantly alter the pore size distribution (**Figure 4D**) except for a slight shift to larger micropores especially for sample DSD2800P. Thus, despite the increase in overall porosity occasioned by compactivation (as per the amount of nitrogen adsorbed – **Figure 4A** and **C**), the pore size remains largely unchanged (**Figure 4 B** and **D**).

Direct and mild non-hydroxide activation of biomass to carbons with enhanced CO₂ storage capacity

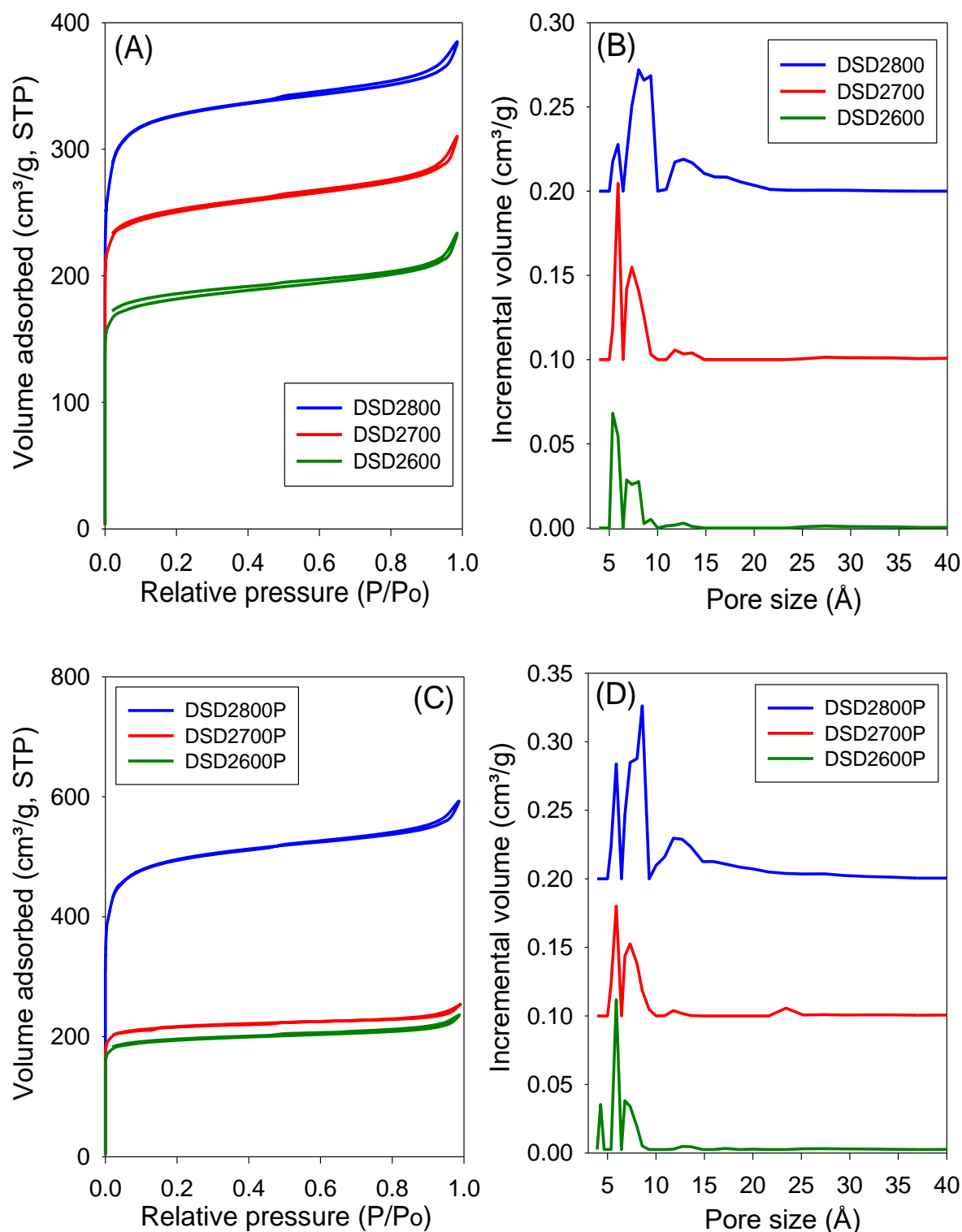


Figure 4. Nitrogen sorption isotherms (A and C) and pore size distributions curves (B and D) of carbons directly activated (A and B) or compactivated (C and D) from sawdust (SD) at 600, 700 or 800 °C, and PO/SD ratio of 2. The PSD curves are offset (y-axis) by 0.1 (DSD2700 and DSD2700P) or 0.2 (DSD2800 and DSD2800P).

Direct and mild non-hydroxide activation of biomass to carbons with enhanced CO₂ storage capacity

Figure 5 shows the nitrogen sorption isotherms and corresponding pore size distribution curves for carbons prepared at PO/SD ratio of 4. The isotherms are typically type I and very similar to those in **Figure 4** both in terms of shape and amount of nitrogen adsorbed. Clearly, increasing the amount of PO does not appear to have any significant effect on the porosity, which is consistent with the results of XRD analysis as described above. The PSD curves in **Figure 5** are comparable to those of in **Figure 4**, which means that increase in the PO/SD ratio does not lead to pore size expansion. This means that control of the porosity of the carbons is best achieved by choice of activation temperature rather than the amount of PO or a combination of both. This is a departure from what is observed for direct activation of sawdust with KOH wherein increase in the KOH/SD ratio from 2 to 4 generated carbons with larger pores and also included the presence of small mesopores.²⁹ According to **Figure 5** (B and D), direct activation at PO/SD ratio of 4 results in the formation of larger micropores with hardly any mesopores even for samples activated at 800 °C. The presence of supermicropores for samples activated at 800 °C could be related to the CO₂ and CO gases released from during the activation at high temperature.¹⁰ Generally, though, the compacted samples show higher nitrogen sorption compared to equivalent powder samples, which is in agreement with previous studies using KOH as activating agent.^{24,30} The increase in porosity induced by compaction is, however, not as high as that observed for KOH activation. This is consistent with the fact that the amount of PO is not a critical factor in determining the porosity. It is likely,

Direct and mild non-hydroxide activation of biomass to carbons with enhanced CO₂ storage capacity

therefore, that PO exists in an excess amount, which means that the close contact with sawdust particles engendered by the compaction does not have any significant effect of the overall efficiency of the activator.

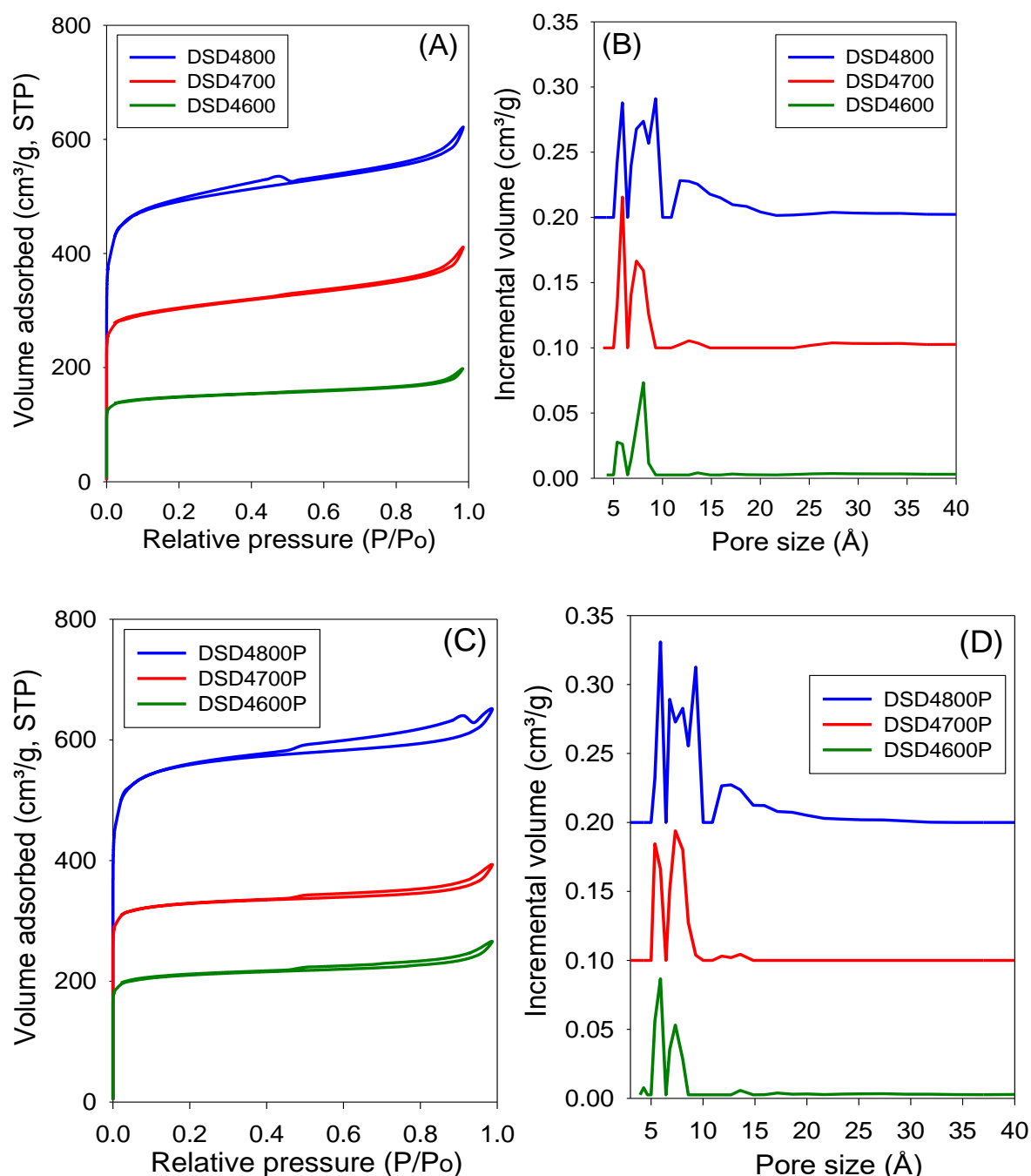


Figure 5. Nitrogen sorption isotherms (A and C) and pore size distributions curves (B and D) of carbons directly activated (A and B) or compactivated (C and D) from sawdust (SD) at 600, 700 or 800 °C, and PO/SD ratio of 4. The PSD curves are offset (y-axis) by 0.1 (DSD4700 and DSD4700P) or 0.2 (DSD4800 and DSD4800P).

Direct and mild non-hydroxide activation of biomass to carbons with enhanced CO₂ storage capacity

One of the key aims of this study was to explore the impact of a simpler direct activation route on the porosity of the activated carbons. This is an important consideration given the mild nature of PO as an activating agent. **Table 2** summarizes the textural properties of the directly activated and compactivated carbons. The surface area of activated carbons is in the range of 550 – 1860 m² g⁻¹ with pore volume of between 0.3 and 0.96 cm³ g⁻¹. The surface area and pore volume are mainly determined by the activation temperature. Both textural parameters increase as activation temperature rises from 600 to 800 °C. The amount of PO (given as PO/SD ratio of 2 or 4) does not appear to have any effect on the surface area and pore volume especially for activation at 600 and 700 °C. However, for activation at 800 °C, a higher amount of PO generates greater surface area and pore volume. Thus the surface area and pore volume of DSD4800 (1859 m² g⁻¹ and 0.96 cm³ g⁻¹, respectively) is higher than that of DSD2800 (1238 m² g⁻¹ and 0.59 cm³ g⁻¹, respectively). The activated carbons exhibit high to very high microporosity as indicated by the magnitude and proportion of surface area and pore volume arising from micropores (**Table 2**). The proportion of surface area arising from micropores is between 80 and 86% while for pore volume it is 59 to 71%. The activation temperature has no effect on the proportion of microporosity. However, a higher amount of PO very slightly reduces the microporosity. It is also clear from the textural data in **Table 2** that compactivation generates carbons with higher surface area and pore volume compared to equivalent activated samples and that, interestingly, this increase in overall porosity does not compromise the microporosity. The microporosity of the compactivated

Direct and mild non-hydroxide activation of biomass to carbons with enhanced CO₂ storage capacity

carbons is either similar or slightly higher than that of equivalent activated carbons.

Table 2. Textural properties and CO₂ uptake at 25 °C of carbons directly activated or compactivated from sawdust at 600, 700 or 800 °C, and PO/sawdust ratio of 2 or 4.

Sample	Surface area (m ² g ⁻¹)	Micropore surface area ^a (m ² g ⁻¹)	Pore volume (cm ³ g ⁻¹)	Micropore volume ^b (cm ³ g ⁻¹)	CO ₂ uptake (mmol g ⁻¹)		
					0.15 bar	1 bar	20 bar
DSD2600	682	574 (84)	0.36	0.23 (64)	1.0	2.7	4.9
DSD2700	945	813 (86)	0.48	0.33 (69)	1.2	4.1	8.5
DSD2800	1238	1053 (85)	0.59	0.42 (71)	0.9	3.4	12.3
DSD4600	556	465 (84)	0.30	0.18 (60)	1.0	2.5	4.8
DSD4700	1131	906 (80)	0.63	0.37 (59)	0.9	3.0	6.8
DSD4800	1859	1497 (81)	0.96	0.60 (63)	0.8	3.2	11.5
DSD2600P	730	638 (87)	0.36	0.26 (72)	1.2	2.9	5.1
DSD2700P	822	699 (85)	0.39	0.28 (72)	1.0	3.6	7.7
DSD2800P	1893	1545 (82)	0.92	0.61 (66)	1.0	4.0	13.0
DSD4600P	793	693 (87)	0.41	0.28 (68)	1.2	2.9	5.2
DSD4700P	1242	1123 (91)	0.61	0.45 (74)	1.6	3.8	7.8
DSD4800P	2121	1816 (86)	1.01	0.73 (72)	1.1	4.3	12.2

The values in the parenthesis refer to: ^a% micropore surface area, and ^b% micropore volume.

Direct and mild non-hydroxide activation of biomass to carbons with enhanced CO₂ storage capacity

It is interesting to note that the porosity of the directly activated carbons is comparable (**Table 3**) to that of equivalent (in terms of amount of PO and activation temperature) conventionally activated samples prepared via HTC prior to activation of the hydrochar. The microporosity of the two sets of samples is also similar especially for carbons prepared at PO/SD or PO/hydrochar ratio of 2. At PO/SD or PO/hydrochar ratio of 4, the directly activated carbons have very slightly lower levels of microporosity. The overall picture that emerges is that direct activation or compactivation of biomass with PO does not compromise the porosity of the resulting carbons. This is similar to what has previously been observed when the harsher activating agent, KOH, is used.²⁹ Thus direct activation or compactivation of biomass with PO offers simplicity but without introducing any disadvantages with respect to achievable porosity.

Direct and mild non-hydroxide activation of biomass to carbons with enhanced CO₂ storage capacity

Table 3. Textural properties and CO₂ uptake at 25 °C of carbons directly activated (DSDxT) or conventionally activated via hydrothermal carbonisation (SDxT) from sawdust at 600, 700 or 800 °C, and PO/sawdust or PO/hydrochar ratio of 2 or 4.

Sample	Surface area (m ² g ⁻¹)	Micropore surface area ^a (m ² g ⁻¹)	Pore volume (cm ³ g ⁻¹)	Micropore volume ^b (cm ³ g ⁻¹)	CO ₂ uptake (mmol g ⁻¹)		
					0.15 bar	1 bar	20 bar
DSD2600	682	574 (84)	0.36	0.23 (64)	1.0	2.7	4.9
DSD2700	945	813 (86)	0.48	0.33 (69)	1.2	4.0	8.5
DSD2800	1238	1053 (85)	0.59	0.42 (71)	0.9	3.4	12.3
SD2600	506	411 (81)	0.27	0.16 (59)	1.2	2.6	4.6
SD2700	893	813 (91)	0.41	0.33 (80)	1.4	3.8	7.6
SD2800	1463	1311 (89)	0.67	0.53 (79)	1.2	4.3	11.9
DSD4600	556	465 (84)	0.30	0.18 (60)	1.0	2.5	4.8
DSD4700	1131	906 (80)	0.63	0.37 (59)	0.9	3.0	6.8
DSD4800	1859	1497 (81)	0.96	0.60 (63)	0.8	3.2	11.5
SD4600	575	499 (87)	0.30	0.20 (67)	1.2	2.9	5.1
SD4700	972	875 (90)	0.46	0.35 (76)	1.2	3.7	7.6
SD4800	1441	1257 (87)	0.68	0.51 (75)	1.0	3.8	11.2

The values in the parenthesis refer to: ^a% micropore surface area, and ^b% micropore volume.

5.3.3 CO₂ uptake of activated and compactivated carbons

Given the high microporosity of the present carbons, we investigated their CO₂ uptake at 25 °C with particular focus on low pressure (> 1 bar) storage capacity. **Figure 6** shows the CO₂ uptake isotherms for activated (i.e., powder) samples, and the storage capacity at 0.15 bar, 1 bar and 20 bar

Direct and mild non-hydroxide activation of biomass to carbons with enhanced CO₂ storage capacity

is summarised in **Table 2**. The CO₂ uptake at 1 bar, which is often used as a measure of performance for post-combustion capture from flue gas streams from fossil fuel power stations, is in the range of 2.5 to 4.1 mmol g⁻¹. The highest CO₂ uptake at 1 bar is for sample DSD2700, which also has the highest proportion of micropore surface area (**Table 2**). The CO₂ uptake rises significantly from ca. 2.5 mmol g⁻¹ (activation at 600 °C) to a high of 4.1 mmol g⁻¹ (700 °C) and then reduces to ca.3.4 mmol g⁻¹ for samples activated 800 °C.

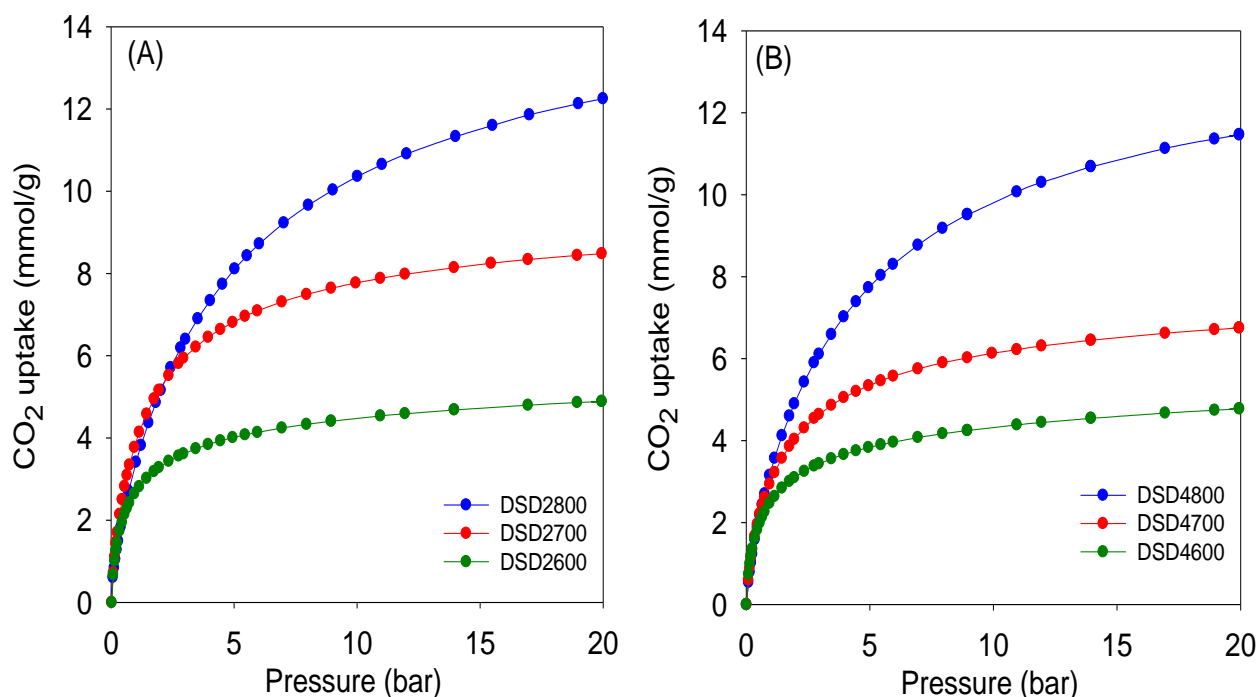


Figure 6. CO₂ uptake isotherms of carbons directly activated from sawdust (SD) at 600, 700 or 800 °C, and PO/SD ratio of 2 (A) or 4 (B).

Figure 7 shows the CO₂ uptake isotherms for compactivated samples, and **Table 2** summarises the uptake at 0.15 bar, 1 bar and 20 bar. For compactivated carbons, the CO₂ uptake at 1 bar is in the range 2.9

Direct and mild non-hydroxide activation of biomass to carbons with enhanced CO₂ storage capacity

– 4.3 mmol g⁻¹, and the highest uptake is for sample DSD4800P. For compacted samples, the rise is from 2.9 mmol g⁻¹ (600 °C) to ca. 3.8 mmol g⁻¹ (700 °C) and up to 4.3 mmol g⁻¹ for the sample compactivated at 800 °C (DSD4800P). The uptake data, therefore, suggest that at 25 °C and 1 bar, the total surface area does not determine CO₂ uptake capacity but rather samples with the largest proportion of micropore surface area have the better performance. This is consistent with previous studies in which the preponderance of small pores (6 – 8 Å) has been noted to determine low pressure CO₂ uptake. It is noteworthy that the highest CO₂ uptake at 1 bar of 4.3 mmol g⁻¹ for the present sawdust-derived direct PO activated carbons is comparable to that previously reported for conventionally (via HTC) PO activated sawdust derived carbons¹⁰ and also for directly activated sawdust-derived carbons with KOH as activating agent.²⁹ A benefit of the current PO activation route is that it is milder and more environmentally friendly and appears to offer a simpler optimisation of pore size by choice of activation temperature. Thus despite being prepared via a simpler, milder, potentially cheaper and more direct route, the directly activated and compactivated carbons show attractive performance for gravimetric CO₂ uptake, which is comparable or better than for current benchmark porous carbons (**Table 3**).^{39–48}

Direct and mild non-hydroxide activation of biomass to carbons with enhanced CO₂ storage capacity

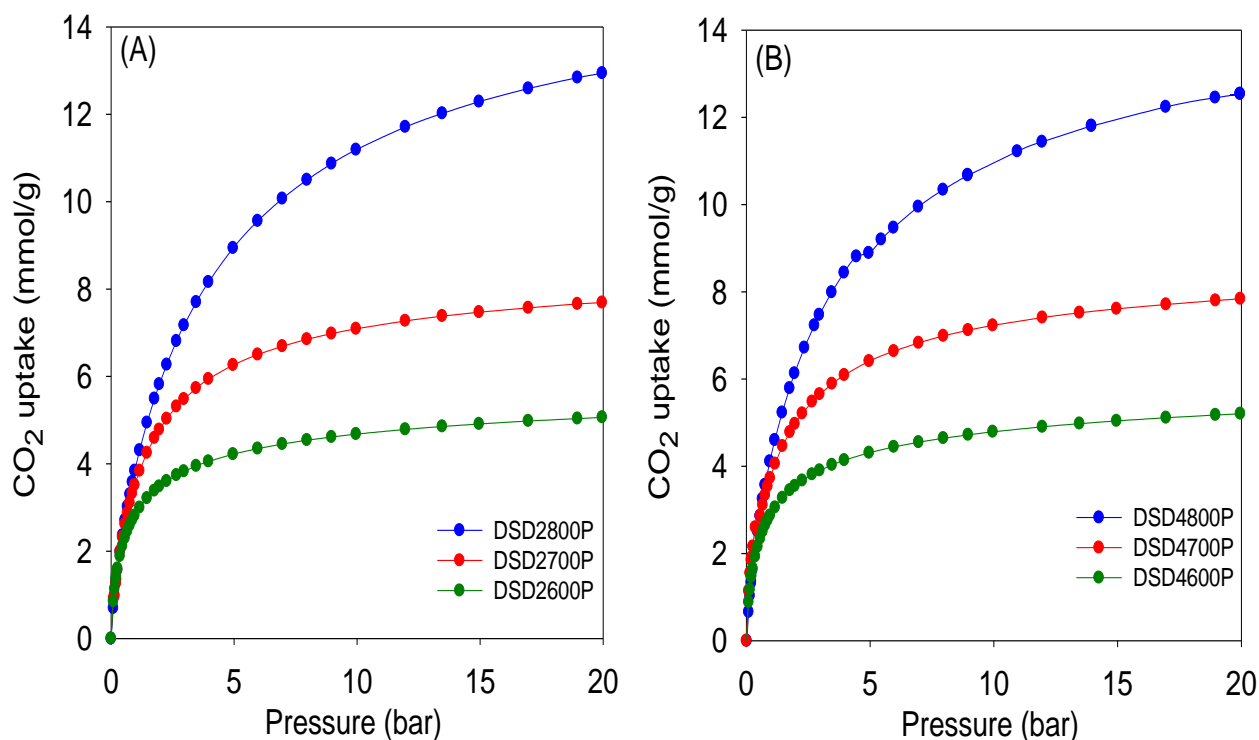


Figure 7. CO₂ uptake isotherms of carbons directly compactivated from sawdust (SD) at 600, 700 or 800 °C, and PO/SD ratio of 2 (A) or 4 (B).

The CO₂ uptake at 0.15 bar is considered to be a close mimic of capture performance from post-combustion flue gas streams emanating from power stations, which typically contain of ca. 15 - 20% CO₂ with the remainder being mainly N₂ (70–75%), and water (ca.10 %).^{49,50} For activated (powder) carbons, the uptake at 0.15 bar is in the narrow range of 0.8 and 1.1 mmol g⁻¹ with samples activated at 800 °C having the lowest storage capacity. For compactivated carbons, the uptake is higher at between 1.0 and 1.6 mmol g⁻¹. The trend generally matches that of uptake at 1 bar and is clearly related to the microporosity of the carbons. It is noteworthy that sample DSD4700P achieves a very high uptake at 0.15 bar of 1.6 mmol g⁻¹, which is one of the highest reported for porous carbons (**Table 3**).^{39-48,51-53}

Direct and mild non-hydroxide activation of biomass to carbons with enhanced CO₂ storage capacity

The trend is reversed for the CO₂ uptake at the higher pressures of 20 bar. The highest uptakes are achieved for samples activated at 800 °C, and the lowest values are achieved for samples activated at 600 °C. This trend mirrors the variation in surface area and confirmed the fact that the CO₂ uptake at moderate to high pressure is dependent on the total surface area rather than pore size, whereas at lower pressure the level of microporosity plays an important role in determining the uptake capacity. Additionally, the CO₂ uptake at 20 bar is not affected by the amount of PO, which is a consequence of the fact that changing the PO/SD ratio from 2 to 4 does not alter the porosity in any significant way. This confirms that in optimising or tailoring the textural properties of the present carbons for targeted CO₂ uptake applications, the activation temperature is more effective than the PO/SD ratio. The possibility of using low amounts of PO whilst still achieving the full range of porosity is also a positive outcome of the present synthesis approach.

Direct and mild non-hydroxide activation of biomass to carbons with enhanced CO₂ storage capacity

Table 3. CO₂ uptake of various porous carbons at 25 °C and 0.15 bar or 1 bar (Table adapted from reference 36)

Sample	CO ₂ uptake (mmol/g)	
	1 bar	0.15 bar
Sawdust-derived activated carbon ⁵⁴	4.8	1.2
KOH-activated templated carbons ⁵⁵	3.4	~1.0
Hierarchical porous carbon (HPC) ⁵⁶	3.0	~0.9
Petroleum pitch-derived activated carbon ⁵³	4.55	~1.0
Activated carbon spheres ⁴²	4.55	~1.1
Phenolic resin activated carbon spheres ⁴¹	4.5	~1.2
Poly(benzoxazine-co-resol)-derived carbon ⁵⁷	3.3	1.0
Fungi-derived activated carbon ⁵⁸	3.5	~1.0
Chitosan-derived activated carbon ⁴³	3.86	~1.1
Polypyrrole derived activated carbon ⁵⁹	3.9	~1.0
Soya bean derived N-doped activated carbon ⁶⁰	4.24	1.2
N-doped ZTCs ⁴⁷	4.4	~1.0
Activated templated N-doped carbon ⁶¹	4.5	1.4
Polyaniline derived activated carbon ³⁹	4.3	1.38
N-doped activated carbon monoliths ⁴⁶	5.14	1.25
Activated N-doped carbon ⁶²	3.2	1.5
Activated hierarchical N-doped carbon ⁵¹	4.8	1.4
Activated N-doped carbon from algae ⁶³	4.5	~1.1

5.4 Conclusion

We have shown that potassium oxalate (PO) is an effective activation agent for the formation of activated carbons from biomass via a direct and simpler synthesis approach. This is notable, as potassium oxalate is milder than the typically used KOH, which is more corrosive/toxic. Carbons were formed directly via activation with PO as powders or by including a compaction step (compactivation), in which the mixture of PO and sawdust are compacted together prior to thermal activation. Highly microporous activated and compactivated carbon materials were generated from sawdust. Direct activation of sawdust, without recourse to hydrothermal carbonisation or pyrolysis, in combination with the use of milder PO as activating agent, offers significant advantages over previous approaches. Despite the clear attractions of the new synthesis approach in terms of reduced steps and a milder activating agent, the properties of the generated carbons were comparable to those prepared via routes that are more complicated. Furthermore, the new approach enabled higher yields of activated carbons. The carbons have surface area in the range 550 to 2100 m² g⁻¹ and pore volume of between 0.3 and 1.0 cm³ g⁻¹. For both powder and compacted samples, surface area increased with increasing activation temperature, but with the amount of PO having little effect this enabling simpler control of the porosity via choice of activating temperature. The carbons, due to the highly microporous nature, were found to be excellent for the uptake of CO₂ at 25 °C, with storage capacity of up to 1.6 and 4.3 mmol g⁻¹ at 0.15 bar and 1 bar,

Direct and mild non-hydroxide activation of biomass to carbons with enhanced CO₂ storage capacity

respectively. Our findings show that the use of potassium oxalate as a mild activating agent via direct activation succeeds in addressing the need for non-corrosive and less toxic activators and also negates the need for hydrothermal treatment or pyrolysis of biomass prior to activation. The resulting activated carbons have attractive performance as sustainable energy materials especially for post-combustion CO₂ capture and storage.

Direct and mild non-hydroxide activation of biomass to carbons with enhanced CO₂ storage capacity

References

- 1 K. V. Kumar, K. Preuss, M. M. Titirici and F. Rodríguez-Reinoso, *Chem. Rev.*, 2017, **117**, 1796–1825.
- 2 B. Li, H. M. Wen, W. Zhou, J. Q. Xu and B. Chen, *Chem*, 2016, **1**, 557–580.
- 3 Y. He, W. Zhou, G. Qian and B. Chen, *Chem. Soc. Rev.*, 2014, **43**, 5657–5678.
- 4 T. A. Makal, J. R. Li, W. Lu and H. C. Zhou, *Chem. Soc. Rev.*, 2012, **41**, 7761–7779.
- 5 G. Singh, K. S. Lakhi, S. Sil, S. V. Bhosale, I. Y. Kim, K. Albahily and A. Vinu, *Carbon N. Y.*, 2019, **148**, 164–186.
- 6 P. González-García, *Renew. Sustain. Energy Rev.*, 2018, **82**, 1393–1414.
- 7 M. Sevilla and R. Mokaya, *Energy Environ. Sci.*, 2014, **7**, 1250–1280.
- 8 M. Sevilla, G. A. Ferrero and A. B. Fuertes, *Chem. Mater.*, 2017, **29**, 6900–6907.
- 9 J. Li, Q. Jiang, L. Wei, L. Zhong and X. Wang, *J. Mater. Chem. A*, 2020, **8**, 1469–1479.
- 10 A. M. Aljumialy and R. Mokaya, *Mater. Adv.*, 2020, **1**, 3267–3280.
- 11 M. Sevilla, N. Alam and R. Mokaya, *J. Phys. Chem. C*, 2010, **114**, 11314–11319.
- 12 M. Sevilla, A. S. M. Al-Jumialy, A. B. Fuertes and R. Mokaya, *ACS Appl.*

Direct and mild non-hydroxide activation of biomass to carbons with enhanced CO₂ storage capacity

Mater. Interfaces, 2018, **10**, 1623–1633.

- 13 J. S. Wei, S. Wan, P. Zhang, H. Ding, X. B. Chen, H. M. Xiong, S. Gao and X. Wei, *New J. Chem.*, 2018, **42**, 6763–6769.
- 14 M. Sevilla, G. A. Ferrero and A. B. Fuertes, *Carbon N. Y.*, 2017, **114**, 50–58.
- 15 J. Ludwinowicz and M. Jaroniec, *Carbon N. Y.*, 2015, **82**, 297–303.
- 16 Y. D. Chen, W. Q. Chen, B. Huang and M. J. Huang, *Chem. Eng. Res. Des.*, 2013, **91**, 1783–1789.
- 17 Q. Jiang, Y. Wang, Y. Gao and Y. Zhang, *Environ. Sci. Pollut. Res.*, 2019, **26**, 30268–30278.
- 18 T. Wang, Y. Zhai, Y. Zhu, C. Li and G. Zeng, *Renew. Sustain. Energy Rev.*, 2018, **90**, 223–247.
- 19 M. M. Titirici and M. Antonietti, *Chem. Soc. Rev.*, 2010, **39**, 103–116.
- 20 M. M. Titirici, R. J. White, C. Falco and M. Sevilla, *Energy Environ. Sci.*, 2012, **5**, 6796–6822.
- 21 M. Sevilla, R. Mokaya and A. B. Fuertes, *Energy Environ. Sci.*, 2011, **4**, 2930–2936.
- 22 A. Altwala and R. Mokaya, *Energy Environ. Sci.*, 2020, **13**, 2967–2978.
- 23 C. Quan, A. Li and N. Gao, *Procedia Environ. Sci.*, 2013, **18**, 776–782.
- 24 N. Balahmar, A. C. Mitchell and R. Mokaya, *Adv. Energy Mater.*, 2015,

Direct and mild non-hydroxide activation of biomass to carbons with enhanced CO₂ storage capacity

- 5**, 1–9.
- 25 N. Soltani, A. Bahrami, M. I. Pech-Canul and L. A. González, *Chem. Eng. J.*, 2015, **264**, 899–935.
- 26 C. R. Lohri, H. M. Rajabu, D. J. Sweeney and C. Zurbrügg, *Renew. Sustain. Energy Rev.*, 2016, **59**, 1514–1530.
- 27 J. F. González, J. M. Encinar, C. M. González-García, E. Sabio, A. Ramiro, J. L. Canito and J. Gañán, *Appl. Surf. Sci.*, 2006, **252**, 5999–6004.
- 28 E. Haffner-Staton, N. Balahmar and R. Mokaya, *J. Mater. Chem. A*, 2016, **4**, 13324–13335.
- 29 N. Balahmar, A. S. Al-Jumialy and R. Mokaya, *J. Mater. Chem. A*, 2017, **5**, 12330–12339.
- 30 B. Adeniran and R. Mokaya, *Nano Energy*, 2015, **16**, 173–185.
- 31 M. Sevilla, W. Sangchoom, N. Balahmar, A. B. Fuertes and R. Mokaya, *ACS Sustain. Chem. Eng.*, 2016, **4**, 4710–4716.
- 32 E. A. Hirst, A. Taylor and R. Mokaya, *J. Mater. Chem. A*, 2018, **6**, 12393–12403.
- 33 N. Balahmar and R. Mokaya, *J. Mater. Chem. A*, 2019, **7**, 17466–17479.
- 34 H. M. Coromina, D. A. Walsh and R. Mokaya, *J. Mater. Chem. A*, 2016, **4**, 280–289.
- 35 W. Sangchoom and R. Mokaya, *ACS Sustain. Chem. Eng.*, 2015, **3**,

Direct and mild non-hydroxide activation of biomass to carbons with enhanced CO₂ storage capacity

- 1658–1667.
- 36 B. Adeniran, E. Masika and R. Mokaya, *J. Mater. Chem. A*, 2014, **2**, 14696–14710.
- 37 B. Adeniran and R. Mokaya, *J. Mater. Chem. A*, 2015, **3**, 5148–5161.
- 38 H. Lin, C. Xu, Q. Wang, J. Wu, Y. Wang, Y. Zhang and G. Fan, *Int. J. Hydrogen Energy*, 2019, **44**, 21527–21535.
- 39 Z. Zhang, J. Zhou, W. Xing, Q. Xue, Z. Yan, S. Zhuo and S. Z. Qiao, *Phys. Chem. Chem. Phys.*, 2013, **15**, 2523–2529.
- 40 A. Almasoudi and R. Mokaya, *J. Mater. Chem. A*, 2014, **2**, 10960–10968.
- 41 N. P. Wickramaratne and M. Jaroniec, *J. Mater. Chem. A*, 2013, **1**, 112–116.
- 42 N. P. Wickramaratne and M. Jaroniec, *ACS Appl. Mater. Interfaces*, 2013, **5**, 1849–1855.
- 43 X. Fan, L. Zhang, G. Zhang, Z. Shu and J. Shi, *Carbon N. Y.*, 2013, **61**, 423–430.
- 44 B. Adeniran and R. Mokaya, *Chem. Mater.*, 2016, **28**, 994–1001.
- 45 A. Almasoudi and R. Mokaya, *J. Mater. Chem.*, 2012, **22**, 146–152.
- 46 M. Nandi, K. Okada, A. Dutta, A. Bhaumik, J. Maruyama, D. Derks and H. Uyama, *Chem. Commun.*, 2012, **48**, 10283–10285.
- 47 Y. Xia, R. Mokaya, G. S. Walker and Y. Zhu, *Adv. Energy Mater.*, 2011,

Direct and mild non-hydroxide activation of biomass to carbons with enhanced CO₂ storage capacity

- 1**, 678–683.
- 48 A. Wahby, J. M. Ramos-Fernández, M. Martínez-Escandell, A. Sepúlveda-Escribano, J. Silvestre-Albero and F. Rodríguez-Reinoso, *ChemSusChem*, 2010, **3**, 974–981.
- 49 Z. Zhang, K. Wang, J. D. Atkinson, X. Yan, X. Li, M. J. Rood and Z. Yan, *J. Hazard. Mater.*, 2012, **229–230**, 183–191.
- 50 J. D. Figueroa, T. Fout, S. Plasynski, H. McIlvried and R. D. Srivastava, *Int. J. Greenh. Gas Control*, 2008, **2**, 9–20.
- 51 D. Lee, C. Zhang, C. Wei, B. L. Ashfeld and H. Gao, *J. Mater. Chem. A*, 2013, **1**, 14862–14867.
- 52 G. Srinivas, J. Burress and T. Yildirim, *Energy Environ. Sci.*, 2012, **5**, 6453–6459.
- 53 J. Silvestre-Albero, A. Wahby, A. Sepúlveda-Escribano, M. Martínez-Escandell, K. Kaneko and F. Rodríguez-Reinoso, *Chem. Commun.*, 2011, **47**, 6840–6842.
- 54 M. Sevilla and A. B. Fuertes, *Energy Environ. Sci.*, 2011, **4**, 1765–1771.
- 55 M. Sevilla and A. B. Fuertes, *J. Colloid Interface Sci.*, 2012, **366**, 147–154.
- 56 G. Srinivas, V. Krungleviciute, Z. X. Guo and T. Yildirim, *Energy Environ. Sci.*, 2014, **7**, 335–342.
- 57 G. P. Hao, W. C. Li, D. Qian, G. H. Wang, W. P. Zhang, T. Zhang, A.

Direct and mild non-hydroxide activation of biomass to carbons with enhanced CO₂ storage capacity

- Q. Wang, F. Schüth, H. J. Bongard and A. H. Lu, *J. Am. Chem. Soc.*, 2011, **133**, 11378–11388.
- 58 J. Wang, A. Heerwig, M. R. Lohe, M. Oschatz, L. Borchardt and S. Kaskel, *J. Mater. Chem.*, 2012, **22**, 13911–13913.
- 59 M. Sevilla, P. Valle-Vigñon and A. B. Fuertes, *Adv. Funct. Mater.*, 2011, **21**, 2781–2787.
- 60 W. Xing, C. Liu, Z. Zhou, L. Zhang, J. Zhou, S. Zhuo, Z. Yan, H. Gao, G. Wang and S. Z. Qiao, *Energy Environ. Sci.*, 2012, **5**, 7323–7327.
- 61 Y. Zhao, L. Zhao, K. X. Yao, Y. Yang, Q. Zhang and Y. Han, *J. Mater. Chem.*, 2012, **22**, 19726–19731.
- 62 M. Saleh, J. N. Tiwari, K. C. Kemp, M. Yousuf and K. S. Kim, *Environ. Sci. Technol.*, 2013, **47**, 5467–5473.
- 63 M. Sevilla, C. Falco, M. M. Titirici and A. B. Fuertes, *RSC Adv.*, 2012, **2**, 12792–12797.

Chapter 6. Porosity modulation of activated carbons via pre-mixed precursors for enhanced methane storage

Abstract

The work reported in this chapter uses knowledge, reported in previous chapters, of the carbonisation stage and how it affects the O/C ratio to tailor the properties of activated carbons. This was achieved by using pre-mixed precursors containing biomass-derived carbonaceous matter of varying O/C ratio as starting materials for activation. The use of pre-mixtures of polypyrrole and CNL carbon (from accidental and uncontrolled burning of wood under fierce fire conditions of the first Carbon Neutral Laboratory, CNL, building at Nottingham) or polypyrrole and ACDS carbon (air-carbonised date seed) generates activated carbons with substantially greater surface area than single use of any of the precursors. Mixing of CNL carbon or ACDS carbon, which are known to generate highly microporous carbons, with polypyrrole, which generates mesoporous carbons, yielded activated carbons with a much wider range of porosity. However, more importantly, it is possible to prepare activated carbon with ultra-high surface area (up to $3890 \text{ m}^2 \text{ g}^{-1}$) and pore volume (up to $2.40 \text{ cm}^3 \text{ g}^{-1}$) in a manner not possible via single use of any of the precursors. The resulting ultra-high surface area carbons have excellent gravimetric methane uptake, which at 25°C and 100 bar, can reach up to 28.4 mmol g^{-1} (or 0.46

Porosity modulation of activated carbons via pre-mixed precursors for enhanced methane storage

g g⁻¹). In addition to the excellent gravimetric uptake, at 25°C and 100 bar, the carbons have total volumetric methane uptake of up to 260 cm⁻³ (STP) cm⁻³, and working capacity (100 – 5 bar) of 210 cm⁻³ (STP) cm⁻³. The combination achieved for gravimetric and volumetric uptake is higher and more attractive than any previous value for porous carbons or metal-organic-frameworks (MOFs).

6.1 Introduction

Currently, the world is facing enormous challenges as a result of rising greenhouse gas emissions, which are causing severe global warming concerns. A number of potential solutions are the focus of on-going research, which is targeted towards the remediation of environmental damage emanating from CO₂ release especially from fossil fuel power stations.¹⁻³ As a consequence of increasing climate change concerns and the tightening of environmental regulations, natural gas, of which the main component is methane, has recently attracted attention as a less environmentally damaging fuel.⁴⁻¹⁰ On the other hand, biogas, which is produced from the breakdown of organic matter and largely consists of methane, and has also attracted interest as a renewable fuel source.^{11,12} Biogas and natural gas, both of which consist of over 70% methane, are readily available and pose a lower environmental risk when used as fuel; although CO₂ is produced, biogas or natural gas burn more cleanly than petroleum-based fuels.

Porosity modulation of activated carbons via pre-mixed precursors for enhanced methane storage

The main obstacles to the more widespread use of methane-rich gases as fuels is to do with their lower energy density and challenges associated with their storage and transportation when compared to gasoline and diesel. Natural gas may be stored in compressed form as compressed natural gas (CNG) or in liquid form as liquefied natural gas (LNG). However, both CNG and LNG are not ideal as they cannot operate under ambient temperature and pressure; while CNG needs high pressure (typically 200 – 300 bar) conditions requiring expensive holding vessels, LNG is dependent on expensive cryogenic cooling techniques.¹³ A promising method that may overcome the pressure and temperature concerns regarding methane storage is the use of adsorbed natural gas (ANG). Storage of adsorbed methane, typically involving physisorption onto the surface of porous adsorbents, can operate at low pressure conditions and at ambient temperature, both of which can reduce costs and offer improved ease of usage.^{4-10,14,15}

Porous carbons are amongst the materials currently being explored for the storage of methane.⁴⁻¹⁰ Porous carbons, and specifically activated carbons, have a number of attractive characteristics including controllable porosity, low cost, chemical and mechanical stability, and ease of preparation and handling.^{16,17} The nature and type of carbonaceous precursor utilised, as well as the activation process and conditions, influence the properties of activated carbons. Activated carbons derived from biomass are potentially the most appealing owing to their low impact on the environment, cost-efficiency, easy access and renewability. Careful

Porosity modulation of activated carbons via pre-mixed precursors for enhanced methane storage

selection of starting materials is critical in order to achieve the optimum properties suited to high methane uptake.

The main focus of the work in this chapter is the judicious use of pre-mixed precursors to synthesis activated carbons that are suited for enhanced methane storage. The pre-mixed precursors, which contain materials that are known to respond variably to similar levels of activation, are used a means to modulate the porosity of activated carbons in a targeted manner. Our improved understanding of the way in which the activation process for biomass is influenced by the carbonisation phase¹⁸⁻²² (see chapter 3) has been combined with the known effects of the oxygen/carbon (O/C) ratio of the precursors used in order to provide activated carbons with optimum porosity and high packing density that are ideal for methane storage.

Great care was taken in choosing the precursors used in this study. The Mokaya group has recently shown that the nature of a carbonaceous precursor has significant influence on susceptibility to activation and, consequently, plays a key role in determining the balance between microporosity and mesoporosity in the resulting carbons.²³⁻²⁸ It is now well established that some biomass-derived carbonaceous matter, depending on the type of biomass and method of carbonisation, can be highly resistant to activation and therefore tends to yield activated carbons with significant microporosity.^{18,20,22,24} In particular, air-carbonisation of biomass yields carbonaceous matter with relative low oxygen content (i.e., low O/C ratio), which is resistant to activation.^{18,20,22} Such resistance to activation results

Porosity modulation of activated carbons via pre-mixed precursors for enhanced methane storage

in highly microporous activated carbons that have high packing density but with surface area that hardly goes above $2800 \text{ m}^2 \text{ g}^{-1}$.^{18,20,22} When used for gas uptake, such carbons have low gravimetric uptake (due to limited surface area) but comparatively high volumetric uptake (due to high packing density).²² On the other hand, polypyrrole is readily activatable and can yield highly mesoporous activated carbons that have much higher surface area of up to $4000 \text{ m}^2 \text{ g}^{-1}$, but also have large pore volume and low packing density.^{21,29-34} This translates to high gravimetric gas uptake but comparatively low volumetric capacity.³³ While the possibility of achieving ultra-high surface area for polypyrrole-derived activated carbons is attractive, the high cost of polypyrrole prohibits its widespread use as a precursor; the cost of the pyrrole ($> \$300/\text{kg}$) used to prepare polypyrrole is several orders higher than that of activated carbon (ca. $\$1/\text{kg}$). However, overall costs can be reduced by blending the polypyrrole with low value waste biomass-derived carbonaceous matter to achieve pre-mixed precursors that may still generate activated carbons with ultra-high surface area but which also have higher packing density. This would enable synthesis of affordable activated carbons that have optimised properties (with respect to surface area and packing density) for which both the gravimetric and volumetric gas uptake is high in a manner not possible for single use of either the polypyrrole or biomass-derived carbonaceous matter.

To this end, Mokaya's group has previously explored the preparation of activated carbons from pre-mixed precursors that contain a mixture of precursors that respond variably to similar levels of activation.²¹ Polypyrrole

Porosity modulation of activated carbons via pre-mixed precursors for enhanced methane storage

was mixed with raw eucalyptus wood sawdust (O/C ratio of 0.773) or hydrochar (O/C ratio of 0.483) derived from the sawdust following hydrothermal carbonisation.²¹ It was possible to prepare highly porous carbons with much higher surface area than was possible from single use of any one of the precursors. However, the O/C ratio of the biomass sources (sawdust or sawdust hydrochar) was still relatively high and they singly generated activated carbons with significant proportion of microporosity.²¹ On the other hand, the work described in this chapter explored the use of pre-mix precursors made up of polypyrrole with biomass-derived carbonaceous matter with much lower oxygen content (i.e., very low O/C ratio), namely, air carbonised date seed (O/C ratio of 0.156)²² and so-called CNL (O/C ratio of 0.185).^{18,22} The motivation for the study was, therefore, three-fold; (i) reduce costs by avoiding the extensive use of polypyrrole, but still achieve ultra-high surface area carbons, (ii) valorisation of cheap biomass-derived carbonaceous matter to activated carbons with porosity that is not achievable directly via use of single precursors, and (iii) optimisation of the porosity of activated carbons targeted at high performance gravimetric and volumetric methane storage. The overall aim of the study is to demonstrate that a logical technique can be used to make activated carbons with appropriate porosity and packing density that enables record methane storage capacity.

In order to enable widespread use of methane, the Advanced Research Projects Agency-Energy (ARPA-E) of the U.S. Department of Energy (DOE) has recently set a volumetric storage capacity target of

Porosity modulation of activated carbons via pre-mixed precursors for enhanced methane storage

350 cm³ (STP) cm⁻³ and gravimetric storage capacity of 0.5 g (CH₄) g⁻¹ at room temperature and pressure of 35 to 100 bar. It is important to note that the target of 350 cm³ (STP) cm⁻³ was set at that level to take into account the use of the crystallographic density of MOFs in calculating volumetric uptake.^{5,7} The crystallographic density of MOFs is typically at least 25% lower than their actual packing density. Therefore, the target of 350 cm³ (STP) cm⁻³ incorporates an expected reduction of at least 25% (down to ca. 263 cm³ (STP) cm⁻³) once MOFs are packed into storage tanks. Crucially, this reduction does not apply to activated carbons for which volumetric uptake is usually calculated using experimentally determined packing density. In this regard, the target for methane storage in carbons can be considered to be 263 cm³ (STP) cm⁻³. The key to achieving high methane storage capacity in porous materials, both in terms of gravimetric and volumetric capacity, is related to having adsorbents with a good balance between surface area and packing density. To present both high surface area and packing density, an adsorbent's porosity should arise predominantly from micropores, which should be accompanied by the presence of small mesopores.^{4-9,48-52} It has previously been suggested that pore channels of size 8 – 15 Å are the most efficient pores for methane storage.^{4-9,48-52}

6.2 Experimental Section

6.2.1 Material preparation

The date seed (5 g) was placed in an alumina boat and heated in a horizontal tube furnace to 400°C under an atmosphere of nitrogen at heating ramp rate of 10°C min⁻¹. Once at 400°C, the date seed was exposed to a flow of air only for 5–10 minutes, after which the furnace was left to cool under a flow of nitrogen gas only. The resulting carbonaceous matter was designated as ACDS (i.e., air carbonized date seed) carbon. CNL carbon, from the surface of a burnt wood log, was washed with distilled water to remove any impurities, dried in an oven at 120°C overnight and sieved to obtain a homogenous particle size ~ 212 μm. Polypyrrole (designated as PPY) was prepared by adding 3 g of pyrrole to 200 mL of 0.5 M FeCl₃ solution and stirring the mixture for 2 h at room temperature. The polypyrrole was recovered, washed with distilled water and dried in an oven at 120°C. The yield from pyrrole to polypyrrole was close to 100%. For activation, three sets of samples were prepared from mixtures of PPY/CNL or PPY/ACDS. Mixtures of PPY:CNL:KOH or PPY:ACDS:KOH at weight ratio of 1:2:4, 1:1:4 or 2:1:4 were activated at 800°C. The amount of KOH and activation temperature (800°C) were identical for all preparations. The mixtures were ground until homogeneous and placed in a tube furnace and heated under nitrogen for 1 h at 800°C following a heating ramp rate of 3°C min⁻¹. After cooling, the activated carbons were thoroughly washed with 10 wt% HCl, followed by washing with distilled water until neutral pH

Porosity modulation of activated carbons via pre-mixed precursors for enhanced methane storage

was achieved for the filtrate. The activated carbons were dried overnight in an oven at 120 °C and designated as PPyCNLxyzT or PPyDSxyzT where xyz is ratio (x:y:z) of the x = PPy, y = CNL or ACDS, and z = KOH, and T is temperature of activation (800°C).

6.2.2 Material Characterisation

Thermogravimetric analysis (TGA) was performed using a TA Instruments Discovery analyser or TA Instruments SDT Q600 analyser under flowing air conditions (100 mL/min). A PANalytical X'Pert PRO diffractometer was used to perform powder XRD analysis using Cu-K α light source (40 kV, 40 mA) with step size of 0.02° and 50 s time step. Elemental, CHN, analysis was performed on an Exeter Analytical CE-440 Elemental Analyser. Nitrogen sorption analysis (at -196 °C) with a Micromeritics 3FLEX sorptometer was used for porosity assessment and to determination of textural properties. Prior to analysis the carbon samples were degassed under vacuum at 200 °C for 12 h. Surface area was calculated using the Brunauer-Emmett-Teller (BET) method applied to adsorption data in the relative pressure (P/P_0) range of 0.02 – 0.22, and pore volume was estimated from the total nitrogen uptake at close to saturation pressure ($P/P_0 \approx 0.99$). The micropore surface area and micropore volume were determined via *t*-plot analysis. The pore size distribution was determined using Non-local density functional theory (NL-DFT) applied to nitrogen adsorption data. Scanning electron microscopy (SEM) images were recorded using an FEI Quanta200 microscope, operating at a 5 kV accelerating voltage.

Porosity modulation of activated carbons via pre-mixed precursors for enhanced methane storage

Transmission electron microscopy (TEM) images were obtained using a JEOL 2100F instrument operating at 200 kV equipped with a Gatan Orius CCD for imaging. Prior to analysis, the carbon samples were suspended in distilled water and dispersed onto lacey carbon support films.

6.2.3 Methane uptake measurements

Methane uptake was determined using a Hiden Isochema XEMIS Analyser. Before the uptake measurements, the carbon samples were degassed at 240 °C under vacuum for several hours. Methane uptake isotherms were obtained at 25 °C over the pressure range of 0 to 100 bar.

6.3 Results and Discussion

6.3.1 Yield, nature and elemental composition of activated carbons

When preparing activated carbon, choosing the right starting materials is essential in order to generate the targeted porosity. In this chapter, pre-mixed precursors was employed, with the hope that they would offer superior potential for porosity generation compared to single precursors. A further important consideration is the elemental analysis of the starting materials and in particular their O/C atomic ratio. Based on our knowledge, from chapter 3, date seed (*Phoenix dactylifera*) was chosen as a starting material due to its low elemental oxygen content. Additionally, and for completeness, CNL carbon was chosen as the other biomass source since it also exhibit a low O/C atomic ratio. When referenced against a variety of

Porosity modulation of activated carbons via pre-mixed precursors for enhanced methane storage

biomass sources, the elemental composition of the biomass-derived precursors employed in this chapter were found to have comparatively low O/C atomic ratios, i.e., 0.185 and 0.156 for CNL carbon and ACDS carbon, respectively. These are the lowest oxygen contents across a wide range of biomass sources for which the O/C ratio is typically in the range of 0.77 to 1.0 (**Table 1**).

Table 1. Elemental composition and O/C atomic ratio of a range of activatable biomass precursors.

Biomass source	C [%]	H [%]	O [%]	(O/C) ^a	Reference
Eucalyptus sawdust	46.4	5.8	47.8	0.773	35
Seaweed ^b	39.6	5.9	51.6	0.977	19
<i>Camellia Japonica</i>	46.2	5.4	48.4	0.786	25
Cellulose	44.4	6.2	49.4	0.830	35
ACDS carbon	78.5	4.0	16.3	0.156	This work
CNL carbon	77.7	3.1	19.2	0.185	This work
Polypyrrole ^c	55.5	2.7			This work

^aAtomic ratio, ^bSeaweed contains 2.9 wt% N, ^cPolypyrrole contains 16 wt% N.

The next consideration was selection of flash air-carbonisation as the method for converting the raw date seed into carbonaceous matter that would then be activated. This would not only negate the requirement for hydrothermal carbonisation (HTC) and pyrolysis but additionally achieve

Porosity modulation of activated carbons via pre-mixed precursors for enhanced methane storage

carbonaceous material with the lowest O/C ratio. Although both HTC and air-carbonisation diminish the O/C ratio compared to raw biomass, previous studies have demonstrated that the former causes a bigger decrease.^{18,20,22,35} For example, when eucalyptus sawdust is exposed to HTC, the O/C ratio reduces from 0.773 to 0.484 (a 40% reduction), while air carbonisation lowers the O/C ratio to 0.251. (ca. 70% decrease).²⁰ In addition, the CNL carbon chosen as precursor was sourced from the charred remains of the accidental and uncontrolled burning of wood under fierce fire conditions in the School of Chemistry's first CNL building.¹⁸ Thus, both the ACDS and CNL carbons are derived from air carbonisation of, respectively, wood or date seeds.

The yields of the activated carbons are shown in **Table 2**. The yields are related to the ease of activation of the precursor. PPY is the least resistant to activation and accordingly sample PPY4800 has the lowest yield of 12 wt%. The yields of CNL4800 and ACSD4800 are, respectively 32 and 50 wt%, which is in line with the trend in their O/C ratios. For both series of samples, the yields from pre-mixed precursors are lower than for the single use of biomass precursor and reduce as the amount of PPY in the mixture increases. At any given pre-mixture level, the PPY/ACDS mixtures have higher yield, which again is consistent with the fact that the ACDS carbon has a lower O/C ratio compared to the CNL carbon.

Porosity modulation of activated carbons via pre-mixed precursors for enhanced methane storage

Table 2. Elemental composition of precursors (polypyrrole, CNL carbon and ACDS Carbon) and activated carbons derived from pre-mixed precursors

sample	Yield [wt %]	C%	H%	N%	O%	O/C ^a
PPY		55.5	2.7	16.0		
PPY4800	12	89.0	0.1	0.7	10.2	0.084
CNL		77.7	3.1	0	19.2	0.185
CNL4800	32	84.2	0.0	0.0	15.8	0.141
PPYCNL124	30	83.0	0.0	0.0	17.0	0.154
PPYCNL114	20	91.0	0.0	0.0	9.0	0.074
PPYCNL214	20	91.0	0.0	0.0	9.0	0.074
Raw DS		49.0	7.0	1.6	42.4	0.649
ACDS		78.5	4.0	2.1	16.3	0.156
ACDS4800	50	84.3	0.1	0.1	15.5	0.138
PPYDS124	36	85.0	0.2	0.4	14.4	0.127
PPYDS114	22	90.5	0.2	0.2	9.1	0.075
PPYDS214	20	90.0	0.0	0.0	10.0	0.083

^aAtomic ratio

The elemental composition of the precursors, i.e. PPY, ACSD carbon and CNL carbon, and the activated carbons are shown in **Table 2**. The C content of the activated carbons increases compared to that of the precursors, which is accompanied by a decrease in N, H and O. The carbon content of PPY increases from 55.5 to 89 wt% when it is activated (sample PPY4800), whereas the N and H contents decrease from 16.0 and 2.7 to 0.7 and 0.1 wt%, respectively. On activation of the CNL carbon (sample CNL4800), the C content increases from 77.1 to 84.2 wt% and the H (1.0 wt%) and N (2.9 wt%) fractions are virtually removed. When ACDS carbon

Porosity modulation of activated carbons via pre-mixed precursors for enhanced methane storage

is subjected to activation (sample ACDS4800), the carbon content rises from 78.5 to 84.3 wt% along with a decrease in the N and H component from 2.1 and 4.0, respectively to 0.1 wt%. All the activated carbons, regardless of the precursor, have a C content of between 78.5 and 91 wt%. It can be surmised from the elemental composition data in **Table 2** that the activated carbons have comparable C and O contents, independent of the form of the pre-mixed precursor from which they are derived. Furthermore, the N and H content of both sets of samples remains low, and becomes practically eradicated in samples made from pre-mixed precursors containing a high quantity of PPY or CNL.

Figure 1 shows the TGA curves of the activated carbons. The carbons were thermally treated to 800 °C at a rate of 10°C min⁻¹ under flowing air conditions. TGA was performed in order to determine the carbon purity, i.e., the absence of inorganic matter, as well as their thermal stability. The TGA curves show that the carbons are stable up to 450 °C following an initial mass loss of 2–5 wt% below 300 °C, which is due to the loss of water or volatiles. This is followed by the main mass loss event due to carbon burn-off at temperatures ranging from 450 to 620 °C. The carbons have similar burn-off temperature range. This indicates that they have similar thermal stability, which is a consequence of the fact that they were all activated at the same temperature (800°C). All the carbons have a residual mass of less than 2%, and most have no residual mass indicating that they are fully carbonaceous with trace amounts or no inorganic matter.

Porosity modulation of activated carbons via pre-mixed precursors for enhanced methane storage

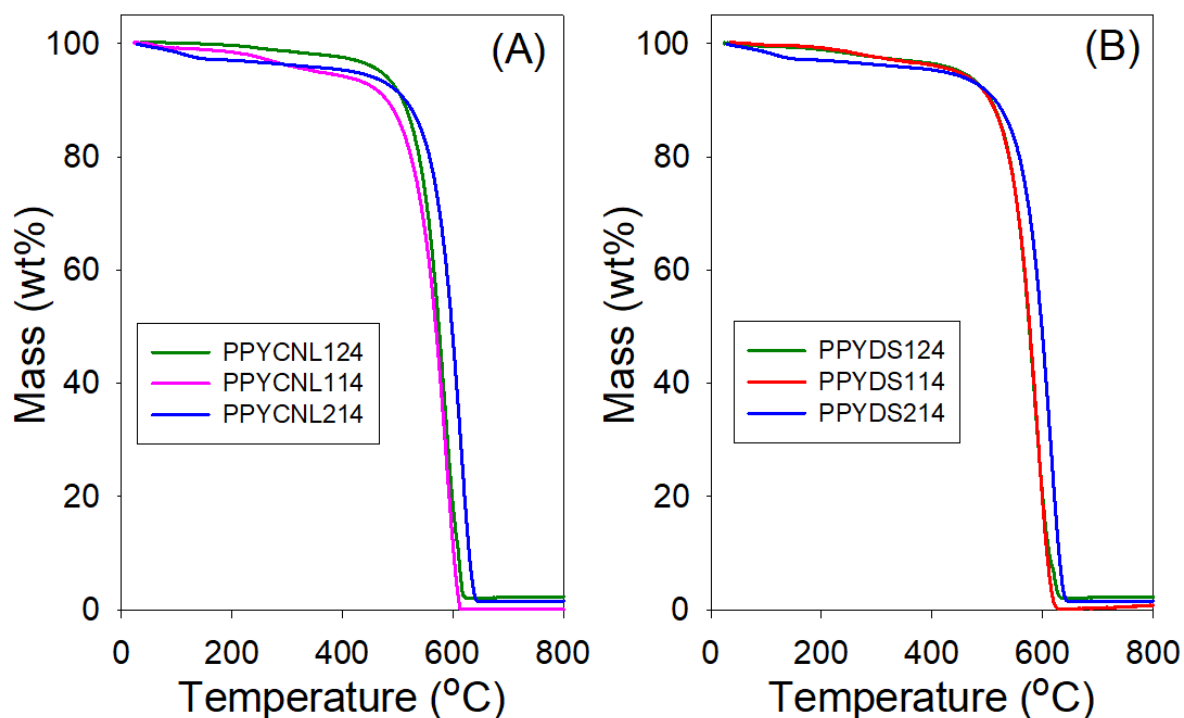


Figure 1. Thermogravimetric analysis (TGA) curves of activated carbons derived from pre-mixed mixtures of polypyrrole (PPY) and (A) CNL carbon or (B) ACDS carbon.

The powder XRD patterns of Polypyrrole, CNL carbon and ACDS carbon, and of the activated carbons are shown in **Figure 2**. XRD is useful in determining the nature (with respect to graphitisation) of the carbons and also for confirming the absence of any crystalline inorganic phases that would show sharp peaks. The XRD patterns of the precursors are featureless except for weak and broad peaks at 2-theta of 22° and 44°, which may be ascribed to very limited graphene stacking. The XRD patterns of the activated carbons hardly show the peaks due to graphene stacking, which is consistent with the expectation that activation would disrupt any graphitic domains. It is clear from the XRD patterns that the

Porosity modulation of activated carbons via pre-mixed precursors for enhanced methane storage

carbons generated from pre-mixed precursors are largely amorphous, as is characteristic of KOH-activated carbons. Given the heterogeneous nature of the starting carbonaceous matter, it is interesting to observe that the activated carbons are homogeneous (one-phase) materials.

Porosity modulation of activated carbons via pre-mixed precursors for enhanced methane storage

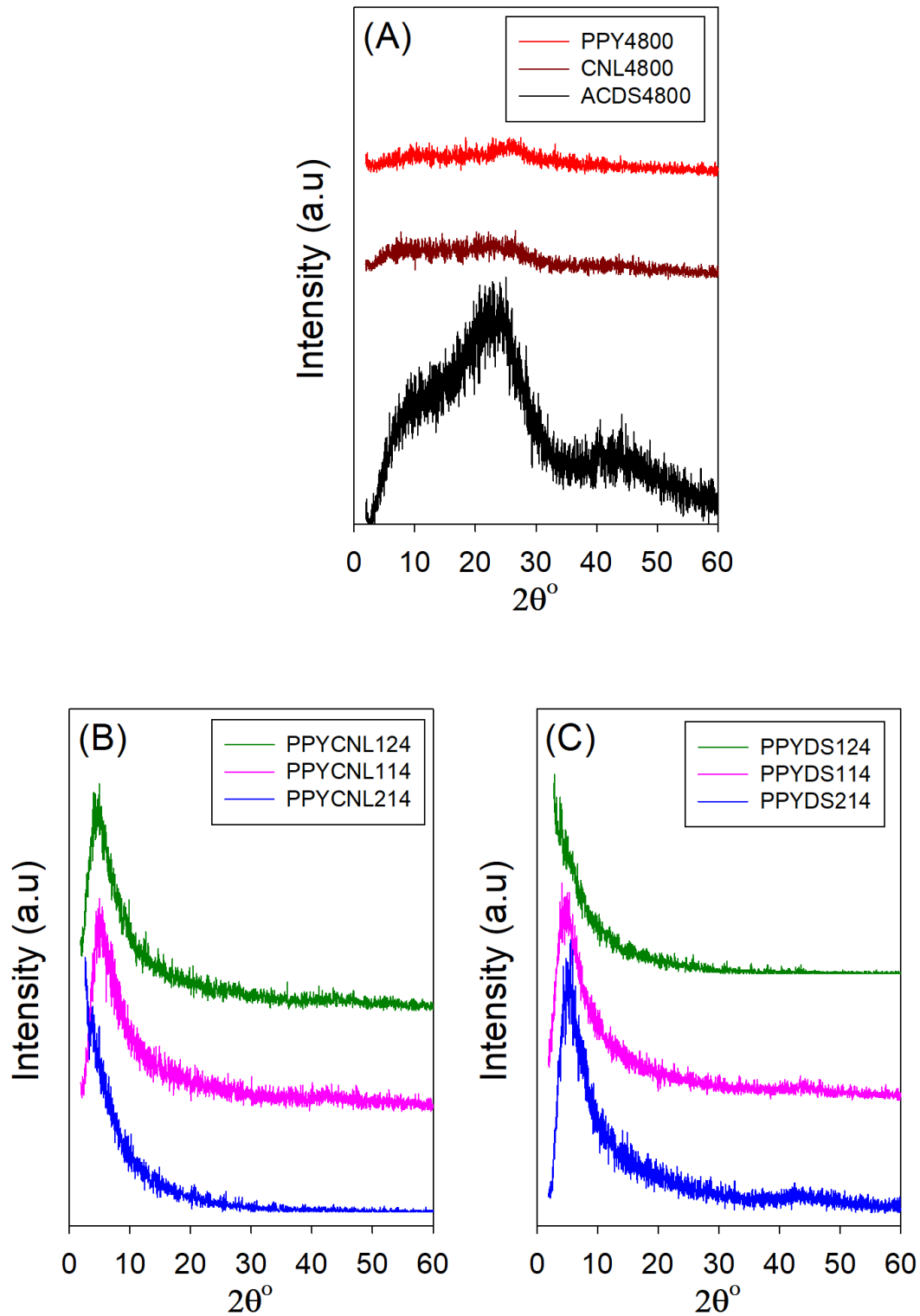


Figure 2. Powder XRD pattern of (A) Polypyrrole, CNL carbon and ACDS carbon precursor materials, and (bottom panels) of activated carbons derived from pre-mixed mixtures of polypyrrole (PPY) and (B) CNL carbon or (C) ACDS carbon.

Porosity modulation of activated carbons via pre-mixed precursors for enhanced methane storage

Scanning electron microscopy was used to examine the surface structure and morphology of the activated carbons. Polypyrrole is known to have globular morphology with globular and spherical particles loosely grouped into bigger assemblies,³⁶ while both CNL carbon and ACDS carbon have previously been shown to retain, respectively, the woody or extended honeycomb structure of the biomass sources.^{18,20,22} The SEM images of representative activated carbons are shown in Figure 3, and indicate that, regardless of the composition of the pre-mixed precursor, the resulting activated carbons have a particle shape that is drastically different from the precursors. The activated carbons comprise of smooth-surfaced particles with extensive conchoidal cavities. This particle morphology is similar to that observed in activated carbons produced from a variety of sources.^{16,18-25,34,37,38} This is consistent with the fact that it is now well-recognised that all activated carbons produced by KOH activation have a similar appearance, and that the type of precursor material has little effect on the morphology. The TEM images of the activated carbons (**Figure 4**) demonstrate wormhole-type pore channels with no indication of graphitic domains which is consistent with the XRD patterns and previous research on biomass-derived activated carbons.¹⁸⁻²⁷

Porosity modulation of activated carbons via pre-mixed precursors for enhanced methane storage

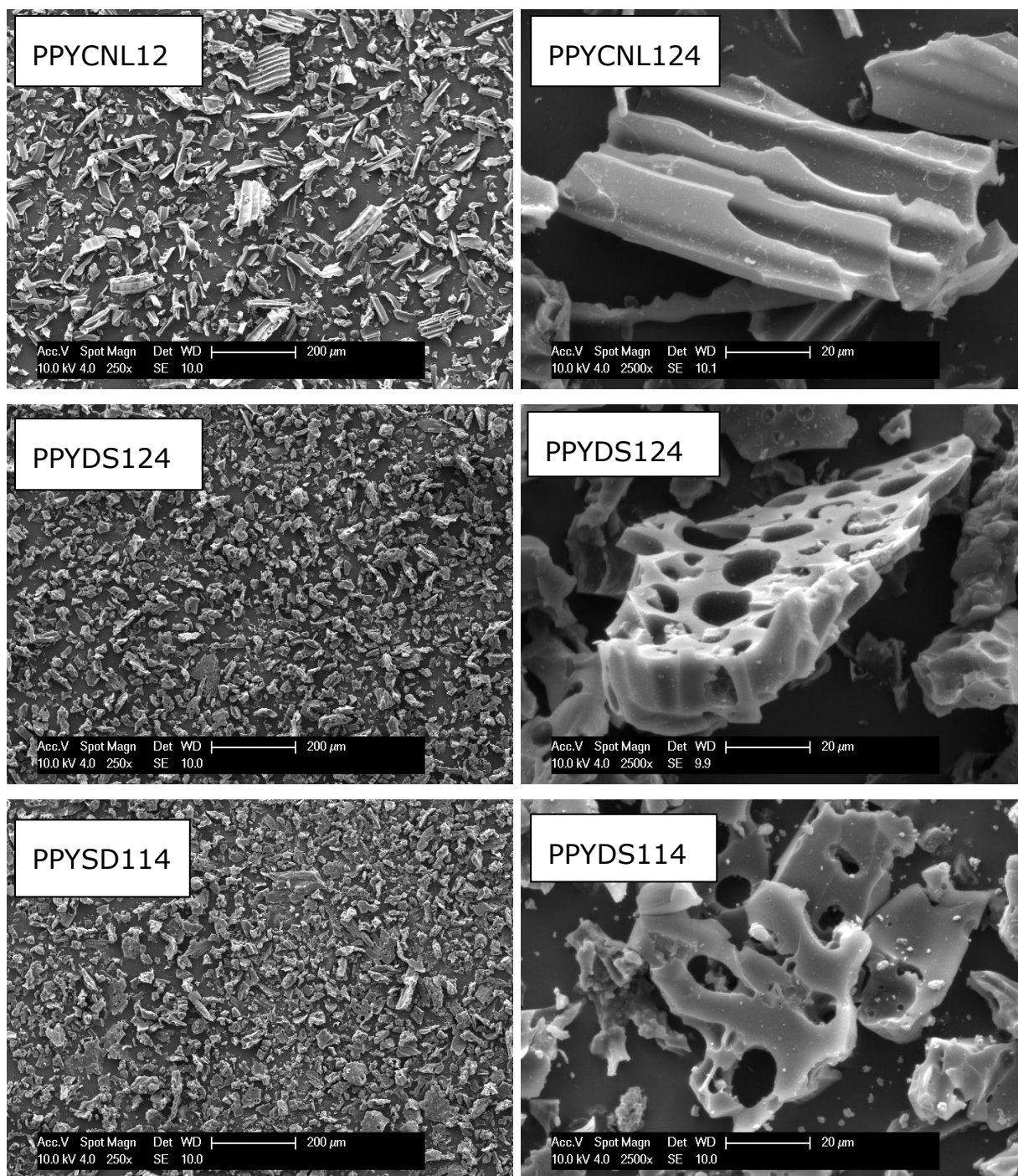


Figure 3. Representative SEM images of activated carbons derived from pre-mixed precursors

Porosity modulation of activated carbons via pre-mixed precursors for enhanced methane storage

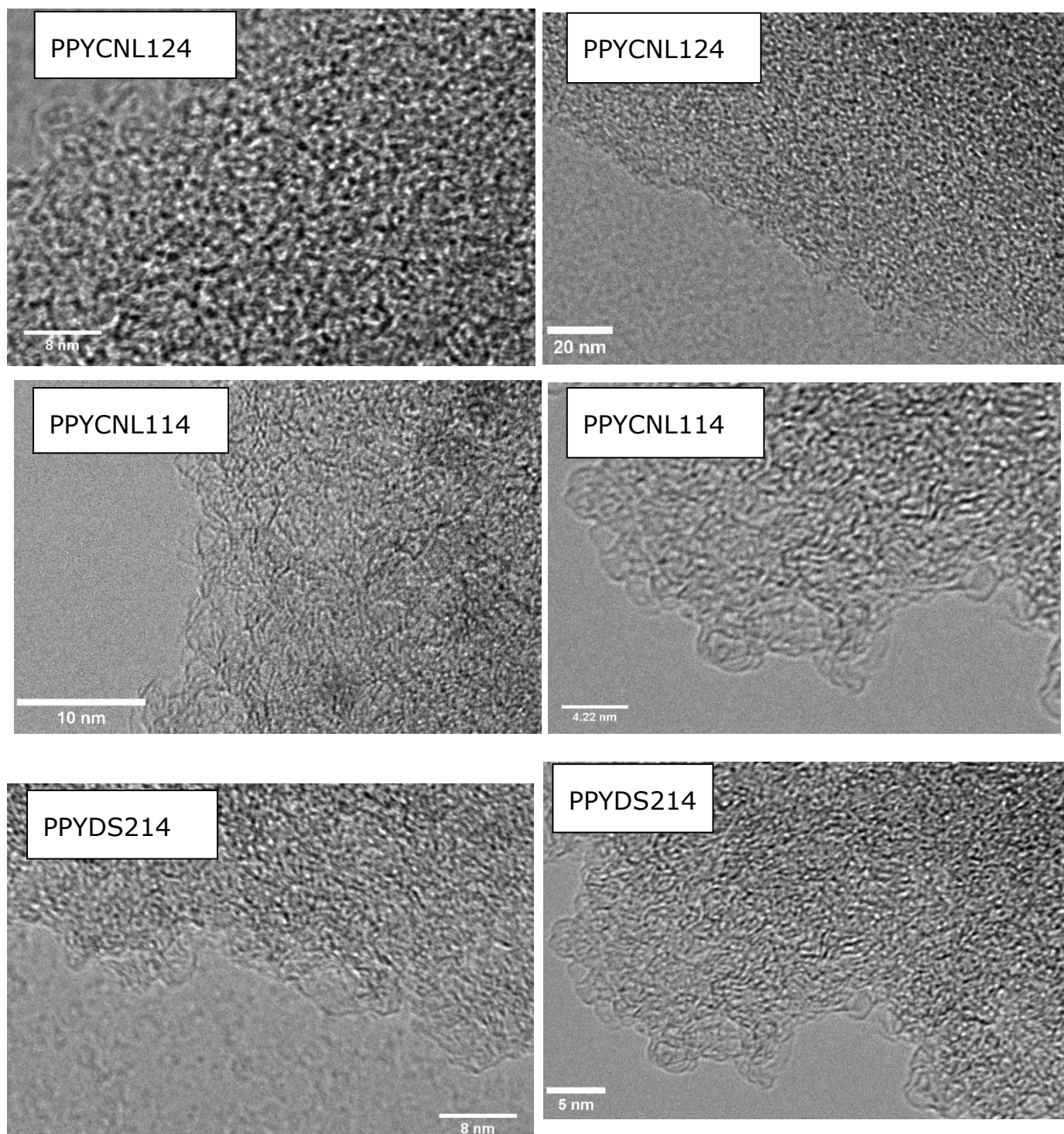


Figure 4. Representative TEM images of activated carbons derived from pre-mixed precursors

Porosity modulation of activated carbons via pre-mixed precursors for enhanced methane storage

6.3.2 Textural properties and porosity

The nitrogen sorption isotherms and corresponding pore size distribution (PSD) curves for the PPY/CNL set of samples, and the PPY-only derived sample (PPY4800) and the CNL-only derived sample (CNL4800) are shown in **Figure 5**. It is worth noting that the PPY-only derived sample (PPY4800) displays an isotherm that is typical of primarily mesoporous materials, whilst the isotherm for the CNL-only derived sample (CNL4800) indicates the presence of a significant proportion of micropores and supermicropores with only a small proportion of small mesopores.^{18,20,22,31-34} The isotherms of the PPY/CNL activated carbons show some clear trend with respect to the nature of the pre-mix precursors. Firstly, the total amount of nitrogen adsorbed, which is an indication of the overall porosity generated, increases as the amount of PPY in the pre-mixture rises in the order CNL4800 < PPYCNL124 < PPYCNL114 < PPYCNL214. Secondly, the shape of the isotherms gradually change with the proportion of PPY. The isotherm of CNL4800 is type I with a relatively sharp adsorption 'knee', which is typical for a mainly microporous material that has supermicropores and some small mesopores. When PPY is added to CNL carbon at a ratio of 1:2 (PPY:CNL carbon), the isotherm of the resulting sample (PPYCNL124) exhibits a much gentle 'knee' suggesting a greater proportion of mesopores. Further increase in the proportion of PPY in the pre-mix results in activated carbons (PPYCNL114 and PPYCNL214) that exhibit type IV isotherms typical of mesoporous materials. Indeed, the isotherms of PPYCNL114 and PPYCNL214 are very similar to that of PPY4800, but with

Porosity modulation of activated carbons via pre-mixed precursors for enhanced methane storage

higher amounts of adsorbed nitrogen. The presence of CNL carbon in the pre-mixtures hinders the generation of mesoporosity to the extent that the isotherm of sample PPYCNL124 suggests a lack of any significant mesoporosity. This trends observed confirm that the nature of the pre-mix precursors has a major impact on the micropore/mesopore combination in the activated carbons.

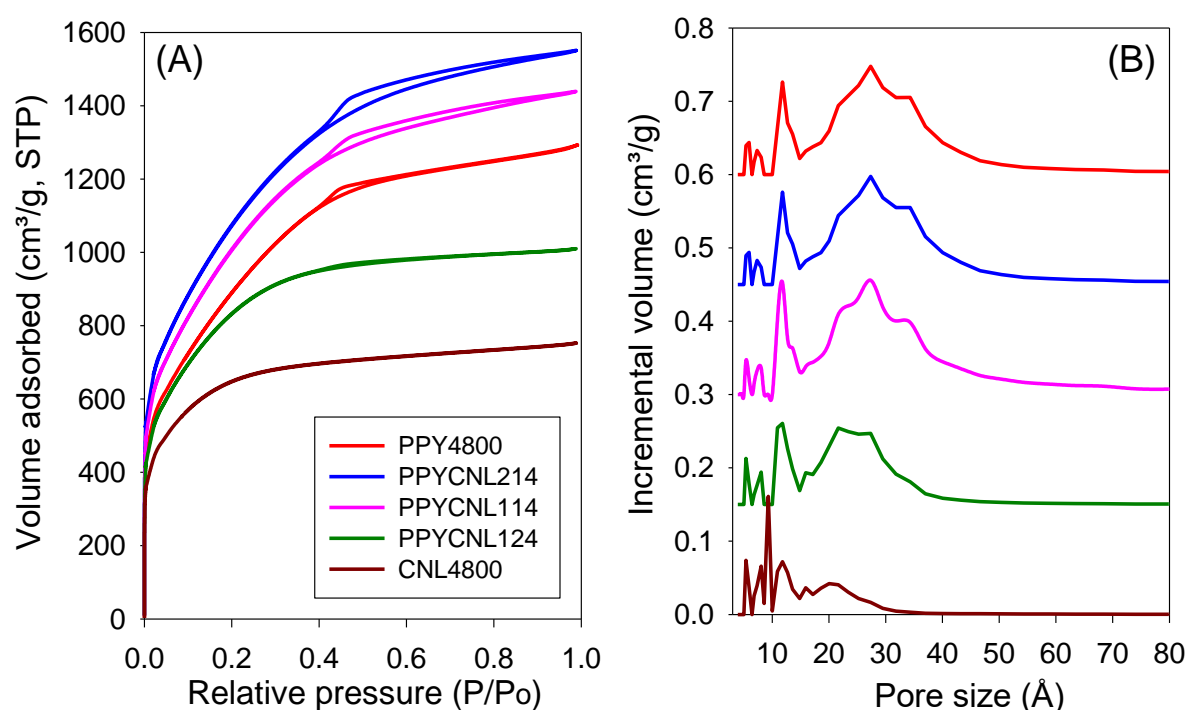


Figure 5. (A) Nitrogen sorption isotherms and (B) pore size distribution curves of activated carbons derived from single precursor, PPY4800 (polypyrrole, PPY) and CNL4800 (CNL carbon) and from pre-mixed precursors containing PPY and CNL carbon at various weight ratios.

Porosity modulation of activated carbons via pre-mixed precursors for enhanced methane storage

The nitrogen sorption isotherms and corresponding PSD curves for the PPY/ACDS set of samples, and the PPY-only derived sample (PPY4800) and ACDS-only derived sample (ACDS4800), are displayed in **Figure 6**. The ACDS4800 sample has an isotherm that is typical of a microporous material. Use of a mix of PPY and ACDS as precursors generates activated carbons with isotherms whose shape and amount of nitrogen adsorbed is significantly altered compared to ACDS4800. Pre-mix precursors with a 1:2 (PPYDS124) or 1:1 (PPYDS114) ratio of PPY/ACDS generate activated carbons with isotherms that have a much gentler adsorption 'knee' consistent with the amount of PPY used. The isotherms of these two samples show a significant proportion of supermicropores and small mesopores that, in terms of the micropore/mesopore mix, lies between the levels of the PPY4800 and ACDS4800 samples. On the other hand, the isotherm of PPYDS214 is similar to that of PPY4800. It is clear to see that mixing polypyrrole and ACDS carbon in the precursor mix lowers mesoporosity, and that the amount of the reduction is greater for higher amounts of ACDS carbon.

Porosity modulation of activated carbons via pre-mixed precursors for enhanced methane storage

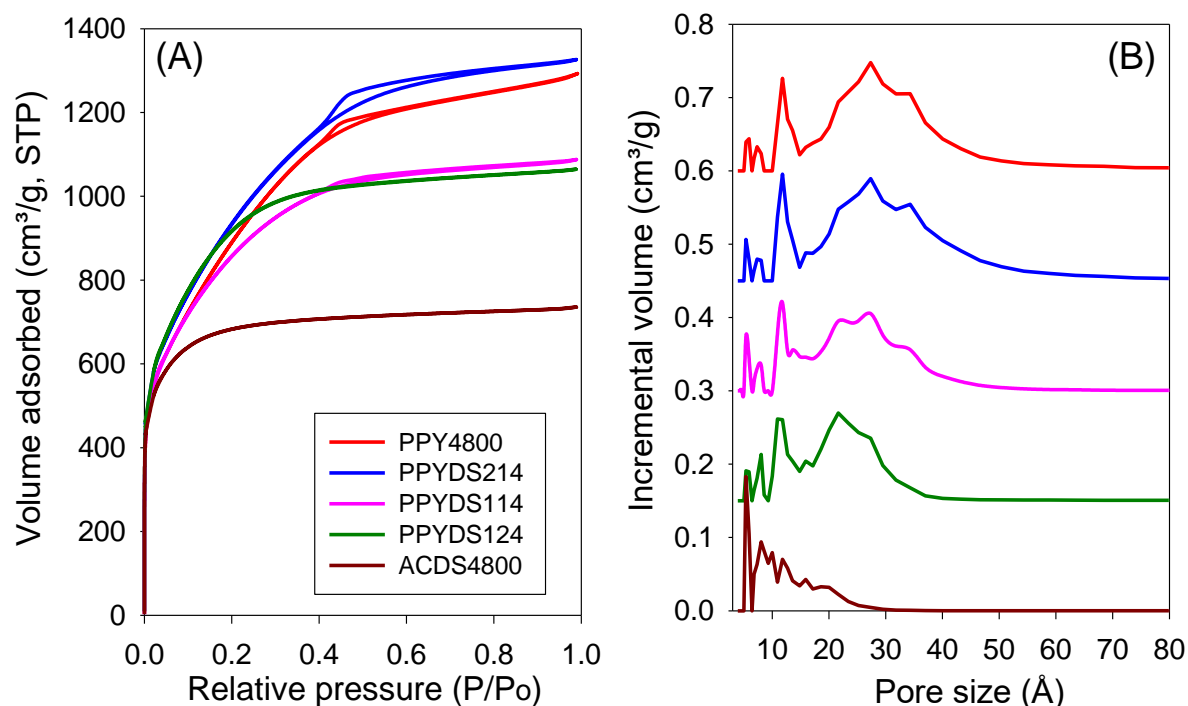


Figure 6. (A) Nitrogen sorption isotherms and (B) pore size distribution curves of activated carbons derived from single precursor, PPY4800 (polypyrrole, PPY) and ACDS4800 (ACDS carbon) and from pre-mixed precursors containing PPY and ACDS carbon at various weight ratios.

The porosity data in **Figure 5** and **6** clearly shows that the nature of the precursors in the pre-mixtures determines the extent to which micropores or mesopores are generated in the activated carbons. Samples prepared from 1:2 mixture of PPY and CNL (PPYCNL124) or 1:2 and 1:1 mixtures of PPY and ACDS (PPYDS124 and PPYDS114) have a moderate level of mesoporosity, which, according to the isotherms, is somewhat intermediate between that of the biomass-derived (CNL4800 and ACDS4800) carbons and PPY4800. We interpret the lower mesoporosity in the pre-mix samples as arising from greater resistance to activation for the CNL and ACDS carbons.

Porosity modulation of activated carbons via pre-mixed precursors for enhanced methane storage

Table 3 gives the pore size maxima values determined from the pore size distribution curves in **Figure 5** and **6**. The CNL-only sample (CNL4800) possess pores mainly within the micropore/supermicropore to small mesopore range, with most pores being of size below 20 Å and hardly any pores wider than 30 Å. The PPY-only (PPY4800) sample, on the other hand, exhibits bimodal pore size distribution with a small proportion of micropores centred at ca. 8 Å and 11Å, and a much larger proportion of mesopores centred at ca. 34 Å. The pore size distribution of the PPY/CNL carbons differs significantly from that of PPY4800 and CNL4800. It is clear to see that the proportion and size mesopores varies depending on the PPY: CNL ratio. The sample made from a 1:2 mixture of PPY/CNL carbon (PPYCNL124) has a relatively smaller proportion of mesopores centred at ca. 24 Å, which is consistent with the observation that the sample tends towards being supermicroporous with small mesoporous and hardly any pores larger than 30 Å. On the other hand, the samples made from 1:1 or 2:1 mixture of PPY and CNL (PPYCNL114) and (PPYCNL214), contain a large proportion of mesopores centred at ca. 27 Å, and their pore size distribution is quite similar to that of PPY4800.

Porosity modulation of activated carbons via pre-mixed precursors for enhanced methane storage

Table 3. Pore size distribution maxima of activated carbons derived from single precursors (Polypyrrole (PPY), CNL carbon and ACDS carbon) and pre-mixed mixtures of the precursors

Sample	Pore size maxima (Å)
PPY4800	12/27
CNL4800	8/12/20
PPYCNL124	12/23
PPYCNL114	12/27
PPYCNL214	12/27
ACDS4800	6/12
PPYDS124	11/22
PPYDS114	12/25
PPYDS214	12/27

The ACDS-only (ACDS4800) sample possess a relatively wide size range of pores but still mainly within the micropore/supercapillary to small mesopore range, with most pores being of size below 20 Å and hardly any pores wider than 25 Å. The sample made from 1:2 or 1:1 mixture of PPY and ACDS (PPYDS124) or (PPYDS114) has a relatively smaller proportion of mesopores centred at 22 Å and 25 Å, respectively, which is consistent with the samples tending towards being supermicroporous with small mesoporous and hardly any pores larger than 30 Å. On the other

Porosity modulation of activated carbons via pre-mixed precursors for enhanced methane storage

hand, the samples made from a 2:1 mixture of PPY and ACDS (PPYDS214) contains a large proportion of mesopores centred at 27 Å, and has a pore size distribution similar to that of PPY4800. It can be concluded that the amount of PPY in the precursor mix is related to the presence of mesopores in the PPY/CNL or PPY/ACDS set of samples, and the size of the mesopores varies based on the PPY:CNL or PPY:ACDS ratio. The quantity and size of mesopores vary, indicating that the pre-mixture has significant effect on the size of pores formed in activated carbons.

The textural parameters of the activated carbons are summarised in **Table 4**. The PPY-only derived sample (PPY4800) has surface area of 3279 m² g⁻¹ and pore volume of 2.0 cm³ g⁻¹, while the CNL-only derived sample (CNL4800) has surface area of 2134 m² g⁻¹ and pore volume of 1.16 cm³ g⁻¹. All the PPY/CNL carbons possess high or ultra-high surface areas which range between 2907 and 3890 m² g⁻¹, and pore volumes within the range of 1.5–2.40 cm³ g⁻¹. The highest surface area for a PPY/CNL sample is for PPYCNL214 (3890 m² g⁻¹) followed by PPYCNL114 (3669 m² g⁻¹), values that are higher than those for either the PPY-only (3279 m² g⁻¹) or CNL-only (2134 m² g⁻¹) derived carbons, and follow the trend in amount of PPY in the pre-mixture. The ACDS-only derived sample (ACDS4800) has a surface area of 2609 m² g⁻¹ and pore volume of 1.1 cm³ g⁻¹. The PPY/ACDS carbons possess moderate to high surface areas in the range 3101 to 3390 m² g⁻¹, and a pore volume of between 1.65 and 2.0 cm³ g⁻¹. The highest surface area is for PPYDS214 (3390 m² g⁻¹), which

Porosity modulation of activated carbons via pre-mixed precursors for enhanced methane storage

is greater than that for either PPY-only derived carbon (3279 m² g⁻¹) or ACDS-only derived carbon (2609 m² g⁻¹).

Table 4. Textural properties of activated carbons derived from single precursors (Polypyrrole (PPY), CNL or ACDS Carbon) and pre-mixed mixtures of the precursors

Sample	Surface area (m ² g ⁻¹)	Micropore surface area ^a (m ² g ⁻¹)	Pore volume (cm ³ g ⁻¹)	Micropore volume ^b (cm ³ g ⁻¹)	Surf.area density ^c (m ² cm ⁻³)	Packing density ^d (g cm ⁻³)	Vol. surface area ^e (m ² cm ⁻³)
PPY4800	3279	1320 (40%)	2.0	0.62 (31%)	1640	0.37	1213
CNL4800	2134	1819 (85%)	1.16	0.90 (78%)	1840	0.67	1430
PPYCNL124	2907	2215 (76%)	1.5	1.07 (71%)	1938	0.52	1512
PPYCNL114	3669	1741 (48%)	2.23	0.82 (37%)	1645	0.39	1431
PPYCNL214	3890	1717 (44%)	2.4	0.81 (34%)	1621	0.36	1400
ACDS4800	2609	1825 (70%)	1.1	0.70 (64%)	2372	0.69	1774
PPYDS124	3132	2631 (84%)	1.65	1.28 (78%)	1898	0.47	1472
PPYDS114	3101	2007 (65%)	1.7	0.93 (55%)	1824	0.47	1457
PPYDS214	3390	1372 (41%)	2.0	0.64 (32%)	1695	0.40	1356

^aValues in parenthesis are % of surface area from micropores. ^bValues in parenthesis are % of pore volume from micropores. ^cSurface area density is obtained as ratio of total surface area to total pore volume. ^dThe packing density was determined by pressing a given amount of carbon in a 1.3 cm die at pressure of 7 MPa for 5 min. Alternatively, relatively similar values are obtained using the general equation; $d_{\text{carbon}} = (1/\rho_s + VT)^{-1}$ where ρ_s is skeletal density and VT is total pore volume. ^eVolumetric surface area determined as surface area x packing density.

Porosity modulation of activated carbons via pre-mixed precursors for enhanced methane storage

The addition of CNL and ACDS carbons to the mixtures increases microporosity and reduces the overall pore volume, with the reductions being greatest for samples prepared from 1:2 or 1:1 PPY/CNL or ACDS ratios (PPYCNL114, PPYDS124 and PPYDS114). The microporosity (given as % of surface area or pore volume from micropores) of activated carbons derived from pre-mix precursors decreases with the proportion of PPY in the mixtures. The textural data clearly demonstrate modulation of porosity of the activated carbons based only on systematic variation of the precursor mixtures. However, in all cases the microporosity does not go below that of the PPY4800 sample despite some of the samples having higher surface area and pore volume. It is also interesting to note that the data in **Table 4** suggests that, in general, the textural parameters of the PPY/ACDS carbons is lower than that of the PPY/CNL equivalents, which is consistent with the fact that ACDS carbon has a lower O/C ratio (0.156) compared to CNL carbon (0.185).

Table 4 also gives the surface area density, which is defined as the ratio of total surface area to total pore volume, of the activated carbons. The surface area density is a parameter that can be used to assess carbonaceous matter's susceptibility or resistance to activation as shown in chapter 3.^{21,22} The surface area density of PPY4800, CNL4800 and ACDS4800 carbons is, respectively, 1640, 1840 and 2372 m² cm⁻³. The trend is consistent with the O/C ratio of the respective precursors, with low ratios signifying resistance to activation and therefore a higher surface area density.^{21,22} ACDS4800 has the highest surface area density, which is

Porosity modulation of activated carbons via pre-mixed precursors for enhanced methane storage

consistent with the fact that the ACDS carbon is the most resistant to activation.²² It has previously been shown that a high surface area density, i.e., the tendency to generate micropores as opposed to larger pores, arises because air-carbonisation of biomass enriches the proportion of lignin products, which are less susceptible to activation.^{18-21,39-45} These results confirm that the O/C ratio is an inherent property of the starting carbonaceous material and that it can be used as a predictor of activation resistance and therefore the type of porosity to be generated.

The surface area density of the pre-mix activated carbons is in the range 1621 – 1938 m² cm⁻³. It is clear that activated carbons derived from pre-mixtures with high amounts of PPY have a lower surface area density, i.e., that the surface area density is inversely proportion to the amount of PPY in the pre-mixture. In particular, samples PPYCNL114, PPYCNL214 and PPYDS214, which are lowly microporous (i.e., have the highest proportion of mesoporosity), display lower surface area densities of 1621, 1645 and 1695 m² cm⁻³, respectively. However, the surface area density of these samples is still higher or comparable to that of PPY4800. Indeed, only sample PPYCNL214, with an extremely high surface area of close to 3900 m² g⁻¹, has surface area density lower than that of PPY4800. Due to their microporous nature, sample CNL4800 and ACDS4800 have relatively high packing density of 0.67 and 0.69 g cm⁻³, respectively, which is significantly higher than that (0.37 g cm⁻³) of the more mesoporous PPY4800. The packing density of the pre-mix activated carbons ranges between 0.36 and 0.52 g cm⁻³. It is interesting to note that despite the higher porosity of

Porosity modulation of activated carbons via pre-mixed precursors for enhanced methane storage

some of the pre-mix samples (PPYCNL114, PPYCNL214 and PPYDS214), their packing density is higher or similar to that of PPY4800. This may be attributed to the packing density enhancing contribution of the CNL and ACDS carbon ingredients.

The volumetric surface area (defined as surface area \times packing density) of the carbons in **Table 4** shows some interesting trend. We note that volumetric surface area of porous materials has previously been used as a proxy for gas storage performance especially for methane.^{22,46} The volumetric surface area of PPY4800, CNL4800 and ACDS4800 carbons is, respectively, 1213, 1430 and 1774 $\text{m}^2 \text{cm}^{-3}$. Once again, the trend is consistent with the O/C ratio of the respective precursors, with low ratios resulting in activated carbons with higher volumetric surface area. The volumetric surface area of the pre-mix activated carbons is in the range 1400 – 1512 $\text{m}^2 \text{cm}^{-3}$ for PPYCNL carbons and between 1356 and 1472 $\text{m}^2 \text{cm}^{-3}$ for PPYDS samples. The volumetric surface area is inversely proportion to the amount of PPY in the pre-mixture, and consequently reduces for samples that have a high proportion of mesoporosity. It is noteworthy that the volumetric surface area of all pre-mix samples, including those with very high surface area (PPYCNL114, PPYCNL214 and PPYDS214) is higher than that of PPY4800. The volumetric surface area of the present pre-mix carbons is amongst the highest reported for porous materials. There have been reports of MOFs with higher volumetric surface area (e.g., 2060 $\text{m}^2 \text{cm}^{-3}$ for NU-1501-Al) but such values are an

Porosity modulation of activated carbons via pre-mixed precursors for enhanced methane storage

overestimation as they are computed using crystallographic density rather than packing density.⁴⁷

To get further insights on the trends discussed above, it is useful to consider the behaviour of a variety of carbonaceous matter with variable O/C ratio in order to more fully understand the effect of elemental composition, particularly the O/C ratio, on the activation of various precursors and the generation of mesoporosity. In this regard, the porosity of PPY4800, CNL4800 and ACDS4800 was compared to that of previously reported activated carbons derived from raw sawdust, sawdust-derived hydrochar²¹ and Jujun grass.²⁵ All carbonaceous precursors were activated in a similar manner, i.e., at 800 °C and KOH/precursor ratio of 4. The O/C ratio varied between 0.156 and 0.773 in the order: raw sawdust > Jujun grass > sawdust hydrochar > CNL carbon > flash air-carbonised date seed (ACDS). The porosity data in **Table 5** demonstrates a link between the O/C ratio of the precursors and the degree of mesoporosity generated in the activated carbons. The carbonaceous precursors with high O/C ratio generated activated carbons, e.g. SD4800D and ACGR-4800, with greater mesoporosity. In contrast, the porosity of activated carbons obtained from precursors with a low O/C ratio, e.g. CNL4800 and ACDS4800, exhibited low levels of mesoporosity.

Porosity modulation of activated carbons via pre-mixed precursors for enhanced methane storage

Table 5. Surface area and level of mesoporosity of activated carbons prepared from precursors with varying atomic O/C ratio. All the activated carbons were prepared at activation temperature of 800°C and KOH/precursor ratio of 4.

Sample	Precursor	O/C ratio	Surface area ^a (m ² g ⁻¹)	Meso SA (%)
ACDS4800	ACDS carbon	0.156	2609 (1825)	30
CNL4800	CNL carbon	0.185	2134 (1819)	15
SD4800	Sawdust hydrochar	0.483	2783 (694)	75
ACGR-4800	Grass hydrochar	0.517	2957 (1578)	47
SD4800D	Raw sawdust	0.773	2980 (478)	84

The values in the parenthesis refer to: ^amicropore surface area.

As previously stated, precursors with a greater O/C ratio produce activated carbons, e.g. PPY4800, that are essentially mesoporous since they are easier to activate, whereas those with lower O/C ratio generate more microporous carbons, such as ACDS4800 and CNL4800. The level of mesoporosity is, therefore, a measure of the ease with which the precursors can be activated; high O/C ratio precursors can be activated more rapidly or to a greater degree to generate larger pores, whereas low O/C precursors are more resistant to KOH activation and hence predominantly yield micropores. Thus, samples ACDS4800 and CNL4800 are almost totally microporous with microporosities of 70% and 85%, respectively, whereas sample PPY4800 has only 40% microporosity. Furthermore, a previous

Porosity modulation of activated carbons via pre-mixed precursors for enhanced methane storage

study reported an inability to directly activate cellulose acetate, which has a high O/C ratio of 0.93, and had no carbon yield on activation.^{23,28} The absence of any yield signifies complete burn-off since cellulose acetate is most readily activated. In terms of the effect of a high O/C ratio, it is likely that a higher O content means a higher proportion of O-containing polar functional groups, which makes activation easier. Low O/C ratio, on the other hand, is related to the presence of stable carbon forms that are resistant to activation.²⁶

6.3.3 Methane Storage

In order for a porous material to achieve efficient methane storage at moderate to high pressures, e.g. 35 – 100 bar, it should be essentially microporous with low mesoporosity and a large surface area. Pore channel dimensions with a diameter of 8 to 15 Å offer the most efficient adsorption of 2 or 3 methane molecules whilst optimising the packing of the adsorbed phase within the pores.^{4-9,46,47} The current carbons should be ideal candidates to attain high methane storage capacity at moderate to high pressures, particularly given their combination of micro- and mesoporosity characteristics (**Table 3 and 4**). The methane uptake capacity of the current carbons was determined at pressures of between 0 and 100 bar, and at ambient temperature, i.e., 25 °C. Focus was placed on uptake at 35, 65 and 100 bar, pressures that have been widely benchmarked in previous studies and which allow for simple comparison of the performance

Porosity modulation of activated carbons via pre-mixed precursors for enhanced methane storage

of the present carbons to existing state-of-the-art materials. The methane uptake measurements facilitated direct determination of the excess uptake. The total methane storage capacity was then determined from the excess data by considering the density of methane at any temperature and pressure and the total pore volume of the adsorbing activated carbon. This was achieved by applying the equation:

$$\theta_T = \theta_{Exc} + d_{CH_4} \times V_T$$

where; θ_T is total methane uptake, θ_{Exc} is excess methane uptake, d_{CH_4} is density (g cm^{-3}) of methane gas under the prevailing temperature and pressure, and V_T is total pore volume ($\text{cm}^3 \text{g}^{-1}$) of the activated carbon. The methane density (d_{CH_4}) was obtained from the National Institute of Standards and Technology website (<http://www.nist.gov/>).

Figure 7 shows the excess methane uptake isotherms of PPY4800, CNL4800 and ACDS4800 along with those of the PPY/CNL and PPY/ACDS pre-mix carbons. **Table 6** summarises the methane storage capacity at 35, 65 and 100 bar. For all the activated samples, the methane uptake isotherms are completely reversible with no hysteresis. At 35 bar, PPY4800 stores 12.6 mmol g^{-1} whereas CNL4800 and ACDS4800 store 11.1 and 10.9 mmol g^{-1} , respectively. For the PPY/CNL samples, the methane storage capacity at 35 bar is between 11.8 and 12.7 mmol g^{-1} , while for the PPY/ACDS carbons it varies 11.8 and 12.8 mmol g^{-1} . The excess methane uptake is generally in line with the surface area of the carbons. At 25°C and 35 bar, excess methane uptake of up to 12.8 mmol g^{-1} is amongst the

Porosity modulation of activated carbons via pre-mixed precursors for enhanced methane storage

most optimal reported for any porous material and shows the potential of the pre-mix carbons as methane stores at moderate pressure.^{4-9,46,47} The excess methane uptake of the pre-mixed carbons is in the range of 14.1 - 15.7 mmol g⁻¹ and 15.0 - 17.1 mmol g⁻¹ at 65 and 100 bar, respectively, with samples of PPYCNL214 and PPYDS214 having the highest methane uptake. It is clear to see that samples prepared from pre-mixtures with a higher amount of PPY store greater amounts of methane, which surpasses that of single precursor carbons (PPY4800, CNL4800 and ACDS4800). This is the first indication that the strategy of using pre-mixtures as precursors, which transfers to modulated porosity, also has a positive effect on methane storage capacity.

Porosity modulation of activated carbons via pre-mixed precursors for enhanced methane storage

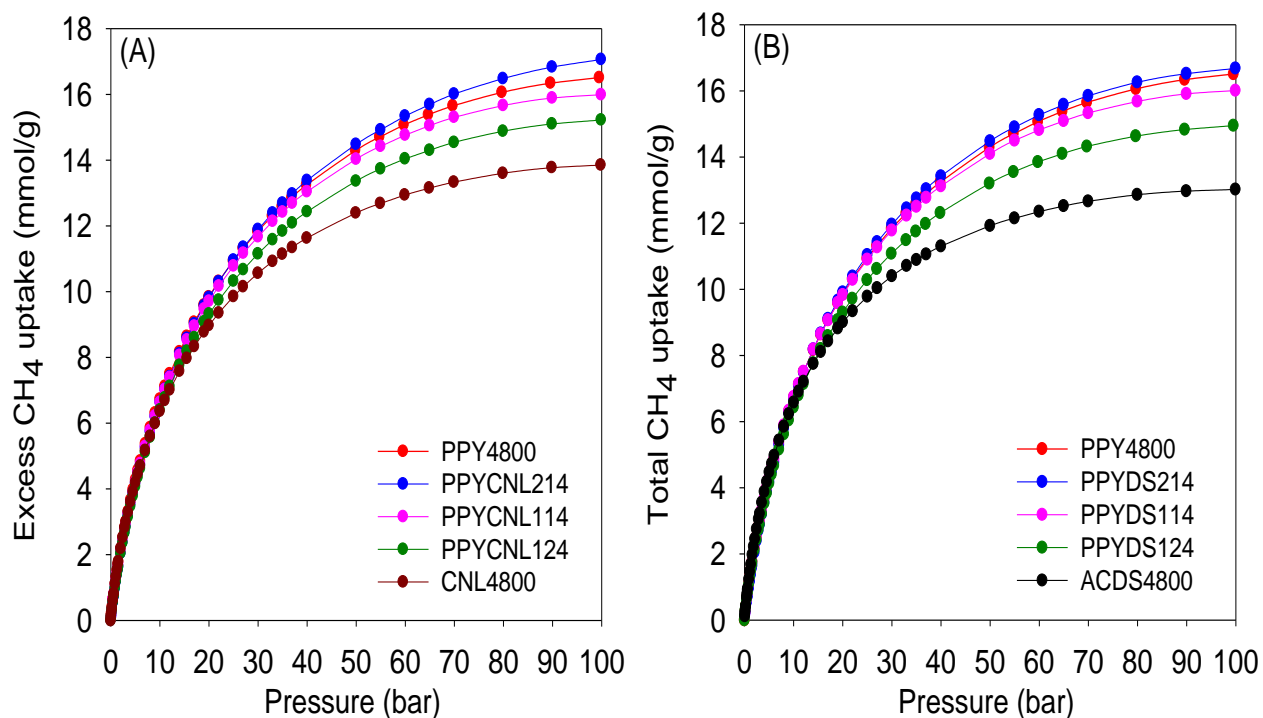


Figure 7. Excess gravimetric methane uptake of activated carbons derived from single precursor, PPY4800 (polypyrrole, PPY), CNL4800 (CNL carbon) and ACDS4800 (ACDS carbon) and from pre-mixed precursors containing PPY and (A) CNL carbon or (B) ACDS carbon at various weight ratios.

Porosity modulation of activated carbons via pre-mixed precursors for enhanced methane storage

Table 6. Excess gravimetric methane uptake of activated carbons derived from single precursor, PPY4800 (polypyrrole, PPY) and CNL4800 (CNL carbon) and from pre-mixed precursors containing PPY and CNL carbon at various weight ratios.

sample	Excess gravimetric methane uptake (mmol g^{-1})		
	35 bar	65 bar	100 bar
PPY4800	12.6	15.4	16.5
CNL4800	11.1	13.2	13.9
PPYCNL124	11.8	14.3	15.2
PPYCNL114	12.4	15.1	16.0
PPYCNL214	12.7	15.7	17.1
ACDS4800	10.9	12.5	13.0
PPYDS124	11.8	14.1	15.0
PPYDS114	12.5	15.1	16.0
PPYDS214	12.8	15.6	16.7

From the data in **Figure 7** and **Table 6**, the excess gravimetric methane uptake appears to be determined by several factors: (i) the level of microporosity, which appears to have an inverse relationship with the excess methane uptake; (ii) the total surface area, with excess methane uptake increasing for higher surface area carbons; and (iii) the nature of the pre-mixture with greater amounts of PPY being associated with increased methane uptake due to higher surface area. To get a clearer view of the methane storage efficiency, we explored the methane uptake density

Porosity modulation of activated carbons via pre-mixed precursors for enhanced methane storage

(expressed as $\text{mmol CH}_4 \text{ m}^{-2}$) of the carbons as shown in **Figure 8**. For PPY/CNL carbons, the uptake density appears to be related to the level of microporosity with sample CNL4800 having both the highest density and micropore surface area, followed by PPYCNL124. There is little variation in the uptake density of PPY4800 and the PPY/CNL samples, which is line with the pore maxima of these carbons (**Table 3**) with pores of size 12 Å and 23 - 27 Å. The higher uptake density of CNL4800 may be related to the presence of significant proportion of pores of size 8 - 10 Å, which is consistent with previous reports that 8 to 11 Å diameter pores offer the most efficient adsorption of methane with optimised packing of the adsorbed phase within the pores.^{4-9,46,47,52} For PPYDS samples (**Figure 8B**), there is only a slight link to the level of microporosity. It is surprising that the uptake density of ACDS4800 is only slightly higher (especially at low pressure (**Figure 9**) to that of the PPY/DS samples. This may be explained by the fact that ACDS4800 is unique in having a significant proportion of 6 Å pores and that such pores are not efficient for high density methane storage as they are too small to optimise packing of 2 or 3 CH_4 molecules. This is consistent with previous reports that pores of size 11 Å are the most suited for methane storage.⁵²

Porosity modulation of activated carbons via pre-mixed precursors for enhanced methane storage

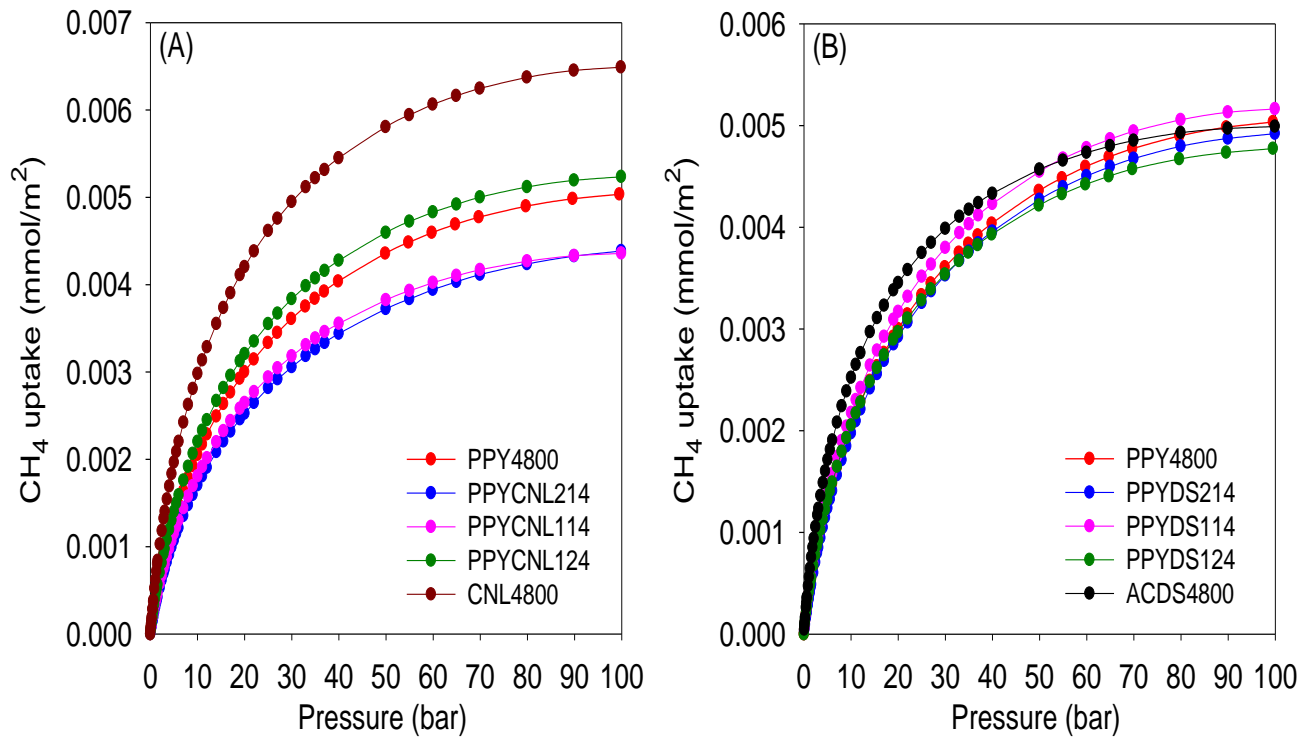


Figure 8. Excess gravimetric methane uptake density of activated carbons derived from single precursor, PPY4800 (polypyrrole, PPY), CNL4800 (CNL carbon) and ACDS4800 (ACDS carbon) and from pre-mixed precursors containing PPY and (A) CNL carbon or (B) ACDS carbon at various weight ratios.

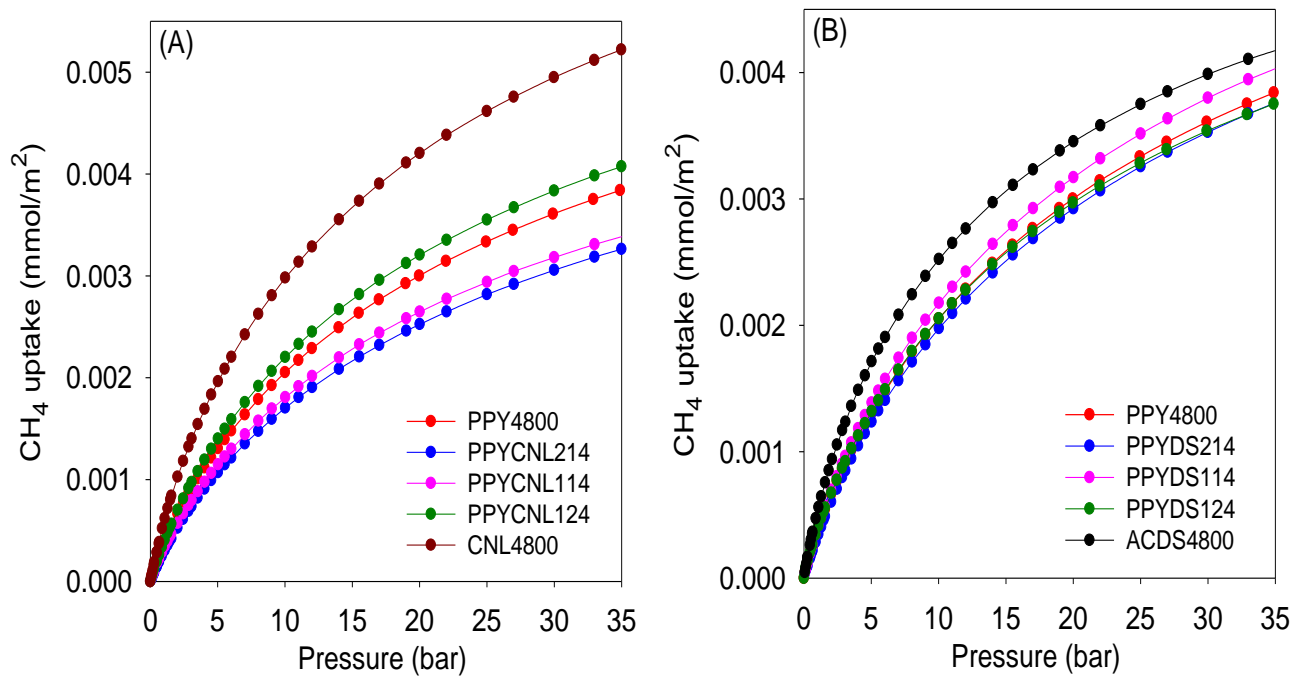


Figure 9. Excess gravimetric methane uptake density at low pressure (0 – 35 bar) of activated carbons derived from single precursor, PPY4800 (polypyrrole, PPY), CNL4800 (CNL carbon) and ACDS4800 (ACDS carbon) and from pre-mixed precursors containing PPY and (A) CNL carbon or (B) ACDS carbon at various weight ratios.

Porosity modulation of activated carbons via pre-mixed precursors for enhanced methane storage

The total gravimetric methane uptake isotherms of PPY4800, CNL4800 and ACDS4800 along with those of the PPY/CNL and PPY/ACDS carbons are shown in **Figure 10**. The total gravimetric methane uptake at 35, 65 and 100 bar, are summarised in **Table 7** and **Table 8** and generally follow the trends discussed above for the excess methane uptake. For the single precursor materials, the total methane storage was, respectively for PPY4800, CNL4800 and ACDS4800, 15.6, 12.9 and 12.6 mmol g⁻¹ (at 35 bar) 21.2, 16.6 and 15.7 mmol g⁻¹ (at 65 bar) and 26.0, 19.3 and 18.2 mmol g⁻¹ (at 100 bar). For PPY/CNL carbons the total methane uptake at 35 bar varies from 14.1 to 16.3 mmol g⁻¹ at 35 bar, while for PPY/DS samples it is between 14.2 and 15.8 mmol g⁻¹. The mixed precursors offer carbons with total methane uptake that outperforms previously reported carbon materials,^{10,53-55} including those reported in chapter 3. Moreover, the total gravimetric uptake of some of the pre-mixed carbons also surpasses that of PPY4800. At 65 bar, the total methane uptake varies from 18.7 to 22.7 mmol g⁻¹ for PPY/CNL carbons, and is between 18.9 and 21.4 mmol g⁻¹ for PPY/DS samples. The mixed precursors offer carbons with total methane uptake that outperforms previously reported carbon materials,^{10,47-58} including those reported in chapter 3. At 100 bar, the total methane uptake varies from 22.2 to 28.4 mmol g⁻¹ for PPY/CNL carbons, and ranges from 22.8 to 26.1 mmol g⁻¹ for PPY/DS samples. Such gravimetric uptake is amongst the best reported to date for carbon or MOF materials.^{4-10,47-58}

Porosity modulation of activated carbons via pre-mixed precursors for enhanced methane storage

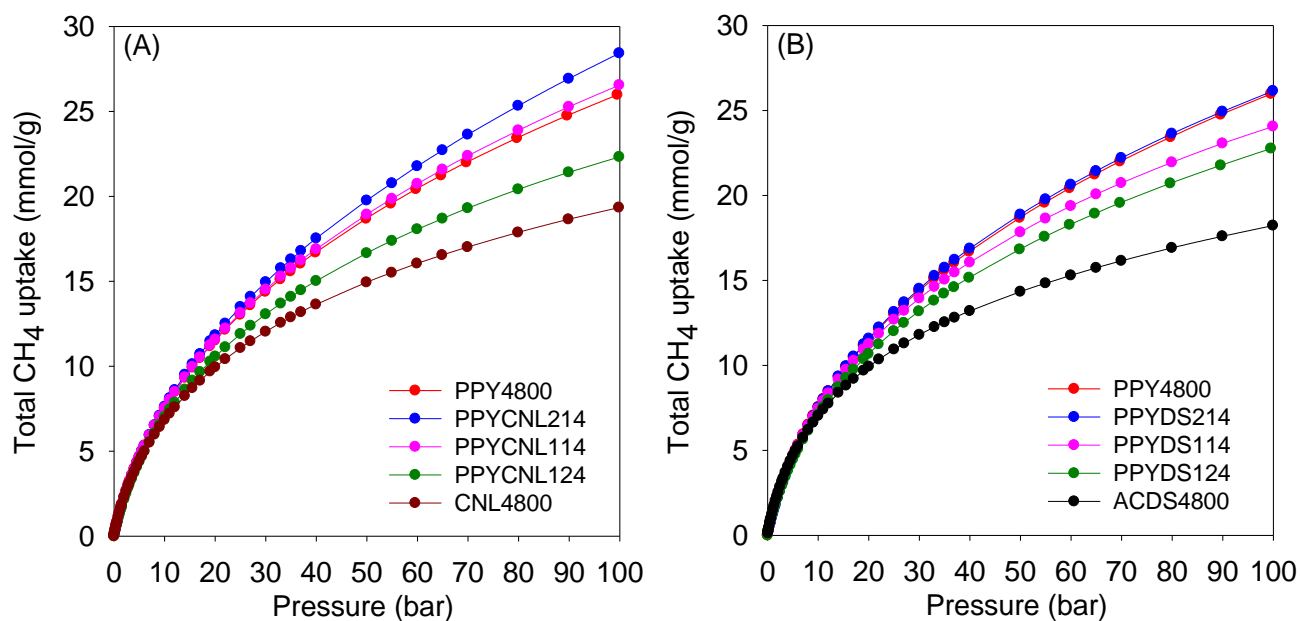


Figure 10. Total gravimetric methane uptake of activated carbons derived from single precursor, PPY4800 (polypyrrole, PPY), CNL4800 (CNL carbon) and ACDS4800 (ACDS carbon) and from pre-mixed precursors containing PPY and (A) CNL carbon or (B) ACDS carbon at various weight ratios.

Porosity modulation of activated carbons via pre-mixed precursors for enhanced methane storage

Table 7. Total gravimetric methane uptake of activated carbons derived from single precursor, PPY4800 (polypyrrole, PPY) and CNL4800 (CNL carbon) and from pre-mixed precursors containing PPY and CNL carbon at various weight ratios.

Sample	Total gravimetric methane uptake (mmol g ⁻¹)		
	35 bar	65 bar	100 bar
PPY4800	15.6	21.2	26.0
CNL4800	12.9	16.6	19.3
PPYCNL124	14.1	18.7	22.3
PPYCNL114	15.8	21.6	26.6
PPYCNL214	16.3	22.7	28.4
ACDS4800	12.6	15.7	18.2
PPYDS124	14.2	18.9	22.8
PPYDS114	15.1	20.1	24.1
PPYDS214	15.8	21.4	26.1

A gravimetric methane uptake target of 0.5 g g⁻¹ has been set by the US DOE. As shown in **Table 8**, the methane uptake, at 100 bar, of some of the pre-mix samples is very close to the DOE target; 0.43 g g⁻¹ (PPYCNL114), 0.46 g g⁻¹ (PPYCNL214) and 0.42 g g⁻¹ (PPYDS214). These values, along with that of PPY4800 (0.42 g g⁻¹) are significantly higher than any previously reported for carbons or other porous materials.^{4-10,47-58} It is

Porosity modulation of activated carbons via pre-mixed precursors for enhanced methane storage

noteworthy that while the pre-mix samples have uptake that is comparable or better than that of PPY4800, they have much higher gravimetric storage than CNL4800 and ACDS4800 by up to 25% (35 bar), 40% (at 65 bar) and 50% (at 100 bar). Such gravimetric uptake, if coupled with good volumetric uptake, would make the pre-mix samples very attractive for methane storage.

Table 8. Total gravimetric methane uptake (expressed as g g^{-1}) of activated carbons derived from single precursor, PPY4800 (polypyrrole, PPY) and CNL4800 (CNL carbon) and from pre-mixed precursors containing PPY and CNL carbon at various weight ratios.

Sample	Total gravimetric methane uptake (g g^{-1})		
	35 bar	65 bar	100 bar
PPY4800	0.25	0.34	0.42
CNL4800	0.21	0.26	0.31
PPYCNL124	0.23	0.30	0.36
PPYCNL114	0.25	0.35	0.43
PPYCNL214	0.26	0.36	0.46
ACDS4800	0.20	0.25	0.29
PPYDS124	0.23	0.30	0.36
PPYDS114	0.24	0.32	0.39
PPYDS214	0.25	0.34	0.42

Porosity modulation of activated carbons via pre-mixed precursors for enhanced methane storage

At 25 °C and up to 100 bar, the targeted porosity development in the current pre-mix carbons clearly achieves excellent gravimetric methane storage capacity. The volumetric uptake, which takes into account an adsorbent's packing density, is a key measure of methane storage performance. Thus the volumetric uptake capacity, which is defined as cm^3 (STP) cm^{-3} , i.e., cm^3 of methane per unit tank volume occupied by the adsorbent. Along with the gravimetric uptake mentioned above (0.5 g g^{-1}), the United States Department of Energy (DOE) has set a target of 263 cm^3 (STP) cm^{-3} at ambient temperature of 25 °C and moderate pressure, i.e., 35–100 bar. **Figures 11** shows the total volumetric methane storage isotherms. **Table 9** summarises the volumetric methane uptake at 35, 65 and 100 bar. Table 9 also gives the working capacity (i.e., deliverable methane) defined as the difference in uptake between 5 bar and the storage pressure (35, 65 or 100 bar). For the single precursor materials, the total methane volumetric storage (given as cm^3 (STP) cm^{-3}) was, respectively, for PPY4800, CNL4800 and ACDS4800, 129, 194 and 194 (at 35 bar) 176, 249 and 243 (at 65 bar) and 215, 291 and 282 (at 100 bar). The total volumetric capacity of PPY/CNL carbons at 35 bar varies from 132 to 164 cm^3 (STP) cm^{-3} at 35 bar, while for PPY/DS samples it is in the range 141 to 159 cm^3 (STP) cm^{-3} . It is noteworthy that, in all cases, the total volumetric uptake of the pre-mixed carbons surpasses that of PPY4800. At 65 bar, the total methane uptake varies from 183 to 217 cm^3 (STP) cm^{-3} for PPY/CNL carbons, and 199 – 211 cm^3 (STP) cm^{-3} for PPY/DS samples.

Porosity modulation of activated carbons via pre-mixed precursors for enhanced methane storage

At 100 bar, the total methane uptake varies from 229 to 260 cm^3 (STP) cm^{-3} for PPY/CNL carbons, and from 234 to 254 cm^3 (STP) cm^{-3} for PPY/DS samples. Such volumetric uptake, calculated based on experimentally determined packing density, is amongst the best reported to date for carbon or MOF materials.^{4-10,47-58}

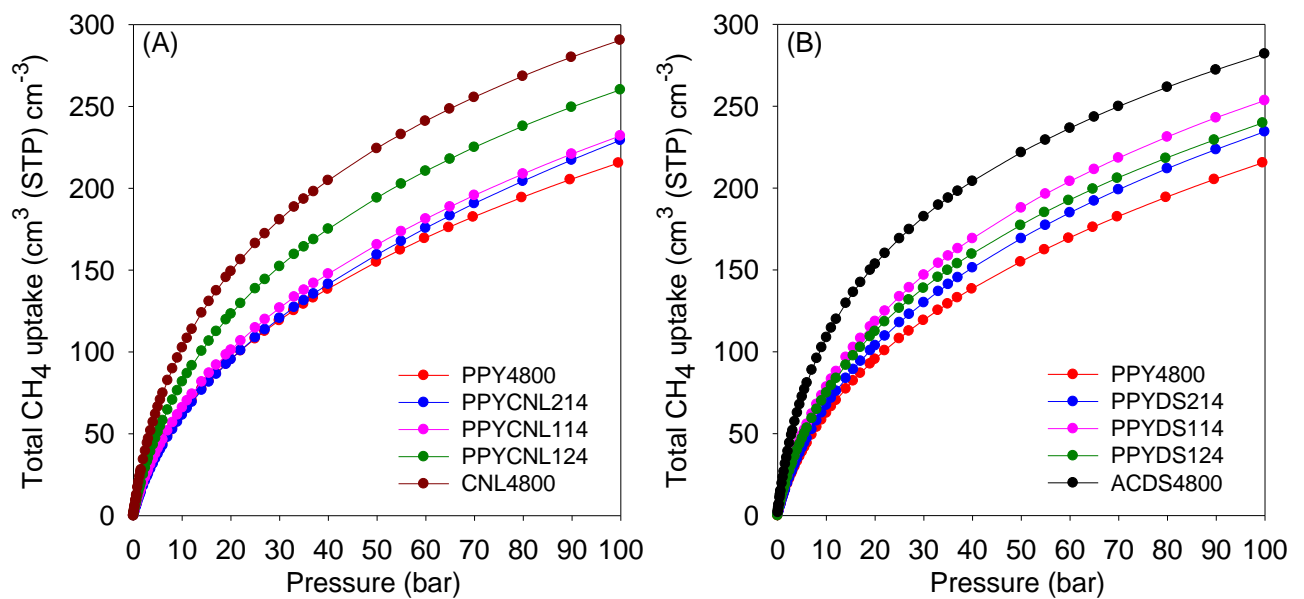


Figure 11. Total volumetric methane uptake of activated carbons derived from single precursor, PPY4800 (polypyrrole, PPY), CNL4800 (CNL carbon) and ACDS4800 (ACDS carbon) and from pre-mixed precursors containing PPY and (A) CNL carbon or (B) ACDS carbon at various weight ratios.

Porosity modulation of activated carbons via pre-mixed precursors for enhanced methane storage

Table 9. Total volumetric methane uptake and working capacity of activated carbons derived from single precursor, PPY4800 (polypyrrole, PPY) and CNL4800 (CNL carbon) and from pre-mixed precursors containing PPY and CNL carbon at various weight ratios.

Sample	Total volumetric methane uptake ^a (cm ³ (STP) cm ⁻³)		
	35 bar	65 bar	100 bar
PPY4800	129 (90)	176 (137)	215 (177)
CNL4800	194 (127)	249 (182)	291 (224)
PPYCNL124	164 (113)	217 (167)	260 (209)
PPYCNL114	138 (97)	189 (148)	232 (191)
PPYCNL214	132 (94)	183 (146)	229 (192)
ACDS4800	194 (122)	243 (171)	282 (209)
PPYDS124	150 (103)	199 (152)	240 (193)
PPYDS114	159 (110)	211 (162)	254 (205)
PPYDS214	141 (100)	192 (151)	234 (193)

The values in parenthesis are the volumetric working capacity defined as the difference in uptake between the stated pressure (35, 65 or 100 bar) and 5 bar.

In all cases, the volumetric uptake of the pre-mix samples outperform that of PPY4800. This is due to the low packing density of PPY4800 arising from a highly mesoporous nature. Thus despite a high gravimetric uptake, the performance of PPY4800 is limited by low volumetric uptake and working capacity. On the other hand, some of the pre-mix samples have

Porosity modulation of activated carbons via pre-mixed precursors for enhanced methane storage

impressive volumetric uptake in addition to high gravimetric storage capacity. Although samples CNL4800 and ACDS4800 have the highest volumetric uptake, their performance is compromised by low gravimetric uptake that only reaches ca. 0.3 g g^{-1} at 100 bar. It is interesting to note that the volumetric uptake of the best performing pre-mix samples is only 10 – 20% lower than that of CNL4800 and ACDS4800 but with comparable volumetric working capacity despite gravimetric uptake that is up to 50% higher. The pre-mix samples, therefore, offer optimised performance as methane stores with respect to the balance between gravimetric and volumetric storage capacity.

A positive consequence, on the methane uptake, of lowering the mesoporosity in comparison to PPY4800 has been achieved. Whilst the highest total volumetric methane uptake was exhibited by samples with the greatest microporosity and the highest packing density, i.e., CNL4800 and ACDS4800, these samples have low gravimetric uptake. The decreased mesoporosity of the pre-mix precursor samples offers the benefit of increased packing density. As discussed above, packing density is inversely related to pore volume. The packing density of porous solids is critical for their use as methane stores since it dictates how much gas can be kept in a limited space, such as a storage tank, when the material is packed to its full volumetric storage capacity. Storage materials therefore need to fulfil both gravimetric and volumetric storage targets, which is best demonstrated by the best performing pre-mix samples. For example, the best performing porous carbons reported to date for total volumetric

Porosity modulation of activated carbons via pre-mixed precursors for enhanced methane storage

methane storage at 25 °C and 35 bar are mesophase pitch derived activated carbons, LMA738 (165 cm³ cm⁻³) DO00-3:1_700 that (184 cm³ cm⁻³), zeolite templated carbons, ZTC, (BEA-ZTC) that stores 148 cm³ cm⁻³ and thermally treated BEA-ZTC (BEA-ZTC-873) that stores 165 cm³ cm⁻³ (**Table 10**). In comparison, the present pre-mixed carbons have comparable volumetric uptake but much higher gravimetric storage capacity.

Table 10. Gravimetric and volumetric methane uptake at 25 °C and pressure of 35 bar for PPY4800, CNL4800, ACDS4800 and PPYCNL124 compared to the best performing carbons

Sample	Total uptake g g ⁻¹	Total uptake cm ³ (STP) cm ⁻³	Reference
PPY4800	0.25	129	This work
ACDS4800	0.20	194	This work
CNL4800	0.21	194	This work
PPYCNL124	0.23	164	This work
DO00-3:1_700	0.18	184	10
LMA738	0.17	165	53
BEA-ZTC	0.16	148	54
BEA-ZTC-873	0.17	165	54
AX21	0.16	154	5

For a more comprehensive understanding of the methane storage performance of the present carbons, their performance was compared to

Porosity modulation of activated carbons via pre-mixed precursors for enhanced methane storage

current benchmark materials. Metal organic frameworks (MOFs) have been reported as the current record holders for methane storage in powdered solids. **Figure 12** shows a comparison between the present carbons and benchmark MOFs, namely, HKUST-1, Ni-MOF-74, Co-MOF-74 and PCN-14.^{4-9,59} The volumetric uptake of the present carbons is comparable to the benchmark materials even though crystal density is used to calculate the uptake of the MOFs. The use of crystallographic density leads to overestimated volumetric uptake values results and suggest impractical scenarios requiring MOFs are packed as single crystals into confined spaces such as storage tanks/cylinders. The reality is that MOF packing density is often substantially lower (up to 50% lower) than its crystallographic density.⁴⁶ As a result, when used in real-world applications, MOF values are expected to reduce by 25 to 50%, meaning that they would actually be mostly lower than for the present carbons as shown in **Figure 13**. The performance of the present carbons is, in particular, significantly higher at pressures above 50 bar (**Figure 13**).

Porosity modulation of activated carbons via pre-mixed precursors for enhanced methane storage

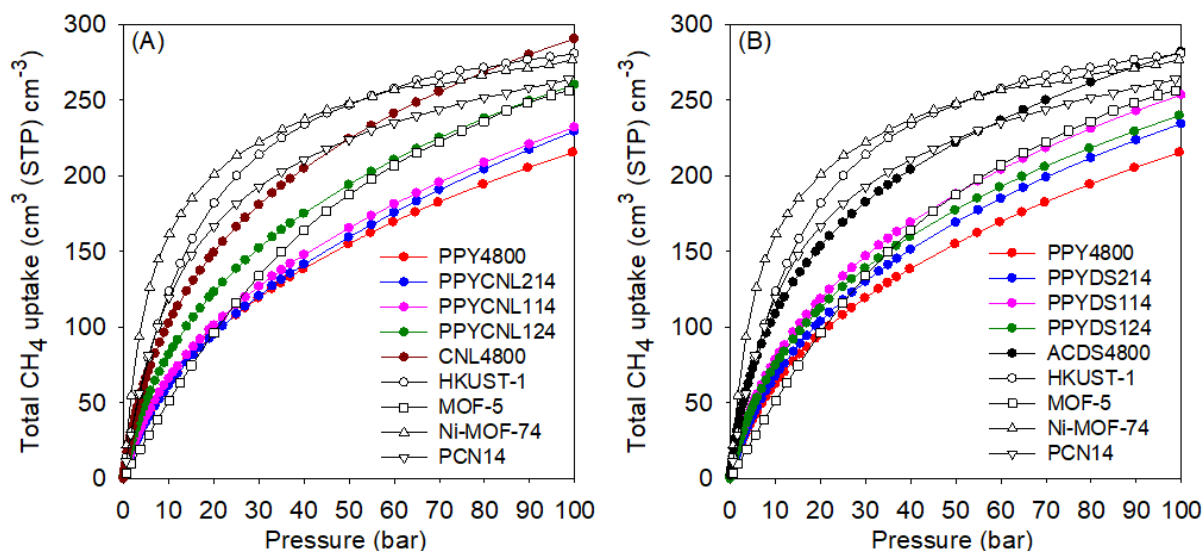


Figure 12. Total volumetric methane uptake of activated carbons derived from single precursors (PPY4800, CNL4800, ACDS4800) or (A) PPY/CNL or (B) PPY/DS pre-mixtures compared to benchmark MOF materials. The uptake of MOFs was calculated using crystallographic density.

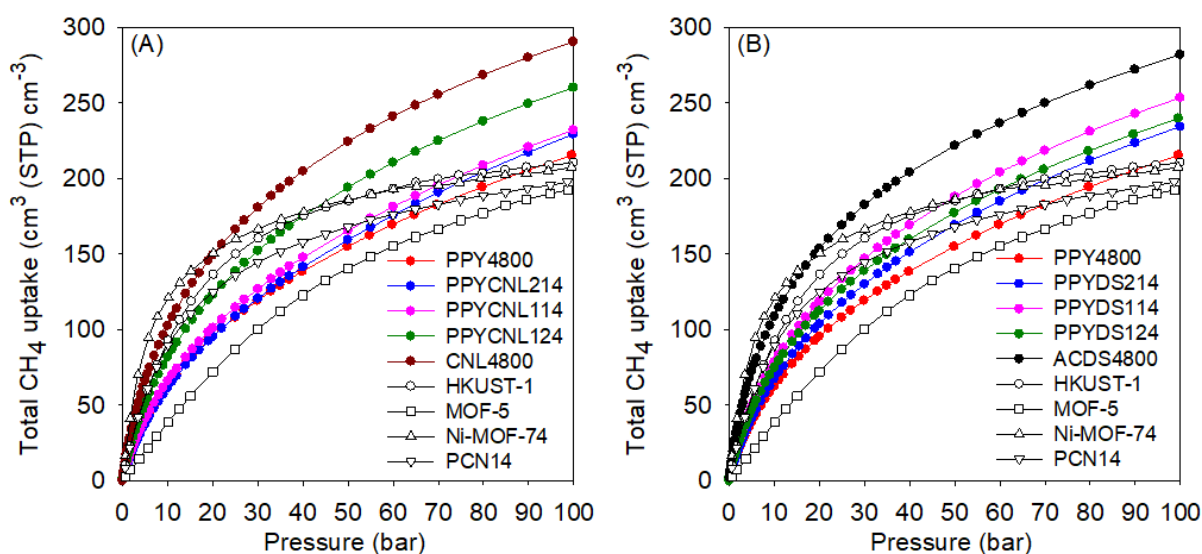


Figure 13. Total volumetric methane uptake of activated carbons derived from single precursors (PPY4800, CNL4800, ACDS4800) or (A) PPY/CNL or (B) PPY/DS pre-mixtures compared to benchmark MOF materials. The uptake of MOFs, allows for a 25% reduction of values calculated using crystallographic density.

A more realistic comparison that avoids the ambiguity associated with the use of crystallographic density (for MOFs) is the recent work of Tian and

Porosity modulation of activated carbons via pre-mixed precursors for enhanced methane storage

co-workers who reported on monolithic MOFs, designated as monoHKUST-1 , which have high packing density (1.06 g cm^{-3}) and enhanced volumetric methane uptake.⁴⁶ The monoHKUST-1 and related monolithic MOFs, such as the more practical monoUiO-66_D , are the current record holders for methane storage at $25 \text{ }^\circ\text{C}$ and pressure of up to 100 bar.^{46,56} In **Figure 14**, performance of the present carbons is compared with that of monoHKUST-1 and monoUiO-66_D . The volumetric uptake of the present carbons is impressive over the full pressure range and is better or comparable to that of monoUiO-66_D . The uptake of the carbons is lower than that monoHKUST-1 , which though claimed to be at least 50% better than any other MOF reported to date, is not a practical material for methane storage.^{46,56} The comparison in **Figure 14** illustrates the attraction of the present carbons as practical methane stores given that they can be readily prepared via low cost routes. A further attraction of the present carbons is that they have much higher gravimetric uptake compared to monoHKUST-1 and monoUiO-66_D as shown in **Figure 15**.

Porosity modulation of activated carbons via pre-mixed precursors for enhanced methane storage

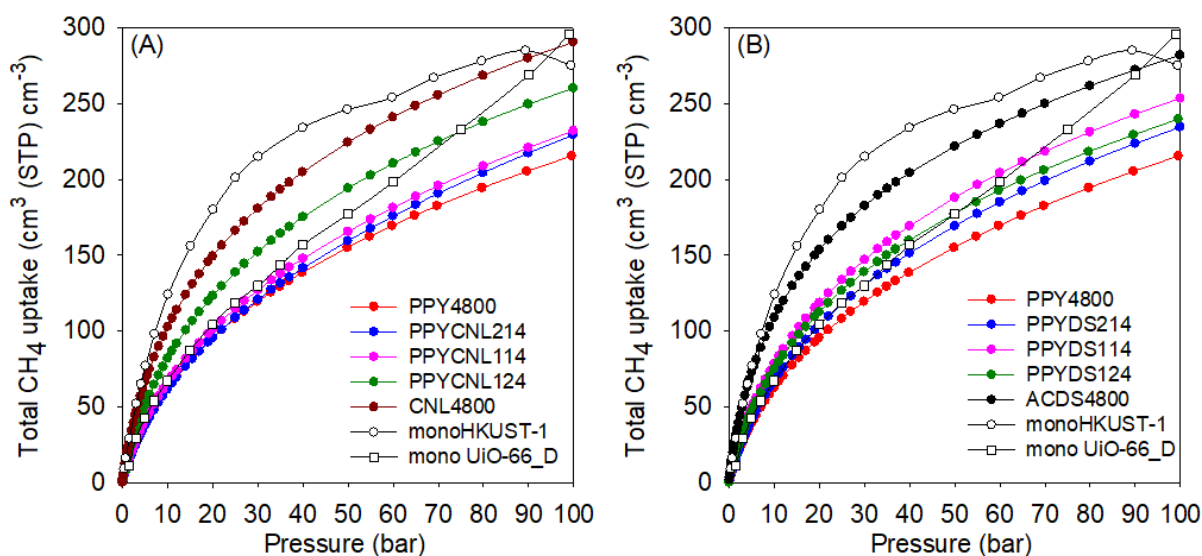


Figure 14. Total volumetric methane uptake of activated carbons derived from single precursors (PPY4800, CNL4800, ACDS4800) or (A) PPY/CNL pre-mixtures or (B) PPY/DS pre-mixtures compared to storage capacity of monolithic *mono*HKUST-1 and *mono*UiO-66_D.

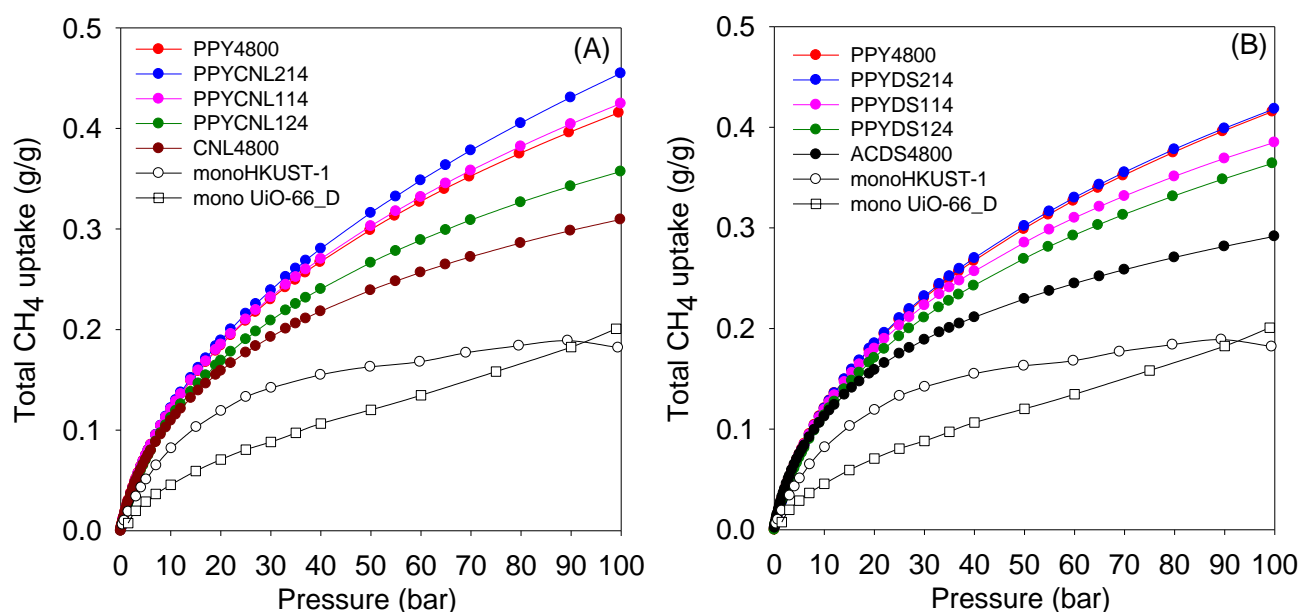


Figure 15. Total gravimetric methane uptake (gCH₄ g⁻¹) of activated carbons derived from single precursors (PPY4800, CNL4800, ACDS4800) or (A) PPY/CNL pre-mixtures or (B) PPY/DS pre-mixtures compared to storage capacity of monolithic *mono*HKUST-1 and *mono*UiO-66_D.

For a desorption pressure of 5 bar, the present carbons show good working capacity values that is comparable to that of *mono*HKUST-1 and *mono*UiO-66_D as shown in **Table 11**. Although *mono*HKUST-1 is the current

Porosity modulation of activated carbons via pre-mixed precursors for enhanced methane storage

record holder for volumetric methane storage in porous materials and is claimed to be 50% better than any other MOF, its practical use is limited by chemical instability associated with loss of crystallinity when exposed to moisture.^{46,56} The more relevant comparison for the present carbons is, therefore, with the more robust and stable monoUiO-66_D . As shown in **Table 11**, at 35 bar, the total volumetric uptake and working capacity of the carbons is better than that of monoUiO-66_D . At 65 bar, the performance of the carbons is comparable to that of monoUiO-66_D . Only at 100 bar is the working capacity of monoUiO-66_D noticeably higher than that of the carbons.

Porosity modulation of activated carbons via pre-mixed precursors for enhanced methane storage

Table 11. Total volumetric methane uptake and working capacity of activated carbons derived from single precursor carbons (PPY4800, and CNL4800) and from pre-mixed precursors compared to _{mono}HKUST-1 and _{mono}UiO-66_D.

Sample	Total volumetric methane uptake ^a (cm ³ (STP) cm ⁻³)		
	35 bar	65 bar	100 bar
PPY4800	129 (90)	176 (137)	215 (177)
CNL4800	194 (127)	249 (182)	291 (224)
PPYCNL124	164 (113)	217 (167)	260 (209)
PPYCNL114	138 (97)	189 (148)	232 (191)
PPYCNL214	132 (94)	183 (146)	229 (192)
ACDS4800	194 (122)	243 (171)	282 (209)
PPYDS124	150 (103)	199 (152)	240 (193)
PPYDS114	159 (110)	211 (162)	254 (205)
PPYDS214	141 (100)	192 (151)	234 (193)
_{mono} HKUST-1	224 (147)	261 (191)	275 (235)
_{mono} UiO-66_D	143 (100)	211 (172)	296 (261)

The values in parenthesis are the volumetric working capacity defined as the difference in uptake between the stated pressure (35, 65 or 100 bar) and 5 bar.

6.4 Conclusions

Pre mixtures of polypyrrole (PPY) with biomass derived CNL carbon or ACDS carbon, were successfully used to generate activated carbons. The carbons made from pre-mixed precursors were compared to those produced from single use of any one of the precursors under similar activation conditions. The use of pre-mixed precursors enables the relationship between level of activation and surface area to be optimised in a manner that cannot be achieved with single precursors. Thus, the pre-mixed precursors provide carbon materials with an ultra-high surface area and pore volume, i.e. of up to $3890 \text{ m}^2 \text{ g}^{-1}$ and $2.40 \text{ cm}^3 \text{ g}^{-1}$, respectively.

The pore size distribution of the pre-mixed carbons is primarily made up of micropore (6–12 Å) and small mesopores (20–30 Å). The combination of mesoporosity, arising from PPY, and microporosity from the biomass sources (CNL or ACDS carbons) means that the porosity of the pre-mix carbons can be readily tailored to exhibit varying combinations of micropores, supermicropores and small mesopores. This is achieved under identical activation conditions, i.e. $800 \text{ }^\circ\text{C}$ and a KOH/precursor ratio of 4, wherein the porosity is modulated by the ratio of PPY and the biomass carbons in the precursor.

This study offers further evidence that the elemental composition of the precursors (carbonaceous starting materials), and in particular the molar ratio of oxygen to carbon (i.e., O/C molar ratio), is the genesis of the ability to modulate porosity based on the precursor mix. A high O/C ratio

Porosity modulation of activated carbons via pre-mixed precursors for enhanced methane storage

favours ease of activation and the formation of mesopores, while a low ratio is associated with resistance to activation and the formation of micropores. We show that knowledge of the O/C ratio of carbonaceous matter allows prediction of activation behaviour, porosity, and micropore/mesopore mix. The carbons developed in this study are excellent stores for methane owing to their tailored porosity and packing density. The methane storage performance of the carbons is better than all previously reported carbons and powder MOFs, and comparable to that of monolithic MOFs that are the current record holders for volumetric methane storage in porous solids.

Porosity modulation of activated carbons via pre-mixed precursors for enhanced methane storage

References

1. U. Eberle, B. Muller and R. von Helmot, *Energy Environ. Sci.*, 2012, **5**, 8780.
2. M. E. Boot-Handford, J. C. Abanades, E. J. Anthony, M. J. Blunt, S. Brandani, N. Mac Dowell, J. R. Fernandez, M. C. Ferrari, R. Gross, J. P. Hallett, R. S. Haszeldine, P. Heptonstall, A. Lyngfelt, Z. Makuch, E. Mangano, R. T. J. Porter, M. Pourkashanian, G. T. Rochelle, N. Shah, J. G. Yao and P. S. Fennell, *Energy Environ. Sci.*, 2014, **7**, 130.
3. K. Z. House, A. C. Baclig, M. Ranjan, E. A. van Nierop, J. Wilcox and H. J. Herzog, *Proc. Natl. Acad. Sci. U.S.A.*, 2011, **108**, 20428.
4. T. A. Makal, J. R. Li, W. Lu and H. C. Zhou, *Chem. Soc. Rev.*, 2012, **41**, 7761.
5. J. A. Mason, M. Veenstra and J. R. Long, *Chem. Sci.*, 2014, **5**, 32.
6. K. V. Kumar, K. Preuss, M. M. Titirici, F. Rodriguez-Reinoso, *Chem. Rev.*, 2017, **117**, 1796.
7. B. Li, H.-M. Wen, W. Zhou, J. Q. Xu and B. Chen, *Chem*, 2016, **1**, 557.
8. Y. Lin, C. L. Kong, Q. J. Zhang and L. Chen, *Adv. Energy Mater.*, 2017, **7**, 1601296.
9. Y. He, W. Zhou, G. Qian and B. Chen, *Chem. Soc. Rev.*, 2014, **43**, 5657.
10. M. E. Casco, M. Martínez-Escandell, E. Gadea-Ramos, K. Kaneko, J. Silvestre-Albero and F. Rodríguez-Reinoso, *Chem. Mater.*, 2015, **27**,

Porosity modulation of activated carbons via pre-mixed precursors for enhanced methane storage

959.

11. I. Angelidaki, L. Treu, P. Tsapekos, G. Luo, S. Campanaro, H. Wenzel and P. Kougias, *Biotechnol. Adv.*, 2018, **36**, 452.
12. Z. Bacsik, O. Cheung, P. Vasiliev and N. Hedin, *Appl. Energy*, 2016, **162**, 613.
13. M. I. Khan, T. Yasmin and A. Shakoor, *Renew. Sust. Energ. Rev.*, 2015, **51**, 785.
14. M. Namvar-Asl, M. Soltanieh and A. Rashidi, *Energy Convers. Manag.*, 2008, **49**, 2478.
15. M. Feroldi, A. C. Neves, C. E. Borba and H. J. Alves, *J. Clean. Prod.*, 2018, **172**, 921.
16. M. Sevilla and R. Mokaya, *Energy Environ. Sci.*, 2014, **7**, 1250.
17. Z. Hu, M. P. Srinivasan and Y. Ni, *Carbon*, 2001, **39**, 877.
18. E. Haffner-Staton, N. Balahmar and R. Mokaya, *J. Mater. Chem. A*, 2016, **4**, 13324.
19. N. Balahmar, A. S. Al-Jumialy and R. Mokaya, *J. Mater. Chem. A*, 2017, **5**, 12330.
20. E. A. Hirst, A. Taylor and R. Mokaya, *J. Mater. Chem. A*, 2018, **6**, 12393.
21. N. Balahmar and R. Mokaya, *J. Mater. Chem. A*, 2019, **7**, 17466.
22. A. Altwala and R. Mokaya, *Energy Environ. Sci.*, 2020, **13**, 2967.

Porosity modulation of activated carbons via pre-mixed precursors for enhanced methane storage

23. T. S. Blankenship, N. Balahmar and R. Mokaya, *Nat. Commun.*, DOI: 10.1038/s41467-017-01633-x.
24. W. Sangchoom and R. Mokaya, *ACS Sustainable Chem. Eng.*, 2015, **3**, 1658.
25. H. M. Coromina, D. A. Walsh and R. Mokaya, *J. Mater. Chem.*, 2016, **4**, 280.
26. X. Zhu, Y. Liu, F. Qian, C. Zhou, S. Zhang and J. Chen, *ACS Sustainable Chem. Eng.*, 2015, **3**, 833.
27. M. Sevilla, W. Sangchoom, N. Balahmar, A. B. Fuertes and R. Mokaya, *ACS Sustainable Chem. Eng.*, 2016, **4**, 4710.
28. T. S. Blankenship and R. Mokaya, *Energy Environ. Sci.*, 2017, **10**, 2552.
29. M. Sevilla, R. Mokaya and A. B. Fuertes, *Energy Environ. Sci.*, 2011, **4**, 2930.
30. M. Sevilla, P. Valle-Vigon and A. B. Fuertes, *Adv. Funct. Mater.*, 2011, **21**, 2781.
31. N. Balahmar, A. C. Mitchell and R. Mokaya, *Adv. Energy Mater.*, 2015, **5**, 1500867.
32. B. Adeniran and R. Mokaya, *Nano Energy*, 2015, **16**, 173.
33. M. Cox and R. Mokaya, *Sustainable Energy Fuels*, 2017, **1**, 1414.
34. J. S. M. Lee, M. E. Briggs, T. Hasell and A. I. Cooper, *Adv. Mater.*, 2016, **28**, 9804.

Porosity modulation of activated carbons via pre-mixed precursors for enhanced methane storage

35. M. Sevilla, A. B. Fuertes and R. Mokaya, *Energy Environ. Sci.*, 2011, **4**, 1400.
36. I. M. Minisy, U. Acharya, L. Kobera, M. Trchová, C. Unterweger, S. Breitenbach, J. Brus, J. Pflieger, J. Stejskal, P. Bober, *J. Mater. Chem. C*, 2020, **8**, 12140.
37. J. Wang and S. Kaskel, *J. Mater. Chem.*, 2012, **22**, 23710.
38. C. Robertson and R. Mokaya, *Microporous Mesoporous Mater.*, 2013, **179**, 151.
39. M. J. Antal, E. Croiset, X. Dai, C. DeAlmeida, W. S-L. Mok, N. Norberg, J-R. Richard and M. Al Majthoub, *Energy Fuels*, 1996, **10**, 652.
40. M. J. Antal, S. G. Allen, X. Dai, B. Shimizu, M. S. Tam and M. Gronli, *Ind. Eng. Chem. Res.*, 2000, **39**, 4024.
41. W. M. A. W. Daud and W. S. W. Ali, *Bioresour. Technol.* 2004, **93**, 63.
42. H. Yang, R. Yan, H. Chen, C. Zheng, D. H. Lee and D. T. Liang, *Energy Fuels*, 2006, **20**, 388.
43. M. Bbebu and C. Vasile, *Cellulose Chem. Technol.*, 2010, **44**, 353.
44. R. K. Sharma, J. B. Wooten, V. L Baliga, X. Lin, W. G. Chan and M. R. Hajaligol, *Fuel* 2004, **83**, 1469.
45. Z. Fang, T. Sato, R. L. Smith Jr, H. Inomata, K. Arai and J. A. Kozinski, *Bioresour. Technol.*, 2008, **99**, 3424.
46. T. Tian, Z. Zeng, D. Vulpe, M. E. Casco, G. Divitini, P. A. Midgley, J. Silvestre-Albero, J.-C.Tan, P. Z. Moghadam and D. Fairen-Jimenez,

Porosity modulation of activated carbons via pre-mixed precursors for enhanced methane storage

Nat. Mater., 2018, **17**, 174.

47. Z. Chen, P. Li, R. Anderson, X. Wang, X. Zhang, L. Robison, L. R. Redfern, S. Moribe, T. Islamoglu, D. A. Gómez-Gualdrón, T. Yildirim, J. F. Stoddart, O. K. Farha, *Science*, 2020, **368**, 297.
48. D. Lozano-Castello, J. Alcaniz-Monge, M.A. de la Casa-Lillo, D. Cazorla-Amoros, A. Linares-Solano, *Fuel*, 2002, 81, 1777.
49. P. Pfeifer, L. Aston, M. Banks, S. Barker, J. Burrell, S. Carter, J. Coleman, S. Crockett, C. Faulhaber, J. Flavin, M. Gordon, L. Hardcastle, Z. Kallenborn, M. Kemiki, C. Lapilli, J. Pobst, R. Schott, P. Shah, S. Spellerberg, G. Suppes, D. Taylor, A. Tekeei, C. Wexler, M. Wood, P. Buckley, T. Breier, J. Downing, S. Eastman, P. Freeze, S. Graham, S. Grinter, A. Howard, J. Martinez, D. Radke, T. Vassalli and J. Ilavsky, *Chaos*, 2007, **17**, 041108.
50. J. Romanos, S. Sweany, T. Rash, L. Firlej, B. Kuchta, J. C. Idrobo, P. Pfeifer, *Adsorpt. Sci. Technol.*, 2014, **32**, 681.
51. D. A. Gómez-Gualdrón, C. E. Wilmer, O. K. Farha, J. T. Hupp, R. Q. Snurr, *J. Phys. Chem. C*, 2014, **118**, 6941.
52. C. M. Simon, J. Kim, D. A. Gomez-Gualdron, J. S. Camp, Y. G. Chung, R. L. Martin, R. Mercado, M. W. Deem, D. Gunter, M. Haranczyk, D. S. Sholl, R. Q. Snurr and B. Smit, *Energy Environ. Sci.*, 2015, **8**, 1190.
53. M. E. Casco, M. Martínez-Escandell, K. Kaneko, J. Silvestre-Albero and F. Rodríguez-Reinoso, *Carbon*, 2015, **93**, 11.

Porosity modulation of activated carbons via pre-mixed precursors for enhanced methane storage

54. S. Choi, M. A. Alkhabbaz, Y. Wang, R. M. Othman and M. Choi, *Carbon*, 2019, **141**, 143.
55. P. N. Quirant, C. Cuadrado-Collados, A. J. Romero-Anaya, J. S. Albero and M. M. Escandell, *Ind. Eng. Chem. Res.*, 2020, **59**, 5775.
56. B. M. Connolly, M. Aragonés-Anglada, J. Gandara-Loe, N. A. Danaf, D. C. Lamb, J. P. Mehta, D. Vulpe, S. Wuttke, J. Silvestre-Albero, P. Z. Moghadam, A. E. H. Wheatley and D. Fairen-Jimenez, *Nat. Commun.*, 2019, DOI:10.1038/s41467-019-10185-1
57. B. M. Connolly, D. G. Madden, A. E. H. Wheatley and D. Fairen-Jimenez, *J. Am. Chem. Soc.* 2020, **142**, 8541.
58. V. Rozyyev, D. Thirion, R. Ullah, J. Lee, M. Jung, H. Oh, M. Atilhan and C. T. Yavuz, *Nat. Energy*, 2019, **4**, 604.
59. S. Ma, D. Sun, J. M. Simmons, C. D. Collier, D. Yuan and H. C. Zhou, *J. Am. Chem. Soc.*, 2008, **130**, 1012.

Chapter 7. Conclusion

In view of increasing global pollution, possible mitigations to counter the effects of pollution are discussed in this Thesis. The focus of the research described in this Thesis is the development of tailorable porous materials with optimised porosity that is suitable for uptake and storage of gases, CO₂ and methane, which are relevant to pollution and sustainable energy provision. In particular, the Thesis focused on activated carbon, an example of an environmentally friendly and sustainable material that can be used for gas storage owing to large internal surface area. Activated carbons were prepared using biomass as starting material. Such biomass as was used is an attractive feedstock in terms of abundance, low cost and renewability. The low cost of the biomass means that conversion to activated carbon is essentially a valorisation process, which adds to their attraction as feedstock. Activated carbons were obtained from biomass via a variety of synthesis routes, including direct activation, flash air-carbonisation before activation, and activation as part of pre-mixed precursors containing up to three different ingredients. The carbons developed in this Thesis were employed for carbon capture and storage, and methane storage. A range of characterisation techniques, including TGA, BET, XRD and SEM, were used to assess the purity, porosity and stability of the carbons.

Four main themes are explored in this thesis. In the first study, it was demonstrated that activated carbon properties can be predictably tailored. Selection of the biomass precursor and mode of carbonisation was able to

Conclusion

produce carbons with high surface area density, volumetric surface area and packing density that were optimised for enhanced methane storage at medium pressure, i.e., 35 bar. It was established that the elemental composition of the biomass precursor, specifically, a low O/C atomic ratio, can be used as a universal predictor of the nature of porosity generated for activated carbon prepared via KOH activation. Activated carbons were obtained with an optimised mix of microporosity and mesoporosity, and high surface area density, volumetric surface area and packing density using date seeds (*Phoenix dactylifera*) as starting biomass material. The technique employed, i.e., flash air-carbonisation, is of a much lesser duration, i.e. 10 minutes, and requires a lower temperature of 400 °C. Following the examination of a wide range of materials, surface area density was found to be inversely related to the O/C ratio of the precursor carbonaceous matter. Even after severe activation, the carbonaceous matter obtained from flash air-carbonisation of date seeds was resistant to activation, resulting in highly microporous activated carbons with a surface area of 995 – 2609 m² g⁻¹, pore volume of 0.43 – 1.10 cm³ g⁻¹ and high packing density. The resulting carbons had pores of size 0.8 – 1.2 nm, which are suitable for methane uptake. At 25 °C and 35 bar, the carbons have an excess and total methane uptake of up to 196 cm³ (STP) cm⁻³ and 222 cm³ (STP) cm⁻³, respectively, which is superior to any previously reported carbon and comparable to the best MOFs, but at a much lower cost.

Conclusion

In the second study, activated carbons were generated from seed using both PO and KOH as activators. In previous studies, the action of the two activating agent was compared but on different starting materials. In this Thesis, identical procedures were used to synthesise the carbons with the respective both KOH and OP, a study design that facilitated comprehension of their respective effects on porosity. The activated carbons resulting from PO activation had surface area of up to $1747 \text{ m}^2 \text{ g}^{-1}$, with up to 94% of the surface area being attributed to micropores. Their porosity could be tailored towards 6–8 Å pore channels, which are excellent for CO_2 storage at low pressure. At pressures of 0.15 and 1 bar, up to 1.9 and 4.8 mmol g^{-1} , respectively, of CO_2 were captured by PO activated carbons at a $25 \text{ }^\circ\text{C}$. Unlike hydroxide activation, changing the PO/ACDS ratio between 2 and 4 did not affect porosity. It was determined that the CO_2 uptake of PO activated air carbonised date seed at 0.15 bar and at $25 \text{ }^\circ\text{C}$ was up to 1.9 mmol g^{-1} , which is one of the highest reported for any porous material. However, carbons similarly activated, but with KOH, have a surface area of up to $2738 \text{ m}^2 \text{ g}^{-1}$ and, depending on the level of activation, exhibit a high pre-combustion CO_2 capture capability of 18.3 mmol g^{-1} at 20 bar compared to a high of 11 mmol g^{-1} for PO activated carbons.

In the third study, highly microporous activated carbon materials were generated from sawdust (SD). A direct activation procedure was used, eliminating the need for hydrothermal carbonisation or pyrolysis, and utilising potassium oxalate (PO) as a less corrosive and less toxic activating agent compared to KOH. The resulting activated carbons demonstrated

Conclusion

relatively high surface area ranging from 550 to 2100 m² g⁻¹, and pore volumes between 0.3 and 1.0 cm³ g⁻¹. Unlike hydroxide activation, the PO/SD ratio does not exert a significant effect on porosity; however, the activation temperature plays a critical role in determining the textural properties. Thus, through variation of the activation temperature, porosity could be precisely regulated. PO is a mild activating agent, with relatively environmentally friendly properties compared to KOH. This is an important observation, as it confirms a more ecologically sound and direct route to activation, using a milder activating agent, does not compromise achievable porosity. The direct activation technique, with PO as the activating agent, generated activated carbons with pore sizes of 6–8 Å, facilitating the carbons to capture up to 1.6 and 4.3 mmol g⁻¹ of CO₂ at 0.15 and 1 bar, respectively, at a temperature of 25 °C.

In the fourth study, activated carbons with ultra-high surface area were generated from pre mixtures of polypyrrole (PPY) with CNL carbon or ACDS carbon. The pre-mixtures, which combined precursors that would ordinarily give mesoporous carbons with high pore volume (PPY) or microporous carbons with moderate pre volume (CNL and ACDS carbons), generated activated carbons with ultra-high surface area of up to 3890 m² g⁻¹) and pore volume of up to 2.40 cm³ g⁻¹. The use of pre-mixed precursor generates carbons with a substantially greater surface area than single use of any one of the precursors. Overall, the study shows that the O/C molar ratio of the precursor is a significant determinant in controlling the development of mesopores, with a high ratio favouring increased

Conclusion

mesoporosity. The porosity of the high surface area carbons generated from pre-mixtures translated to exceptional gravimetric methane uptake at 25°C. The volumetric uptake was also found to improve due to the positive contribution of using CNL or ACDS carbon to packing density. The activated carbons, therefore, exhibited greater methane uptake capacity (gravimetric and volumetric) than those produced from single use of the precursors. The carbons had a total gravimetric methane uptake of up to 28.4 mmol g⁻¹ (or 0.46 g g⁻¹) at 100 bar. At 25 °C and at 100 bar, the carbons were able to store up to 260 cm³ (STP) cm⁻³ methane, which is notably superior to previous values reported for porous carbons and is comparable to the best storage capacities documented for MOFs. However, activated carbons have the advantage of being cheaper compared to MOFs.